UNIVERSITY OF OKLAHOMA

GRADUATE COLLEGE

CLOSURE OF THE SURFACE ENERGY BUDGET

A Dissertation

SUBMITTED TO THE GRADUATE FACULTY

in partial fulfillment of the requirements for the

degree of

Doctor of Philosophy

By

JERALD ANDREW BROTZGE
Norman. Oklahoma
2000

UMI Number: 9988514

CLOSURE OF THE SURFACE ENERGY BUDGET

A Dissertation APPROVED FOR THE
SCHOOL OF METEOROLOGY

BY

Kenneth C. Crawford

Acknowledgments

The people who have shaped this dissertation both personally and professionally are numerous. First, I must thank my advisor, Dr. Ken Crawford. Ken has taught me that no dream is too great. His diligence and perseverance is amazing, and I'll never forget his honesty and kindness. Thanks Dr. C!

Thanks also are due all of OCS. Scott, you've taught me a lot, and I couldn't have done this without you. You and Yvette are wonderful. David, Sherman, and James- I could not have survived those first few years (and latter years!) without your expertise and friendship. Thanks too to all the techs- Ken, Gavin, Leslie, and Thomas- for all the hard work over the years. Kudos also to Amy, Cerry, Sridhar, Jessica, Chris F., Derek, and all the other programmers and staff who've shown a great deal of patience with me over the years.

More importantly are all the friends who have made my personal time here in Oklahoma a most enjoyable one. Bill and Rob, you have shown me that indeed there are good and sane people from California. Besides that, you've made my weekends fun, humiliated me in tennis, listened to my rants and raves, and have been the best friends anyone could imagine. Laurie and MyShelle, you're included in that as well. I will forever share a much deeper "appreciation" for Rage, "spewing", and hearts. Ernani, Ken, Paul and Elaine, Chris, Erin – thanks for such a good time!

Jeff, thanks for making the office fun. I've learned a lot from you, and I hope our paths continue to cross in the future. You help bring a lot of enthusiasm to what we do, and I'm going to miss all those office talks.

Eric, thanks for being such a great roommate all these years. You've been incredibly kind and patient.

Also, I'll never forget all my tremendous friends from church who have kept me thinking, level-headed, and straight in our Christian walk – Blake, Chandra, Debbie, Dorain, Helen, Kevin, Lisa, Mecca, Mel, Mike, and Uwem. Thanks for all the good times!

Finally and above all, I thank my parents. I have been blessed by all measure to have such an honorable and respected family. They have opened my eyes to the world around me, filled me with wonder, and taught me right from wrong. Thanks for a lifetime of fun.

Table of Contents

List of Tables

Abstract

Radiative energy incident upon the earth's surface is either absorbed by the earth, reflected back to the atmosphere, or converted into sensible (SH) and latent heat (LH) fluxes. This principle of conservation of energy defines the surface energy budget, Rn = SH + LH + GH where Rn is net radiation and GH is the ground heat flux. A common standard for representing the accuracy of measurement of the energy budget is defined by the degree of "closure" (C) as defined by a percentage:

$$C = \frac{(SH + LH)}{(Rn - GH)} * 100\%$$

Eddy correlation systems provide the only direct method for independently measuring sensible and latent heat fluxes. Unfortunately, measurements using eddy correlation (EC) systems often have failed to close the energy budget (Rn ≠ SH + LH +GH). Previous field experiments such as FIFE, Monsoon-90, and SGP-97 have consistently underestimated closure. This lack of closure casts doubt on the accuracy of EC measurements. A systematic error in measurement of the surface energy budget has profound implications for model and satellite verifications. The exact cause(s) for this systematic underestimate in closure is unknown.

The OASIS Project became operational 1 January 2000 and permits measurement of net radiation and ground heat flux as well as sensible and latent heat fluxes via eddy correlation at ten Mesonet sites across Oklahoma. In this dissertation, the closure issue is investigated using over 5 million observations collected during a one-year period from the OASIS and ARM projects.

Instrument error, a mismatch in source area, horizontal flux divergence, surface heterogeneity, and fetch are examined as possible sources of error.

Results outline appropriate procedures for limiting instrument and system error in measurement of the surface energy budget. A systematic error was identified from an examination of closure at ten OASIS sites, and a comparison between an EC and Bowen ratio system recognized several specific problems. Problems with closure were found limited to measurement of the latent heat flux, and several reasons for the underestimate in latent heat flux were identified.

Chapter 1: Introduction

According to Brutsaert (1982), Anaximander of Miletos (ca. 565 B.C.) of ancient Greece was among the first to recognize the unifying bonds between the land and atmosphere. As recorded by Hippolytus, Anaximander spoke of the water cycle when he described "rains generated from the evaporation that is sent up from the earth toward under the sun" (Brutsaert 1982). His description is but one example of the interplay between components of our climate system – the atmosphere, lithosphere, cyrosphere, oceans, and biosphere - and it is as important to our understanding of meteorology today as it was during the days of ancient Greece.

Fortunately, modern meteorology more clearly understands these processes of energy exchange at the earth's surface. Solar radiation impinges upon the top of the atmosphere where it is either reflected back into space, absorbed by the atmosphere, or transmitted to the earth's surface. Radiative energy incident upon the earth's surface is then either absorbed by the earth, reflected back to the atmosphere, or converted into sensible and latent heat energies at the surface. The principle of conservation of energy prevents the production or destruction of energy. Thus, the surface budget is conserved. The surface energy budget has the components:

$$Rn = SH + LH + GH + P \qquad (1.1)$$

It confines the 5 terms to equality where net radiation (Rn), sensible heat (SH), latent heat (LH), and ground heat (GH) dominate. Photosynthetic activity (P) remains negligible during the day and is less than 2% of the nocturnal radiation budget (Fritschen and Simpson 1989). While components of the surface energy budget vary widely on spatial and temporal scales according to surface heterogeneity, the total energy budget remains conserved across all land surface types. Such energetic processes play a critical role in momentum, heat, and moisture transfers between climate systems.

Despite these important influences, difficulties remain in the measurement of these basic meteorological parameters associated with the land surface. Precise measurements are difficult to obtain because of instrumentation error, system design limitations, and the empirical nature of corrective measures. Advection of meteorological parameters, topographical features, variable source regions, heterogeneity of soil and vegetation properties, and the nonstationarity of weather patterns severely limit the sample representativeness of observations on the meso- and regional scales.

The hypothesis of this study is that *the surface energy budget can be closed even in complex terrain if instrumentation error, topography, heterogeneity, and sampling differences are addressed with care.* This hypothesis will be investigated by integrating one year of data from the Oklahoma Atmospheric Surface-layer Instrumentation System Project (OASIS; Brotzge et al. 1999b), a component of the Oklahoma Mesonet (Brock et al. 1995), with topographical and vegetation data sets, and by conducting a series of field experiments.

First, a literature review outlines previous attempts at resolving the surface energy budget and explores hypotheses as to why closure remains an unresolved issue. Next, data used in the study are described in Chapter 3. Chapter 4 details instrumentation error and measurement limitations for each component of the energy budget. Chapter 5 quantifies the instrument measurement uncertainty associated with each of the components.

The final chapters explicitly examine closure in context with the known errors developed in Chapters 1 to 5. A detailed comparison of a Bowen ratio and eddy correlation system is described in Chapter 6. Next, closure is examined at ten Mesonet sites across the state to assess climatic influences. The influence of topography and fetch is explicitly investigated. Finally, Chapter 8 reviews possible causes for non-closure as proposed by the literature in lieu of results from Chapters 6 and 7. A summary of results and concluding remarks are provided in Chapter 9.

Chapter 2: Prior Field Experimentation and Theory

Introduction

Improved modeling and measurement of the surface energy budget have progressed through synergistic efforts over many years. More precise measurement of fluxes has enabled more realistic modeling. Improved modeling has prompted refined field measurements and field programs specifically aimed at improving targeted areas of model performance. Because model development is dependent upon observations, instrumentation error must be minimized. In addition, site-specific errors must be limited because point observations normally are assumed (sometimes unjustifiably) to be representative of the regional area (Shuttleworth 1991).

One physical requirement of every atmospheric model is that all energy incident upon the land surface must be conserved. Ideally, the observations reflect this conservation of energy, and the summation of all measured fluxes should equal zero. The challenge is to design observational systems that both minimize instrumentation error and limit microscale effects while best capturing regional land-surface and PBL properties.

2.1 Measurement of the Surface Energy Budget

The degree of "closure" of the energy budget is considered a common standard for representing the accuracy of any field experiment involving the energy budget. Closure provides a theoretical basis by which system error can be evaluated. Closure (C) is commonly defined as a percentage as:

$$C = \frac{(SH + LH)}{(Rn - GH)} * 100\% \tag{2.1}$$

where the sum of the sensible (SH) and latent heat (LH) fluxes are divided by the net available energy, the difference between the net radiation (Rn) and ground heat flux (GH). Eq. (2.1) is considered a reliable measure because the numerator and denominator represent different source regions. Note, however, that C = 100% does not ensure perfect observations; offsetting errors in 2 or more components also could lead to C = 100%. Nevertheless, as is shown in the scientific literature, even reasonable closure within 5% is difficult to obtain in many circumstances. In most cases, the SH and LH terms attained via eddy correlation techniques typically are underestimated relative to the net available energy (McNeil and Shuttleworth 1975; Shuttleworth et al. 1984; Dugas et al. 1991; Fritschen et al. 1992). Note that in some cases (e.g., during low flux periods), it is more appropriate to use the residual (R) of closure (Wm^{-2}):

$$R = Rn - GH - SH - LH \tag{2.2}$$

The first attempts at examining the surface energy budget used the Bowen ratio technique (Bowen 1926) which forces closure. The Bowen ratio is assumed proportional to the ratio of a vertical gradient of heat and moisture; it is obtained from measurements of temperature (T_1, T_2) and specific humidity (q_1, q_2) at two heights. The Bowen ratio is defined as:

$$\beta = \frac{C_p}{L_v} \frac{K_h}{K_w} \frac{(T_1 - T_2)}{(q_1 - q_2)} \tag{2.3}$$

where C_p is the specific heat of dry air, L_v is the latent heat of vaporization, and K_h and K_w are the eddy diffusivities for heat and water vapor, respectively (Ohmura 1982). The eddy diffusivities for heat and water vapor are assumed to be equal. The energy budget is estimated from:

$$LH = \frac{Rn - GH}{1 + \beta} \tag{2.4}$$

where Rn and GH are measured independently, and SH is the residual of the energy balance.

Despite its continuing popularity, work by Fuchs and Tanner (1968), Blad and Rosenberg (1974) and Ohmura (1982) identified numerous possible errors in using the Bowen ratio method. Even Bowen recognized that the assumption of the equality of eddy diffusivities was not always valid (Bowen 1926). Ohmura identified three specific operational limitations: 1) errors made in the Rn and GH terms are cumulative; 2) estimated fluxes could be of the wrong sign; and 3) estimated fluxes could be of the correct sign but of the wrong magnitude. Indeed, the accuracy of the Bowen ratio method relies on the accuracy of the difficult-to-measure terms of Rn and GH (e.g., see Chapter 6).

With advances in PBL theory and instrumentation technology, other methods were developed to measure the surface energy budget. Monin-Obukhov theory allowed surface-layer profiles to be estimated from measured vertical gradients (Holtslag and Van Ulden 1983; Halliwell and Rouse 1989). Improved computer hardware permitted direct sensing techniques, such as eddy correlation, where sensible and latent heat could be estimated directly (Suomi 1957). The use of profile and direct measurement techniques now allow each of the four components of the energy budget to be estimated independently.

2.2 Small-scale Field Experiments

Large-scale mixing above forests limit vertical gradients in heat and moisture and inhibit the use of Bowen ratio methods. In an effort to measure fluxes above forest canopies, eddy correlation methods began to be used more frequently. McNeil and Shuttleworth (1975) were among the first to compare the eddy correlation (EC) method to the Bowen ratio (BR) technique. Examining flux measurements above a pine forest, they found a marked underestimate of the sensible heat of about 24% by the eddy correlation method when compared to the Bowen ratio technique. Although all four components of the surface budget were measured, unfortunately, closure of the energy budget was not explicitly reported.

Shuttleworth et al. (1984) conducted a similar study above an Amazonian forest. Using a sonic anemometer and infrared absorption hygrometer, the authors explicitly examined closure of the energy budget. In their study, several corrections were applied to the sonic data including the correction proposed by Webb et al. (1980) for density variational dependence, and the correction from Moore (1986) for humidity fluctuations.

Nevertheless, in an examination of 8 days of data, Shuttleworth et al. found a 6.5% underestimate in the sum of sensible and latent heat fluxes compared to the available energy (Rn - GH).

Verma et al. (1986) were among the first to perform an energy budget study above a deciduous forest. They, too, explicitly examined the issue of closure. Using eddy correlation to measure the sensible and latent heat fluxes, they found a closure between 70 and 130%; only +/- 20% of the +/- 30% closure error could be accounted for by instrument uncertainty. Thus, at least 10% was not accounted for in the measurement process. A bias was not detected between the EC and BR methods, as other studies have confirmed. Verma et al. suggest such large errors in closure could be caused by either large error in the estimate of the canopy storage term or by the effects of complex terrain upwind of the site.

McMillen (1988) addressed the conclusions of Verma et al. by quantifying the problems of eddy correlation measurement in complex terrain. He identified several limitations of eddy correlation systems unique to inhomogeneous sites. McMillen found that the energy budget could be underestimated by as much as 30% without coordinate rotation to account for tilt error. Tilt error can be caused by either the tilt of the sonic anemometer or by the slope of the terrain. He also determined from observations that closure was maximized (at 0.99) by using a time-averaging interval between 100 and 500 s.

Dugas et al. (1991) reexamined the comparison between eddy correlation and the Bowen ratio techniques by using more advanced instrumentation. They compared four Bowen ratio systems, three eddy correlation systems, and a portable chamber system. The comparison was conducted over an irrigated wheat field to minimize surface heterogeneity. Eddy correlation estimates were corrected for density variation and oxygen dependence (Tanner et al. 1993). Still, the results were not unlike those found by McNeil and Shuttleworth (1975) and Shuttleworth et al. (1984); the EC estimates of sensible heat were 18% and 31% less than those from the BR technique on two successive days of comparison. Estimates of latent heat flux from the sonic were 23% and 33% less than those from the Bowen ratio technique.

Dugas et al. suggested four reasons for the underestimate produced by eddy correlation: 1) The available energy (Rn - GH) was overestimated. However, the authors' estimates of (Rn - GH) were consistent with those of other investigators; 2) Corrections to the frequency response of the sonic were needed as suggested by Moore (1986). This correction would have increased sonic SH by 5%; 3) The time constant of the thermocouple (T) used to estimate SH may have been too slow and resulted in an underestimate of the flux; 4) The SH as measured by the Bowen ratio technique was too large due to the assumption that the heat and vapor diffusivities were equal, $K_h = K_w$. Because of large values of latent heat flux, much of the lack of closure was due to discrepancies in accurately estimating LH by the sonic.

Another comprehensive comparison between the Bowen ratio and eddy correlation methods was conducted by Barr et al. (1994) above a deciduous forest. Data were collected at a height of 4 m above the canopy top. Corrections for wind and humidity fluctuations were applied to the sonic data, and a coordinate transformation of the data was accomplished to minimize slope error. Data were limited by wind direction to minimize fetch and flow interference across instruments. Barr et al. found closure of the energy budget to within 89%. Nevertheless, statistical analysis of the instrument error could only account for 6% of the 11% imbalance, leading to the conclusion that the lack of closure was statistically significant.

Barr et al. cited two additional reasons for the underestimate from the eddy correlation method. First, the averaging period may have been too short, whereby low frequency contributions were not included as described by Kaimal et al. (1972). A second reason given by the authors concerned "dispersive flux" (Shaw 1985; Lee and Black 1993). Eddy correlation assumes a mean vertical velocity of zero. However, given a strongly unstable environment, the vertical velocity could be much greater than zero in the vicinity of a thermal or updraft. Thus, the EC method does not account for large-scale fluxes.

Several studies explicitly investigated the problem with EC underestimating closure. As described by Kizer and Elliott (1991), Tanner (1984) tested two EC systems using Lyman-alpha hygrometers and sonic anemometers. Closure was estimated at 75% and 81%, respectively, from the two systems. Tanner cited a sensor separation of 20 cm between the hygrometer and sonic or air flow obstructions to the hygrometers as the most likely sources of error. Tanner et al. (1985) tested six EC systems, using two Lyman-alpha hygrometers and four krypton hygrometers. Closure estimates ranged between 69% and 102% with a mean closure of 89%.

Kizer and Elliott (1991) conducted a similar study using eddy correlation over a cultivated field of alfalfa. A CA-27 sonic anemometer and KH-20 krypton hygrometer, both manufactured by Campbell Scientific, Inc. (CSI), were mounted at a height of 1.8 m AGL and separated laterally by 20 cm. (Note that the same model instruments are being used by the OASIS Project; they also provided data for use in this dissertation.) Six 24-hour periods of data were collected. A mean closure rate was estimated at 84% with a standard deviation of 3%. However, the mean closure improved to 95% with a standard deviation of 3% after a correction was applied for sensor separation.

2.3 Large-scale Field Projects

During the late 1980s and 1990s, large field projects were used to again investigate the closure issue. The First ISLSCP (International Satellite Land Surface Climatology Project) Field Experiment (FIFE) was a three-year study between 1987 and 1989 that examined the spatial and temporal variability of surface fluxes. The site was a 15 km^2 agricultural area located near Manhattan, Kansas. Some 22 sites were placed across the FIFE region and consisted of six different Bowen ratio systems and five different eddy correlation systems (Kanemasu et al. 1992). Several corrections were applied to the eddy correlation data including coordinate rotation, sensor separation, frequency response errors, and the Webb et al. (1980) correction (Fritschen et al. 1992). Despite these careful considerations, FIFE results repeated those of previous studies: the eddy correlation method underestimated the aerodynamic fluxes (SH + LH) when compared to Bowen ratio estimates (Sellers and Hall 1992).

Individual comparisons among FIFE sites between the eddy correlation and Bowen ratio estimates revealed similar differences. One comparison used a one-dimensional sonic anemometer to determine that eddy correlation underestimated (SH + LH) by as much as 24% (Fritschen et al. 1992). In this case, coordinate rotation could not be applied, and thus, errors due to slope could have affected sonic estimates. (For an explanation of coordinate rotation, see Chapter 4.4.) Other FIFE investigators who examined closure of the surface budget using eddy correlation methods found residuals as large as 160 Wm^{-2} (Nie et al. 1992). As summarized by Sellers and Hall (1992), comparative results from FIFE concluded that an apparent underestimate of (SH + LH) by eddy correlation "is most likely due to problems with 'missing flux' associated with the eddy correlation stations."

The Monsoon '90 experiment (Kustas et al. 1991) examined the hydroclimatology of complex terrain across the 150 km^2 Walnut Gulch watershed near Tucson, Arizona. Flux measurements were made using profile, eddy correlation, and Bowen ratio techniques. As determined in previous studies, Monsoon '90 results revealed that (Rn - G) > (SH + LH), meaning either the available energy was overestimated or the aerodynamic fluxes were underestimated. Mean closure during a two-month period using the eddy correlation method ranged between 1 and 35 Wm^{-2} among five sites; RMS values of closure ranged between 30 and 75 Wm^{-2} (Stannard et al. 1994). In general, the flatter the site, the better the closure due to the assumption that the mean vertical velocity equals zero. Dyer (1981) found that the error of the sonic SH and LH was about 3% per degree of terrain slope. Stannard et al. also suggested that horizontal flux divergence and a mismatch of source areas could account for some nonclosure. Thom (1975) concluded that horizontal flux divergence of sensible heat offsets that of latent heat and that the total flux divergence is limited. The source region of the available energy is restricted to the nadir viewing angle of the radiometer and to the soil around the flux plates. On the other hand, the source region of the sonic, as a function of the stability, roughness, wind speed and direction, may include a fetch in excess of 1 km upwind. Differences in the soil and vegetation properties between source regions introduce a significant source of error. However, Stannard et al. dismissed any mismatch between source areas; they claimed that the sonic delivers a fundamental underestimate in the aerodynamic fluxes. As might be expected, the flatter sites at the Walnut Gulch region in Arizona also contained the more homogeneous vegetation, so attempts were not made to separate the effects of surface homogeneity and slope.

The Hydrologic Atmospheric Pilot Experiment in the Sahel (HAPEX-Sahel) was a field program conducted during 1992 to examine atmospheric-land surface interaction across inhomogeneous surfaces (Lloyd et al. 1997). Both Bowen ratio and eddy correlation methods were applied. Because of the extreme heterogeneity of the terrain, vegetation, and soil properties, closure was not estimated hourly or even daily. Estimates across a three-day period closed the residual to within 3% of the daily totals. Lloyd et al. concluded that, as homogeneity increases under more stable conditions, (e.g., wetter soils which lead to more homogeneity of the soil moisture), the fetch footprint increases. A larger footprint includes greater surface heterogeneity. Thus, any flux average includes a large footprint area and the measurement becomes more representative of the region. Likewise, the higher above ground the measurement, the greater the footprint source region. Thus, the longer the averaging period and with increasing neutrality, the better the expected closure.

In a comprehensive study of the closure issue, Twine et al. (2000) examined the closure of the surface energy budget during the Southern Great Plains '97 (SGP-97) Hydrology Experiment. SGP-97 was conducted in north-central Oklahoma during June and July of 1997. Both eddy correlation and Bowen ratio measurements were acquired at 11 sites across the SGP-97 region. Closure rates for the eddy correlation systems ranged between 67% and 83%. Residuals of the energy budget appear to be greater than 100 Wm^{-2} (J. Norman, U. of Wisconsin, personal communication). Again, as indicated by previous studies, instrument error within data of the available energy (Rn - G), by itself, could not account for the lack of closure. Twine et al. also noted that closure increased to about 90% during dry conditions.

A summary of results from many previous field programs is listed in Table 2.1. As described, many results are similar and have remained so despite varying conditions and improvements and changes in instrumentation. While some observations indicated near perfect closure (McMillen 1988; Stannard et al. 1994), even these studies indicated a rather significant error variance. It is clear, from numerous studies documented in the scientific literature, that reasonable closure of the surface energy budget remains an elusive problem.

The OASIS Project differs from previous field studies in several ways that permit a unique and extensive examination of the closure problem. First, each of the 10 super sites is equipped with two independent methods for measuring net radiation and sensible heat flux. Redundant instruments allow for improved quality assurance of the data. Second, each of the ten super sites are equipped with the same suite of instruments, all calibrated together to minimize site-specific error. Third, each of the super sites is located in a different climate region of Oklahoma. This spatial deployment permits examination of closure under a wide range of atmospheric conditions. In addition, the flux stations are permanent installations, which allow long-term trends to be investigated. Finally, one super site is co-located with a Bowen ratio system to provide an independent and direct comparison of sensible and latent heat flux. As a result of multiple sites, each with duplicate instrument and measurement techniques, and with sites spread across a range of climate zones, data are available to undertake perhaps the most comprehensive examination of closure yet possible.

Table 2.1: Summary of field projects and results.

Author(s), Field Project	Year of Pub.	Land Surface Type	Method	Period of Data Collection	Results
McNeil and Shuttleworth	1975	Pine Forest	EC, BR	2 months	SH: BR > EC by 24%
Shuttleworth et al.	1984	Amazon Forest	EC	8 days	Closure: 93%
Tanner	1984	Crops	EC	NA	Closure: 75%, 81%
Tanner et al.	1985	Crops	EC	NA	Closure: 69% - 102%, mean 89%
Verma et al.	1986	Deciduous Forest	EC	6 days	Closure: 70% to 130%
McMillen	1988	Complex terrain	EC	1 day	Closure: 99%
Dugas et al.	1991	Crops	EC, BR, chamber	2 days	SH: BR > EC by 18%, 31% LH: BR > EC by 23%, 33%
Kizer and Elliott	1991	Crops	EC	6 days	Closure: 84% (95%)
Stannard et al. (Monsoon '90)	1991	Complex terrain	EC, BR, Profile	3 months	Rn-G > SH+LH by 1-35 Wm^{-2} (RMS of 30-75 Wm^{-2})
Fritschen et al. (FIFE)	1992	Crops	EC, BR	15 days	Closure: 81%
Nie et al. (FIFE)	1992	Crops	EC	19 days	Rn-G > SH+LH by ≤ 160 Wm^{-2}
Barr et al.	1994	Deciduous Forest	EC	2 months	Closure: 89%
Lloyd et al (HAPEX-SAHEL)	1997	Complex terrain	EC, BR	32 days	Total 3-day closure within 3%
Twine et al (SGP-97)	2000	Great Plains	EC, BR	2 months	Closure: 67% to 83% (Residuals>100 Wm^{-2})
Brotzge (OASIS)	***	Complex terrain/ crops	EC	1 year	Closure: 76% - 100%, mean 92%

Chapter 3: Data

3.1 The OASIS Project

The Oklahoma Mesonet (Brock et al. 1995) is a meteorological network of 115 stations evenly spaced across the state. Each site measures solar radiation, air pressure, precipitation, wind speed and direction at 10 m, air temperature and relative humidity at 1.5 m, and bare soil and sod temperature at 10 cm depth. A majority of sites also measure the supplemental parameters of wind speed at 2 m and 9 m, air temperature at 9 m, soil moisture at 5, 25, 60, and 75 cm depths, and bare soil and sod temperatures at 5 cm. The Mesonet was installed during 1992 and became operational on 1 January 1994.

During 1999, the Oklahoma Atmospheric Surface-layer Instrumentation System Project (Brotzge et al. 1999b) instrumented approximately 90 Mesonet sites with new sensors to enable routine measurements of the surface energy budget. These measurements include net radiation, sensible heat flux, and ground heat flux. The latent heat flux is estimated as the residual in the energy balance equation:

$$LH = Rn - SH - GH \tag{3.1}$$

Net radiation is measured at 90 "standard" OASIS sites using the Kipp & Zonen NR-Lite (Brotzge et al. 1999a). Sensible heat flux is estimated using a profile technique, employing two temperature and two wind sensors and applying Monin-Obukhov theory (see Appendix A; Brotzge and Crawford 2000). Ground heat flux is estimated using a combination approach (Tanner 1960); the soil heat flux and soil heat storage are calculated separately. The soil heat flux is estimated using two HFT3.1 heat flux plates manufactured by Radiation & Energy Balance Systems, Inc. (REBS). The soil heat storage is estimated using two REBS platinum resistance temperature detectors (PRTDs), soil moisture estimated at 5 cm (using the CSI 229L), and knowledge of the soil properties at each site.

In addition to the 90 standard sites, 10 of the 90 OASIS sites were designated "super" sites (Fig. 3.1). These 10 super sites have additional instrumentation which are used to verify the accuracy of measurements from the standard instrumentation and methods. The analysis techniques used at the super and standard sites are discussed in detail in Chapter 4. Geographical information about each super site is listed in Table 3.1.

Besides the NR-Lite, each super site measures each component of the net radiation budget using the 4-component CNR1 radiometer. Incoming and outgoing shortwave and longwave radiation each are measured explicitly. In addition, each of the 10 super sites directly estimate sensible and latent heat flux using an eddy covariance technique. A CSI CSAT3 sonic anemometer and Krypton hygrometer have been installed at 4.5 m; it samples at 8 Hz.

Because of the expensive cost and high maintenance requirements of the super site instrumentation, only 10 OASIS sites could be equipped with sonic anemometers, 4-component CNR1 radiometers, and self-calibrating heat flux plates. Nevertheless, strategic placement of the 10 super sites across Oklahoma allows for a diverse range of climates to be examined. The 10 super sites are designed to minimize instrumentation error; more specifically, data from these sites are aimed at model initialization and verification. It is at these 10 super sites where closure of the energy budget will be examined.

Meanwhile, the 90 standard sites allow for routine measurements of the energy budget across the entire state of Oklahoma, expanding the spatial coverage of these vital measurements across a large domain. Data from the standard site instrumentation will permit the development of an improved climatology, new land-atmosphere investigations, and studies of the precipitation budget and evapotranspiration. Most importantly, the standard methods for estimating net radiation and sensible heat flux provide an opportunity for a direct comparison with CNR1 and sonic measurements at the super sites. A detailed examination of the instruments and data collection techniques at the standard and super sites of OASIS is discussed below.

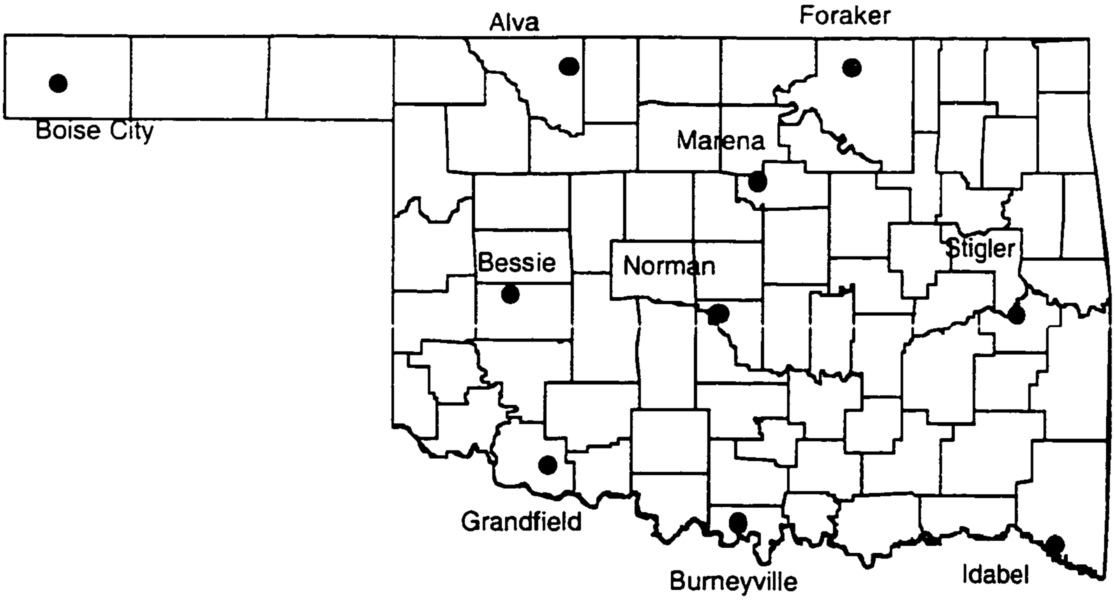

Fig. 3.1: Ten OASIS super sites located in each of Oklahoma's nine climatic regions.

Table 3.1: Geographical information of the ten super sites.

Site ID	Latitude (deg)	Longitude (-deg)	Elevation (m)	Slope (deg)	Aspect (deg)	Primary Land Use
Alv2	36.71	98.71	439.0	0.098	200.62	Agricultural
Bess	35.40	99.06	509.5	1.764	248.04	Pasture
Bois	36.69	102.50	1268.0	0.000	***	Scrub
Burn	33.89	97.27	226.4	0.806	238.28	Pasture
Fora	36.84	96.43	330.1	1.221	20.140	Grassland
Gra2	34.24	98.74	341.0	0.168	203.20	Airport/Scrub
Idab	33.83	94.88	110.0	0.055	73.177	Pasture
Mare	36.06	97.21	330.0	0.840	212.31	Pasture
Norm	35.26	97.48	360.0	0.000	***	Scrub
Stig	35.27	95.18	175.6	0.861	146.31	Pasture

*** No aspect calculated due to estimated slope of zero.

3.2 Net Radiation

Net radiation is measured using a single net radiometer or is estimated as the sum of the net radiation budget using a 4-component radiometer system. Radiation is measured from the amount of energy incident upon a sensing element. The computed radiation is the sum of energy absorbed by the sensor and energy transferred to and from the sensor in the form of conduction and convective currents. Thermopiles or photoelectical devices are often used in construction of radiometers.

3.2.1 NR-Lite Net Radiometer

The NR-Lite net radiometer manufactured by Kipp & Zonen measures the sum of incoming and outgoing shortwave and longwave radiation. The sensor, mounted at 1.5 m AGL, is approximately 1 m south from the tower. Data are excluded during periods of precipitation and when dew is suspected. Observations are gathered every 3 seconds and averaged to yield 5-minute observations.

Prior to installation, each NR-Lite was standardized (calibrated to be consistent with) to an Eppley 4-component Precision Spectral Pyranometer/Precision Infrared Radiometer (PSP/PIR) system at the NCOM (Net Radiation Comparison) facility (Brotzge and Duchon 2000). A simple linear regression was applied to data from each NR-Lite with respect to the reference sensor. Individual calibration coefficients were applied to each unit during post-processing of the data. Brotzge and Duchon (2000) described details of the calibration facility and process.

Brotzge and Duchon (2000) found that error is introduced during the day when wind speeds are greater than 5 ms^{-1}. A comparative study by Smith et al. (1997) used a wind tunnel to test 8 models of radiometers for wind-induced error. Their study showed the NR-Lite to be the most sensitive to wind speed with an error of approximately 0.5% $(ms^{-1})^{-1}$. Brotzge and Duchon developed a wind correction:

$$Rn_{est} = Rn_{obs}, \qquad u < 5.0\ ms^{-1} \qquad (3.2)$$

$$Rn_{est} = Rn_{obs} * [1.0 + a(u-5.0)], \qquad u \geq 5.0\ ms^{-1}$$

where Rn_{obs} is the observed net radiation, u is the measured wind speed (ms^{-1}), and a=0.0213, an empirical constant derived from comparisons of data from the NR-Lite and an Eppley reference. The wind speed correction was applied to the NR-Lite observations during post-processing unless otherwise specified.

3.2.2 CNR1 4-Component Net Radiometer

The Kipp & Zonen CNR1 is a 4-component net radiometer. It consists of two pyranometers (CM3s) and two pyrgeometers (CG3s), housed in a single unit. The unit is mounted at 1.5 m AGL about 2 m (6 feet) south from the tower. The pyranometers measure incoming and reflected shortwave radiation while the pyrgeometers measure incoming and emitted longwave radiation.

Each CNR1 has its own calibration value that is applied in the datalogger; all four components of the CNR1 use the same calibration coefficient. In addition, the longwave radiation must be corrected for the temperature of the longwave sensor. The incoming and outgoing longwave radiation, LW_{cor} (Wm^{-2}), are a function of the temperature of the instrument and are corrected by:

$$LW_{cor} = V/C + \sigma T_{case}^4 \qquad (3.3)$$

where V is the respective measured voltage output, C is the factory-determined calibration factor, σ is the Stefan-Boltzmann constant, and T_{case} is the measured body temperature. These temperature corrections are applied during post-processing of the data.

The net radiation data may become suspect when precipitation or dew occurs. In these circumstances, the CNR1 heater may be used. Because dew is not directly measured via Mesonet instruments, the CNR1 heater is used when conditions are favorable for dew formation (e.g., relative humidity > 95% and wind speeds < 3 ms^{-1}). All net radiation data are flagged as suspect when the heater is used and during precipitation events.

3.3 Ground Heat Flux

A combination method is used to estimate the total ground heat flux (Tanner 1960). The combination approach includes separate estimates for the ground flux and storage terms:

$$GH = -\lambda(\frac{dT}{dz}) - Cdz_2\left(\frac{d\overline{T}}{dt}\right) \tag{3.4}$$

where λ [W $(m\ K)^{-1}$] is the thermal conductivity, dT [K] is the temperature difference across the plate, dz [m] is the plate thickness, C [J $(m^3\ K)^{-1}$] is the soil heat capacity, dz_2 [m] is the depth of the soil layer, and $d\overline{T}/dt$ [K m^{-1}] is the temporal rate of change in the integrated soil temperature between 0 and 5 cm (Fritschen and Gay 1979).

The soil heat flow is estimated from the first term in Eq. (3.4) using two soil heat flux plates. The temperature difference measured across the depth of a plate is equivalent to the vertical movement of heat within the soil. As described above, each of the 90 standard sites have two REBS HFT 3.1 heat flux plates installed at a depth of 5 cm. Thus, the arithmetic mean of data from the two sensors is used. Each plate has an individual calibration that is applied during post-processing.

The second term in Eq. (3.4) is the storage term and includes measurement of the integrated soil temperature within the top 5 cm layer. Like the heat flux plates, two REBS PRTDs are installed at each site and the mean value of observations from the two sensors is used. Each PRTD has an individual calibration that is applied during post-processing. The ground heat storage term also is a function of the soil heat capacity (C), defined by Fritschen and Gay (1979) as:

$$C = X_m C_m + X_o C_o + X_w C_w + X_a C_a \tag{3.5}$$

and is a function of the heat capacity and volume fraction (X) of minerals (m), organic matter (o), water (w), and air (a). In this case, the heat capacity of air is negligibly small compared to the remaining terms. The volume fraction of organic matter, X_o, varies from site-to-site, but it is assumed to have a value of 3% at all sites. The volume fraction of minerals, X_m, is derived as a function of X_o and the soil porosity, ϕ, as:

$$X_m = 1 - X_o - \phi$$

where porosity is defined as a function of the soil bulk density, ρ_b, and particle density, ρ_m, as:

$$\phi = 1 - \rho_b / \rho_m \, .$$

The heat capacity of organic matter is $C_o = 2.51*10^6$ [J $(m^3K)^{-1}$], and the heat capacity of minerals is $C_m = 1.96*10^6$ [J $(m^3K)^{-1}$]. The heat capacity of water is determined by collocated soil moisture sensors buried at a depth of 5 cm. The matric potential sensor (the 229L from CSI) measures the soil water potential. The soil water content is estimated from the matric potential measurement, as shown in Appendix B. The mean values of soil bulk density, soil porosity, and volume fraction of minerals are listed in Table 3.2 for each site.

Table 3.2: Soil bulk density (ρ_b), soil porosity (ϕ), and volume fraction of minerals (X_o) listed for the ten super sites.

Site	ρ_b	ϕ	X_o
Alv2	1.35	0.49	0.48
Bess	1.35	0.49	0.48
Bois	1.40	0.53	0.44
Burn	1.60	0.60	0.37
Fora	1.55	0.58	0.39
Gra2	1.35	0.49	0.48
Idab	1.35	0.49	0.48
Mare	1.48	0.56	0.41
Norm	1.29	0.51	0.46
Stig	1.35	0.49	0.48

3.4 Sensible Heat Flux

3.4.1 Profile Technique

At the 90 standard sites across the Mesonetwork, similar cup anemometers and thermistors are used to monitor vertical gradients in wind and temperature. Vertical gradients of heat and momentum are applied to Monin-Obukhov similarity theory to derive an estimate of the sensible heat flux (Brotzge and Crawford 2000). Previous investigations demonstrated the accuracy of the gradient approach using Mesonet data (Brotzge 1997; Brotzge et al. 1998). The limitations and accuracy of the gradient approach are examined further in Chapter 4.

3.4.2 Covariance Technique

The ten super sites also measure sensible heat flux using eddy correlation. Each of the super sites has a CSI CSAT3 sonic anemometer mounted at 4.5 m AGL and located ~1 m south of the tower. Values of latent heat flux are estimated using a co-located Krypton hygrometer and are included in the estimate of sensible flux to remove effects of moisture (see below and Chapter 4.4).

The CSAT3 sonic anemometer measures wind speed and air temperature using sound wave (sonic) theory. By measuring the speed of sound between two points, the fluctuations of wind and temperature can be calculated. As described by Schotanus et al. (1983), the speed of sound is proportional to the reciprocals of the measured time between the sonic axis as:

$$\frac{1}{t_1} + \frac{1}{t_2} = \frac{2c(\cos\alpha)}{l} \qquad (3.6)$$

where t_1 and t_2 are the time periods between the downward and upward facing sensors, respectively; c is the speed of sound, α is the 3-dimensional angle between the wind vector and sonic wave, and l is the path length of the sonic wave. The speed of sound is defined as:

$$c^2 = \gamma RT(1 + 0.51q) \qquad (3.7)$$

where γ is the ratio of moist air at constant pressure to that at constant volume, R is the gas constant for dry air, T is air temperature, and q is specific humidity. By combining Eqs. (3.6) and (3.7), the sonic temperature (T_s) can be derived as:

$$T_s = \frac{l^2}{4\gamma R}\left[\frac{1}{t_1} + \frac{1}{t_2}\right]^2 \qquad (3.8)$$

Note that $T_s \neq T$ because the sonic temperature is a function of the specific humidity. Thus, as shown in Chapter 4, a correction must be applied to account for fluctuations in atmospheric moisture.

The CSAT3 is a 3-dimensional sonic array, and so all three dimensions of the wind field are determined. Wind speed components of u (east-west), v (north-south), and w (vertical) and temperature (T_s) are sampled at a frequency of 8 Hz and then averaged over 5-minute intervals. Next, the 8 Hz sampling of u, v, w, and T_s are multiplied accordingly to yield the covariances of: u'u', u'v', u'w', v'v', v'w', w'w', u'T_s', v'T_s', w'T_s', and T_s'T_s' where the ' indicates a fluctuation from the 5 minute mean value. These covariances are calculated within the datalogger program and then averaged to yield the 5-minute mean values of flux. The sensible flux is:

$$H = \rho C_p \overline{w'T'} \qquad (3.9)$$

The momentum flux (τ) and friction velocity (u*) also are calculated within the datalogger from the semi-derived sonic variables using:

$$\tau = \rho\left[\left(\overline{u'w'}\right)^2 + \left(\overline{v'w'}\right)^2\right]^{1/2} \qquad (3.10)$$

$$u^* = \left[\left(\overline{u'w'}\right)^2 + \left(\overline{v'w'}\right)^2\right]^{1/4} \qquad (3.11)$$

3.5 Latent Heat Flux

At the standard sites, latent heat flux must be estimated as the residual of the energy budget. However, the super sites measure latent heat flux directly using the sonic anemometer and Krypton KH20 hygrometer. The Krypton hygrometer works using the principle that, at specific emission lines, the krypton gas is a very strong absorber (and emitter) of water vapor. The krypton emits at two specific emission lines: 123.58 nm and 116.49 nm. The amount of absorption (emission) of krypton between the two points of the transducers is proportional to the water vapor density of the air [kg m^{-3}].

Covariances are calculated from the fundamental parameters of the sonic winds and temperature and the hygrometer water vapor density, ρ'_v. The latent heat is calculated using:

$$LE = L_v \overline{w'\rho'_v} \tag{3.12}$$

where L_v [J kg^{-1}] is the latent heat of vaporization. Like the sonic, the sampling of the hygrometer is at 8 Hz with five-minute averaging. The Krypton hygrometer is mounted 15 cm from the sampling volume of the sonic anemometer. The direct measurement of latent heat at the super sites provides a direct comparison to residual estimates obtained from using the standard methodology.

Chapter 4: Instrumentation Error and Measurement Limitations

Introduction

As demonstrated by the field experiments listed in Chapter 2, the instruments used in PBL and land-surface experiments have improved steadily with time, have become more complex, and are more accurate. Nevertheless, measuring the components in the energy budget equation remains difficult. The problem of closure of the surface energy budget is perhaps best defined as the resolving of four separate problems - namely, accurately measuring each of the four components of the surface energy budget. If each component of the budget is measured without error *and if each component is representative of the same source region*, then it is assumed that the surface energy budget is closed.

In this chapter, the instrumentation error and measurement limitations of each component of the energy budget are investigated. The specifications of all OASIS instruments are listed in Table 4.1. A summary of all known instrument errors and limitations are provided in Table 4.2. A complete outline of corrections applied during the generation of a research-ready OASIS data set also are listed in Table 4.2 and displayed in Figure 4.1.

4.1 Net Radiation

The surface energy budget is driven by net radiation. The net radiation budget may be defined as:

$$Rn_{sfc} = SW_{in}(1 - \alpha) - \varepsilon\sigma T^4_{sfc} + LW_{in} \tag{4.1}$$

where SW_{in} (W m^{-2}) is the incoming shortwave radiation (wavelength (λ) < 4 μm), α is the surface albedo, ε is the surface emissivity, σ (W m^{-2} K^{-4}) is the Stefan-Boltzmann constant, T_{sfc} (K) is the skin temperature, and LW_{in} (W m^{-2}) is the incoming longwave radiation (4 μm < λ < 100 μm; Peixoto and Oort 1992). The magnitude of shortwave radiation

Table 4.1: Specifications for OASIS instruments.

Sensor	Height	Inaccuracy	Resolution
CNR1 CM3	1.5 m	+/- 10% (daily totals)	10-35 $\mu V/Wm^{-2}$
CNR1 CG3	1.5 m	+/- 10% (daily totals)	5-35 $\mu V/Wm^{-2}$
NR-Lite	1.5 m	NA	10 $\mu V/Wm^{-2}$
HFT 3.1	-5 cm	NA	NA
PRTDs	-5 cm	NA	0.392 Ω/°C
Thermistors, air (Thermometrics)	1.5 m, 9.0 m	0.4°C	0.03°C
Cup anemometers	2.0 m, 9.0 m	2% reading	0.25 m s^{-1}
Wind direction	10 m	3°	0.05°
Thermistors, soil	-5, -10, -30 cm	0.5°C	0.03°C
Pyranometer (LiCor 200)	1.5 m	5% reading	0.23 W m^{-2}
Rain gauge	0.6 m	1% reading	0.25 mm
Barometer	0.75 m	0.4 mb	0.01 mb

dominates during the day and creates large-scale mixing and momentum transfer. Longwave radiation dominates at night, leading to radiational cooling of the surface and stabilization of the surface boundary layer. Despite its importance, however, net radiation remains among the most difficult atmospheric parameters to measure accurately. Unfortunately, a 5% error in the estimate of net radiation during a typical summer afternoon becomes an approximate 35 Wm^{-2} error in the closure of the surface energy balance.

The foremost difficulty in observing net radiation properly is the absence of a World Meteorological Organization (WMO) standard for longwave radiation (Ohmura et al. 1998). Because of the lack of a uniform standard, calibrations of net radiometers vary greatly among instrument companies. A number of field programs have quantified

Table 4.2: Summary of instrument errors and limitations.

Energy Budget Component	Instrument Problem	Approximate Error	Corrective Measure
Net Radiation	Calibration	$\leq 13\%$	NCOM calibration
	Wind speed error	~ 5% / m s^{-1} if $U > 5$ m s^{-1}	Brotzge correction
	Cosine function	> 20% if < 20°	None
	Precipitation, etc	≥ 100 W m^{-2}	Data unusable
Ground Heat Flux	Calibration	Total error $\leq 10\%$	Lab calibration
	Surface heterogeneity	Variable	Mean of 2 sensors
Sensible Heat (Profile)	Radiational heating	~ 10 - 15%	Brotzge/Crawford correction
	Fetch	Variable	Limit data
Eddy correlation	Flow distortion	$\leq 44\%$, (variable)	Mask data 345° - 15°
	Sensor separation	~5% /10 cm	None
	Tilt of the sensor	~3% / degree	Coordinate axis rotation
Eddy Sensible Heat	Cp(T)	$\leq 10\%$	Stull correction
	Moisture contamination	$\leq 20\%$	Schotanus correction
Eddy Latent Heat	Density variations	≤ 10 %	Webb correction
	Oxygen density	$\leq 20\%$	Oxygen correction

differences among radiometers of various manufacturers. Field et al. (1992) compared seven different models of radiometers used during FIFE. They found daytime radiation differences between manufacturers to be as large as 10 to 15%. Halldin and Lindroth (1992) conducted a similar study when they evaluated six radiometer designs. Differences between these radiometers ranged between 6 and 20%. Stannard et al. (1994) briefly examined three radiometer models used during the Monsoon '90 experiment and found differences up to 14%. Smith et al. (1997) examined nine varieties of radiometers in preparation for the Boreal Ecosystem-Atmosphere Study (BOREAS) program. Differences among these models, representing seven different manufacturers, varied by up to 25%. In

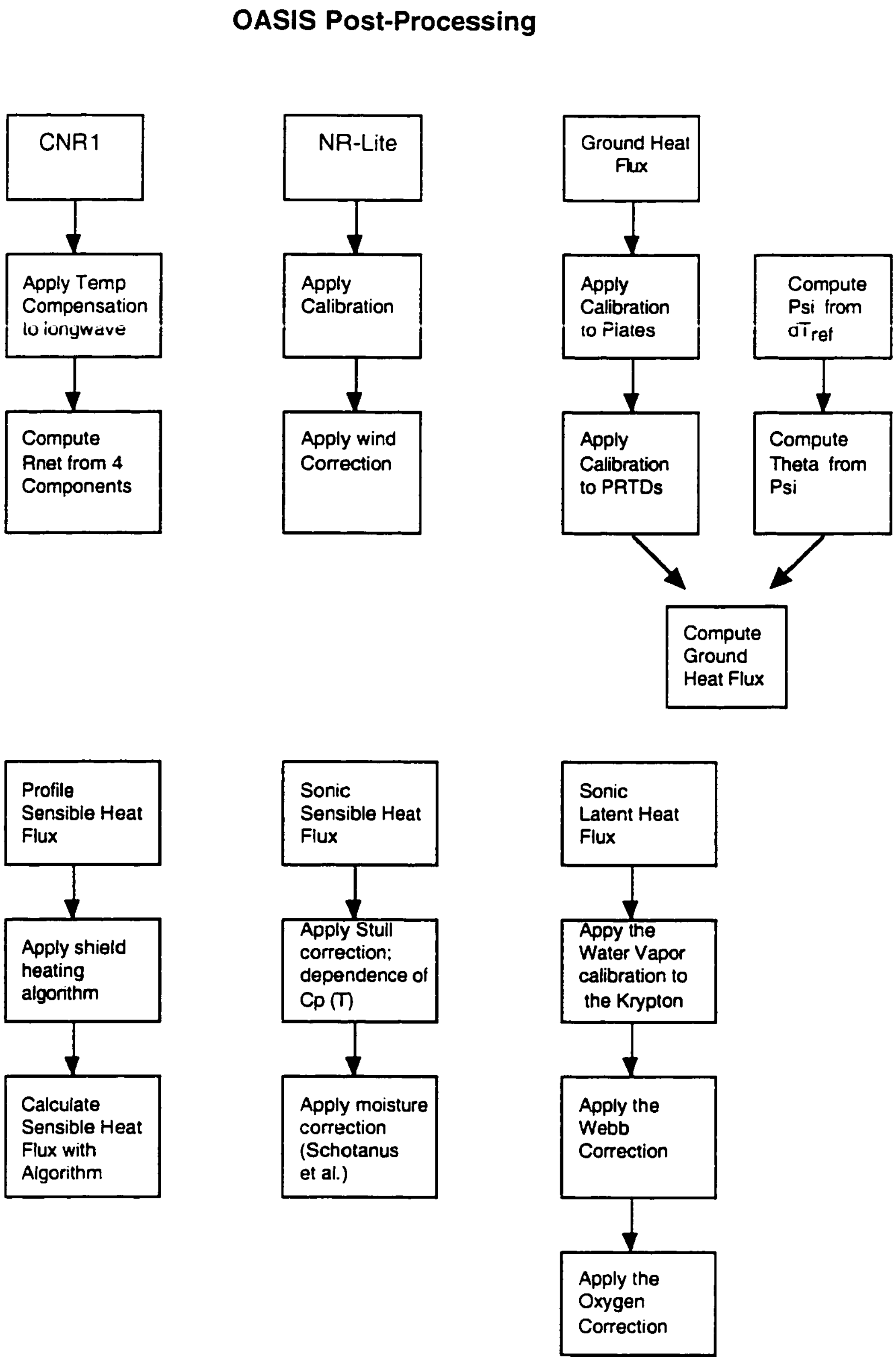

Fig. 4.1: Diagram outlining the post-processing routines applied to all OASIS flux data.

preparation for the OASIS Project (Brotzge et al. 1999). Brotzge and Duchon (2000) tested four models of radiometers, representing three manufacturers, and found daytime differences among them of up to 75 Wm^{-2} (approximately 12%). Daily totals among model types varied by as much as 20%. Halldin and Lindroth concluded that much of the differences between radiometers were due to the lack of a stable, longwave reference standard.

Investigators also determined calibration differences among the *same* model types. Field et al. uncovered daytime differences of approximately 5 to 7%. Brotzge and Duchon (2000) measured daily mean differences of up to 25 Wm^{-2} among 7 NR-Lites; differences among sensors were less than 5% of the total net radiation and were within the manufacturer's specifications. Many authors discovered that these differences result from different sensitivities at short and long wavelengths. This fact would cause radiation estimates to vary as a function of cloudiness as well as to create separate day and night calibrations. Smith et al. (1997) concluded that, because of the differences in the short- and longwave sensitivities, minimum errors in the measurement of net radiation remained at 5 to 10% under conditions of variable cloudiness. Halldin and Lindroth noted changes of calibration with season as well.

A third, commonly observed error of net radiometry concerns the cosine response of the instrument. Differing response to short- and longwave radiation affects how the sensor reacts to beamed verses diffuse radiation. In addition, the material of the sensor plate determines the reflectivity and absorption of radiation by the sensor body. These properties determine the sensitivity of the sensor to the angle of incidence of the radiation, commonly referred to as the cosine response. Flat polyethylene shields developed during the 1950's (Tanner et al. 1960) produced erroneous observations because the sensors were highly reflective to beamed radiation from a low solar elevation angle. Brotzge and Duchon (2000) determined errors with the relatively flat NR-Lite was greater than 20% with the solar elevation angles of < 20° when compared to how the Eppley 4-component system responded. Halldin and Lindroth (1992) identified several radiometers among modern designs that were still impacted by some cosine response.

A fourth problem that limits accurate net radiometry is solar radiative heating of the pyrgeometers. A number of investigators have quantified the problem (Enz et al. 1975; Albrecht and Cox 1977; Halldin and Lindroth 1992) and have developed several corrections that may be applied (Alados-Arboledas et al. 1988; Duchon and Wilk 1994; Perez and Alados-Arboledas 1999). Brotzge and Duchon (2000) compared the longwave radiation of the CNR1 used by OASIS with the reference net radiometer of the Eppley system. Measurement differences in incoming longwave radiation between systems varied between -30 and +50 W m^{-2} depending upon which correction terms were included in the estimate (see Chapter 5).

Common operational problems included snow covering the sensor, precipitation, and ultraviolet (UV) degradation of the domes. Betts and Ball (1997) demonstrated during BOREAS, that short and longwave measurements were severely limited due to snow covering the sensors. Dust also can collect on the radiation sensor limiting the quality of the data. Brotzge and Duchon (2000) found that the NR-Lite used by OASIS was highly sensitive to rainfall; errors as large as 100 Wm^{-2} were observed during precipitation. The sensitivity of the NR-Lite to rain is most likely due to its lack of a dome. A radiometer dome shields the thermopile surface and keeps it dry. On the other hand, degradation of the polyethylene domes due to UV radiation is commonly observed and requires replacement after several months.

4.2 Ground Heat Flux

While only a small part of the daily total energy budget, the ground heat flux is a significant portion of the daytime energy budget, especially under bare soil conditions. Instrumentation error, theoretical assumptions and surface heterogeneity are known to affect the estimates of ground flux.

The combination approach used by OASIS includes three major assumptions (Massman 1993). First, the specific heat capacity of the soil is assumed to remain constant with depth and in time. The heat capacity is a function of the soil moisture, but the OASIS technique includes soil moisture measurements which accounts for the variability of heat capacity. Nevertheless, vertical variations in soil water content and heat capacity variations are not known. Massman noted that absolute errors are typically greater in "soils with large vertical gradients" in the heat capacity and thermal conductivity. He found that the top 10 cm of soil often dries much faster than soils below this layer. If the heat flux plate lies within or above this layer of drying, then the heat flux could be substantially underestimated. This fact may be a problem when the plates are installed at 5 cm, and so Massman recommended plate placement at 10 cm.

Second, it is assumed that there is no horizontal heat flow. Massman determined that lateral heat flow is most severe nearest the surface and recommended placement of soil temperature sensors at 2.5 cm and 7.5 cm. He cautioned that a single integrating sensor, such as a PRTD, could be susceptible to lateral heating errors if placed too close to the skin surface. Lateral heat flow is especially dominant in bare soil and partial ground cover conditions.

Third, most combination techniques estimate the soil heat storage term using two single point measurements in the vertical layer. This approach assumes the soil layer is best characterized using an arithmetic mean of several observations. Massman (1993) demonstrated that this assumption may not be the best method and, in fact, may introduce errors up to 3% to 6%. Each measurement should be weighted according to the soil thermal properties; Massman recommended the mean weights of $W_1 = 0.54$ and $W_2 = 0.45$ where W_1 is the measurement at 2.5 cm and W_2 is the measurement at 7.5 cm. The OASIS technique uses a single integrated thermistor between 0 and 5 cm. However, Massman found that this approach might be less accurate than the weighted point samples depending upon the magnitude of the vertical gradients of soil temperature. Because of these three assumptions of the combination technique. Massman estimated a total error in measurement of between +/- 3% to 10%.

The most common and significant error in ground heat flux measurements occurs when the thermal conductivity of the soil does not match the thermal conductivity of the heat flux sensor. Ideally, the flux plate should have the same conductivity as the mean properties of the soil. Fritschen and Gay (1979) found that the thermal conductivity of sand and clay soil ranges between 0.8 and 2.2 W $(m\ K)^{-1}$. The thermal conductivity of a heat flux plate made from plastic or glass could be as low as 0.17 W $(m\ K)^{-1}$, resulting in errors as high as 44%. When the thermal conductivity of the plate does not match the conductivity of the soil, heat flow may either be deflected around (or drawn towards) the sensor plate. This "deflection error" leads to an underestimate (overestimate) of the ground heat flux (Hukseflux 1999). A difference in thermal conductivity also may lead to "resistance error" by modifying the total thermal resistance in the soil layer (Hukseflux 1999).

The dependence of the ground heat flux upon the soil thermal conductivity is corrected as described by Fritschen and Simpson (1989). The correction is:

$$G_p = G_m \frac{\left(1 - F + (l/d)(1 - k_s/k_t)\right)}{\left(1 - F + (l/d)(1 - k_m/k_t)\right)}$$

where G_m is the measured heat flux by the plates, $F \approx 1.92$ is an empirical constant derived as a function of plate disk shape (van Loon 1998), l is the width of the transducer, d is the diameter of the transducer, k_s is the soil thermal conductivity, k_t is the thermal conductivity of the transducer, and k_m is the conductivity of the medium used for calibration of the transducer. The soil thermal conductivity is estimated at each site as a function of the measured bulk density, ρ_d, and gravimetric soil water percentage, θ_m. The soil thermal conductivity is defined as:

$$k_s = 0.64 + 1.63\theta_m - 0.505\exp\left(-17\theta_m^2\right)$$

and the gravimetric soil water percentage is estimated as:

$$\theta_m = \theta / \rho_d$$

where θ is the estimated soil water content, estimated as shown in Appendix B. Typical corrections to the ground heat flux range as high 5%.

To minimize errors in using a heat flux plate, Fritschen and Gay (1979) recommended careful manufacture and calibration of the ground heat flux plates. First, the plates should be manufactured from a material that shares the same conductivity as the mean properties of the soil. The flux plates used by OASIS have a thermal conductivity of 1.22 [W $(mK)^{-1}$]. Second, each sensor should be calibrated in a material with similar thermal conductivity as the soil properties. The conductivity of the calibration medium is 0.906 [W $(mK)^{-1}$]. The thermal conductivity of the soil approaches the thermal conductivity of the plate during saturated conditions. Note that the thermal conductivity of the soil changes as a function of the soil moisture.

Another significant error in measuring ground heat flux occurs because the heat flux plate itself impedes the vertical flow of heat and moisture in the soil layer (Tanner 1960; van Loon et al. 1998). Tanner (1960) and Fritschen and Gay (1979) recommended a small, thin plate sensor to reduce error in the vertical flow of energy. To further minimize ground flux error, each plate must be in complete thermal contact with the soil. Air gaps between the plate and soil can lead to errors as great as 54% (Fritschen and Gay 1979). Yet another error involves a temperature dependency of the measurement. Standard temperature dependency is about 0.2% K^{-1}. A typical range of 20 °C can lead to an approximate 4% error in ground heat fluxes (Hukseflux 1999).

4.3 Sensible Heat Flux

4.3.1 Profile Gradient Approach

Three specific problems limit the accuracy of the gradient approach. First, gradient methods are sensitive to instrumentation error. A sensitivity test of the profile algorithm demonstrates the error to be a function of both the wind speed and temperature vertical gradients, and implicitly, a function of the stability. An error in the vertical temperature (wind speed) gradient can lead to an approximate 100 Wm^{-2} (30 Wm^{-2}) error in heat flux. Instrumentation error associated with the thermistors and cup anemometers could be assumed to have a Gaussian distribution when averaged across all 90 standard sites. However, instrumentation error observed at any single site could result in biased estimates of sensible flux.

Each instrument was carefully calibrated in the laboratory prior to field installation, and multiple sensors, such as the cup anemometers and thermistors, were paired and installed at the same site to minimize bias error between them. Quality assurance of the profile temperature and wind data provides some limits to the instrument errors. Spatial analysis of monthly means of temperature and wind speed reveals small biases at individual sites. In addition, like instrumentation, such as the Thermometrics and HMP-35C, measure the same variable at the same height. By examining this comparison, some bias and temporal error can be identified and flagged. The wind profile is measured by two (three) cup anemometers at the standard (super) sites in addition to the propeller vane at 10 m. Thus, irregularities in the vertical wind profile can be identified as well.

Second, radiational heating of the temperature shelter during sunny, light wind conditions produces heating of the temperature sensor (Richardson 1995). The air temperature is overestimated when the shelter of the temperature sensor warms. Operational corrections were developed independently by Anderson and Baumgartner (1998) and Brotzge and Crawford (2000). The Brotzge and Crawford method improves sensible heat flux estimates by approximately 5 - 10%.

A third problem with the gradient approach to estimate sensible heat is fetch. As vegetation height changes seasonally, fetch is affected accordingly. The taller the vegetation, the greater the turbulence and mixing near the surface. As a result, low level wind estimates become less reliable. As vegetation increases in height, the height of the sublayer increases, and if the vegetation grows tall enough, the low level wind monitor could find itself within the sublayer. In addition, some sites are within 100 m of trees and fence lines. While the choice of site selection considered fetch carefully, limited obstructions still impact accurate estimates of flux when the wind is from certain directions at each site; these observations subsequently are flagged.

4.3.2 Eddy Correlation Approach

As shown in Chapter 2, failure to close the energy budget generally is associated with problems with EC instrumentation. Nevertheless, a greater understanding of eddy covariance techniques has contributed to its widespread acceptance in the scientific community. Several limitations of eddy correlation such as flow distortion and frequency error have been identified (Dyer et al. 1982; Dugas et al. 1991; Foken and Wichura 1996), and improved quality assurance routines have been developed (Kaimal and Gaynor 1991; Vickers and Mahrt 1997). In addition, universal corrections are routinely applied (Webb et al. 1980; Schotanus et al. 1983; Moore 1986; Tanner et al. 1993). First, the limitations of direct eddy flux measurements are discussed, followed by an examination of corrections applied to the OASIS data set. Finally, quality assurance routines are described which allow for quality control of direct flux estimates.

4.4 Eddy Correlation

4.4.1 Measurement Limitations

Technological advances have permitted more precise and accurate eddy flux measurements. The first eddy flux instruments were the 'Evapotron' (Swinbank 1951; Dyer 1961) and the 'Fluxatron' (Hicks 1970; McNeil and Shuttleworth 1975). These used propeller anemometers to measure the vertical component of wind speed, and fast temperature sensors to measure temperature fluctuations. McBean (1972) found that the propeller anemometer introduced both frequency response errors and cosine function errors that could be as large as 25%. McNeil and Shuttleworth (1975) showed that the slow response of the propellers tended to underestimate the flux by as much as 24%. Advances in digital technology allowed for the development of sonic thermometry where wind and temperature fluctuations could be estimated simultaneously (Suomi 1957; Kaimal and Businger 1963; Kaimal and Gaynor 1991). Advantages of the sonic include its improved resolution of the vertical wind component, sampling over the same volume for both temperature and wind, and improved calibration (Kaimal and Gaynor 1991). Still, sonic measurements are restrained by the common assumptions and limitations of turbulence theory (Panofsky and Dutton 1984).

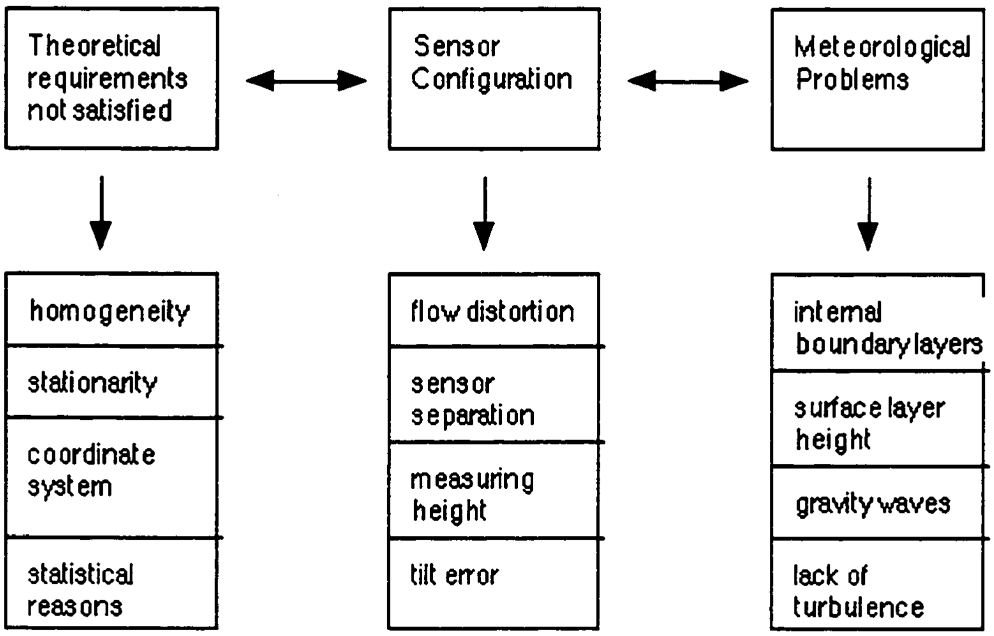

Fig. 4.2: Diagram reproduced from Foken and Wichura (1996) listing possible errors with eddy correlation.

Foken and Wichura (1996) and Panofsky and Dutton (1984) detailed many of the limitations and assumptions that accompanied turbulence measurements. A summary of such problems is given by Foken and Wichura and is reproduced in Figure 4.2. Researchers conveniently overlook many of these problems. Furthermore, the complexities of the sonic anemometer lead many to treat it as a "black box" (Foken and Wichura 1996).

Theoretical requirements of eddy correlation include stationarity and homogeneity. Stationarity requires that the sampling statistics do not change with time. Homogeneity means that the sampling statistics do not change in space. Stationarity and homogeneity are often used synonymously. Given a heterogeneous land surface, homogeneity cannot be observed. Sampling statistics may vary spatially according to changes in albedo, roughness, soil wetness, and vegetation structure among others. Likewise, stationarity may fail in a heterogeneous landscape. Roughness estimates vary with wind direction, which affect stationarity. Variations in the time series of data reflect spatial heterogeneity. The time series is directly reflective of the fetch represented, which is a function of the stability, wind direction, and surface roughness (Foken and Wichura 1996).

Turbulence measurements can be sensitive to sensor configuration problems if they have not been treated properly. Flow distortion from the mounting tower and sonic anemometer has been examined in several studies (Dyer 1981; Dyer et al. 1983). Dyer (1981) quantified and modeled the problem. He found typical errors in the momentum flux to be about 14% per degree of wind direction and caused by flow distortion. Typical error in the heat flux was limited to only 3% per degree. Dyer also developed corrective equations for both the momentum and heat flux as follows:

$$\overline{u'w'} = \overline{u'_m w'_m} \Big/ \left(1 + \frac{\cos\phi}{\gamma r_a} + \overline{u'^2_m} \tan\theta \right) \tag{4.2a}$$

$$\overline{w'\theta'} = \overline{w'_m\theta'} \cos\theta + \overline{u'_m\theta'} \tan\theta \tag{4.2b}$$

where u'_m and w'_m are the distorted flow covariances, ϕ is the polar coordinate, $\gamma = \pi/n$ where $n = m \pi V / a$, m is the source strength, V is the flow velocity, r is the distance between the flow distortion source and the measurement, a is the assumed cylinder radius, and θ is the angle of flow distortion. Wyngaard (1982) and Dyer et al. (1983) suggest that flow distortion error may be as high as 20% but the exact error remains highly variable.

Tilt errors are another serious issue when dealing with sonic anemometry. If the sonic anemometer is titled relative to the actual airflow, then the measured vertical component is contaminated by the horizontal wind component. Two errors may occur: 1) the sonic itself may not be level, and 2) the land surface may be sloping. Both errors introduce similar under- or overestimation of the fluxes. To minimize the former error, electronic levels will be installed with each OASIS sonic. As the sonic responds to the wind, instantaneous corrections theoretically could be applied. Practically, the level is used to track long-term changes in the sonic tilt. To address the latter issue, a Digital Elevation Model (DEM) at 30 m spatial resolution was used to determine the land slope at each OASIS site (Table 3.1). The estimated slope value for the 900 m^2 region centered on the site was used to further examine the orographically induced flow (see Chapter 7). Operationally, tilt error is mathematically corrected by a process called coordinate axis rotation. This is described in detail later in this chapter.

Dyer (1981) found that tilt error closely resembled error created by flow distortion. Again, he devised a corrective formula that could be applied to the momentum and heat flux estimates:

$$\overline{u'w'} = \overline{u'_m w'_m}\cos 2\theta + \frac{1}{2}\sin 2\theta\left(\overline{u'^2_m} - \overline{w'^2_m}\right) \tag{4.3a}$$

$$\overline{w'\theta'} = \overline{w'\theta'}\cos\theta + \overline{u'_m\theta'}\sin\theta \tag{4.3b}$$

where the distorted (or in this case, 'tilted') flow are u'_m and w'_m, and the tilt error is θ. Dyer found these corrective equations to be very similar to those for flow distortion, again yielding an approximate 14% and 3% error for momentum and heat fluxes, respectively.

Sensor separation is another serious issue with dramatic implications for flux estimates. Eddy correlation measurements often require two separate sensors - one measuring the vertical wind component and the second measuring the scalar (temperature, humidity, or atmospheric gas). In the case of the OASIS data set, measurement of latent heat flux requires both the sonic anemometer to estimate the wind component and the Krypton hygrometer to measure water vapor fluctuations. The sensors are separated vertically by 15 cm. Koprov and Sokolov (1973) found the underestimate of flux was caused by the lateral separation of sensors to be an approximate 10% (20%) error in momentum covariance and a 5% (10%) error in heat flux covariance at a sensor separation of 10 cm (20 cm).

Kristensen et al. (1997) conducted a comprehensive study of the sensor separation problem. The authors quantified the separation error as a function of measurement height and vertical and lateral sensor separation. The authors found that the higher above ground level (AGL) the flux measurement was taken, the smaller the error incurred by the sensor separation. The size of eddies increases with measurement height. The error caused by sensor separation decreases with eddy size. Kristensen et al. also realized that the error caused by sensor separation was asymmetric about the vertical. By placing the scalar sensor 20 cm above the anemometer, a flux error of 18% occurred. However, by placing the scalar sensor 20 cm below the anemometer, the flux error was only 2%. As expected, lateral sensor displacement was symmetric. Because of these results, OASIS placed its scalar component (the Krypton hygrometer) 15 cm *below* the sonic anemometer.

As shown in Figure 4.2, meteorological problems may unduly influence and affect flux estimates. Strongly stable nocturnal layers may create a very shallow surface layer of less than 10 m AGL. Gravity waves may propagate within these shallow inversions as well. The sonic anemometers for OASIS were mounted at 4.5 m AGL. This height was chosen to alleviate any problems with a shallow boundary layer; the height was less sensitive to very localized surface heterogeneity. Internal boundary layers can develop, given a change in surface heterogeneity within the flux footprint. When internal boundary layers occur, homogeneity and stationarity are seriously violated.

4.4.2 Corrective Measures Applied to Sensible Heat Flux

Because of the many serious issues that can arise when using eddy correlation, a number of corrections must be applied to the sonic data. Three corrections were applied to the sensible and latent heat fluxes in the OASIS data set; they are described below.

4.4.2.1 Moisture Dependence

The sensible heat flux is a function of the specific heat of air, C_p, which varies as a function of moisture. Thus, the kinematic moisture flux, as measured by the krypton hygrometer, must be included in the estimate of sensible heat flux to account for changes in the specific heat. The sensible heat flux is calculated as defined by Stull (1988):

$$H = \rho C_p\left(\overline{w'T'} + 0.84\overline{T}\,\overline{w'q'}\right) \tag{4.4}$$

where $(C_{p,\text{water vapor}} * C_{p,\text{dry air}}) / (C_{p,\text{dry air}}) = 0.84$.

4.4.2.2 Correction of Schotanus et al.

Schotanus et al. (1983) demonstrated that the measured sonic temperature (T_s), as shown in Eq. (3.8), is a function of both the specific humidity and normal velocity fluctuations:

$$T_s' = T' + 0.61q'\overline{T} - \frac{2\overline{T}}{c^2}\bar{v}_n v_n'. \tag{4.5}$$

Thus, to accurately compute the sensible heat flux as given by Eq. (3.9), one must remove the effects of both the humidity and velocity fluctuations. Schotanus et al. provide the correction:

$$\overline{w'T'} = \overline{w'T_s'} + 2\frac{\overline{T}\overline{u}}{c^2}\overline{u'w'} - 0.61\overline{T}\overline{w'q'} \tag{4.6}$$

Because the krypton hygrometer automatically corrects for the normal velocity fluctuations, Eq. (4.6) is applied to the OASIS data set without using the second term.

4.4.2.3 Coordinate Axis Rotation

Eddy correlation estimates of heat flux are sensitive to tilt errors of the sonic anemometer. As described in a previous section, measurement of the vertical wind component can be in error when either the sonic is tilted relative to the flat ground or the ground surface is sloped. In either case, the measured wind components are not parallel to the mean air flow. To minimize flux error, the sonic anemometer must be exactly perpendicular to the mean air flow.

Methods have been developed to quantify and correct for sonic tilt error. Tilt error can be corrected through a process of coordinate axis rotation. First, as part of the quality control of the data for this study, a visual check of the data was examined as described by T. Horst (NCAR, personal communication, 1999). Elevation (α) and azimuth (β) angles were computed for each time step as:

$$\alpha = Tan^{-1}\left(\frac{w}{\sqrt{u^2 + v^2}}\right) \tag{4.7a}$$

$$\beta = Tan^{-1}\left(\frac{v}{u}\right) \tag{4.7b}$$

and then plotted as a function of wind direction. The results generally follow a sinusoidal curve which represent the sonic tilt error observed at the site. To quantify the error, a least squares fit is applied to the orthogonal wind components (u, v, and w) as:

$$w = a + bu + cv \tag{4.8}$$

where a is the estimated offset in the measured vertical velocity. The dimensionless coefficients of b and c are used to compute the sonic lean angle (θ) and the azimuth of the sonic lean angle (φ) as follows:

$$\theta = Tan^{-1}\left(\sqrt{b^2 + c^2}\right) \tag{4.9a}$$

$$\varphi = Tan^{-1}\left(\frac{c}{b}\right) \tag{4.9b}$$

A sinusoidal fit to the plots made from Eqs. (4.7) can be plotted using Eqs. (4.9) as:

$$\alpha = \theta * \cos(\beta - \varphi). \tag{4.10}$$

Several examples of tilt error are plotted from data collected at the Burneyville, Grandfield, Idabel and Marena sites and are shown in Figures 7.1 and 7.2. Negative values of elevation angle represent downward sloping winds (or negative vertical component contamination), and positive values represent upward sloping winds (positive vertical component contamination). Values for α, β, θ, and φ were computed from five-minute observations of data collected at each super site between 1 - 14 October 1999, 1 – 14 January 2000, and 15 – 31 May 2000. Data were excluded from computations during days with rain and when the observed wind direction was between 345° and 15°, directions that cause flow distortions by the tower. The computed tilt errors for each site are listed in Table 7.2.

Finally, the computed sonic lean and azimuth angles are used to rotate the sonic measurements into the mean air flow. The complete method for sonic rotation of the covariances is shown in Appendix 3.

4.4.3 Corrective Measures Applied to Latent Heat Flux

A number of corrections must be applied to the latent heat flux derived from the eddy correlation method.

4.4.3.1 Correction of Webb et al.

First, the covariance method estimates the density fluctuations of heat and moisture about an arbitrary mean. The heat and moisture fluxes, however, directly modify the density of the air, and thus affect the density fluctuations (Webb et al. 1980). A modified form of the correction for density variability is listed by Tanner et al. (1993) as:

$$LE = LE_{old}\left(1.0 + \frac{e}{P-e} + \left(\frac{0.622 L_v \beta}{C_p T}\right)\left(\frac{P}{P-e}\right)\left[\frac{e}{P-0.378e}\right]\right) \tag{4.11}$$

where β is the uncorrected Bowen Ratio, e is the vapor pressure, P is the atmospheric pressure, C_p is the specific heat at constant pressure, and L_v is the latent heat of vaporization. The second and third terms on the RHS of Eq. (4.11) represent the effects of the sensible and latent heat upon the density fluctuations, respectively. Tanner et al. demonstrated that the general impact of sensible heat is roughly 5 times greater than that of the latent heat and increases with increases in the Bowen ratio.

4.4.3.2 Oxygen Correction

A second correction that should be applied to the estimate of latent flux involves the dependence of the sonic measurement upon the oxygen density of the air. The magnitude of oxygen absorption by the Krypton hygrometer is dependent upon both the sensible and latent heat fluxes. Thus, the correction is dependent upon the Bowen ratio. Tanner et al. (1993) presented this correction as:

$$LE = LE_{old}\left(1.0 + 0.23\frac{k_o}{k_w}\frac{L_v \beta}{T}\right) \tag{4.12}$$

where k_o is the oxygen absorption coefficient, k_w is the water vapor absorption coefficient, T is the sonic-derived temperature, L_v is the latent heat of vaporization, and β is the Bowen ratio.

4.4.3.3 Coordinate Axis Rotation

The same method of coordinate axis rotation applied to the sensible heat flux was applied to the latent heat flux. Details of the technique are described in Appendix 3.

4.5 Quality Control Measures

A series of quality control measures have been formulated in the literature to identify errors in eddy correlation data (Panofsky and Dutton 1984; Heiser and Sellers 1995; Foken and Wichura 1996; Vickers and Mahrt 1997). Data should be limited to use only when the assumptions of turbulence theory are not violated such as stationarity and homogeneity. Most tests involve examination of the covariance response functions and turbulence spectrum. Unfortunately, OASIS does not allow routine collection of the 8 Hz sampling; only five minute averages of covariance are recorded. This limited data set severely restricts quality assurance of the eddy correlation data. Nevertheless, several techniques are available which aid in minimizing instrumentation and sampling error in the data set.

The methods implemented in the generation of the complete OASIS data set are described below. Automatic routines were applied to all flux data. The routines were implemented easily into the data processing and were used primarily to identify instrumentation error. Manual routines were applied only on an "as needed" basis. The combination of the automatic and manual routines allowed for identification of systematic errors that were not otherwise detected. Problems with nonstationarity, fetch, and surface inhomogeneity also were examined (see Chapters 7 and 8).

4.5.1 Automatic Routines

4.5.1.1 Range Tests

Heiser and Sellers (1995) developed a system of quality control measures to ensure consistency in the data among FIFE sites and to limit erroneous data from the data stream. Among their quality control measures were the use of a range test to exclude those energy fluxes outside a range of physically plausible values. The OASIS data set was quality assured in a similar manner using their recommended ranges for energy fluxes:

$$-150 < Rn < 1000\ Wm^{-2} \qquad -100 < LE < 600\ Wm^{-2} \qquad (4.13)$$
$$-200 < SH < 600\ Wm^{-2} \qquad -150 < GH < 300\ Wm^{-2}$$

Shafer et al. (2000) have developed similar range requirements for Mesonet data.

4.5.1.2 Step and Persistent Tests

Instrumentation and sampling error also may cause spurious jumps or spikes in the data stream. Some erroneous data values may remain within range limits, however. Arbitrary step functions were chosen to identify suspected data problems. A step function was defined as the change in value between two successive measurements. The step values used in the quality control of this data set were:

$$\text{SW, in:} > 800\ Wm^{-2} \qquad \text{LW, in:} > 400\ Wm^{-2}$$
$$\text{SW, out} > 400\ Wm^{-2} \qquad \text{LW, out:} > 400\ Wm^{-2} \qquad (4.14)$$
$$\text{SH:} > 200\ Wm^{-2} \qquad \text{GH:} > 100\ Wm^{-2}$$
$$\text{LH:} > 200\ Wm^{-2}$$

A persistence test also should be applied to identify erroneously repeated values. Because nocturnal values of flux are often repeated, only daytime estimates of flux were examined for persistence. Observations were excluded when successive flux estimates were identical.

Note that in development of the data set used in this dissertation, step and persistent tests were not automated. Visual inspection of the data identified problems when possible.

However, future use of the data will include automated routines similar to those described by Schafer et al. (2000).

4.5.1.3 Miscellaneous Tests

Neither the sonic anemometer nor the Krypton hygrometer operates properly once the transducers are wet. Water on the transducers affects the transient signal. Thus, eddy correlation data, collected during or just after precipitation, cannot be used. For this study, all EC data collected during days with precipitation were excluded.

Likewise, net radiation data collected during precipitation is affected by evaporative cooling from the sensor surface. While the CNR1 sensor is designed to minimize such effects, the NR-Lite is not. Brotzge and Duchon (2000) demonstrated the large error associated with precipitation on the NR-Lite. Like the EC data, all data collected from the NR-Lite during days with precipitation were excluded. The CNR1 is equipped with an on-board heating system to reduce precipitation error. Thus, only data collected during precipitation is not used.

Dew also is a problem for the NR-Lite. Thus, during conditions favorable for dew, such as relative humidity > 90% and wind speeds less than 3 ms^{-1}, data from the NR-Lite were not used. However, because the CNR1 included use of a heater, the data were deemed suspect and reexamined manually. If no large outliers were detected, then the data were used.

Snowfall can cover the net radiation sensor as well and has posed a major problem in field experiments in northern climates (Betts and Ball 1997). The winter climate in Oklahoma rarely includes snowfall, and yet snow events can limit the collection of net radiation. A statewide snowfall between 25 – 27 January 2000 was one such example; hence, net radiation data collected during that week were not used.

4.5.2 Manual Quality Assurance

All data are initially quality assured by the automated routines. Then, the four components of the energy balance are computed. Thirty-minute means are produced, and all data are visually inspected to detect obvious flaws.

While digital values of the data appear correct, an understanding of the physical processes of the energy budget dictates exclusion of the data during certain periods. For example, snowfall during 25 - 27 January inhibited accurate measurement of net radiation. All data collected during this period, while passing all automated routines, was manually excluded from the data stream. A second problem occurred when three krypton hygrometers failed completely. However, the failed sensors continued to measure noise, and the automated routines failed to exclude such data. Another problem occurred when gophers dug up several in-ground sensors at Stigler. Most sensors continued to measure correctly; unfortunately, the sensors were simply no longer buried. Only a manual inspection of the data revealed a rather erratic behavior by the soil temperature and moisture sensors.

More difficult problems involve fetch, surface homogeneity, and source area "mismatch" (see Chapters 7 and 8). Identification of these problems requires detailed study of the site, preferably prior to site installation. Once these problems are detected at a site, data should be excluded as a function of wind direction or time of year. For example, fetch could be limited from certain directions at a particular site, or the land-surface could be marked by strong heterogeneity during the growing season in which case data collected during these periods should be excluded.

All days of missing or bad data are listed in Tables 4.3a-b. The tables do not list data excluded during rainfall or days with only partial data missing. Unfortunately, replacement sensors for the krypton hygrometers were not readily available, and so the mere identification of a bad sensor did not necessarily mean a quick replacement. Long periods of missing data were observed at Foraker, Grandfield, and Norman. Problems with gophers at Stigler produced bad ground heat flux data over most of the data collection period. Note that when any one component of the energy balance is not measured, then closure cannot be estimated during that period of time at that site.

Table 4.3a: Periods of data during 1999 with complete days of missing or bad data.

	Jun	Jul	Aug.	Sept.	Oct.	Nov.	Dec.
Rnet							
Burn			225-238				
Stig				244-248			
GH							
Norm	174-181						
Stig					283-304	305-334	335-365
SH/LH							
Fora					302-304	305-334	335-365
Gra2						321-334	335-365
Norm				254-273	274-304	305-334	335-365

Table 4.3b: Periods of data during 2000 with complete days of missing or bad data.

	Jan.	Feb.	Mar.	Apr.	May
Rnet					
Alv2	25-34				
Bois	27-31	32			
Burn				98-104	
Fora	27-30				
Gra2	26-29				
Idab	26-31	32-34			
Mare	26-30				
Norm	26-31	32-33			
GH					
Alv2			72-90	91-121	122-140
Stig	1-31	32-60	61-81		
SH/LH					
Fora	1-31	32-34			
Gra2	1-31	32-60	61-90	91-121	122-138
Norm	1-31	32-60	61-83		

Chapter 5: Quantification of Instrument Error

Introduction

Before closure can be methodically examined, an estimate of instrument error must be developed for each component of the energy budget. At that point, a system is considered "closed" only when the residual of the energy budget lies within the maximum error limitations presented by the independent components of the energy budget. A detailed examination of instrument error allows measurement bias to be easily identified and corrected and allows random error to be minimized. This chapter quantifies instrument error for each component of the energy budget.

Failure to close the energy budget is caused by two primary sources of "error": *instrument error* and *system error*. Instrument error is caused by problems with the engineering, maintenance and/or calibration of the instrument itself. This error is manifest as either random or systematic, static or dynamic (Richardson and Brock 2001). Fortunately, instrument error can be identified and can be reduced by instrument calibrations, field intercomparison between like instruments, and quality assurance routines (Schafer et al. 2000). System error is created when, despite the instrument itself working properly, the observation still does not represent "atmospheric truth"- the measurement intended by a human observer or an automated system. Poor instrument exposure, unrepresentative site location, and surface heterogeneity create system error; these errors are often difficult to recognize in a data stream. "Source area mismatch" is a system problem unique to estimating the surface energy budget and is created because the net radiometer and ground flux sensors measure a very localized footprint area whereas the sensible and latent flux sensors observe a much larger upwind region. Thus, the footprint region estimated by (Rn-GH) often is as much as a magnitude smaller than the area estimated for (SH+LH).

In this chapter, instrument error is quantified when possible for each component of the energy budget through direct instrument intercomparison.

5.1 Net Radiation

Net radiation is the largest component of the surface energy budget, and its correct measurement is critical to minimizing error. Thus, the net radiometer used by OASIS, the CNR1, was investigated for precision and accuracy. First, two CNR1 radiometers were compared directly. Field intercomparisons between like instruments allow for an estimate of the instrument precision and permits verification of instrument specifications provided by the manufacturer. Second, radiation estimates from the CNR1 were tested against observations collected from a second four-component net radiometer, the PIR/PSP system manufactured by Eppley. Comparing the CNR1 to a second, independent system allows for an estimate of the differential bias for each component of the net radiation budget. The Eppley system has been cited as a field reference for radiation by other research programs (e.g., during FIFE; Field et al. 1992).

First, the four components of net radiation collected from two CNR1s were compared directly. One-minute data were collected during 1 – 31 March 1999 at the Norman Intercomparison (NCOM) facility. Both CNR1s were mounted at approximately 3 m AGL, aligned east – west and placed about 1 m apart. Data collected during rainfall and shortwave radiation data less than 10 W m^{-2} were excluded from the comparison. Five-minute averages for both sensors were compared and results are shown in Figs. 5.1a-d and Tables 5.1 and 5.2.

Table 5.1: Linear regression parameters from the comparison of two CNR1s.

Variable	Intercept	Slope	R^2
Net radiation	-0.564	1.009	1.000
Incoming Shortwave	-0.612	1.004	1.000
Outgoing Shortwave	1.724	0.979	0.998
Incoming Longwave	1.162	0.998	0.998
Outgoing Longwave	-2.684	1.010	0.999

Table 5.2: Difference statistics from the two CNR1s (CNR1 #1 – CNR1 #2; Wm^{-2}).

Variable	Mean, X	Standard deviation, σ	Confidence limits at 95%	Sample size, # 5-min averages
Net Radiation	-0.137	3.690	-7.37 – 7.10	8916
Incoming Shortwave	-0.957	3.415	-7.65 – 5.74	4169
Outgoing Shortwave	0.221	3.000	-5.66 – 6.10	3652
Incoming Longwave	-0.489	1.611	-3.65 – 2.67	8916
Outgoing Longwave	-0.855	0.932	-2.68 – 0.97	8916

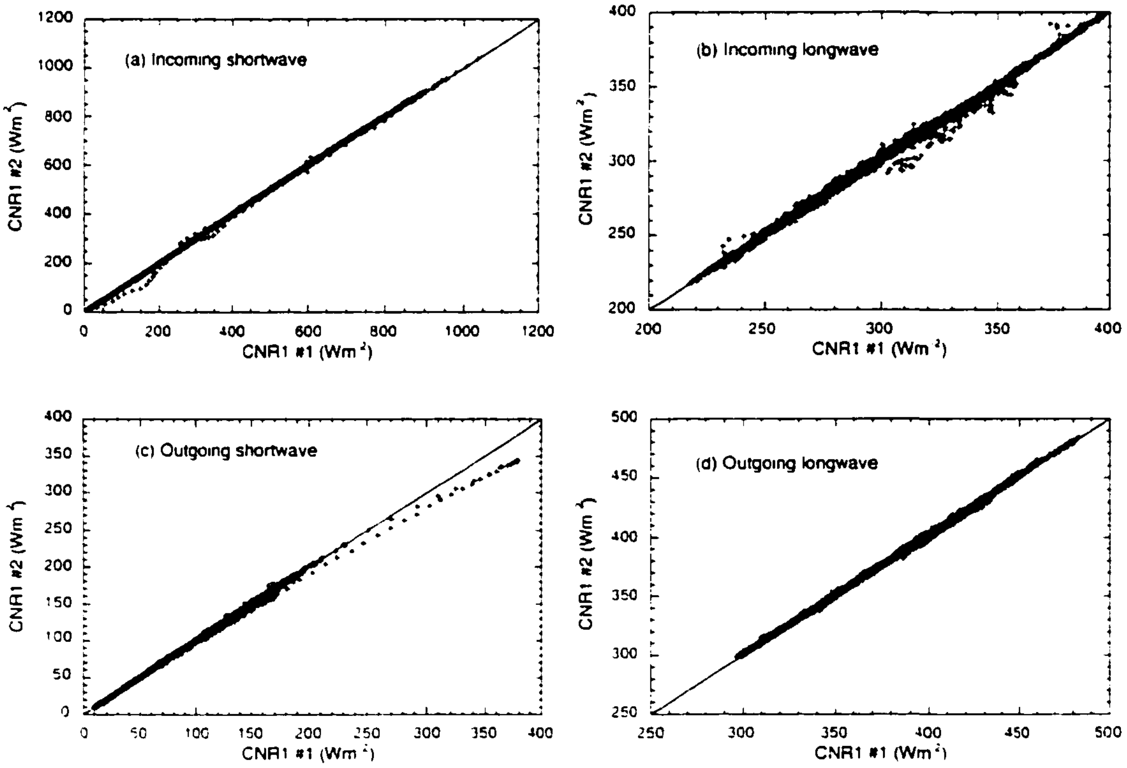

Fig. 5.1a-d: A comparison of the four components of net radiation obtained via two CNR1s. One-minute data were collected between 1 – 31 March 1999.

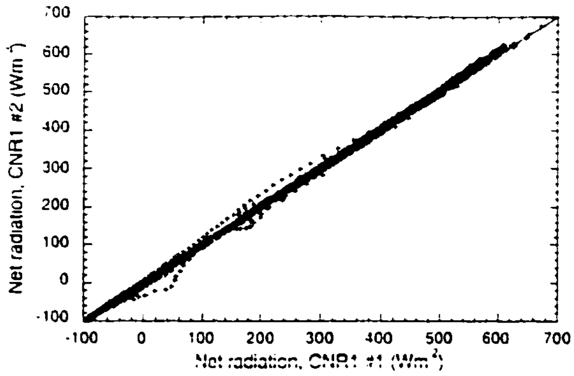

Fig. 5.2: A comparison of net radiation obtained via two CNR1s. One-minute data were collected between 1 – 31 March 1999.

Results from comparing the two CNR1s revealed little relative difference between them. Nearly all components lie within 2%, and mean differences between components were within 1 Wm^{-2}. Confidence limits range between +/- 8 Wm^{-2} for all components (Table 5.2). The results verify the consistency of measurements from the CNR1.

As shown by Halldin and Lindroth (1992) and Field et al. (1992), significant calibration differences may exist between radiation sensors from different models. Thus, to better determine its accuracy, the CNR1 was compared with an independent net radiometer, the PSP/PIR system by Eppley. Data were collected during 7 May - 6 June 1998 at the NCOM and Norman Radiation (NRAD) test facilities. The CNR1 was new while the manufacturer had recalibrated the 4-component Eppley system in 1997. A Q*7.1 manufactured by REBS and an NR-Lite manufactured by Kipp & Zonen also were available. Five-minute averages of radiation were used for this intercomparison study.

First, the net radiation of the CNR1 and Eppley were compared during situations when clear sky conditions were dominant (Fig. 5.3). Data from eight clear days and seven clear nights during May and June (DOY 130-132, 135, 148, 152-154) 1998. The comparison revealed that the CNR1 underestimated radiation by as much as 40 Wm^{-2} at midday relative to the Eppley system. However, a similar comparison between the Q*7.1 and NR-Lite radiometers indicated that these radiometers underestimated radiation by as much as 75 Wm^{-2} and 100 Wm^{-2}, respectively, when compared to the Eppley (see Figs. 6a-c in Brotzge and Duchon 2000). Thus, either all three sensors, the CNR1, Q*7.1, and NR-Lite, underestimated net radiation, or the Eppley system used at NRAD overestimated net radiation, or all four sensors had some diurnally-dependent error. Unfortunately, the "correct" net radiation is not known.

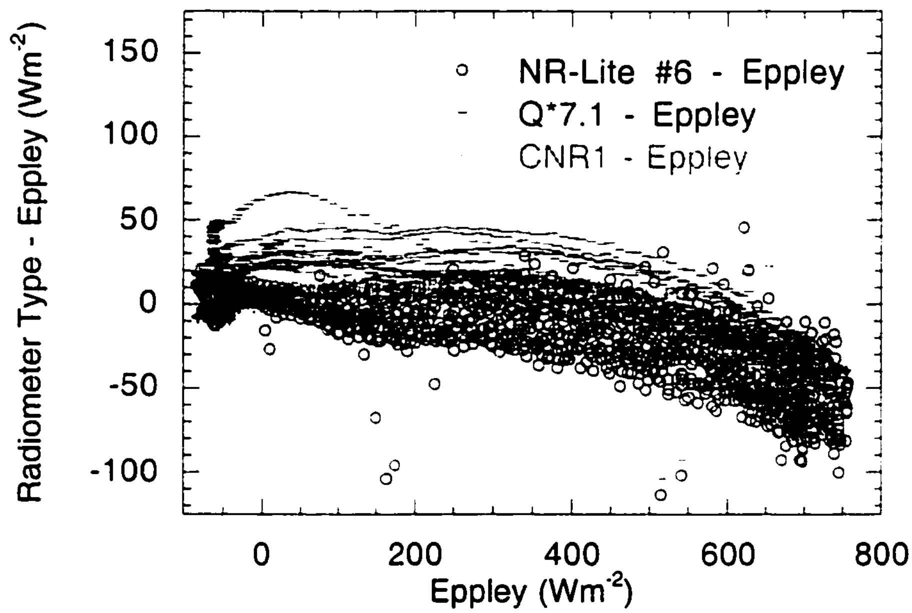

Fig. 5.3: Radiometer type versus the 4-component Eppley system.

Next, individual components of the CNR1 and Eppley were compared: differences revealed several systematic problems (Figs. 5.4 - 5.7 and Tables 5.3 and 5.4). Differences in the shortwave radiation (Fig. 5.6a) are symmetric about solar noon and may be simply a calibration error. Differences in incoming longwave radiation (Fig. 5.6b) show a clear dependence on the diurnal cycle as well. These differences in longwave radiation most likely result from different methods in dealing with heating of the pyrgeometer dome.

Differences in the outgoing shortwave (longwave) radiation from the CNR1 and Eppley systems averaged less than 5% (1%). The shortwave radiation values from the

CNR1 and Eppley were set to zero at night. Shortwave differences during the day may be due to small differences in albedo under the two sensors resulting from non-uniform surface properties such as vegetation type and soil moisture. Similar differences could likewise lead to small differences in longwave radiation. Nevertheless, the incoming and reflected shortwave measurements of the CNR1 remained within 2.2% and 4.4% of the Eppley, respectively, and the longwave measurements of the CNR1 remained within 2% of the Eppley. These estimates lie well within the CNR1 specifications provided by the manufacturer.

Table 5.3: Linear regression parameters from the comparison of data from a CNR1 and an Eppley system. The CNR1 is the independent variable (x), and the Eppley is the dependent variable (y).

Variable	Intercept	Slope	R^2
Net radiation	-2.224	1.022	0.9985
Incoming Shortwave	-0.389	1.044	0.9997
Outgoing Shortwave	1.303	0.980	0.9977
Incoming Longwave	3.127	0.9961	0.9889
Outgoing Longwave	-2.886	1.021	0.9982

Table 5.4: Difference statistics estimated from the CNR1 and Eppley systems.

Variable	Mean, X	Standard deviation, σ	Confidence limits at 95%	Sample size, # Observations
Net Radiation	-0.873	10.946	-22.33 – 20.58	8792
Incoming Shortwave	-9.531	10.878	-30.85 – 11.79	4948
Outgoing Shortwave	-5.965	3.534	-12.89 – 0.96	4948
Incoming Longwave	4.515	5.722	-6.70 – 15.73	2304
Outgoing Longwave	4.663	2.912	-1.04 – 10.37	2304

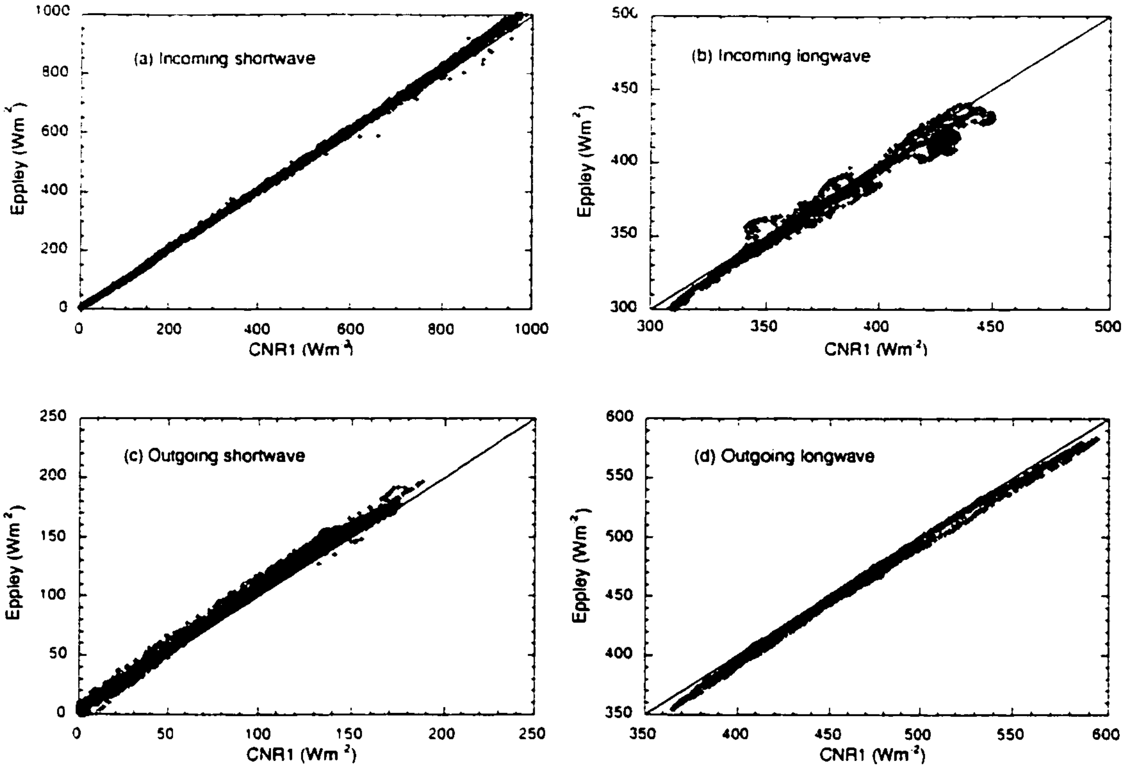

Fig. 5.4: A comparison of four components of net radiation produced by the CNR1 and Eppley systems. Five-minute data were collected between 7 May and 6 June 1998.

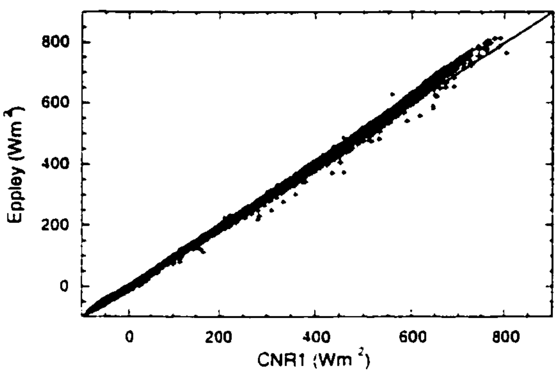

Fig. 5.5: A comparison of net radiation produced by the CNR1 and Eppley systems. Five-minute data were collected between 7 May and 6 June 1998.

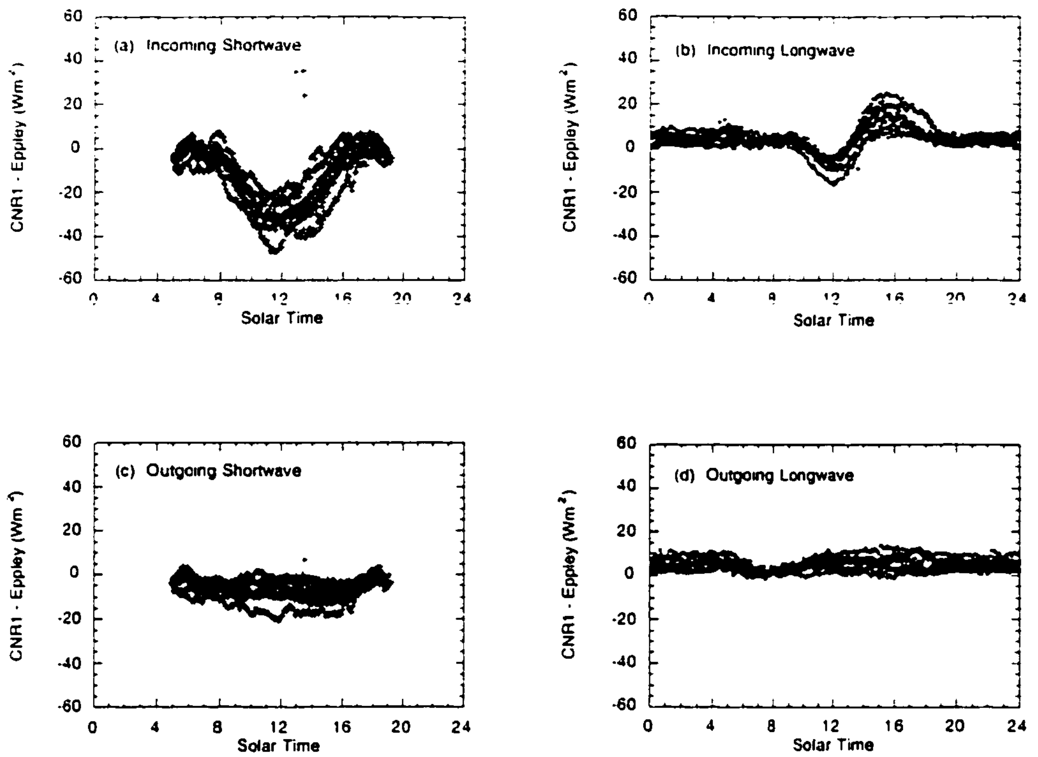

Fig. 5.6a-d: Differences between the K&Z CNR1 and Eppley PSP-PIR system for (a) incoming shortwave, (b) incoming longwave, (c) outgoing shortwave, (d) outgoing longwave from 7 May – 6 June, 1998.

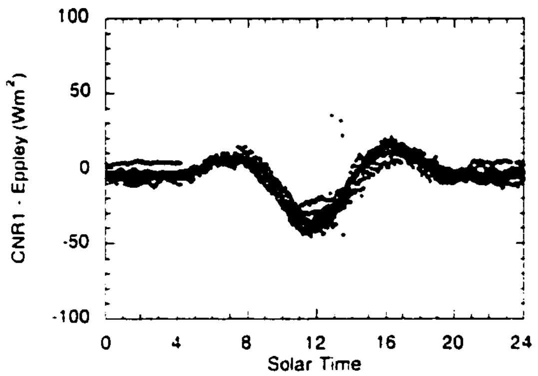

Fig. 5.7: Difference in net radiation between the CNR1 and Eppley systems.

Differences between the incoming longwave data from the Eppley and CNR1 were examined further by studying the effect of applying different radiative heating correction measures (Fig. 5.8). The Eppley pyrgeometers were manufactured with a single dome temperature sensor while a case temperature sensor was already installed. Thus, longwave estimates from the Eppley system included a case temperature (T_{case}) and dome temperature (T_{dome}). The formula for the incoming or outgoing longwave radiation, Lw_{cor} (Wm^{-2}), was that proposed by Delaney and Semmer (1998), and is given by:

$$Lw_{cor} = V/C + \sigma T^4_{case} - a\sigma(T^4_{dome} - T^4_{case}) - bQ \qquad (5.1)$$

The first term on the right calculates the uncorrected longwave radiation where V is the measured voltage output, and C is the determined calibration factor. The second term corrects for an underestimate of longwave radiation by the pyrgeometer because it

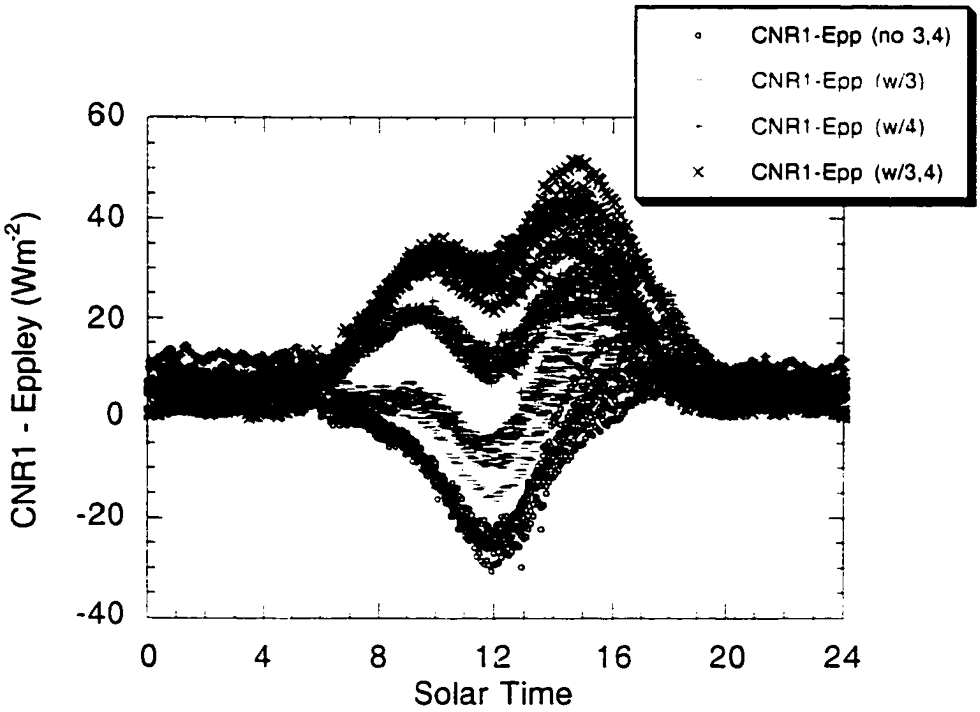

Fig. 5.8: Differences between data from the K&Z CNR1 and Eppley systems for incoming longwave radiation with and without corrections applied to the Eppley for solar heating. The 3rd and 4th terms of Eq. (5.1) are defined in the figure as (3) and (4).

reemits radiation that is proportional to the temperature of the top surface of the thermopile. In addition, σ is the Stefan-Boltzmann constant, and T_{case} is the measured case temperature. The third term accounts for the temperature difference between the dome and case where a = 2.5 is the dome opaqueness coefficient (A. C. Delany, 1998, personal communication). The last term subtracts contamination by shortwave radiation (shortwave radiation getting through the domes) where Q is the incoming shortwave radiation and b = 0.036 is an empirically derived coefficient (Alados-Arboledas et al. 1988).

Longwave estimates from the Eppley and CNR1 were compared for the clear days of the data set (Fig. 5.8). First, both the incoming longwave radiation from the Eppley and CNR1 were compared without correcting for dome heating or solar contamination, the 3rd and 4th terms on the right hand side in Eq. (5.1). Daytime differences ranged up to 30 Wm^{-2}. Next, only the dome heating (and cooling) correction was applied. Differences decreased substantially to within +/- 15 Wm^{-2}. The solar contamination term was also included but with less success, increasing the difference to +30 Wm^{-2}. Inclusion of both terms 3 and 4 lead to even greater differences of nearly 50 Wm^{-2}. This examination suggests that only the dome heating correction term be included in Eq. (5.1). Nevertheless, applying both corrective terms can change the longwave estimates by as much as 60 Wm^{-2}.

As further verification of the accuracy of the 4-component CNR1, data from a CNR1 were directly compared against a 4-component SIRS (Solar Infrared Radiation System) in operational use by the ARM (Atmospheric Radiation Measurement) Program (Stokes and Schwartz 1994). As described in more detail in Chapter 6, a Mesonet and ARM site near Foraker, Oklahoma, are co-located within 100 m which allow for direct comparisons between sites (see Fig. 6.1). For this study, data were compared for the periods 11 - 20 August 1999 and 24 February – 4 March 2000. Half-hourly data were examined. Because the CNR1 was replaced at the Foraker site during January 2000, results may vary between the August and February/March periods.

Data collected during August revealed differences between instruments was limited to less than 9% for all radiation components (Figs. 6.2 - 6.5 and Tables 6.1 - 6.2). The largest absolute differences appeared in the incoming shortwave radiation. This observation is consistent with results from the Norman study described previously. Ironically, shortwave radiation is the simplest and most straightforward measurement to validate the calibration of a sensor against an international standard (Ohmura et al. 1998). The incoming shortwave radiation from the CNR1 and SIRS were validated against the Mesonet's pyranometer measurement. The pyranometer itself is calibrated against the Eppley PSP, which is in use at the Norman intercomparison facility. Results indicated consistency between the pyranometer and SIRS during the two periods with mean differences of 13.2 Wm^{-2} and 15.8 Wm^{-2}, respectively. Results from comparing data produced by the CNR1 and the pyranometer appeared to improve between periods as the standard deviation decreased from 31.8 Wm^{-2} to 8.4 Wm^{-2}. This decrease may have resulted from replacement of the CNR1 between the two data-collection periods.

Table 5.5: Linear regression statistics estimated using data from the CNR1 and SIRS and Mesonet pyranometer. Thirty-minute data were used.

	Independent Variable	Dependent Variable	Intercept (Wm^{-2})	Slope	R^2
11-20 August	LiCor 200	CNR1	-31.871	1.0473	0.9916
1999	LiCor 200	SIRS	-10.33	0.9947	0.9965
24 February - 4	LiCor 200	CNR1	-6.672	0.9965	0.9990
March 2000	LiCor 200	SIRS	-9.617	0.9842	0.9961

Table 5.6: Difference statistics produced using data from the CNR1 and SIRS and the Mesonet pyranometer. Thirty-minute data were used.

		X (Wm^{-2})	σ (Wm^{-2})	95% Confidence Interval	Sample size, # Obs
11 – 20	CNR1 – LiCor 200	-6.00	31.796	-68.32 – 56.32	266
August 1999	SIRS – LiCor 200	-13.22	17.457	-47.44 – 21.00	266
24 February –	CNR1 – LiCor 200	-8.02	8.364	-24.41 – 8.37	211
4 March 2000	SIRS – LiCor 200	-15.77	17.035	-49.16 – 17.62	211

Differences between outgoing shortwave radiation were less than 15 Wm^{-2} (a difference of about 7.6%). The differences in incoming shortwave radiation may indicate some heating of the pyrgeometer domes with either one or both shortwave sensors. Differences in albedo between the two sites may create some difference in reflected solar radiation. The longwave radiation data collected from the CNR1 and SIRS indicated differences of less than 20 Wm^{-2} for all time periods, an approximate difference of less than 9%. Spatial differences in surface properties between sites also could account for some variation in the emitted longwave radiation.

Data collected during February and March showed many of the same results as during August. However, significant differences were noted in the measurements of incoming shortwave radiation. While the magnitude of the differences between sites remained less than 60 Wm^{-2}, the differences as a function of time indicated a change between test periods. Likewise, differences between the two sets of outgoing shortwave radiation also showed change in the diurnal pattern. The February/March data set indicated measurements that were much larger in value from the CNR1 relative to SIRS versus the differences indicated by the August data.

To summarize the results using the CNR1, tentative confidence limits were created for each component of the net radiation based upon differences observed when comparing data from the CNR1, Eppley and SIRS. These differences were used to formulate an expected mean "error", assuming the Eppley and SIRS data represent the "truth". The total confidence limits are summarized:

$$\begin{array}{ccccccccccc} Rn & = & Sw_{in} & - & Sw_{out} & + & Lw_{in} & - & LW_{out} \\ 5\% & & 5\% & & 2\% & & 2\% & & 3\% \end{array} \qquad (5.2)$$

Note that during periods of minimal radiation (< 100 Wm^{-2}), the percentage given in Eq. (5.2) is not used but is replaced by the constant error value of 10 Wm^{-2}.

5.2 Sensible and Latent Heat Flux

The precision of measurements of the sensible and latent heat fluxes could not be determined as with net radiation. Unfortunately, a pair of identical CSAT3 sonic anemometers or krypton hygrometers was not available for direct comparison. Instead, two separate field experiments were conducted in part to evaluate the accuracy of the eddy correlation technique estimated using Mesonet data. The accuracy of estimating the sensible and latent fluxes were determined from the OASIS-98 and OASIS-2000 field programs.

During OASIS-98 (McAloon et al. 1999), an ISFF (Integrated Surface Flux Facility) sonic anemometer was placed on a 10 m tower located approximately 10 m west of the Mesonet tower at Norman. This co-location allowed a direct comparison between the CSAT3 sonic anemometer used by OASIS and the ATI sonic anemometer used by the ISFF. Data were collected during an approximate 5 week period at the Norman Mesonet site between 1 July and 8 August, 1998. Data collected between 15 July and 5 August was used for this study. Data from eight clear days (DOY 196, 197, 200, 204, 207, 208, 211, and 212) were examined in closer detail. Data from the CSAT3 and ATI sonic anemometers were examined to identify any systematic error and to quantify the random error associated with each measurement.

First, five-minute data from the eight clear days were compared (Tables 5.7 and 5.8). The Mesonet had a slightly lower sensible flux and latent flux by approximately 4%

when compared to the NCAR measurements. A higher correlation was observed between the two sets of sensible flux estimates than was found between the two sets of latent flux estimates. The standard deviation of error was significant at 41.3 Wm^{-2} and 27.3 Wm^{-2}, respectively. Results were similar using data from all sky conditions (a total of 22 days of data).

Table 5.7: Linear regression statistics estimated from the NCAR and Mesonet measurements of sensible and latent heat fluxes for both clear sky and all-sky conditions. Five-minute data were used.

		Intercept (Wm^{-2})	Slope	R^2
Clear skies	Sensible heat	1.984	0.9611	0.8984
	Latent heat	6.931	0.9639	0.7760
All sky	Sensible heat	2.439	0.9702	0.8941
conditions	Latent heat	6.574	0.9545	0.7620

Table 5.8: Difference statistics estimated from the NCAR and Mesonet measurements of sensible and latent heat fluxes for both clear sky and all-sky conditions. Five-minute data were used.

		X (Wm^{-2})	σ (Wm^{-2})	95% C.I.	Sample size #
Clear skies	SH, NCAR-Meso	-1.19	41.3	-30.85 – 11.79	4948
	LH, NCAR-Meso	5.18	27.3	-12.89 – 0.96	4948
All sky	SH, NCAR-Meso	0.21	39.8	-6.70 – 15.73	2304
conditions	LH, NCAR-Meso	4.46	27.6	-1.04 – 10.37	2304

Next, the diurnal averages of sensible and latent heat flux were estimated to better identify systematic errors between the two systems (Fig. 5.9). As described above, five-minute data were used from the eight clear days during July. A histogram of the differences indicated a near-Gaussian curve about 0 Wm^{-2}. The majority of Mesonet values of sensible flux were overestimates by 0-10 Wm^{-2} and were underestimates for latent flux

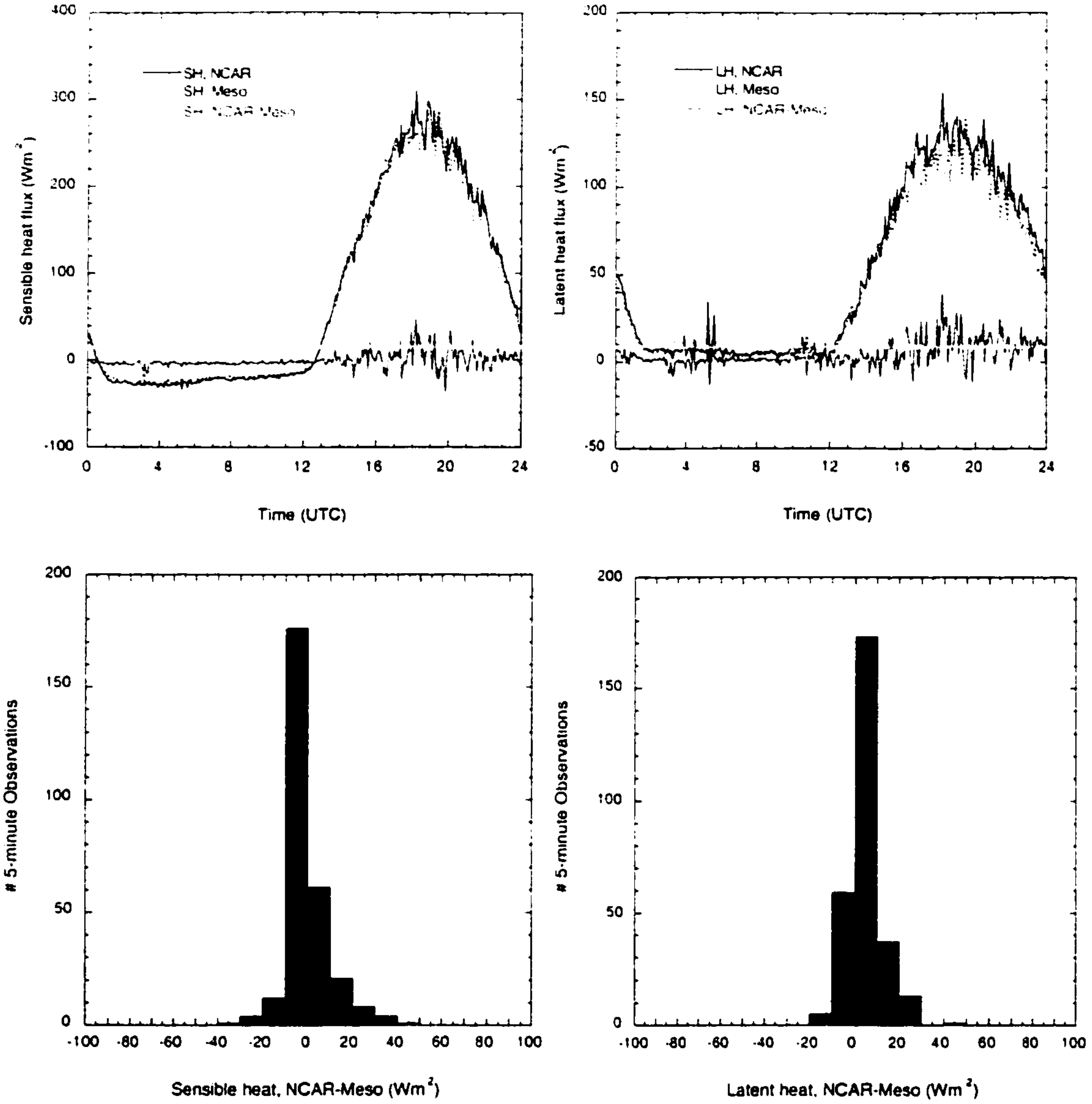

Fig. 5.9: Five-minute data collected at Norman, OK, during OASIS-98, between 15 July and 5 August 1998.

by 0-10 Wm^{-2} when compared to NCAR. However, true values were not known. Results were similar when all 22 days of data were considered. Thus, while large variance may be observed between any particular 5-minute period, over daily or even 30-minute periods, little bias is noted with either measurement of sensible or latent heat flux.

As further verification of the consistency of sensible and latent fluxes measured by OASIS, OASIS-2000 (McAloon et al. 2000) was a second field study which examined the eddy correlation fluxes at five of the ten super sites. During OASIS-2000, ISFF sonic anemometers were placed at several super sites for approximate 3 - 4 week periods. As during OASIS-98, the two sonic anemometers from NCAR and OASIS provided data for direct comparison of the relative accuracy between sensors. A 10 m tower from ISFF was approximately 10 m west of each Mesonet site. Both sonic anemometers were mounted at 4.5 m. Sites at Foraker and Marena were tested during Phase 1 of the project, Stigler during Phase 2, Grandfield during Phase 3, and Alva during Phase 4. Thirty-minute data were used.

Flux data from this project are plotted in Figs 5.10 and 5.11 and in Tables 5.9 - 5.12. Results indicate good agreement between the two systems. A comparison of sensible flux during the four phases of the field experiment revealed that Mesonet data at Stigler and Bessie differed significantly from the NCAR data. The other sites were within 5% of the NCAR measurements. Stigler data was well behaved with a high correlation of 0.968 and a low standard deviation. Only the site at Bessie provided poor quality data relative to the other sites; the Mesonet site underestimated fluxes by 8.3% relative to NCAR. A correlation of 0.864 and a large standard deviation of over 43 Wm^{-2} were evidence of the poorer quality data from Bessie. Complex topography at Bessie is likely responsible for such poor results (see Chapter 7).

Latent heat fluxes compared less favorably between the two systems. Some instrument problems with the NCAR krypton hygrometers were suspected at Stigler and Grandfield, and the data should not be used. Phase 1 of the project occurred before spring "green-up" of the vegetation, and thus, minimal latent heat flux was observed. As a result, a comparison of latent flux data between the two systems at Foraker and Marena was difficult. Results from Bessie were similar as the sensible flux comparison revealed a poor correlation between systems and an underestimate by the Mesonet of 13.3% when compared to NCAR. Only at Alva could the observed latent flux by the two systems be described as "good"; even so, the Mesonet site estimated a lower flux by ~ 5% but the correlation was 0.956 between the two systems.

As observed in the data from OASIS-98 and OASIS-2000, the measurement of latent flux is more difficult and less accurate than is the measurement of sensible flux. Based upon results from the two field experiments, percentage of uncertainty associated with the sonic anemometer and the krypton hygrometer is assumed to be ~ 5% for sensible heat flux and 10% for latent heat flux. Because the exact sensible and latent fluxes were not known, the "correct" sensor value was not known and only a semi-objective percentage of uncertainty can be assigned.

5.3 Ground Heat Flux

Instrument error associated with the heat flux plates and PRTDs, provided by the manufacturer, are listed in Table 4.1. While instrument error is relatively small (< 5%), system error can lead to significant errors in estimating ground heat flux as described in Chapter 4. The most significant problem to measure accurately the ground flux is created by surface heterogeneity. This problem is discussed in detail in Chapter 8.

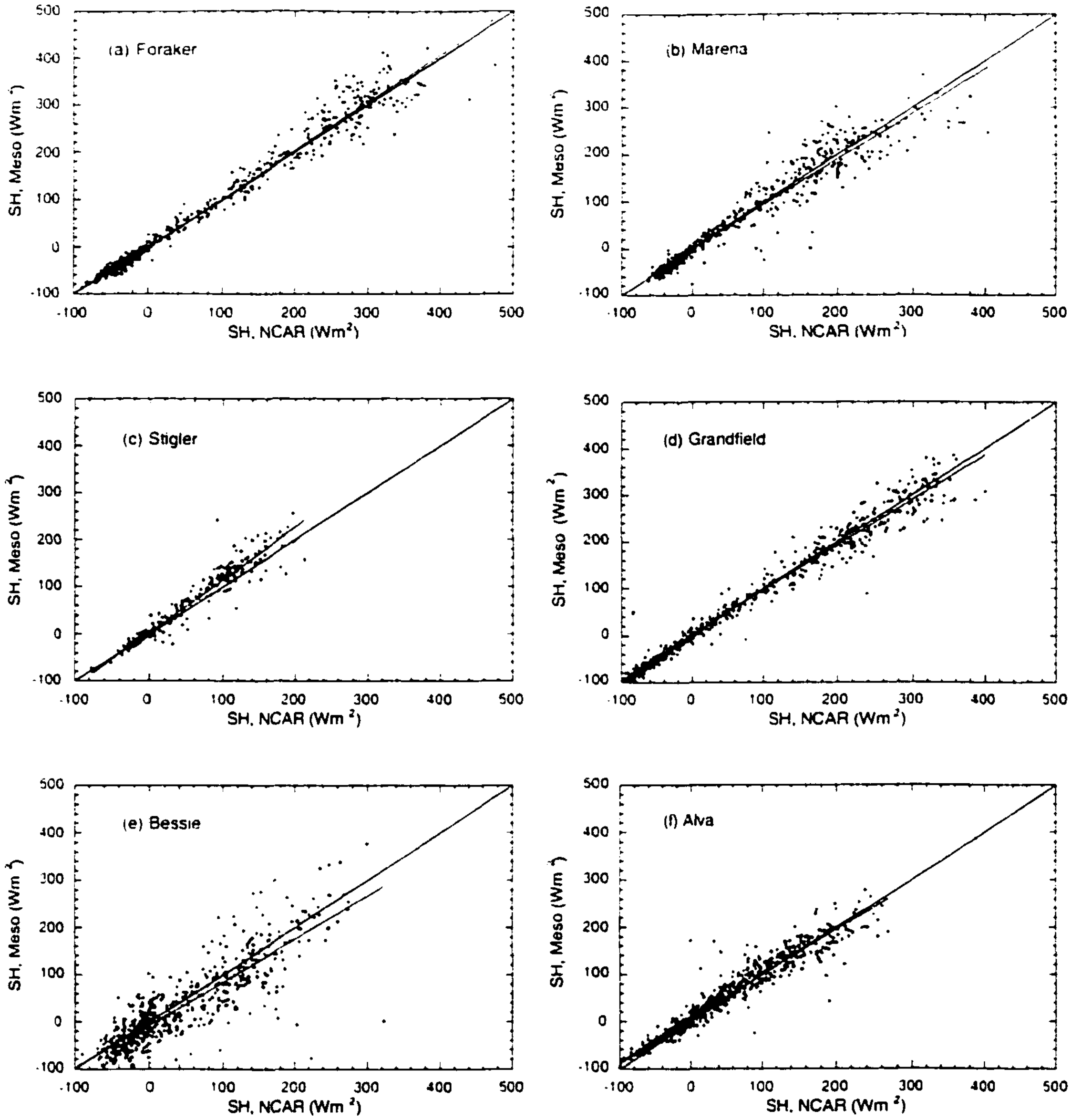

Fig. 5.10a-f: Comparison of sensible heat fluxes (Wm^{-2}) as measured by NCAR and by Mesonet during OASIS-2000. Note that periods of data collection vary at each site.

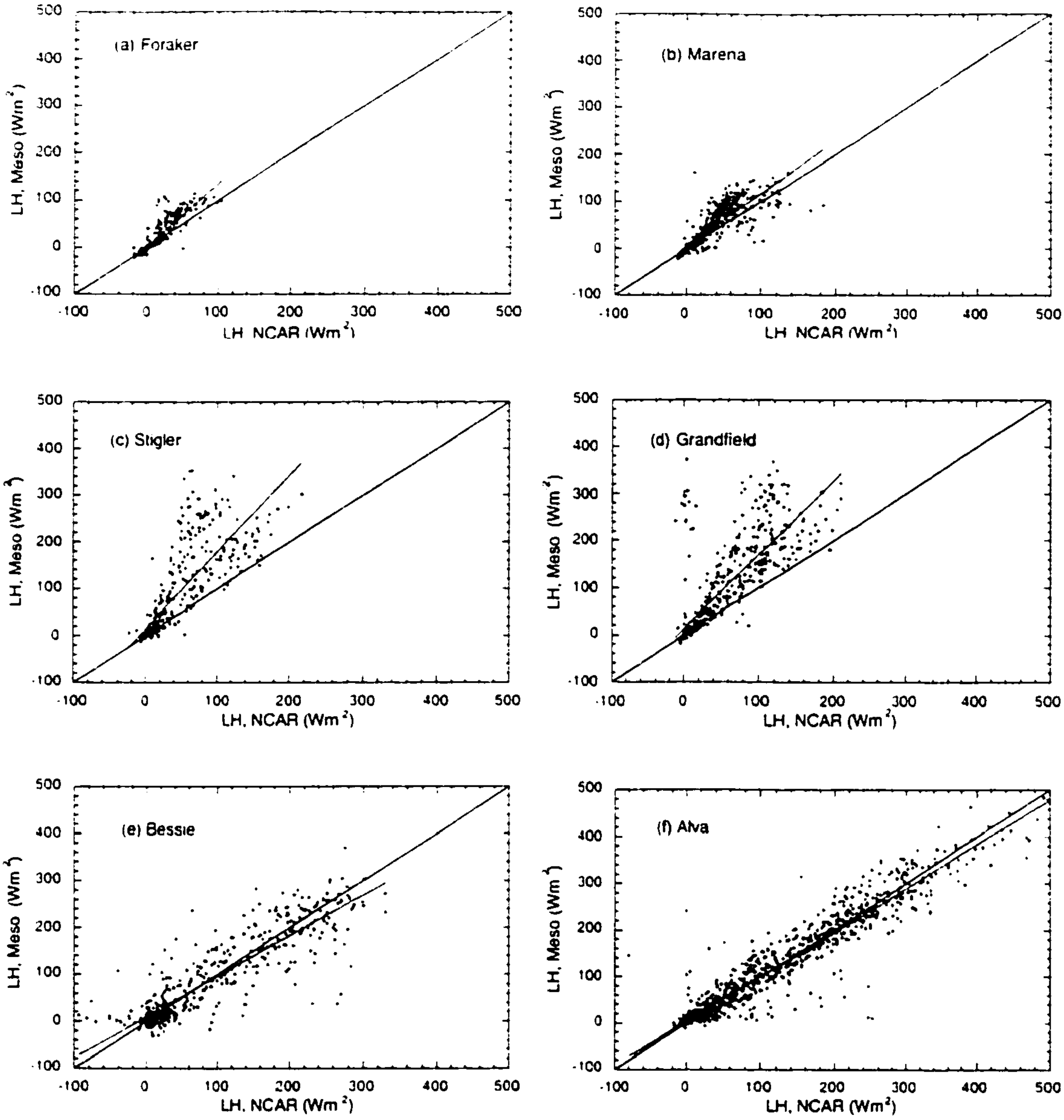

Fig. 5.11a-f: Comparison of latent heat fluxes (Wm^{-2}) as measured by NCAR and by Mesonet during OASIS-2000. Note that periods of data collection vary at each site.

Table 5.9: Difference in sensible heat flux between the NCAR and Mesonet systems.

Site	Collection period (Day of Year)	Mean, X (Wm^{-2})	Standard deviation, σ (Wm^{-2})	Sample size, n (# 30-min. Obs)
Foraker	55 – 85	-0.98	18.1	892
Marena	55 – 85	3.13	24.1	780
Stigler	92,94, 104-116	-6.56	18.5	397
Grandfield	129 – 151	2.15	19.7	740
Bessie	137 – 151	10.94	43.0	636
Alva	156 - 182	-2.75	18.3	1008

Table 5.10: Difference in latent heat flux between the NCAR and Mesonet systems.

Site	Collection period (Day of Year)	Mean, X (Wm^{-2})	Standard deviation, σ (Wm^{-2})	Sample size, n (#30-min Obs)
Foraker	55 – 85	-6.75	17.3	338
Marena	55 – 85	-7.18	20.4	749
Stigler	92,94, 104-116	-40.34	66.4	395
Grandfield	129 – 151	-38.85	66.0	564
Bessie	137 – 151	1.18	42.8	500
Alva	156 - 182	0.65	32.7	1061

Table 5.11: Linear regression of sensible heat flux between NCAR and Mesonet systems.

Site	Collection period (Day of Year)	Intercept (Wm^{-2})	Slope	R^2
Foraker	55 – 85	0.18	1.018	0.9791
Marena	55 – 85	-1.67	0.965	0.9364
Stigler	92,94, 104-116	2.50	1.122	0.9367
Grandfield	129 – 151	-0.50	0.970	0.9766
Bessie	137 – 151	-7.91	0.917	0.7469
Alva	156 - 182	4.13	0.953	0.9376

Table 5.12: Linear regression of latent heat flux between the NCAR and Mesonet systems.

Site	Collection period (Day of Year)	Intercept (Wm^{-2})	Slope	R^2
Foraker	55 – 65	1.39	1.343	0.7523
Marena	55 – 85	3.70	1.136	0.7487
Stigler	92,94, 104-116	19.80	1.505	0.5868
Grandfield	129 – 151	12.58	1.578	0.6285
Bessie	137 – 151	9.57	0.867	0.7945
Alva	156 - 182	4.76	0.950	0.9138

Chapter 6: Evaluation of Eddy Correlation and Bowen Ratio Systems

Introduction

As listed in Table 2.1 of Chapter 2, prior studies evaluated the performance of co-located, surface layer measurement systems. A reliable method to measure the surface energy budget is critical to improve the evaluation and initialization of numerical models as well as to develop new parameterization schemes.

The most significant contention centers on the accuracy of an eddy correlation (EC) system when compared to a Bowen ratio (BR) system. All studies that compared EC and BR systems concluded that $(SH + LH)_{BR} > (SH + LH)_{EC}$. In other words, the sum of aerodynamic fluxes are greater when measured from a BR system than when measured via an EC system (Dugas et al. 1991; Fritschen et al. 1992; Stannard et al. 1994; Lloyd et al. 1997; and Twine et al. 2000). Even more disagreement arises when the fluxes are compared directly. Dugas et al. (1991) claimed that most differences between systems are due to differences in the measured latent heat flux. Twine et al. (2000) claimed the differences were evenly distributed between the latent and sensible heat fluxes as a function of the true Bowen ratio. To determine whether the sensible or latent fluxes are measured accurately would improve the estimates of closure and provide insight into the use of EC and BR methods.

For this study, it was important to duplicate previous work comparing EC and BR systems. OASIS data collected from the Mesonet site at Foraker, Oklahoma, was compared directly against Bowen ratio data collected from the co-located Atmospheric Radiation Measurement (ARM) site.

6.1. Description of the ARM Bowen Ratio Site and Instrumentation

The Mesonet site at Foraker is co-located with an ARM energy balance Bowen ratio (EBBR) system. The ARM site is ~ 100 m north-northwest of the Mesonet tower, which allows measurements of the energy budget to be compared. The site, located at ~ 36.841 north latitude and 96.427 west longitude, is an extended facility site of the ARM Program which began operating in June 1995. The site is equipped with an Energy Balance Bowen Ratio system, Solar Infrared Radiation Station (SIRS), Multi-Filter Rotating Shadowband radiometers (MFRSRs), and Soil Water and Temperature Sensors (SWATS). The site is located in the Tallgrass Prairie Preserve in northcentral Oklahoma near Pawhuska. Native prairie grasses are the dominant vegetation; bison graze on much of the nearby land. Typical soil type is silt loam. The site slopes downward from south to north; the ARM site is approximately 1-2 m lower in elevation than is the Mesonet site. An overhead view of the ARM and Mesonet site locations are shown in Fig. 6.1.

The EBBR system used by ARM directly measures net radiation, ground heat flux, and vertical gradients of temperature and relative humidity. Latent heat flux is estimated using Eq. (2.4); sensible heat flux is estimated as the residual of the energy budget. Net radiation is measured at a height of 3 m using the REBS' model Q*6.1. Ground heat flow is estimated as the average of data from five soil heat plate sensors, REBS' model HFT-3.1s, which are buried at a depth of 5 cm. The ground heat storage term is computed from soil moisture estimated at a depth of 2.5 cm and the mean of data from five platinum resistance temperature detectors buried between 0 and 5 cm. Vertical gradients in air temperature and moisture are measured using temperature and humidity sensors mounted at heights of 2 and 3 m. An automatic exchange mechanism (AEM) switches the two temperature and humidity sensors vertically every 15 minutes to minimize systematic error due to instrument offset and drift. The average of data produced by two 15 minute averages yields a final 30-minute mean of sensible and latent flux.

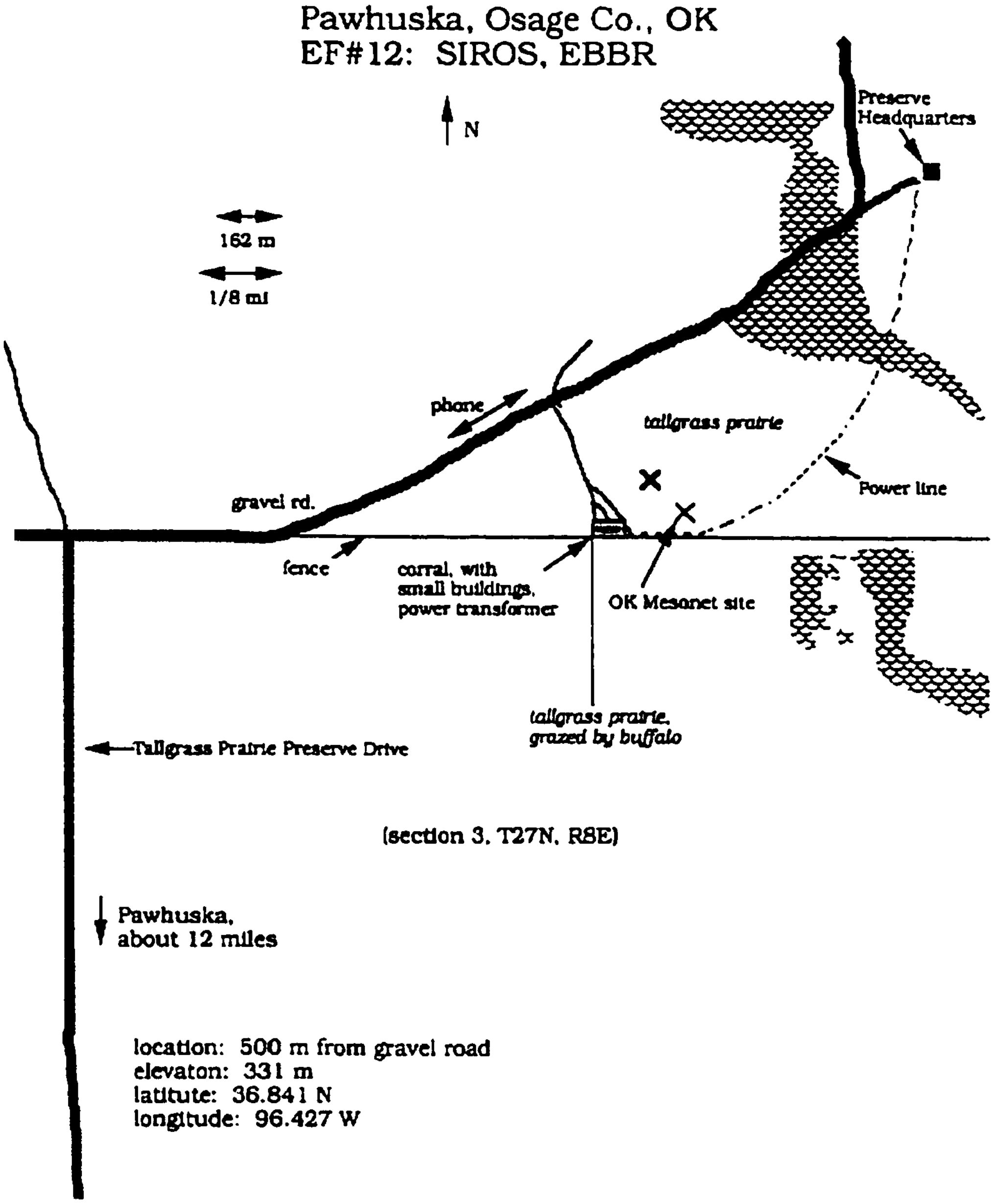

Fig. 6.1: Overhead view of the ARM and Mesonet sites at Foraker site. The ARM site is marked by the bold X northwest of the Mesonet site. Map provided by the ARM Program.

6.2. Comparison of EC and BR Systems

Eddy correlation estimates from the Mesonet site and Bowen ratio data from the ARM site were directly compared. Net radiation and ground heat flux estimates also were compared as they represent the available energy for the Bowen ratio technique. Thus, the entire energy budget was examined. For this study, 5-minute data from Mesonet sites were averaged over 30-minute periods to match the EBBR data from ARM.

Two ten-day periods of data were chosen from the year-long data set for a more detailed examination. Quiescent conditions prevailed during most of the two periods; partly to mostly clear skies dominated. Each period represented different synoptic conditions, however. The first period of data collected during 11 – 20 August 1999, represented an excellent "dry-down" period. Mostly clear and hot conditions prevailed. The second period of data, collected between 24 February and 4 March 2000, represented much wetter soil conditions. Partly to mostly sunny skies and cool temperatures prevailed along with several days of rainfall. The second test period coincided with the OASIS-2000 field project during which additional eddy correlation equipment provided by NCAR was installed at the site. No precipitation was recorded during the August period; data were not used when rain occurred during the February to March period. Shortwave data were not included if values were less than 10 Wm^{-2}.

To evaluate properly the EC and BR techniques, it was critical to estimate the error associated with the available energy components, Rn and GH, as well as the sensible and latent heat components. The Bowen ratio method forces closure; the technique assumes the sum of the aerodynamic fluxes (SH + LH) are equal to the available energy (Rn – GH). Subsequently, any error associated with the net radiation and/or ground flux affects both estimates of sensible and latent heat flux. To compare sensible and latent fluxes properly, the available energy must be examined as well.

6.2.1 Net Radiation

The Mesonet site at Foraker has been designated as a super site of OASIS and is equipped with both the NR-Lite and four-component CNR1 radiometers while the nearby ARM site is equipped with a REBS Q*6.1 and SIRS system. Net radiation from the CNR1 was estimated using the sum of four separate components of radiation. The longwave components were corrected by Eq. (3.3). The CNR1 was replaced on 18 January 2000 due to a faulty temperature sensor. The NR-Lite was corrected for the effects of wind as given by Eq. (3.2).

The ARM EBBR site is equipped with a REBS Q*6.1 net radiometer. In addition, the 4-component SIRS system is co-located at the site and is comprised of direct component and diffuse radiometers. The Q*6.1 was not corrected for wind speed. The direct shortwave component of SIRS was corrected by the cosine of the zenith angle.

The SIRS and CNR1 radiometers measure each component of the radiation budget explicitly and are considered more accurate instruments for observing net radiation than either the Q*6.1 or NR-Lite sensors. Because the CNR1 also is used for closure of the energy budget, a critical issue is the accuracy with which net radiation is measured. The four components of the radiation budget are examined during each collection period. Results are summarized in Tables 6.1 and 6.2 and Figures 6.2 – 6.5. Note that the CNR1 was replaced between test periods so that similar results may not be expected between the August and February periods. However, a direct comparison between 1999 data from two CNR1s showed excellent agreement between the sensors (see Section 5.1).

Table 6.1: Direct comparison of the 4 components of the radiation budget as measured by the CNR1 and SIRS instrumentation.

	Variable	Mean diff. X (Wm^{-2})	Std. Dev. σ (Wm^{-2})	Sample size, # 5-min obs
11 – 20 Aug 1999				
	SW, in	+ 7.15	27.12	260
	SW, out	- 6.96	4.39	257
	LW, in	- 0.25	6.13	480
	LW, out	- 1.66	5.58	480
24 Feb – 4 Mar 2000				
	SW, in	+7.55	21.88	152
	SW, out	+2.29	4.58	142
	LW, in	+2.28	4.39	386
	LW, out	+0.32	5.65	386

Table 6.2: Linear regression of data representing the 4 components of the radiation budget using the CNR1 and SIRS instrumentation. The CNR1 is the independent variable, and the SIRS is the dependent variable.

	Variable	Intercept	Slope	R^2
11 – 20 Aug 1999				
	SW, in	1.722	0.974	0.9973
	SW, out	-0.626	1.076	0.9974
	LW, in	26.685	0.931	0.9691
	LW, out	38.873	0.917	0.9899
24 Feb – 4 Mar 2000				
	SW, in	-3.21	0.987	0.9972
	SW, out	-0.43	0.972	0.9942
	LW, in	-13.40	1.039	0.9879
	LW, out	32.37	0.911	0.9918

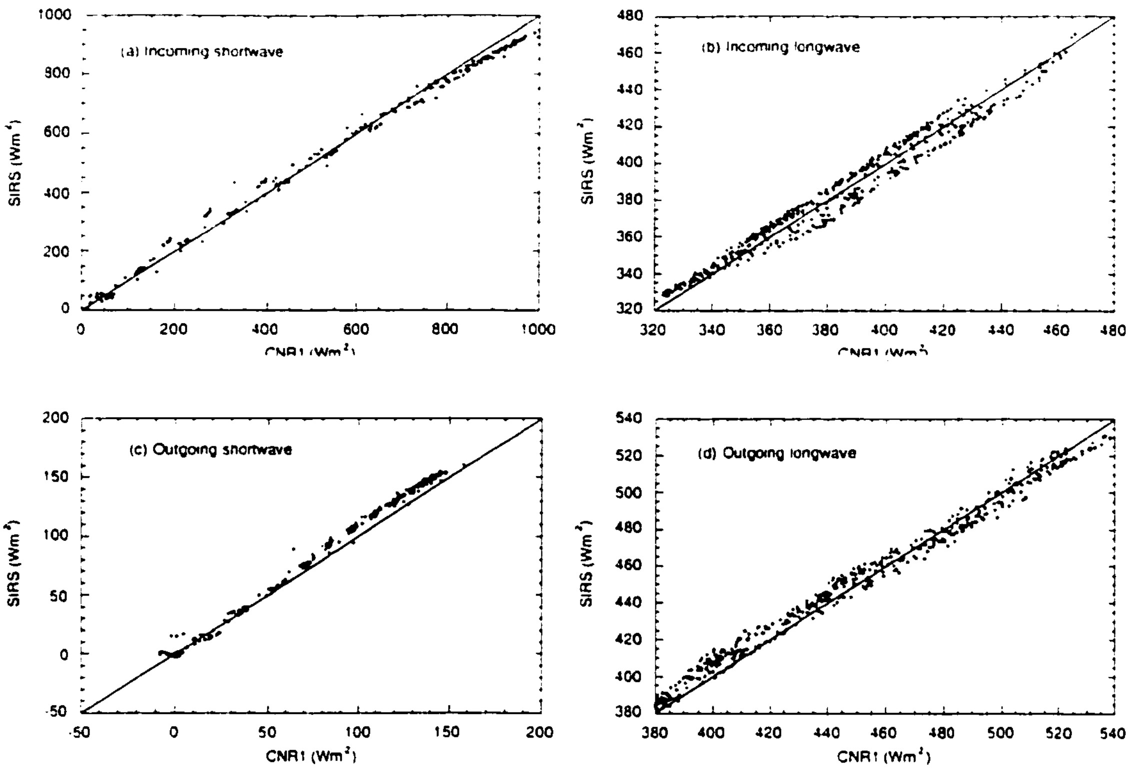

Figs 6.2a-d: Comparison of data from the K&Z CNR1 and ARM SIRS for (a) incoming shortwave, (b) incoming longwave, (c) outgoing shortwave, and (d) outgoing longwave from 11 – 20 August 1999.

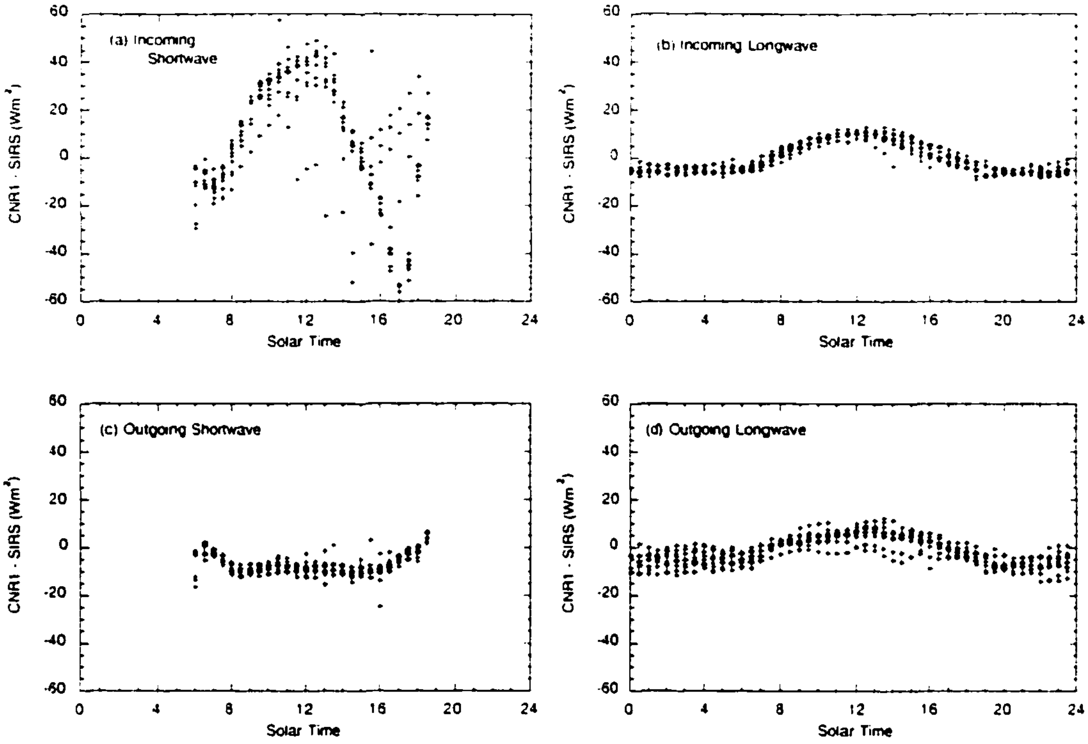

Fig. 6.3a-d: Differences of data from the K&Z CNR1 and ARM SIRS for (a) incoming shortwave, (b) incoming longwave, (c) outgoing shortwave, and (d) outgoing longwave from 11 – 20 August, 1999, plotted as a function of solar time.

The greatest uncertainty in data produced by the CNR1 and SIRS radiometers was in the measurement of incoming solar radiation. The CNR1 overestimated shortwave radiation by 2.6% and 1.3% when compared to SIRS during the respective periods. The SIRS system explicitly measures both the direct and diffuse incoming solar radiation and is considered a more accurate sensor. The *overestimate* by the CNR1 leads to an underestimate in closure. However, the CNR1*underestimates* incoming shortwave radiation when compared to the 4-component Eppley system (see Section 5.1). Thus, the "true" radiation value is not known. It is possible that each CNR1 has variations in calibration accuracy; however, the two sensors that were compared revealed little difference in their measurements.

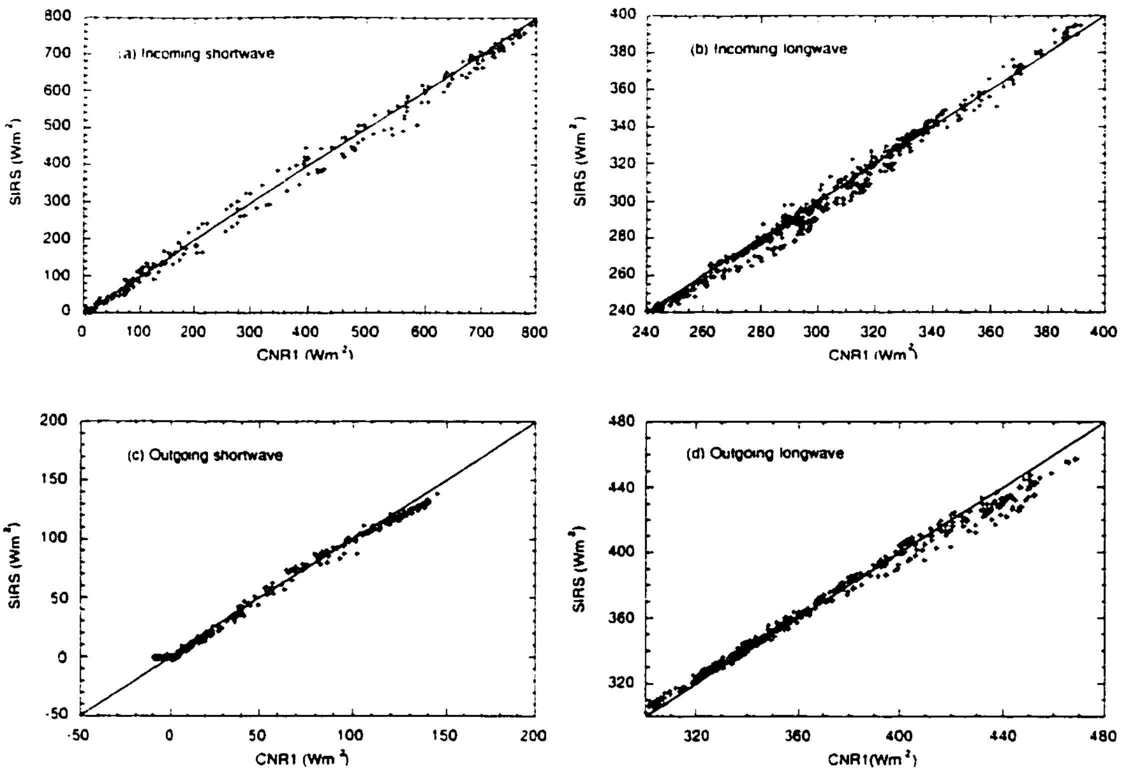

Fig. 6.4a-d: Comparison of data from the K&Z CNR1 and ARM SIRS for (a) incoming shortwave, (b) incoming longwave, (c) outgoing shortwave, and (d) outgoing longwave from 24 February – 4 March 2000.

Variations in reflected shortwave radiation also were significant. However, such differences could be due to slight variations in albedo during this observing period, vegetation height and geometry, and vegetation coverage of the land surface. During the August period, a 7.6% underestimate in the reflected shortwave combined with a +2.6% overestimate in the incoming shortwave could lead to significant underestimates in closure. A slight underestimate in closure was observed during this period (Table 6.11). However, replacement of the CNR1 by the SIRS sensor improved daily closure rates only by 1.4%; the average daily closure rate was still underestimated slightly at approximately 96.1%. A

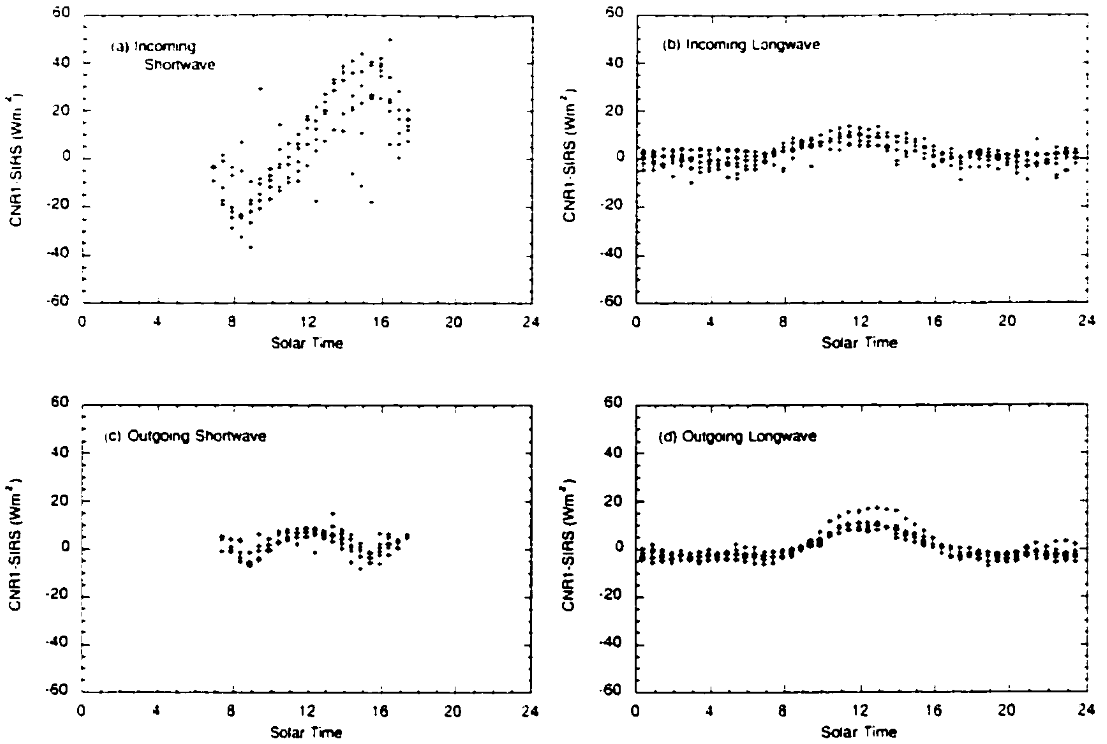

Fig. 6.5a-d: Differences of data from the K&Z CNR1 and ARM SIRS for (a) incoming shortwave, (b) incoming longwave, (c) outgoing shortwave, and (d) outgoing longwave from 24 February – 4 March 2000, plotted as a function of solar time.

similar underestimate in closure was observed during the February/March period. The SIRS estimate increased closure by 4.7%.

Differences in the measurement of incoming longwave radiation were significant; the sensors overestimated by 6.9% during August but only slightly underestimated (3.8%) during the February to March period. Differences of 7 - 9% were observed in outgoing longwave radiation. However, these differences are attributed to observed differences in the features of land cover.

Differences in radiation between the CNR1 and SIRS are plotted as a function of solar time (Figs. 6.3 and 6.5). During August some diurnal dependence was observed. The difference in shortwave radiation may be indicative of some slight calibration error by one or both sensors. The presence of this calibration error is consistent with radiation differences being symmetric about solar noon. During the February to March period, differences between systems were not significant as a fraction of the incoming net radiation. However, noteworthy differences in measurements of the incoming shortwave radiation were asymmetric about solar noon. Such differences could be attributed to either tilt off vertical by one of the sensors or by pyranometer heating due to radiation or both. Prior to solar noon, the CNR1 underestimated shortwave radiation relative to the SIRS system; during the afternoon, the CNR1 overestimated the radiation relative to SIRS. Thus, either the CNR1 was tilted toward the west or one component of the SIRS system was tilted to the east or both. All four components of the CNR1 are combined into a single unit; thus, no tilt error is suggested by the reflected shortwave data. Accordingly, an eastward tilt of only a few degrees by the SIRS unit could account for the incoming shortwave being underestimated.

Net radiation from the REBS Q*6.1 and the NR-Lite and the summed components of radiation from the CNR1 and SIRS system were compared with each other. A result of this comparison of data from the two test periods is shown in Figures 6.6 – 6.7. The results also are summarized in Tables 6.3 and 6.4. Comparative results changed significantly between the two periods.

The net radiation difference between the CNR1 and SIRS system decreased from +5.4% during the August period to –0.3% during the February/March period. The very hot temperatures and strong radiational heating during August could have created some of the observed difference. Note that two different CNR1s were used during these two periods. A sensor problem occurred with the NR-Lite during the August period, data from this sensor were not included in the study. However, during the second study period, the NR-Lite measured within –0.6% of the SIRS and within –0.4% of the CNR1.

A year-long comparison between the CNR1 and NR-Lite revealed an approximate 50-day period when the NR-Lite produced underestimated values of radiation. This period occurred between DOY 218 and 250. The cause for this sudden underestimation is not

Table 6.3: Comparison of data from the CNR1, SIRS, REBS Q*6.1, and NR-Lite for 11 – 20 August 1999 and for 24 February – 4 March 2000.

		Mean Diff, X (Wm^{-2})	Std. Dev., σ (Wm^{-2})	Sample Size, n
11 – 20 Aug 1999				
	CNR1 – SIRS	+ 10.8	22.1	480
	CNR1 – REBS	+ 2.0	36.0	479
	CNR1 – NR-Lite	+ 41.3	51.5	477
	SIRS – REBS	- 8.8	18.3	479
	SIRS - NR-Lite	+ 30.7	36.6	477
	REBS - NR-Lite	+ 39.7	23.2	476
24 Feb – 11 Mar 2000				
	CNR1 – SIRS	+ 5.5	11.9	386
	CNR1 – REBS	+ 6.2	30.5	385
	CNR1 – NR-Lite	+5.1	7.2	386
	SIRS – REBS	- 5.5	11.9	386
	SIRS – NR-Lite	- 0.4	13.6	386
	REBS – NR-Lite	- 1.1	30.1	385

Table 6.4: Linear regression using data from the CNR1, SIRS, REBS Q*6.1, and NR-Lite for 11 – 20 August 1999 and for 24 February – 4 March 2000.

	Dependent variable	Independent variable	Intercept	Slope	R^2
11 – 20 Aug 1999	CNR1	SIRS	1.56	1.054	0.9964
	Q*6.1	SIRS	18.37	0.945	0.9981
	Q*6.1	CNR1	17.61	0.893	0.9938
24 Feb – 4 Mar 2000	CNR1	SIRS	5.69	0.997	0.9963
	Q*6.1	SIRS	8.43	0.858	0.9947
	Q*6.1	CNR1	3.68	0.859	0.9941
	NR-Lite	SIRS	0.84	0.993	0.9952
	NR-Lite	CNR1	-4.82	0.996	0.9987
	NR-Lite	Q*6.1	-8.71	1.154	0.9938

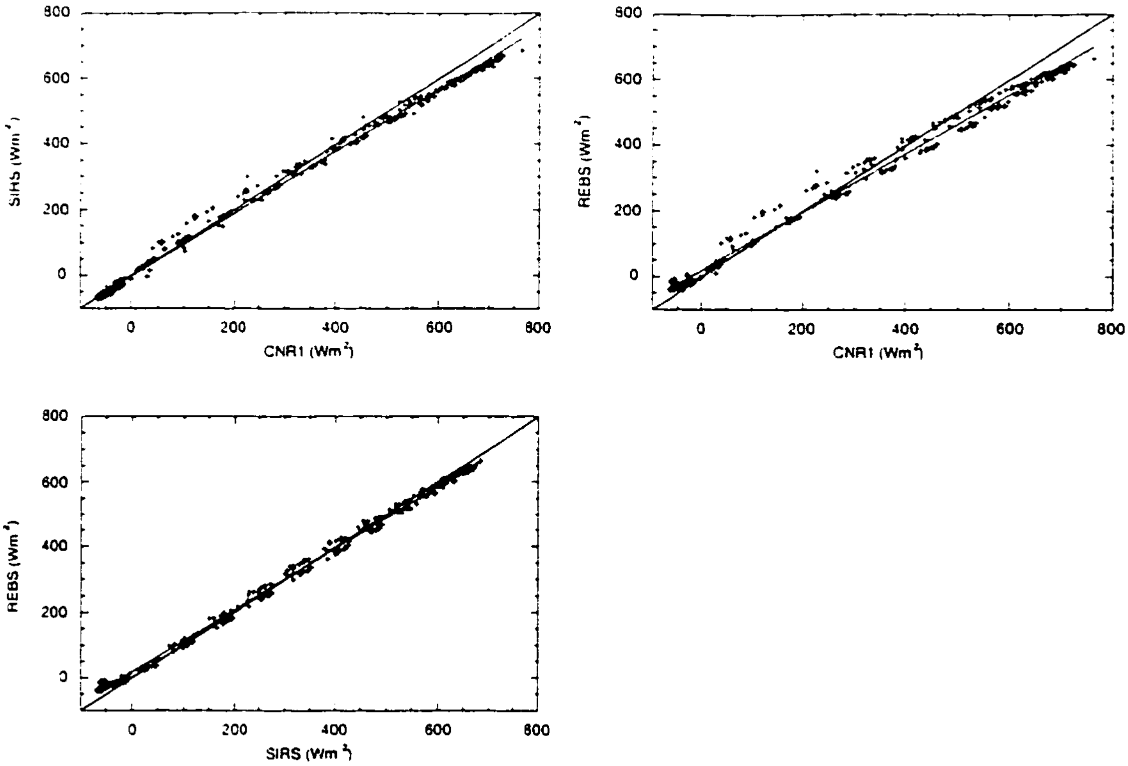

Fig. 6.6: Comparison of net radiation data from the ARM SIRS and REBS radiometers with data from the Mesonet's CNR1 net radiometer. Half-hourly data were collected from 11 – 20 August 1999.

known. The error does not appear to be a function of air temperature, relative humidity, or precipitation. However, rain showers a day prior to DOY 218 indicated a frontal passage which could have deposited residue and dust on the sensor. A second heavy rain event near DOY 250 appears to have cleaned the sensor and corrected the problem. This hypothesis cannot be verified. Nevertheless, data acquired during the first study period from the NR-Lite were in error and could not be used.

The REBS Q*6.1 appeared to deteriorate during the second period (Fig. 6.7) when compared to the performance of the other radiometers. During the August period, the Q*6.1 was within –5.5% and –10.7% relative to the SIRS and CNR1; during February/March, the Q*6.1 underestimated net radiation by –14.2% and 14.1%, respectively. Yet, the performance of the REBS Q*6.1 is critical to evaluate the closure problem because radiation from the Q*6.1 is used by the EBBR system to estimate the fluxes of sensible and latent heat.

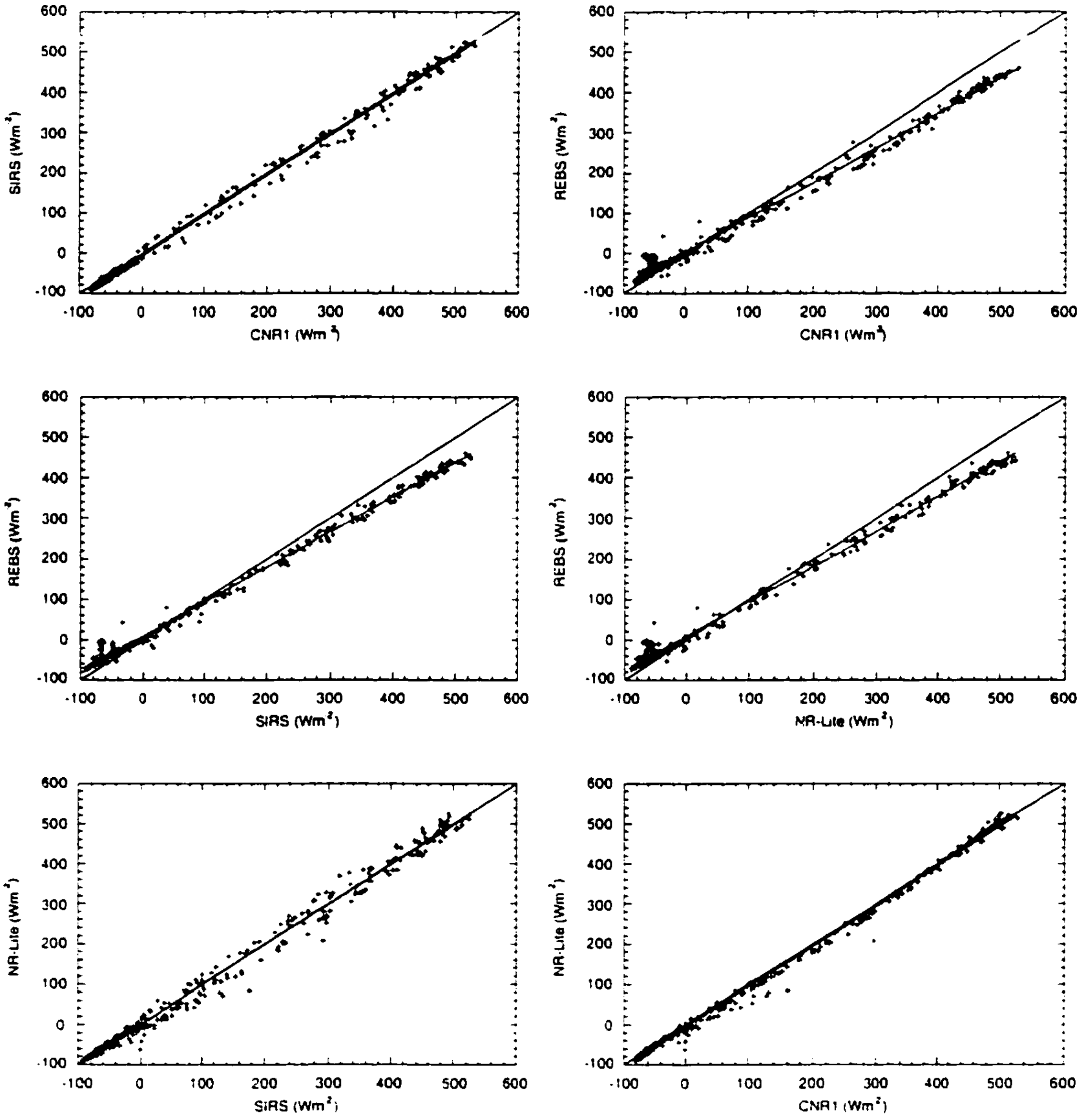

Fig. 6.7: A comparison of net radiation data from the ARM SIRS and Q*6.1 net radiometers and the Mesonet's CNR1 and NR-Lite net radiometers. Data were collected from 24 February through 4 March 2000.

6.2.2 Ground Heat Flux

The ground heat flux is the sum of the soil heat flow near the surface and the time-integrated change in energy storage. The soil heat flow and the total ground flux were compared using data from the ARM and Mesonet systems. The soil water content measured at both sites was compared because the soil water content strongly modulates the storage term.

Soil heat flow is measured at the Mesonet and ARM sites using the same model of heat flux plate, the HFT3.1 manufactured by REBS. Two sensors were installed at the Mesonet site, while five sensors were installed at the ARM site. All sensors were installed at a depth of 5 cm. A comparison of data from all seven plates obtained during August and February/March is plotted in Figures 6.8 and 6.9.

Despite using the same instruments, large differences in measurements are noted between sites. The August data revealed that the five sensors installed at the ARM facility provided data with a damped diurnal cycle; a daily maximum of soil heat flow was ~20 Wm^{-2}. The Mesonet sensors produced data containing daily peak amplitude of 60 - 80 Wm^{-2}. Nighttime values from the two Mesonet sensors reached a minimum of –20 to –40 Wm^{-2}; ARM sensors reached a minimum of 0 to –10 Wm^{-2}. The February/March data were strikingly similar.

The much larger amplitude of soil heat flow at the Mesonet site may theoretically result from a distinct difference in soil and vegetation characteristics. A thicker and denser vegetation cover at the ARM site produced a damped diurnal cycle; less vegetation and more bare soil at the Mesonet site yielded a diurnal cycle with a larger amplitude. However, a visual inspection of the site did not indicate differences in vegetation between the sites. Dense vegetation covered sensors at both sites. The impact is that, if Mesonet sensors overestimate ground flux, the closure residual *increases*. Thus, large differences in soil heat flow indicate the difficulty and uncertainty in soil measurements, even when the same type of instrument is used.

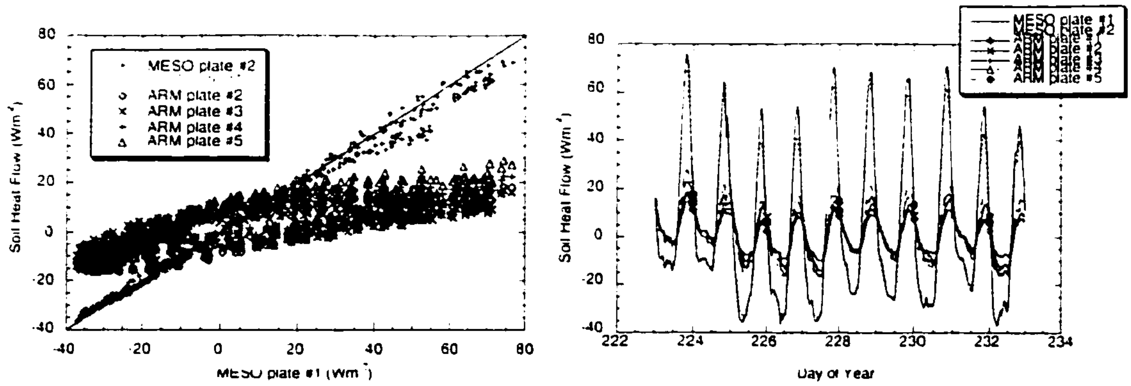

Figs. 6.8: Soil heat flow (Wm^{-2}) as measured during 11 – 20 August 1999.

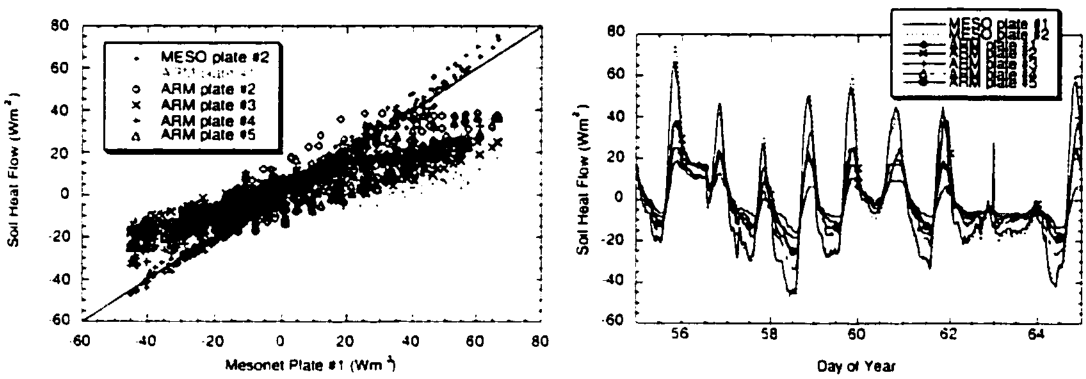

Figs. 6.9: Soil heat flow (Wm^{-2}) as measured during 24 February to 4 March 2000.

Next, measurements of the soil water content from the sites were compared. The ARM facility measures soil water content directly using five soil moisture sensors, a model SMP-2 manufactured by REBS. An average value of data from the five sensors is used. The Mesonet measures soil water potential using a single 229L manufactured by Campbell Scientific, Inc. (CSI). The soil water potential is converted to soil water content using empirical soil water retention curves, which are unique to each site. The Mesonet sensors are installed at a depth of 5 cm; soil moisture sensors at ARM sites are installed at a depth of 2.5 cm. All soil moisture observations were acquired at 30-minute intervals.

The August data captured a dry-down period when precipitation did not occur and a high evaporation rate was evident. On the other hand, soils during the February/March

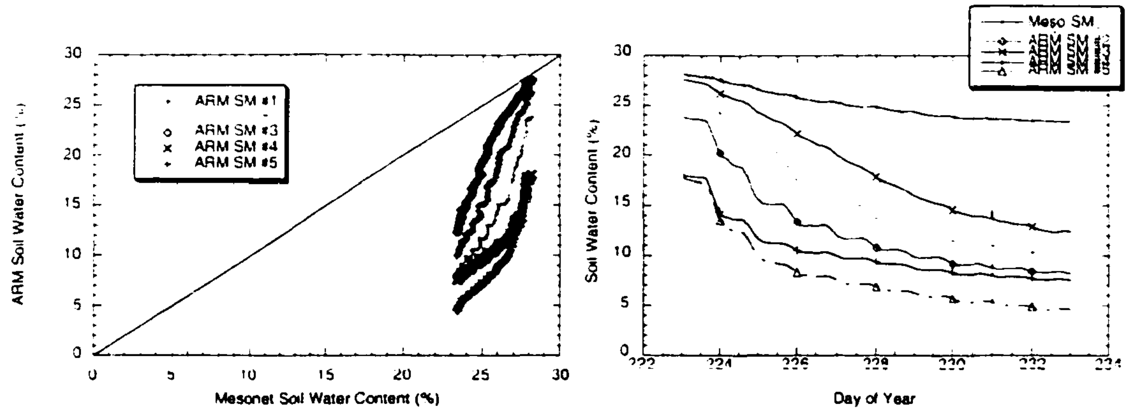

Figs. 6.10: Soil water content (%) as measured during 11 – 20 August 1999.

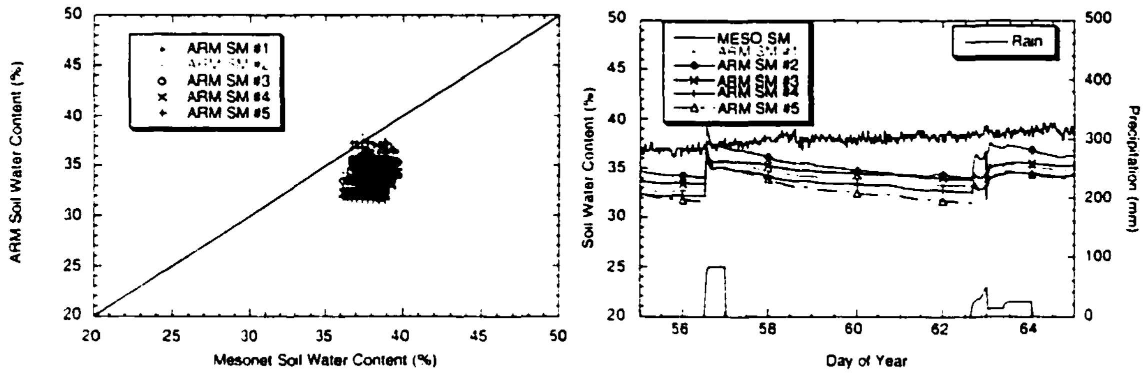

Figs. 6.11: Soil water content (%) as measured during 24 February to 4 March 2000.

period remained nearly saturated as a result of several rain events. Direct comparisons of data from the ARM and Mesonet sites are shown in Figures 6.10 and 6.11. Large differences are noted in the data from the ARM and Mesonet sites, particularly during dry conditions.

Beginning with DOY 223 in 1999, the soil water content ranged between 18 and 27% as measured by the ARM sensors; the Mesonet sensor estimated soil water content of 28%. However, 10 days later, the soil water content at the ARM site ranged between 5% and 12%; the Mesonet sensor still measured between 23 - 24%. It is possible that these differences are, in fact, real and that a distinct hydrologic difference exists between sites, because both sites are on sloped terrain. *Nevertheless, much uncertainty remains in the*

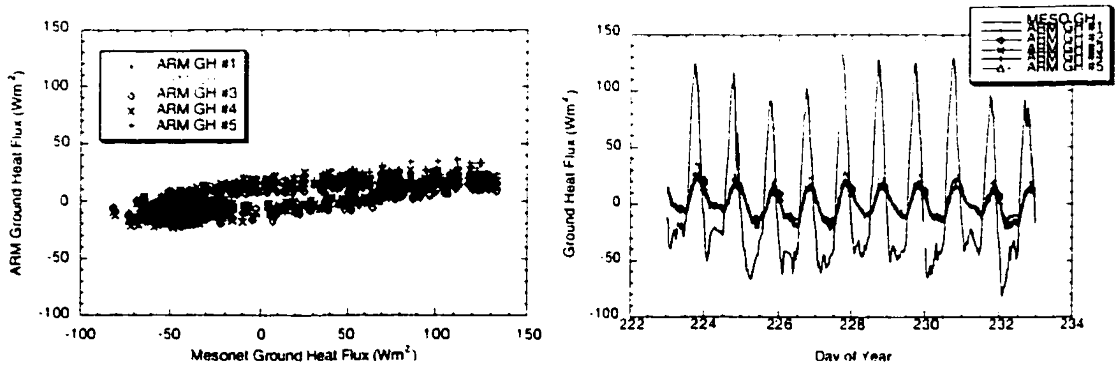

Figs. 6.12: Ground heat flux (Wm^{-2}) as measured during 11 – 20 August 1999.

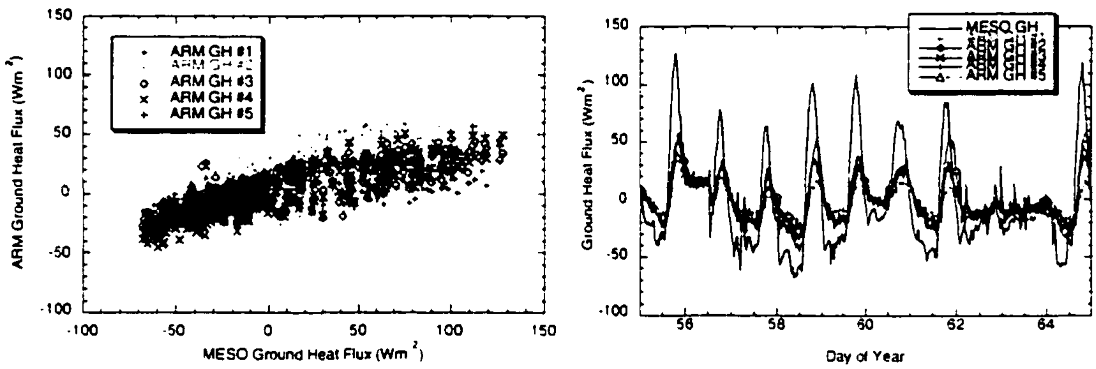

Figs. 6.13: Ground heat flux (Wm^{-2}) as measured during 24 February to 4 March 2000.

accuracy of the conversion method from soil water potential to soil water content (personal communication from K. Humes and J. Basara). Such large estimates of soil moisture from the Mesonet site "create" higher estimates of soil heat capacity when compared to data from ARM. As discussed by Lloyd et al. (1997), inhomogeneities in soil moisture alone can cause an under- or overestimate in energy closure.

The spring period remained saturated with soil water content ranging between 30% and 40% (Fig. 6.11). Although daily mean values of soil moisture from ARM and Mesonet were closer in value to each other than during August, the Mesonet observations did not respond as quickly to rain events as did the sensors from ARM. This circumstance

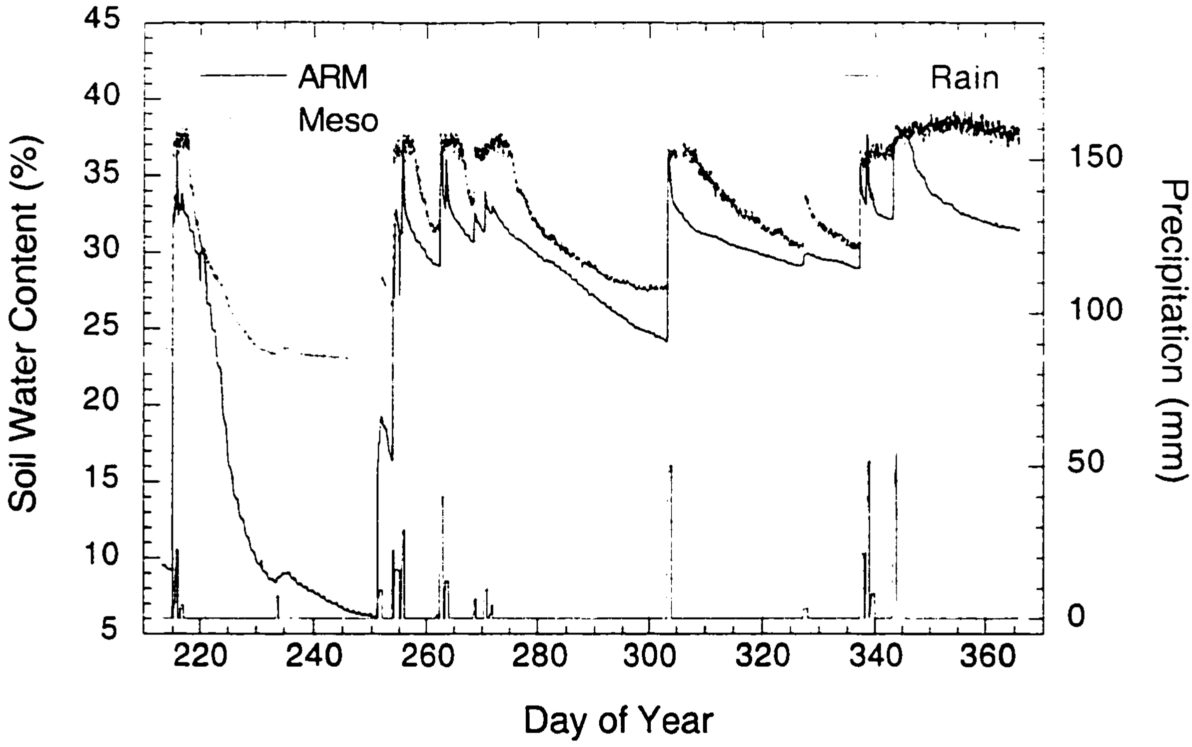

Fig. 6.14: Daily average values of soil water content as measured by ARM and the Mesonet. Thirty-minute data were collected during 1 August – 31 December 1999.

could result from the fact that the ARM sensors were buried at 2.5 cm while the Mesonet sensors were installed at a 5 cm depth. This slight difference in depths could account for this difference in sensitivity to rain events. In addition, variations in ground cover also could have had some impact.

To better understand the variability in soil moisture observations between the ARM and Mesonet sites, a five-month comparison of soil moisture was examined (Fig. 6.14). Data were collected between 1 August and 31 December 1999. With two exceptions, soil moisture values from the two sites compared relatively well. Large differences were noted during the dry August period (approximately DOY 220 – 250) and during the wet period of December (after DOY 340). Calibration differences among sensors are the most likely cause for differences in soil moisture values observed during August. However, the difference in installation depth may have created the differences observed during December.

The much shallower depth of 2.5 cm is more likely to dry quickly during the cool seasons than at lower depths.

The ground heat flux between sites was substantially different (Figs. 6.12 and 6.13). The ground flux estimated at the ARM site was approximately half that measured at the Mesonet site. The higher values of soil heat flow at the Mesonet site combined with the larger estimated values of soil water content produced a much greater value of ground heat flux versus the ground flux estimated at the ARM site. While differences in vegetation density and percentage of ground cover could have contributed to variation in measurements between sites, differences were not visually evident. Both sites made use of the REBS HFT-3.1 heat flux plate and both sets of sensors were installed at a depth of 5 cm. At the ARM site, the energy storage term was determined using the mean of five PRTDs and soil moisture. The energy storage term at the Mesonet site was estimated using the mean value of data from two PRTDs and the soil moisture sensor. It is worth noting again that when Mesonet estimates of soil heat flux are overestimated, the closure residual *increases*.

The estimated values of available energy at the ARM and Mesonet sites are shown in Figures 6.15 - 6.18 and summarized in Table 6.5. Using data from the ARM site, the available energy was calculated using measurements of net radiation from the Q*6.1 and using measurements from the more accurate SIRS. Likewise, the available energy at the Mesonet site was estimated using measurements from the CNR1 and SIRS radiometers. The comparison reveals that large values of ground flux from the Mesonet site versus small values of ground flux from the ARM site created available energy at the ARM site that was between 2 and 23% larger than estimates of available energy at the Mesonet site. The apparent underestimate of net radiation by the REBS sensor during February/March leads one to conclude that the actual difference in available energy as estimated by the two systems lies between 13 and 23%. Thus, if the available energy is underestimated at the Mesonet site, the residual of closure increases.

Table 6.5: Linear regression based upon available energy measured at the ARM and Mesonet sites during the August and February/March time periods.

	Independent variable	Dependent variable	Intercept	Slope	R^2
11 – 20 Aug 1999	$Rn_{,CNR1}-GH_{,Meso}$	$Rn_{,Q*6.1}-GH_{,ARM}$	-23.14	1.144	0.9893
	$Rn_{,CNR1}-GH_{,Meso}$	$Rn_{,SIRS}-GH_{,ARM}$	-43.43	1.208	0.9905
	$Rn_{,SIRS}-GH_{,Meso}$	$Rn_{,Q*6.1}-GH_{,ARM}$	-24.46	1.226	0.9944
	$Rn_{,SIRS}-GH_{,Meso}$	$Rn_{,SIRS}-GH_{,ARM}$	-44.71	1.293	0.9945
24 Feb – 4 Mar 2000	$Rn_{,CNR1}-GH_{,Meso}$	$Rn_{,Q*6.1}-GH_{,ARM}$	-7.87	1.018	0.9849
	$Rn_{,CNR1}-GH_{,Meso}$	$Rn_{,SIRS}-GH_{,ARM}$	-19.77	1.181	0.9832
	$Rn_{,SIRS}-GH_{,Meso}$	$Rn_{,Q*6.1}-GH_{,ARM}$	-2.30	1.018	0.9904
	$Rn_{,SIRS}-GH_{,Meso}$	$Rn_{,SIRS}-GH_{,ARM}$	-13.75	1.187	0.9929

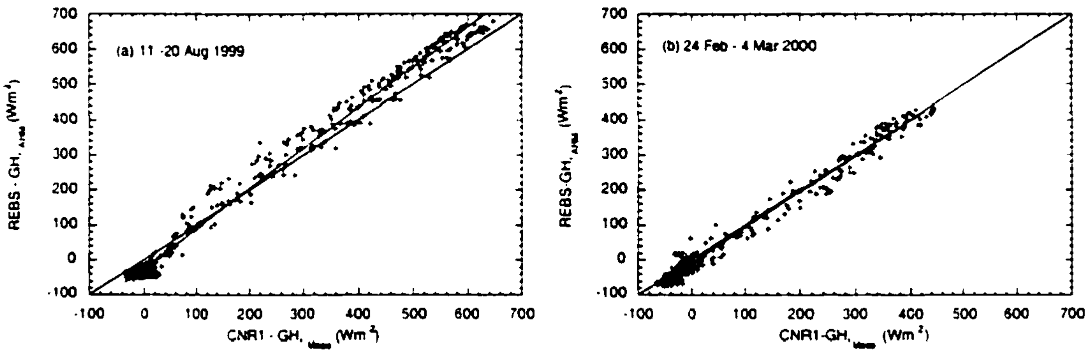

Fig. 6.15a-b: Estimated available energy (Rn – GH) at the ARM and Mesonet sites.

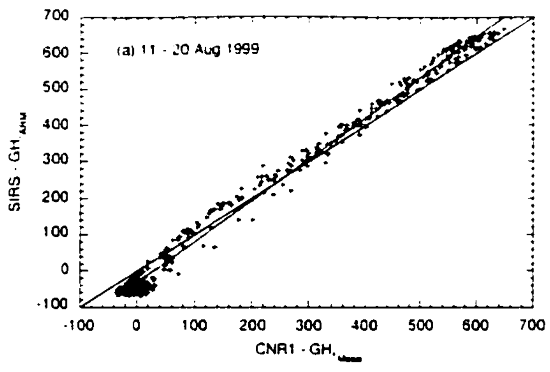

Fig. 6.16a-b: Estimated available energy (Rn - GH) except using the SIRS net radiometer instead of the REBS Q*6.1.

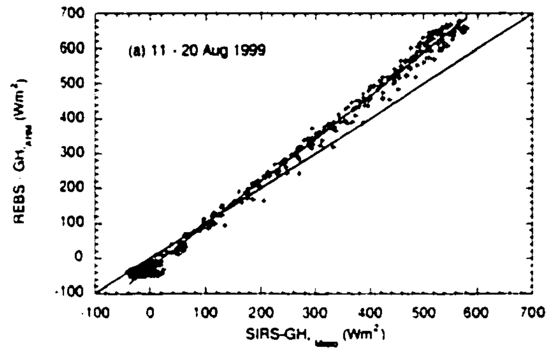

Fig. 6.17a-b: Estimated available energy except using the SIRS net radiometer instead of the CNR1.

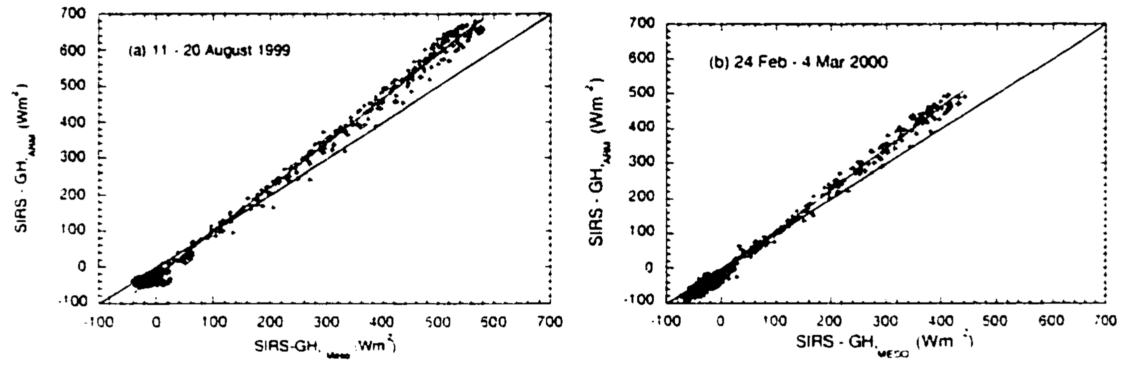

Fig. 6.18a-b: Estimated available energy except using the SIRS net radiometer instead of the CNR1 and Q*6.1.

Several questions remain. Do differences in available energy result from instrument error or from surface heterogeneity? Is it coincidental that differences in soil moisture correspond to significant differences in soil heat flow? Because of natural heterogeneity in surface properties, some variation was expected. Nevertheless, differences in available energy must be considered when the fluxes of sensible and latent heat are derived from different systems.

6.2.3 Sensible and Latent Heat Flux

Sensible and latent heat fluxes at the ARM site were calculated using the Bowen ratio technique (Eqs. 2.3 and 2.4). Sensible and latent heat fluxes at the Mesonet site were calculated using the methodology of Chapters 3, 4 and 5. All corrections were applied to the eddy correlation data unless otherwise stated. Days with rainfall were excluded from the data. In addition, Bowen ratio data were not used when $-2.0 < BR < -0.5$ because small vertical gradients in temperature and moisture occasionally create spuriously large flux estimates (Ohmura 1982).

Based upon sensible and latent fluxes calculated using data from the Mesonet and from ARM, the response of these fluxes to changing synoptic and land surface conditions was unexpected. Despite the hot and dry conditions which prevailed during August, the Bowen ratio remained very low (approximately 0.19). On the other hand, during the cool, wet winter and spring period of February/March, the Bowen ratio remained very high

Table 6.6: Surface parameters measured during 11 – 20 August 1999 and 24 February – 4 March 2000.

	Bowen ratio, Mesonet (ARM)	NDVI	Soil water potential (kPa)	Soil water content (%)
11 -20 Aug 1999	0.19 (0.08)	0.56	-233.37	25.1
24 Feb – 4 Mar 2000	2.52 (3.38)	0.19	-5.80	38.0

(approximately 2.52). In addition, soil moisture values during February/March were much higher than during August. Thus, values of the Bowen ratio were opposite to what might have been expected (see Table 6.6).

A comparison of the NDVI imagery during these two periods revealed the overwhelming factor that led to such differences in the BR. A wet and warm period during June and July of 1999 created a very "green" land cover during August despite the drying soil. Evapotranspiration (ET) was very large as revealed by the large estimates of latent flux (Fig. 6.19). However, the senescence of winter created small values of latent flux during February/March because ET was near zero. The strong correlation between ET and NDVI has important implications when one estimates fluxes across large regions using satellite imagery. Such studies warrant further investigation.

The primary goal of this section is to determine whether any of the fluxes from the eddy correlation methodology – either sensible or latent or both or neither – were underestimated assuming Bowen ratio fluxes measured by the EBBR system were correct. In Chapter 7 it is shown that $(Rn - GH)_{EC} > (SH+LH)_{EC}$. In Section 6.2.2 it was shown that $(Rn - GH)_{ARM} \geq (Rn - GH)_{MESO}$. To begin this determination, eddy correlation and Bowen ratio data were compared without any adjustments made to the net available energy. These results are listed in Table 6.7 and 6.8 and are shown in Figures 6.19 and 6.20. Next, the Bowen ratio data were recalculated assuming the net available energy measured using SIRS values for radiation. These results are listed in Tables 6.9 and 6.10 and Figures 6.21 and 6.22.

The EC and BR data during August revealed that the EC technique overestimated SH by 1.2% prior to EC corrections; after corrections, the difference increased to 12.5%. However, given the minimal values of sensible flux during August, the mean error was less than 20 Wm^{-2}. During February/March, the EC technique underestimated SH by about 5.0% (4.1%) prior to (after) corrections. In spite of the season, sensible heat flux increased to reach a daytime maximum of ~ 400 Wm^{-2}; the standard deviation of errors were less than 30 Wm^{-2}.

While SH flux differences between the two observing systems were relatively small, large discrepancies were observed in the measurement of latent heat flux. The EC method underestimated LH by 24.1% during August, even after all EC corrections were applied. During this period, LH was large and reached midday values of 550 Wm^{-2}. As a result, LH flux errors were as large as 230 Wm^{-2}.

Much smaller values of LH occurred during February/March (generally < 100 Wm^{-2}). These low values led to more variable results in latent flux. The EC technique underestimated LH by 6.1% prior to applying corrections but overestimated LH by 21.5% after corrections were applied.

Several caveats should be mentioned. First, the krypton hygrometer was not regularly cleaned prior to 11 January 2000. Thus, some uncertainty exists as to the accuracy of the LH estimate prior to this time. Ultraviolet radiation emanating from the KH20 reacts with atmospheric constituents to form a residue on the windows of the sensor. This reaction is known as "scaling" and can lead to calibration changes as large as 8% (Tanner 1988). However, changes in calibration only affect the mean values of moisture and do not affect the variance of moisture. The latent flux is estimated from the variance about the mean. The scaling problem is corrected simply by wiping the sensor windows clean. The OASIS Project has volunteers at each of the ten super sites who regularly clean the hygrometers once every two weeks. While scaling does not mean a measurement is incorrect or inaccurate, scaling can lead to much greater variance and noise in the data. To address this question, a one-year long data set of ARM and Mesonet fluxes was examined (see Section 6.4). An attempt was made to quantify the improvement in LH flux after routine cleaning of the sensor became established. However, little difference was noted in the quality of the data before and after the sensor was cleaned.

The substantial differences between data from the REBS Q*6.1 and from the assumed-to-be more accurate SIRS system raised questions about the accuracy of BR fluxes. Differences between the two observing systems ranged between an underestimate

Table 6.7: Comparison of the ARM Bowen ratio and Mesonet eddy correlation estimates of sensible (SH) and latent heat (LH) with and without corrections (corr.) applied. All estimates using ARM data were based upon estimates of net radiation from the REBS sensor.

	Variable (ARM –Meso)	Mean diff, X (Wm^{-2})	Std. Dev. σ (Wm^{-2})	Sample size, n
11 – 20 Aug 1999				
	SH, no corr	-9.2	23.3	450
	SH, all corr	-16.1	22.4	373
	LH, no corr	53.0	65.4	450
	LH, all corr	39.3	47.5	373
24 Feb – 4 Mar 2000				
	SH, no corr	1.7	27.3	446
	SH, all corr	2.5	23.9	399
	LH, no corr	1.0	19.8	403
	LH, all corr	-5.3	19.7	393

Table 6.8: Linear regression based upon sensible and latent heat fluxes from the ARM and Mesonet sites (with and without sonic corrections applied). Mesonet data were assumed to be the independent data (x) and ARM data were assumed to be the dependent (y) data.

	Variable	Intercept	Slope	R^2
11 – 20 Aug 1999	SH, no corr	-8.76	0.988	0.898
	SH, all corr	-11.83	0.875	0.916
	LH, no corr	9.25	1.364	0.944
	LH, all corr	6.38	1.241	0.974
24 Feb – 4 Mar 2000	SH, no corr	0.43	1.050	0.973
	SH, all corr	0.42	1.041	0.971
	LH, no corr	-0.17	1.061	0.709
	LH, all corr	0.39	0.785	0.756

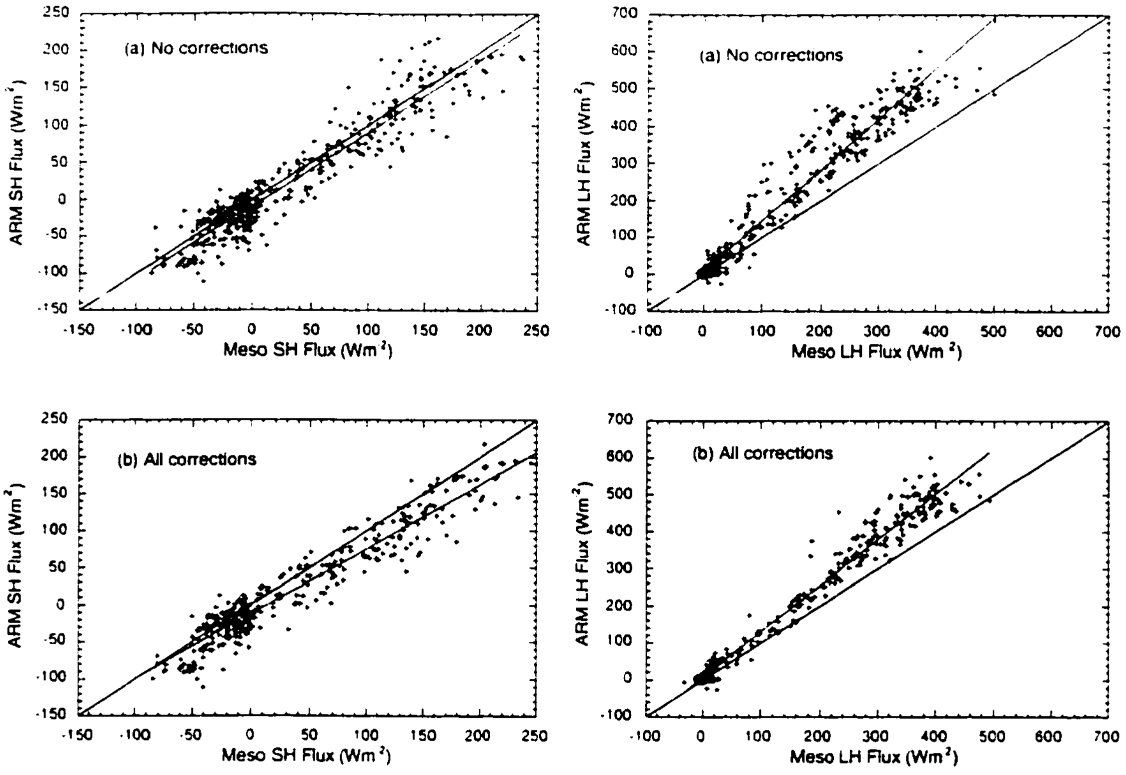

Figs. 6.19: Sensible and latent heat flux estimated during 11 – 20 August 1999 (with and without sonic corrections).

of 5.5% by the Q*6.1 during August to an underestimate of 14.2% during February/March. Assuming the SIRS system produced the most accurate data, estimates using SIRS data were substituted for the Q*6.1 estimates to calculate SH and LH fluxes at the ARM site. The BR flux estimates were multiplied by the ratio $(Rn_{SIRS}\text{-}GH)/(Rn_{REBS}\text{-}GH)$ to adjust the available energy to a more correct value. Results are listed in Tables 6.9 and 6.10 and shown in Figures 6.21 and 6.22.

The larger estimates of net radiation by SIRS increased the BR flux estimates of SH and LH particularly during the February/March period. Sensible flux differences between the ARM and Mesonet systems improved to 1.8% (14.1%) with (without) corrections during August, but worsened during the February/March period to 23.1% (23.5%) with (without) corrections. Latent flux differences improved slightly during August to 23.6% (35.9%) and to -11.0% (+53.5%) with (without) corrections during the February/March period.

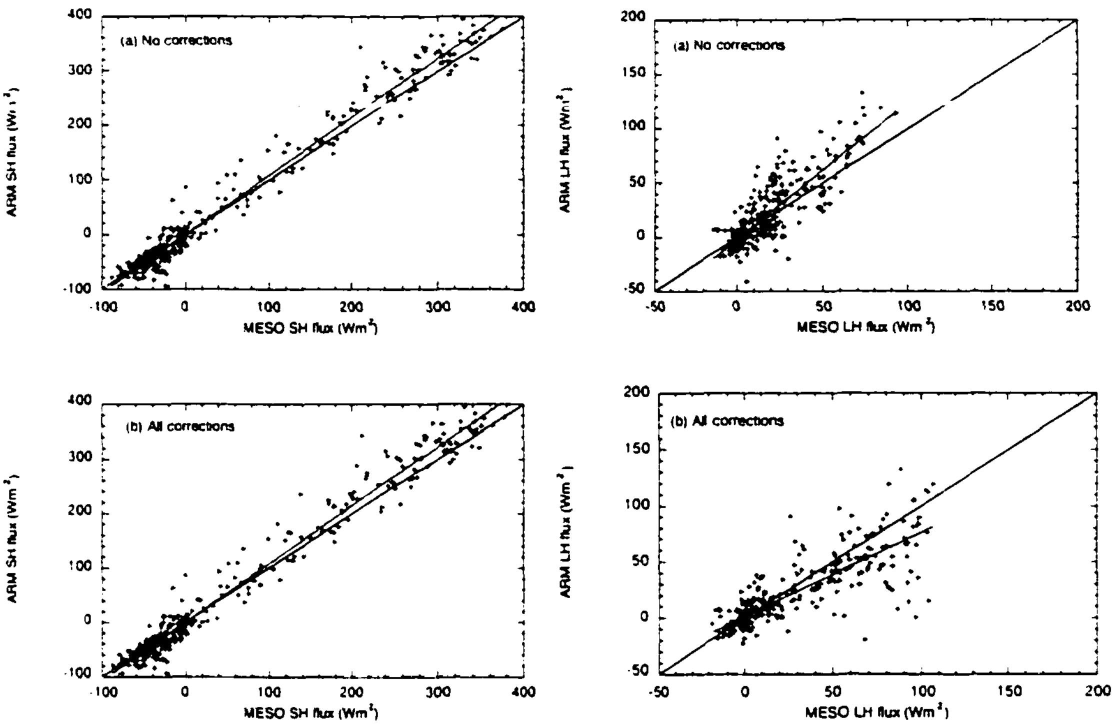

Figs. 6.20: Sensible and latent heat flux estimated during the period of 24 February and 4 March 2000 (with and without sonic corrections).

Table 6.9: Comparison of the ARM Bowen ratio and Mesonet eddy correlation estimates of sensible (SH) and latent heat (LH) with and without corrections (corr.) applied. This data have been adjusted using SIRS net radiation instead of REBS net radiation.

	ARM (y) - MESO (x)	Mean diff, X (Wm^{-2})	Std. Dev. σ (Wm^{-2})	Sample size, n
11 - 20 Aug 1999				
	SH, no corr	-18.3	34.7	450
	SH, all corr	-25.5	31.2	373
	LH, no corr	59.0	66.3	450
	LH, all corr	46.1	49.8	373
24 Feb – 4 Mar 2000				
	SH, no corr	2.4	40.8	374
	SH, all corr	1.7	40.4	372
	LH, no corr	3.7	20.5	375
	LH, all corr	- 3.4	20.7	372

Table 6.10: Linear regression based upon sensible and latent heat fluxes from the ARM and Mesonet sites (with and without sonic corrections applied). Mesonet data were assumed to be the independent data (x), and ARM data were assumed to be the dependent (y) data. ARM data have been adjusted using SIRS net radiation instead of REBS net radiation.

	Variable	Intercept	Slope	R^2
11 – 20 Aug 1999	SH, no corr	-22.31	1.141	0.852
	SH, all corr	-26.06	1.018	0.862
	LH, no corr	15.82	1.359	0.939
	LH, all corr	13.88	1.236	0.967
24 Feb – 4 Mar 2000	SH, no corr	-8.51	1.235	0.971
	SH, all corr	-9.20	1.231	0.972
	LH, no corr	-4.25	1.535	0.739
	LH, all corr	-1.02	0.890	0.655

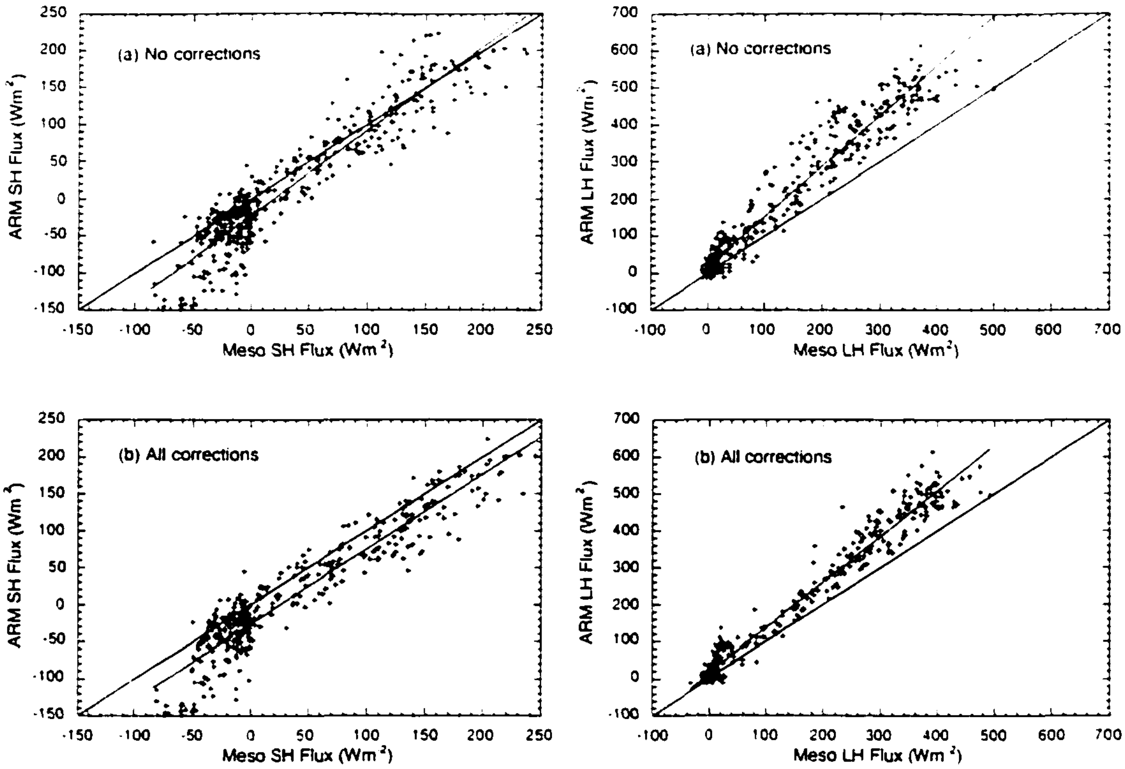

Figs. 6.21: Sensible and latent heat flux estimated during 11 – 20 August 1999 (with and without sonic corrections) substituting data from the SIRS system in place of data from the Q*6.1 system.

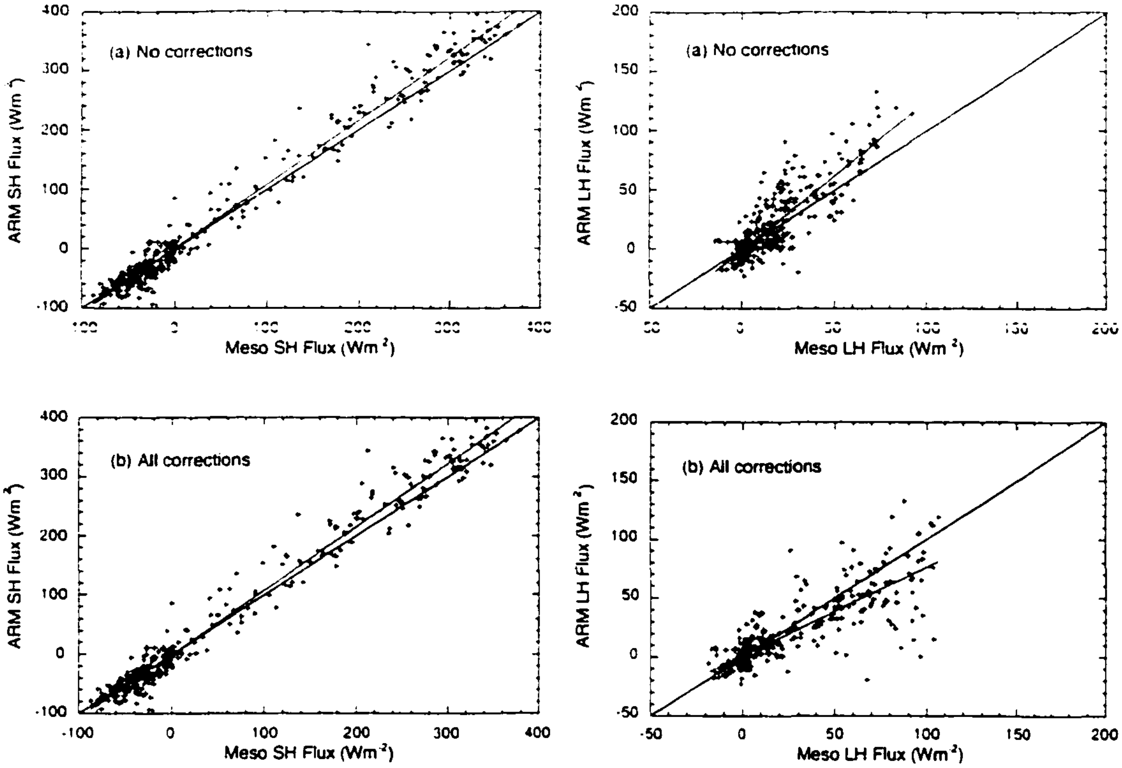

Figs. 6.22: Sensible and latent heat flux estimated during 24 February – 4 March 2000 (with and without sonic corrections) substituting data from the SIRS system in place of data from the Q*6.1 system.

6.3 Closure at the Foraker Mesonet site

Closure of the energy budget was investigated at the Foraker Mesonet site during the August and February/March periods. A detailed examination of the closure issue yields greater insight into the evaluation of the EC and Bowen ratio methods and provides clues to the errors associated with each component of the energy budget. Estimates of closure were computed for each set of 30-minute observations. All data from days when rain occurred were excluded from further analysis. Data also were excluded if (Rn-GH) < 50 Wm^{-2} or if (SH+LH) < 50 Wm^{-2} as small values of flux creates spuriously large percentages of closure. Statistics of closure from the data are listed in Table 6.11.

Table 6.11: Mean closure rates for the Foraker Mesonet site during 11 – 20 August 1999 and 24 February – 4 March 2000.

		Mean closure (%)	Std Dev (%)	Sample size, n (# 30 –min obs)
11 – 20 Aug 1999				
	CNR1, no corr	81.9	16.6	214
	CNR1, all corr	94.7	13.3	178
	SIRS, no corr	83.2	15.7	214
	SIRS, all corr	96.1	13.0	178
24 Feb – 4 Mar 2000				
	CNR1, no corr	87.7	11.4	132
	CNR1, all corr	97.4	13.9	132
	SIRS, no corr	91.9	16.5	129
	SIRS, all corr	102.1	19.4	129

The corrections described in Chapter 4 were applied to the data set obtained from the Foraker site. The corrections include those developed by Stull (1988) and Schotanus et al. (1983) for sensible flux and those developed by Webb et al. (1980) and (Tanner et al. 1993) for latent flux. The tilt correction to account for terrain slope also was included. In addition, data were excluded when winds were from the north (330° – 30°) because the sonic anemometer and the krypton hygrometer are mounted south of the tower. According to Dyer (1981) and Dyer et al. (1983), flow distortion from north winds significantly reduces the measured covariance of flux. When plotted as a function of wind direction, closure is reduced significantly when winds are from the north (Figs. 6.23a-b). In this situation, sensible and/or latent fluxes were underestimated due to flow distortion created by the tower.

Closure rates when estimated using the CNR1 ranged from 94.7% during August to 97.4% during the February/March after corrections were applied. After including all corrections, closure improved significantly by nearly 13% during August and nearly 10% during February/March. Because of differences in net radiation between the two four-component systems, closure was recalculated using the SIRS data instead of the CNR1 data. Closure improved by 1.4% and 4.7% during the respective periods. Even so, these results do not prove that the SIRS system is more accurate than the CNR1. Only if other components of the energy budget could be assumed to be accurate could the SIRS system be superior in accuracy to the CNR1. Nevertheless, such differences account for variation in closure estimates.

Despite the high estimates of mean closure in Table 6.11, the standard deviation of the observations remained between 10% and 20%. To explain this variability and using SIRS net radiation, the diurnal mean of closure was plotted at monthly intervals for the period September 1999 through May 2000. (The krypton hygrometer was out of order during November through January, and so no closure estimates could be computed during this time.) A strong diurnal dependence is evident (Figs. 6.36a-f). Early morning periods appear to have minimal closure. However, closure reaches its maximum at midday before decreasing during the late afternoon. Barr et al. (1994) detected a similar diurnal pattern in closure.

The diurnal dependence of closure errors is not unexpected (Barr et al. 1994). It has been suggested that closure rates should be at their minimum values prior to mixing of

Table 6.12: Daily-averaged value of closure at the Foraker Mesonet site during 11-20 August 1999 and 24 February – 4 March 2000.

		Mean closure (%)	Std Dev (%)	Sample size, n
Aug 11 – 20 1999				
	CNR1, no corr	83.0	5.8	8
	CNR1, all corr	89.5	7.5	6
	SIRS, no corr	87.9	5.9	8
	SIRS, all corr	94.6	8.0	6
24 Feb – 4 Mar 2000				
	CNR1, no corr	84.2	5.0	7
	CNR1, all corr	94.7	7.5	7
	SIRS, no corr	90.2	5.9	7
	SIRS, all corr	101.5	8.2	7

the boundary layer during the early to mid-morning hours. This then suggests the question- does closure improve when averaged over longer time periods? To address this question, mean closure was computed using 24-hour totals of the four components. Data were excluded when 5 or more observations were missing or failed quality assurance routines. Data also were excluded during days with rainfall (e.g., DOY 56, 62, and 63) and during periods of northerly winds (e.g., DOY 225 and 231). The statistics of closure are listed in Table 6.12 and are shown in Figures 6.24a-b.

Daily averaged estimates of closure varied slightly from those computed using the 30-minute observations. Closure estimates improved during the February/March period versus during the August period. Sonic corrections increased closure by approximately 6% during August and by 11% during February/March. Use of SIRS data improved closure an additional 5% during August and by almost 7% during February/March. Although closure rates near 100% are ideal, day-to-day variations are large and are difficult to explain.

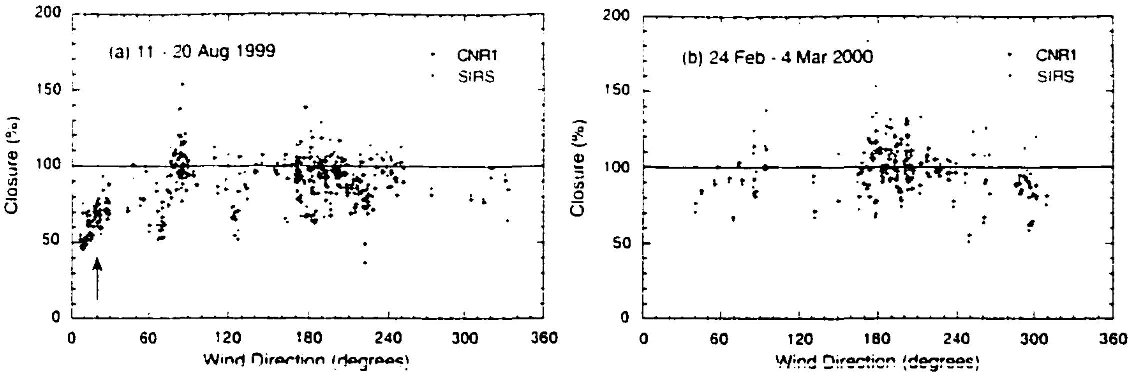

Figs. 6.23a-b: Closure estimated as a function of wind direction. When the winds were northerly (330° – 30°), closure of the surface energy budget decreased significantly.

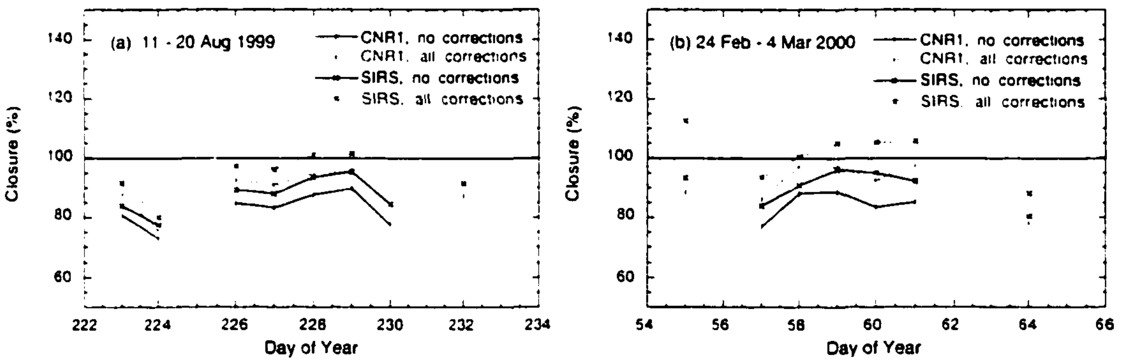

Figs. 6.24a-b: Daily mean closure estimated using 24-hour totals of components in the energy budget.

6.4 The EC and BR Systems – A One Year Comparison

The ARM-Mesonet comparison reveals that closure varies widely during the day. The accuracy of the various net radiation sensors varied as a function of the time of day (e.g., Figs. 6.3a versus 6.5a). Significant differences (> 40 Wm^{-2}), which varied with the diurnal cycle, were observed in the ground heat flux between the ARM and Mesonet sites (Figs. 6.10 and 6.13). Thus, daily averaged values of closure yielded the most consistent estimates. Fortunately, daily totals of components in the energy budget have been found to be important for climatological and hydrological applications (Shuttleworth 1991).

Long-term trends in flux measurements should yield unique insights into the closure problem. Because previous field experiments have been limited to a few days or weeks (Table 2.1), seasonal variations have rarely been observed. Only one example has been documented (Barr et al. 1994). Nevertheless, large-scale changes in vegetation and surface wetness occur during the year, which could create an opportunity to improve our understanding of the closure problem. For instance, if errors with closure were only associated with the latent heat flux, annual trends in closure could be linked to changes in the measured Bowen ratio, soil moisture, rainfall, and Normalized Difference Vegetation Index (NDVI).

A year-long data set from the ARM and Mesonet sites at Foraker was examined. Net radiation, ground, sensible and latent heat fluxes were summed to produce daily totals in MJ m^{-2} day^{-1}. Thirty-minute data were used; if more than 4 of the 48 observations were missing, that day of data was excluded. In this situation, missing data were interpolated to complete the time series.

The annual mean difference of net radiation between the two observing systems was within 0.5 MJ m^{-2} day^{-1} (as shown in Table 6.13 and Fig. 6.25). The trends of net radiation remained constant throughout the year (Fig. 6.26). The remarkable stability of these observing systems increased our confidence in the OASIS measurement of net

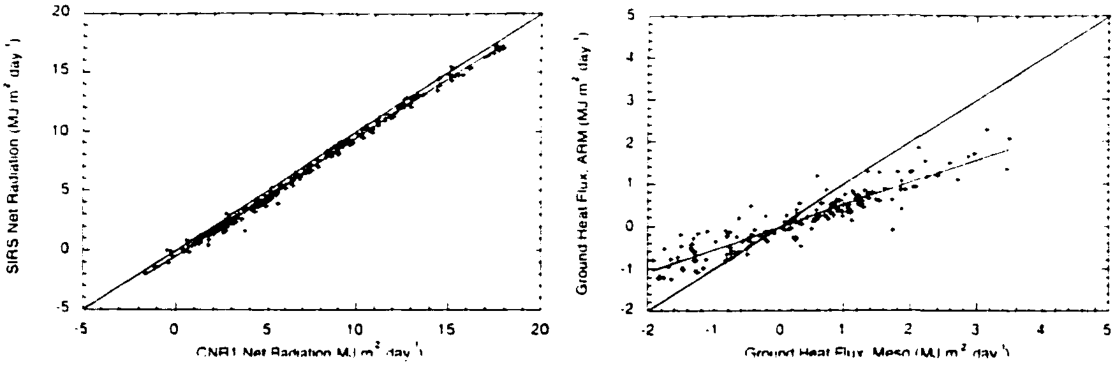

Figs. 6.25: Daily totals of net radiation and ground heat flux collected between 1 June 1999 and 31 May 2000.

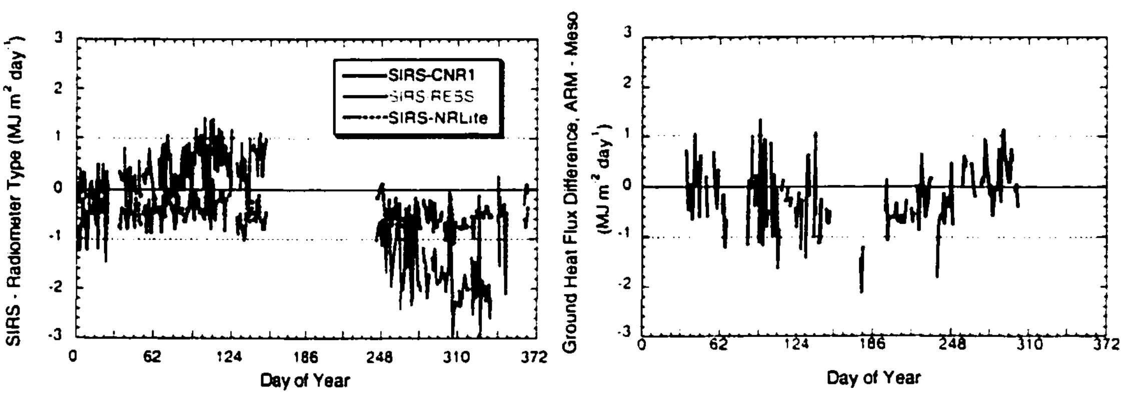

Figs. 6.26: Differences in net radiation and ground heat flux between the ARM and Mesonet sites during an annual cycle.

Table 6.13: Differences in measurement of net radiation, ground heat, sensible heat, and latent heat fluxes between ARM and Mesonet systems (1 June 1999 – 31 May 2000).

All units: MJ m^{-2} day^{-1} unless otherwise noted.		X	σ	n (days)	Min Diff	Max Diff
Net radiation	SIRS - CNR1	-0.501	0.307	233	-2.10	0.48
	SIRS - REBS	-0.413	1.090	228	-2.94	1.41
	SIRS - NR-Lite	-0.458	0.280	114	-1.06	0.32
Ground heat	ARM - Meso	-0.211	0.639	167	-2.12	1.32
Sensible heat	ARM/SIRS - Meso	0.951	1.477	87	-1.26	5.42
	ARM/REBS - Meso	0.681	1.330	130	-2.06	4.92
Latent heat	ARM/SIRS - Meso	-0.607	1.292	80	-3.92	2.39
	ARM/REBS - Meso	0.169	1.805	121	-4.03	4.96

radiation.

Based upon an examination of closure results using radiometer data from the Q*6.1 and NR-Lite radiometers (Table 6.13), mean differences compared to the SIRS averaged less than 0.5 MJ m^{-2} day^{-1}. However, long-term variations were noted. Annual trends from each system revealed significant errors (Fig. 6.26). The trend in results based upon the REBS measurement was significant, decreasing from a difference of approximately -1.0 MJ m^{-2} day^{-1} in September to nearly -2.5 MJ m^{-2} day^{-1} by November. A dome replacement during December and a calibration correction appears to have corrected the difference based upon the Q*6.1 and SIRS systems. However, results based upon the REBS and SIRS diverged again from near 0 MJ m^{-2} day^{-1} during January to +0.5 MJ m^{-2} day^{-1} by May. Differences in results obtained using data from the NR-Lite and SIRS remained constant throughout the year; this comparison had the smallest standard deviation of difference from the SIRS (Table 6.13). One problem, perhaps dust on the sensor, created divergence between sensor observations during DOY 220 - 250. Sensor measurements converged following a heavy rain event (see Section 6.2.1).

Ground heat fluxes between the ARM and Mesonet sites (Fig. 6.25) revealed large amplitudes in the daily ground flux observed by the Mesonet. When the true ground flux is at a minimum, the residual of closure increases. The annual mean difference in ground heat flux between the ARM and Mesonet sites varied by -0.211 MJ m^{-2} day^{-1} (Table 6.13). However, the annual cycle reveals a trend (Fig. 6.26). Differences are at a maximum during the summer months and appear related to the increase of net radiation. These differences could be real and may represent heterogeneity at the site. The ground flux estimates are consistent with the fact that the Mesonet site is sparsely vegetated and has more bare soil than does the ARM site. Such heterogeneity at a site could limit the accuracy of closure.

Daily-averaged values of sensible and latent heat flux also were compared. The sensible and latent fluxes were estimated by the Bowen ratio system of ARM using the net radiation acquired by the Q*6.1 and recalculated using data from the 4-component SIRS. A comparison of estimates from the Mesonet and ARM is shown in Figure 6.27a-b. Net radiation from SIRS did not become available until I September 1999. Thus, fluxes could not be recalculated during July and August, a period when latent heat flux was at its largest value during the annual period.

Differences were examined (Fig. 6.28) in the sensible and latent heat flux during an annual cycle at the ARM and Mesonet sites. Sensible heat flux differed the most during spring months, at a time when the Mesonet underestimated SH relative to values obtained at the ARM site. However, during the same period, the Mesonet overestimated latent heat flux relative to ARM. Thus, the sum of (SH + LH) was similar at both sites. It is the ratio of these fluxes, which produced different measurements. Closure estimates from the EC method were ~100% during the spring, which increased our confidence in measurements from the Mesonet. In estimating the Bowen ratio, it appears that the ARM system favored SH flux, while the Mesonet favored LH flux.

Large differences in latent heat flux were observed during the autumn period. The Mesonet underestimated latent flux by as much as 4 MJ m^{-2} day^{-1} relative to values produced at ARM, and unlike the spring period, closure estimates were at their minimum values of the year. Values of sensible flux were small. Thus, differences in SH measured by both systems remained small. A period between DOY 200 – 250 coincided with very dry conditions but large values of latent flux resulted from large values of greenness or NDVI. As the soil dried during the period, LH fluxes declined, and closure improved. By DOY 250 closure estimates were ~ 100%.

Differences between the net available energy and aerodynamic fluxes using data from both sites are shown in Figure 6.29a-b. Note that the difference in values of the

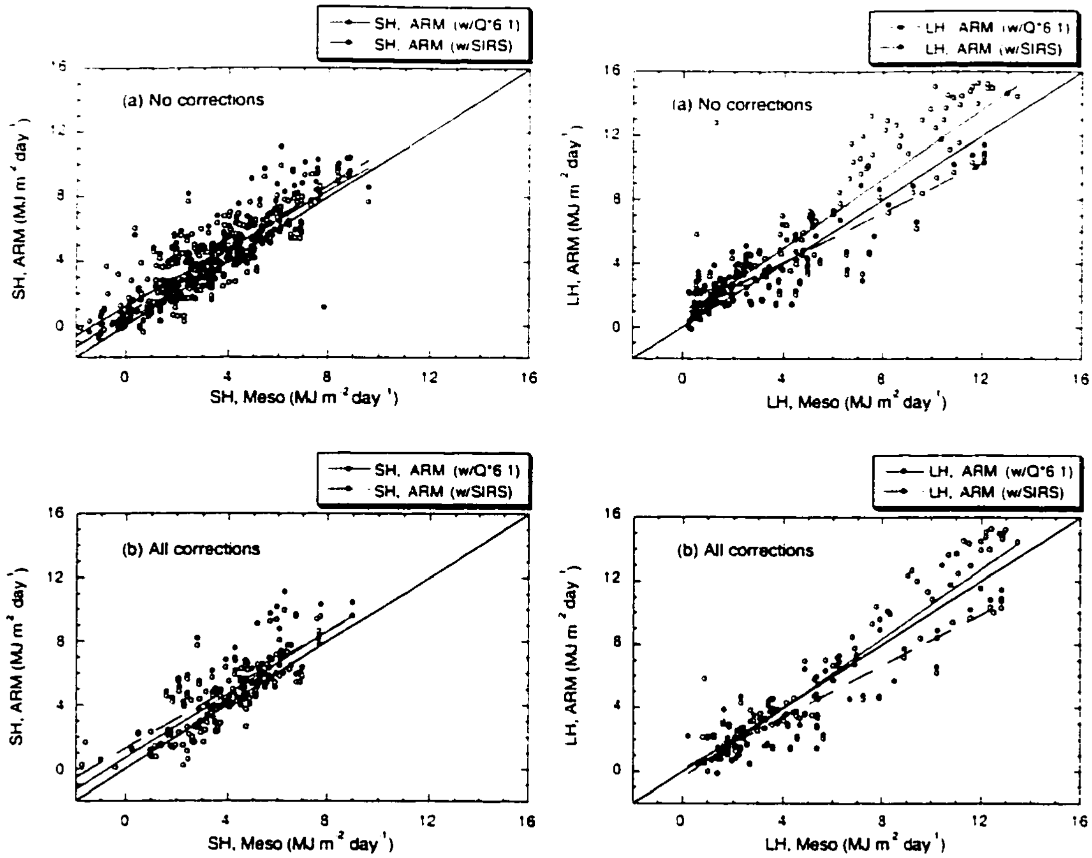

Figs. 6.27: Daily totals of sensible and latent heat collected between 1 June 1999 and 31 May 2000 as estimated at the ARM and Mesonet sites (with and without corrections).

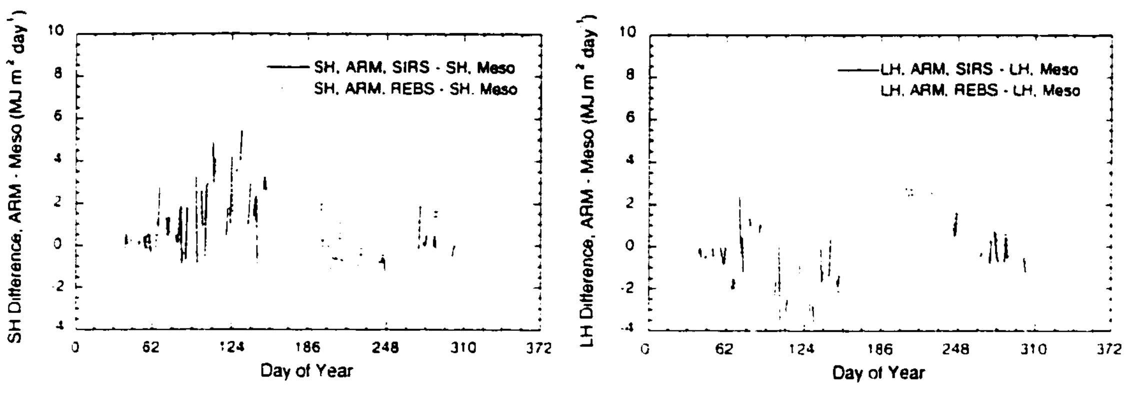

Figs. 6.28: Differences in sensible and latent heat fluxes during an annual cycle at the ARM and Mesonet sites.

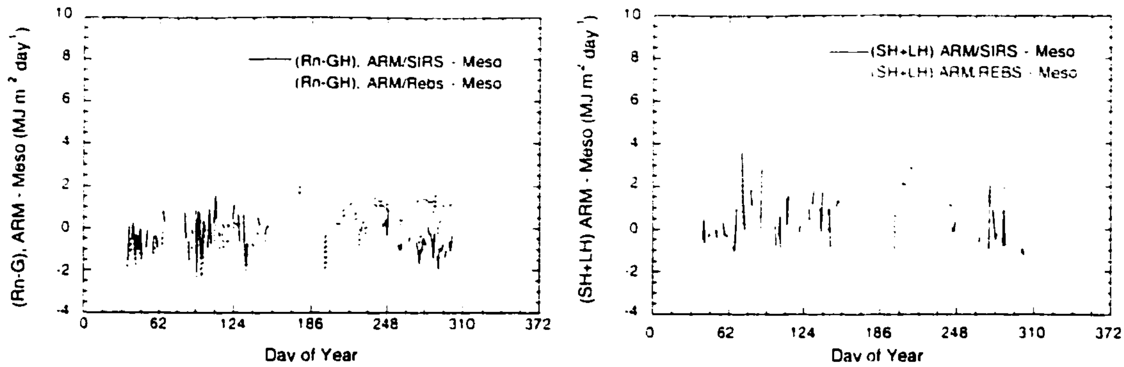

Fig. 6.29: Differences in sensible and latent heat fluxes during an annual cycle at the ARM and Mesonet sites.

available energy between the two sites was ~ +/- 1.0 MJ m^{-2} day^{-1} throughout the year. On the other hand, the difference in aerodynamic fluxes obtained by both systems varied as a function of the available energy and with changes of season.

An examination of daily estimates of closure at the Mesonet site at Foraker reflects the differences in observations between the ARM and Mesonet sites (Figs. 6.29 and 6.30). The percentage of closure, which seemed to be a function of the available energy, decreased to minimum values during the summer months. Closure estimated as a residual also shows a similar annual cycle and primarily reflects differences observed between the aerodynamic terms. Note that the residual appears to be inversely proportional to the Bowen ratio (Fig. 6.31a). To determine better the relationship between closure and the Bowen ratio, daily closure rates were plotted as a function of Bowen ratio (Fig. 6.31b). A systematic decrease in closure was noted when the BR < 1.0. However, when the BR > 1.0, a rather large variance in closure about 100% was observed. Although closure rates declined systematically with increasing moisture, other influences such as terrain and fetch appeared to adversely affect closure as well.

As differences between the ARM and Mesonet observations decreased, closure rates improved (Fig. 6.32). This improved closure was expected because the Bowen ratio

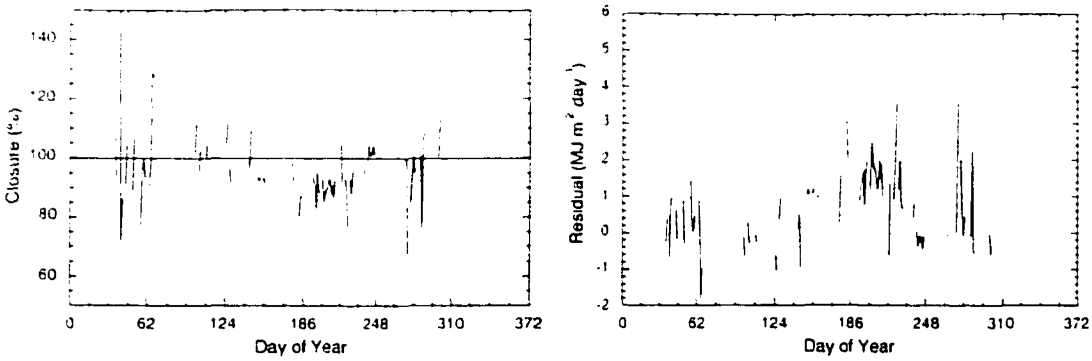

Fig. 6.30: Closure (%) and residual (MJ m^{-2} day^{-1}) of the energy balance plotted as a function of the day of the year.

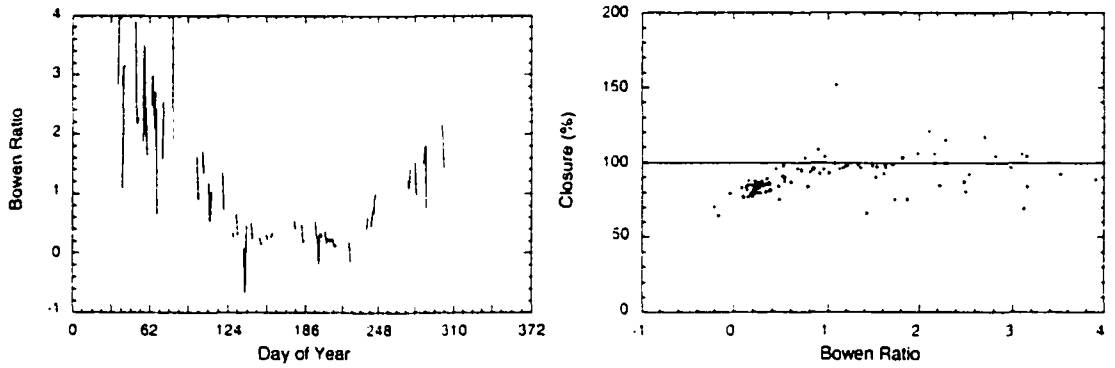

Fig. 6.31: a) Bowen ratio as a function of time of day. b) Closure as a function of daily estimates of Bowen ratio.

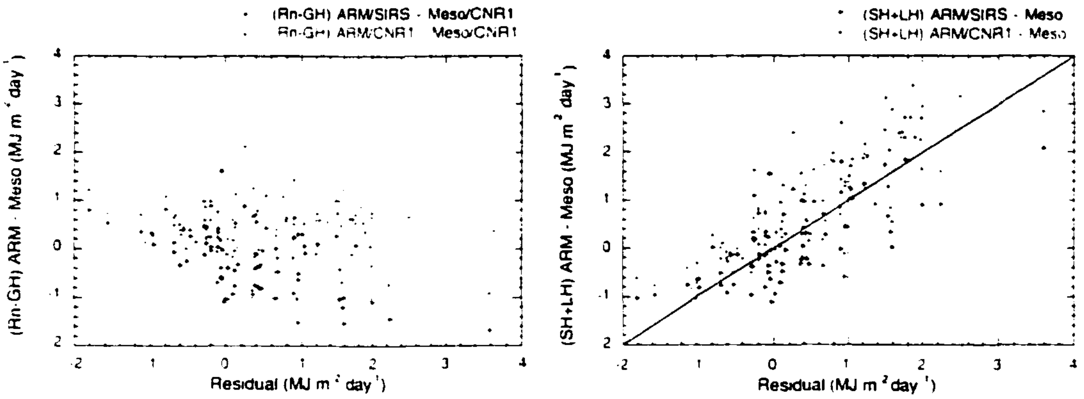

Fig. 6.32: Residuals of the energy budget as a function of difference between the ARM and Mesonet systems.

method forces closure, but an examination of the differences in observations allows for specific errors in closure to be identified better. Note that data from the SIRS were not available during much of the summer period when the residual of closure was at its largest value. For this reason, the ARM estimates of closure were recomputed using data from the CNR1.

An analysis of the site differences as a function of the closure residual shows that the error due to the measured available energies is generally limited to +/- 1 MJ m^{-2} day^{-1}. Thus, the lack of closure at the Foraker Mesonet site cannot be explained by the available energy when differences between the observing systems are greater than +/-1 MJ m^{-2} day^{-1}. In other words, because differences in the available energy are limited to +/-1 MJ m^{-2} day^{-1}, only those days when the residual of closure is less than 1 MJ m^{-2} day^{-1} can a lack of closure be explained. For those days when the residual of closure was greater than 1 MJ m^{-2} day^{-1}, the observation problem lies either with an underestimate in sensible heat or latent heat, or a combination of both.

A similar examination of the aerodynamic fluxes as a function of the closure residual shows errors as large as 4 MJ m^{-2} day^{-1}. Linear regression of the data revealed a minimal relationship between differences in net radiation versus closure (R^2 = 0.292). However, linear regression of the difference within the aerodynamic fluxes versus closure supported a much stronger correlation of 0.710 (0.451) when the CNR1 (SIRS) was used.

Diurnal averaging of the sensible and latent fluxes from the ARM and Mesonet sites could yield new insight into which component of the energy budget remains in error when closure fails. Assuming the difference between the Bowen ratio and eddy correlation approaches to energy balance can be linked with failure to close the energy budget, examining differences between individual components of sensible and latent flux produced by the observing systems may conclusively identify which components are in error.

The net radiation, ground heat, sensible and latent heat fluxes were averaged on a diurnal basis for each month during the period from 1 September 1999 through 31 May 2000. The krypton hygrometer at Foraker did not operate during 29 October 1999 to 3 February 2000, and so data was excluded during this period. All ARM data were excluded when the Bowen ratio was between –0.5 and –2.0 as large spurious fluxes could result (Ohmura 1982). All EC data were quality assured as described in previous sections.

First, net radiation from the 4-component radiometers and ground heat flux from both ARM and Mesonet sites (Fig. 6.33a-f) were averaged on a monthly basis. Little change is noted during the 9-month period. Daily difference in net radiation between the CNR1 and SIRS changed little during the year as shown in Figure 6.26.

Greater daytime differences between observing systems were observed in the ground heat flux. In fact, little correlation existed between ground flux estimates produced by the two observing systems (ARM and Mesonet). The Mesonet estimates of ground flux reach a maximum value near midday while ARM estimates of ground flux achieve a broad peak near dusk. At the ARM site, the maximum amplitude is less than 50 Wm^{-2}. Greater (more positive) values of ground flux at the ARM site during the night create daily differences of +/- 1 MJ m^{-2} between the ARM and Mesonet systems (Fig. 6.26). Together, the greater midday estimates of net radiation at the Mesonet site combined with much larger estimates of ground flux to yield lower daily-averaged values of available energy when compared to similar estimates from ARM.

Next, the sensible and latent fluxes (Figs. 6.34 – 6.35) were estimated at the ARM and Mesonet sites. To minimize errors created by differences in the measurement of available energy, the BR fluxes measured by ARM were rescaled according to the available energy from the Mesonet. In this manner, all relative differences between observing systems could be attributed to the measurement of the sensible and latent fluxes.

The diurnal cycles of sensible and latent heat were averaged on a monthly basis at the Mesonet and ARM sites (Figs. 6.34 – 6.35). Differences between observing systems versus closure rates (Figs. 6.36a-f) revealed several trends. First, sensible heat fluxes during the daytime were underestimated by the EC method compared to the BR method during five of the six months. On the other hand, latent heat fluxes were overestimated by the EC method compared to the BR method during the same five months. Only during September was the situation reversed when the EC method overestimated sensible flux and underestimated latent flux. This result is surprising because either (a) real differences exist between the two observing sites, or (b) the BR system overestimates the Bowen ratio, or (c) the EC system underestimates the Bowen ratio. The monthly-averaged Bowen ratios estimated from the EC and BR methods (Figs. 6.37a-f) clearly indicate strong diurnal patterns.

Measured differences in soil water content and soil heat flow indicate actual differences in the energy budget at the two sites. A lower Bowen ratio is expected over the wet soil observed at the Mesonet site; likewise, a higher Bowen ratio is expected over the drier soil at the ARM site. If surface heterogeneity exists across an area of less than 100 m in width, the accurate measurement and modeling of the surface budget across a heterogeneous landscape could be impossible to achieve. In fact, if such heterogeneity exists, then measurement from a single tower is not representative of a larger scale region.

Tanner (1988) demonstrated how changes in surface properties upwind of an observing site create significant differences in Bowen ratio with height. Tanner mounted two sonic systems 4 m apart at a height of 1.35 m AGL. The ground surface directly beneath his sensors was wheat stubble; however, a soybean field was upwind of his site. The two sonic systems measured nearly the same Bowen ratio. On the third day of data collection, one of the sonic systems was lowered to a height of 0.9 m. At this point, the second system measured a greater Bowen ratio because the system at 1.35 m was affected by the LH flux advected from the soybean field. On the other hand, the system at 0.9 m was dominated by sensible heat flux from the wheat stubble.

Another cause of the observed differences between systems may be due to the theoretical assumptions imposed by the Bowen ratio system and not caused by heterogeneity of the landscape. The Bowen ratio technique assumes the eddy diffusivities of heat and water vapor are equal ($K_h = K_m$). Several studies determined that $K_h \neq K_m$ during stable and neutral conditions (Motha et al. 1979; Lang et al. 1982; Dugas et al. 1991).

Lang et al. (1981) determined a method to study eddy diffusivities when both BR and EC methods were available. The definitions used by Lang et al. are:

$$K_H = -H \Big/ \left(\rho C_p \frac{\partial \theta}{\partial z} \right) \tag{6.1a}$$

$$K_W = \lambda E \Big/ \left(\rho \lambda \frac{\partial Q}{\partial z} \right) \tag{6.1b}$$

$$H = \rho C_p \overline{w\theta} \tag{6.2a}$$

$$\lambda E = \rho \lambda \overline{wq} \tag{6.2b}$$

Bowen ratios of flux (β_f) and gradient (β_g) are formed from Eqs. (6.1) and (6.2), as

$$\beta_f = \frac{C_p \overline{w\theta}}{\lambda \overline{wq}} \tag{6.3a}$$

$$\beta_g = \frac{C_p \Delta\theta}{\lambda \Delta Q} \tag{6.3b}$$

Lang et al. demonstrated how the ratio of diffusivities of heat to vapor equals the Bowen ratio of flux to gradient as defined by Eqs. (6.3):

$$\frac{K_H}{K_W} = \frac{\beta_f}{\beta_g} \tag{6.4}$$

Because closure is near 100%, the BR and EC methods determine the behavior of the eddy diffusivities. From observations shown in Figures 6.34 – 6.35, the Bowen ratio measured by the gradient BR method (in this case, β_g) is greater than the Bowen ratio measured from the EC method (β_f), or $\beta_f > \beta_g$. Thus, from Eq. (6.4), $K_W > K_H$. Motha et al. (1979) demonstrated that $K_H > K_W$ occurs during the advection of sensible heat. Lang et al. further demonstrated that instances of sensible heat advection and inequality of diffusivities were accompanied by a downward-gradient of sensible heat flux. In other words, an inequality of diffusivities occurs during instances of positive latent flux and negative sensible flux. In general, the ratio of K_H to K_W decreases with increasing stability.

A second feature observed in the diurnal cycles of flux (Figs. 6.34 and 6.35) is the rapid increase in latent heat flux at sunrise. This sudden jump in flux is particularly noteworthy during October, February, and March. The EC method often fails to measure this rapid increase, and failure to capture this feature results in a repeated underestimate of closure at sunrise. As shown in Figure 6.36, closure is often at its worst near sunrise and near sunset. This problem appears to be common to the ten super sites (see Chapter 7). This problem begets two questions: (1) Why does the EC method fail to measure a sudden increase in latent heat? (2) Is this rapid increase in latent flux real? If not, then is the BR method simply appropriating the available energy into its subsequent aerodynamic fluxes?

One cause of divergent behavior between observing systems arises from the height at which the sensors are located. The BR system is close to the ground and any vertical moisture gradient is sampled between 2 and 3 m. The sonic anemometer and krypton hygrometer of the EC system are mounted at a height of 4.5 m AGL. During the early morning hours, a stable boundary layer is dominant and an inversion could set up between 2 m and 4.5 m. Low level moisture gradients very near the surface could be detected by the Bowen ratio system but missed by the EC technique.

Finally, even the diurnal estimates of closure (Fig. 6.36) appear dependent upon the Bowen ratio (Fig. 6.37). Closure rates are ~ 100% during the mid- to late afternoon when Bowen ratios are the largest; closure rates are worst near sunrise and sunset when the ratio of sensible to latent flux diminishes. The error in closure appears to result from an underestimate of the latent heat flux. Reasons for this underestimate are discussed in detail in Chapters 7 and 8.

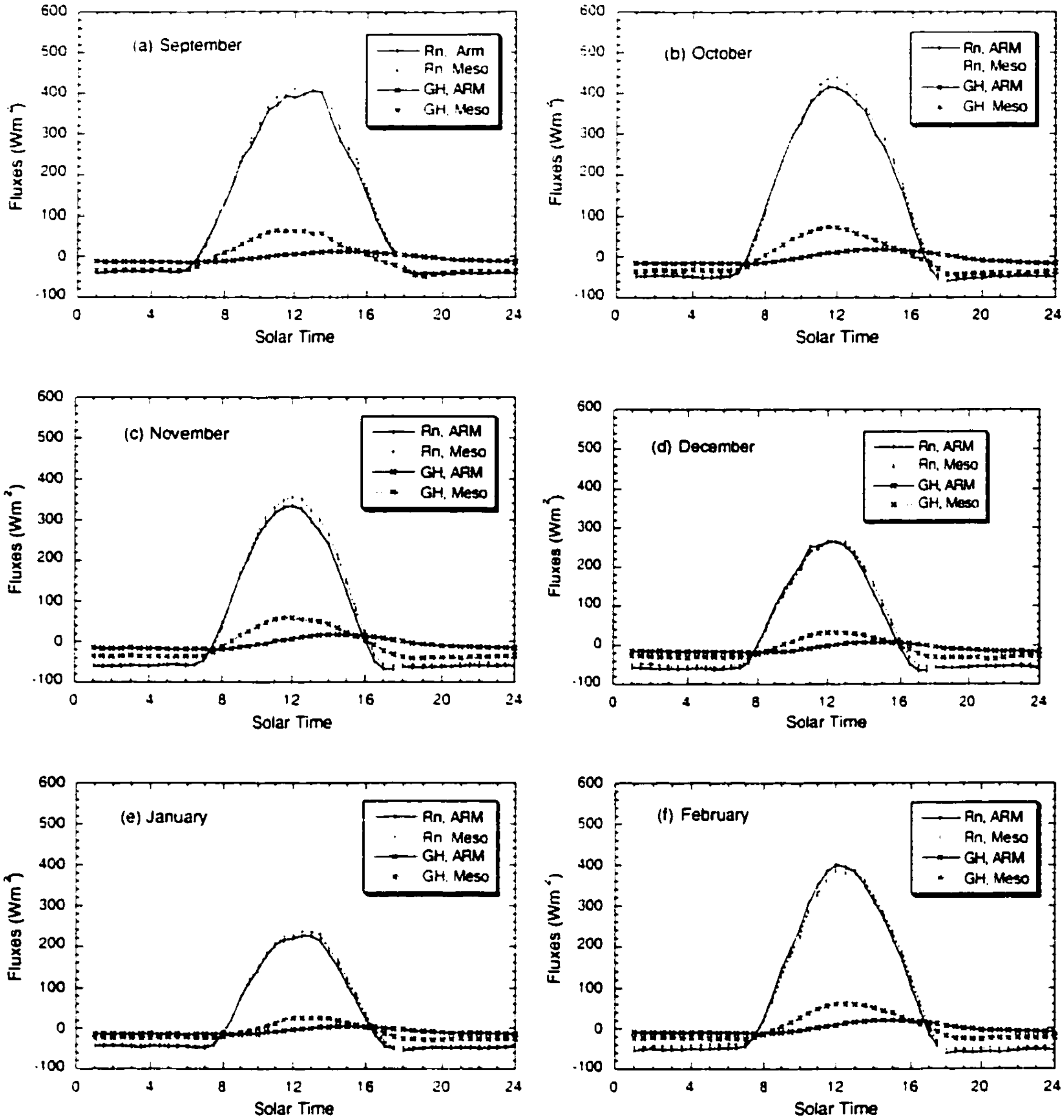

Fig. 6.33a-f: Net radiation and ground heat flux as measured at the ARM and Mesonet sites at Foraker between 1 September 1999 and 29 February 2000.

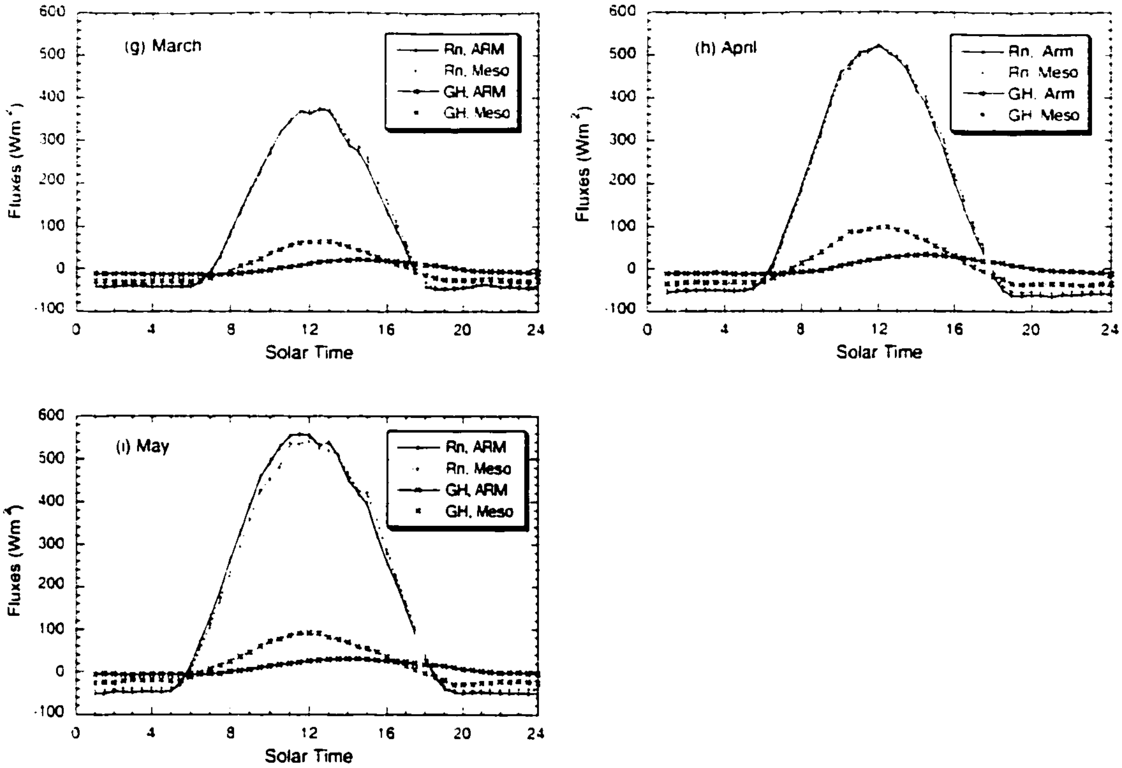

Fig. 6.33g-i: Net radiation and ground heat flux as measured at the ARM and Mesonet sites at Foraker between 1 March 2000 and 31 May 2000.

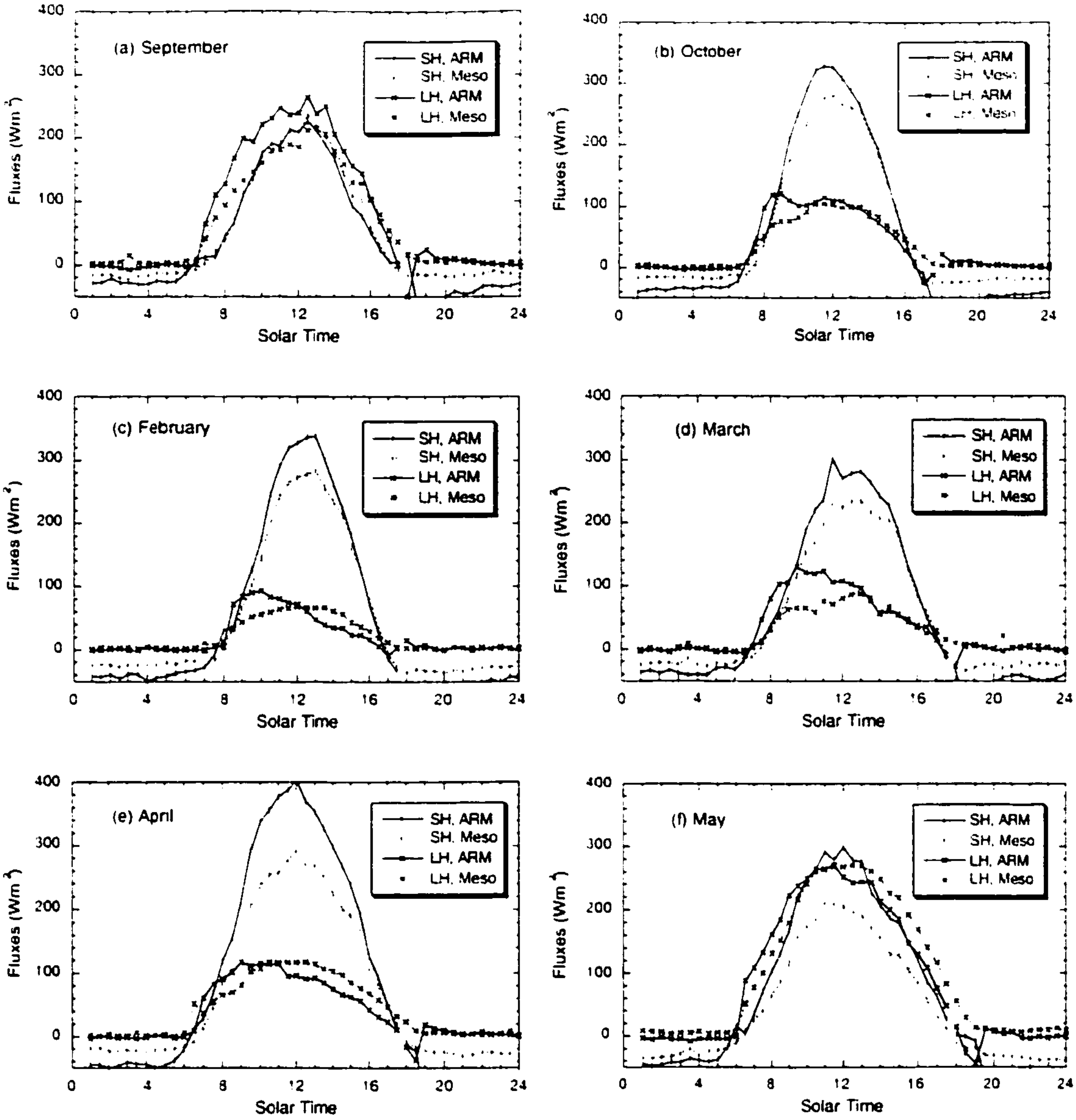

Fig. 6.34a-f: The diurnal cycle of sensible and latent heat flux averaged on a monthly basis as estimated at the ARM and Mesonet sites at Foraker. The ARM estimates of flux used the net radiation measured by the 4-component SIRS.

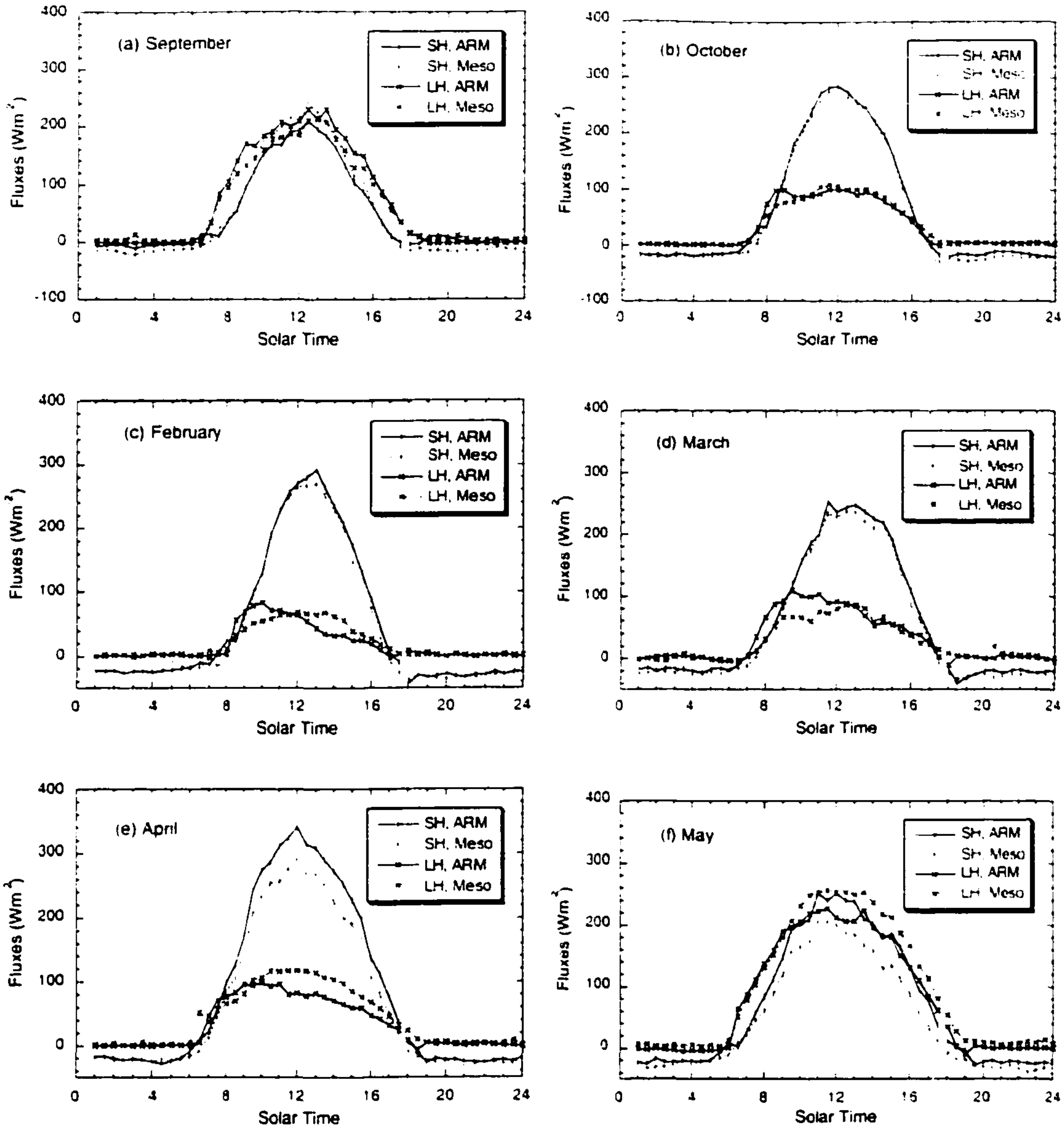

Fig. 6.35a-f: The diurnal cycle of sensible and latent heat flux as estimated at the ARM and Mesonet sites at Foraker. The ARM estimates of flux used the estimated available energy from the Mesonet.

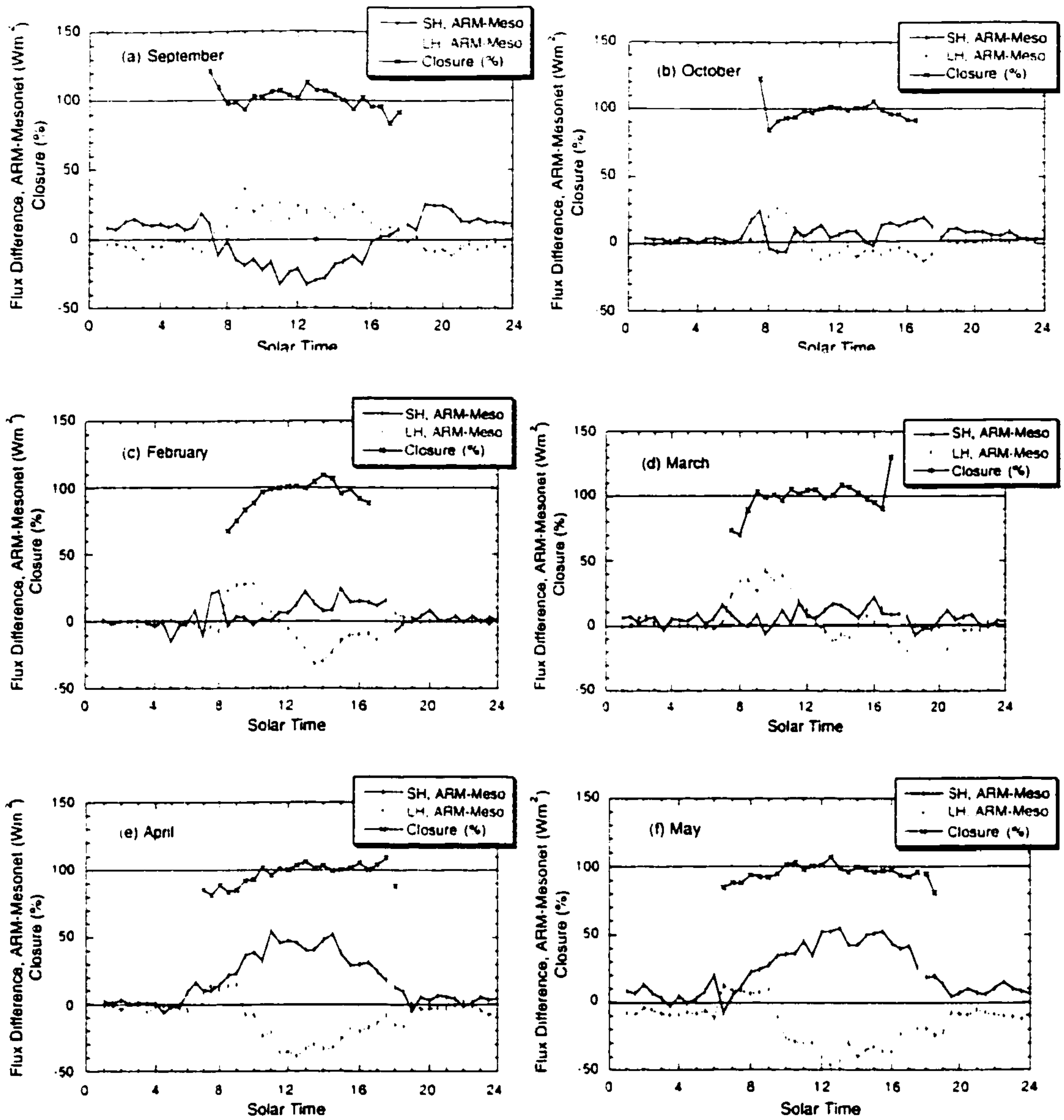

Fig. 6.36a-f: Flux differences between sensible and latent heat as measured at the ARM and Mesonet sites. Percent of closure is estimated at the Mesonet site. The ARM estimates of flux used the available energy from the Mesonet.

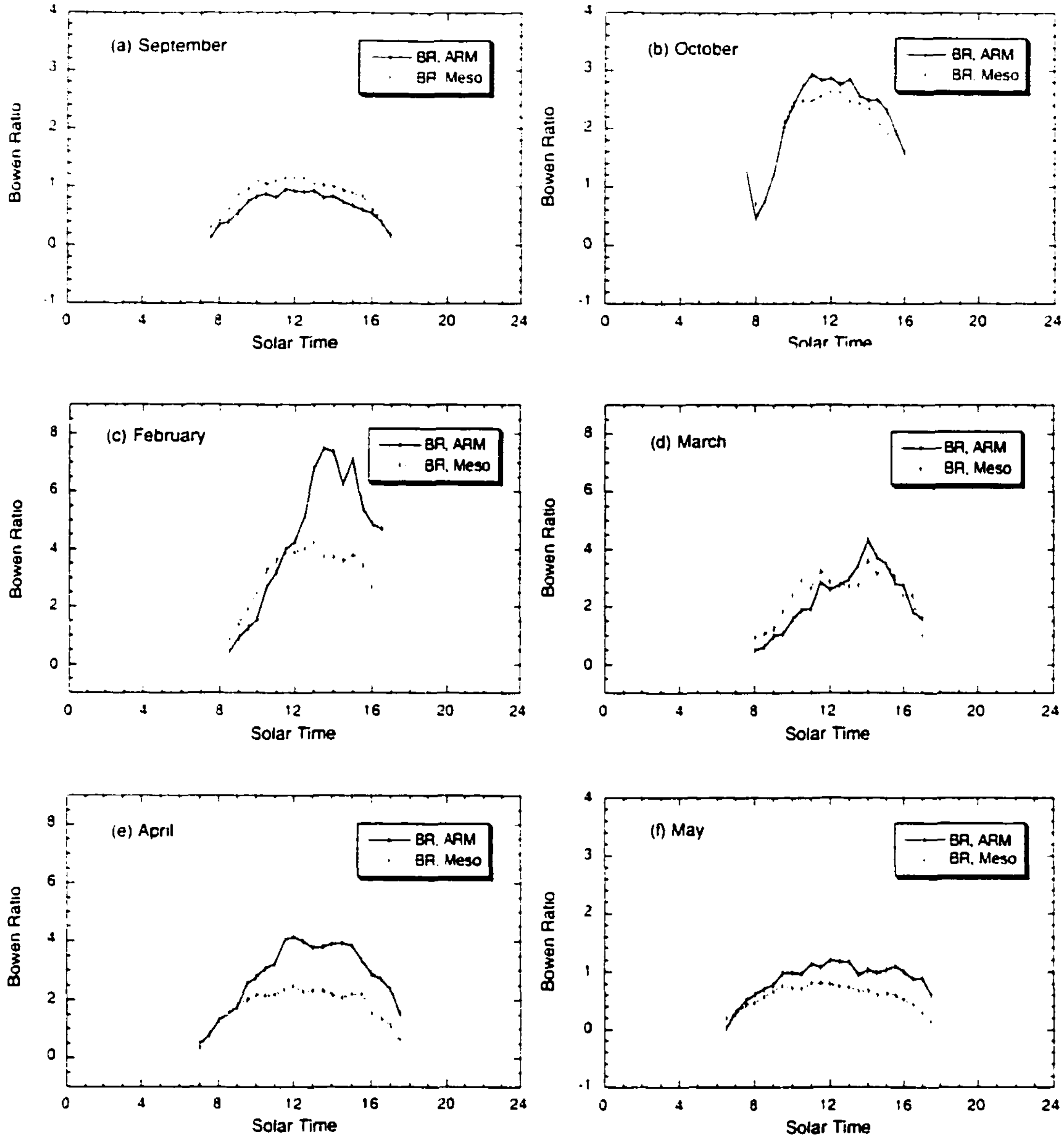

Fig. 6.37a-f: The diurnal cycle of Bowen ratio as estimated at the ARM and Mesonet sites at Foraker. The ARM estimates of flux used the available energy from the Mesonet.

Chapter 7: Closure Estimated at the 10 OASIS Super Sites

Introduction

One unique aspect of this investigation is that the OASIS network provides an opportunity for studies of the closure budget which can be conducted simultaneously at ten sites located in ten unique and varying climate regimes. Such a diverse selection of site locations, each with variable land surface properties, permits explicit study of the effects of climate, topography, surface heterogeneity and fetch. If similarity in closure is uncovered among the ten sites, local effects can be eliminated as possible causes for non-closure. Because the EC methodology appears to underestimate terms of the energy budget on a systematic basis, all sites should measure a similar underestimate in closure. If the underestimate in closure is due to latent heat flux (proposed in Chapter 6), closure should vary with climate and be a function of the Bowen ratio. These hypotheses are considered in this chapter. A one-year long data set has been collected from the ten super sites of OASIS and is the foundation for this chapter.

Data were collected between 1 June 1999 and 31 May 2000 from the ten OASIS super sites. All data were averaged over 30-minute periods, and all data were quality assured. If more than 4 of the 48 observations per day (each representing a 30-minute average) were missing, then that day of data was excluded from further analysis. Otherwise, missing data were interpolated from the time series. Twenty-four hour flux totals were summed for each of the four components of the energy budget.

7.1 Underestimation of Sensible and Latent Flux

The fundamental problem in estimating closure is the consistent underestimate of all aerodynamic fluxes – sensible and latent heat – when compared to the available energy of net radiation and ground heat flux. A majority of previous experiments, ranging from FIFE to SGP-97, support this conclusion (Fritschen et al. 1992; Nie et al. 1992; Twine et al. 2000). Thus, the primary focus of this research becomes identifying (and possibly correcting) the source(s) of this imbalance.

The initial step in identifying the source of closure imbalance becomes one of repeating previous results. The OASIS data set was examined at each of the ten super sites to assess the underestimate of aerodynamic fluxes (SH+LH) when compared to the available energy (Rn-GH). If previous conclusions from the scientific literature were correct, closure should be less than 100% at each of the ten OASIS sites regardless of instrumentation or site conditions.

The question presents itself as a classical statistical problem. A simple one-sided hypothesis was evaluated with a rejection level (p) equal to 5%. A null hypothesis (H_o) and an alternative hypothesis (H_A) were defined as:

H_o: $(Rn - GH) \leq (SH + LH)$

H_A: $(Rn - GH) > (SH + LH)$

with the null distribution assumed Gaussian based upon plots of observed data. A two-sample t-test was applied with the two sets of data represented by (Rn-GH) and (SH+LH).

The two sets of data were serially correlated with the annual cycle of incoming solar radiation. A single parabolic curve was fitted to the data, and the annual trend was removed. In addition, the two sets of data were determined to be cross-correlated. For example, as the net radiation increased, the sensible and latent fluxes likewise increased. The following equation was used to determine statistical significance because of the correlation between data sets:

$$z = \frac{\overline{x_1} - \overline{x_2}}{\left[\left(s_1^2 + s_2^2 - 2\rho_{1,2}s_1s_2\right)/n\right]^{1/2}} \tag{7.1}$$

The variables x_1 and x_2 are the sample means of (Rn-GH) and (SH+LH), respectively; s_1^2 and s_2^2 are the sample variances of each data set; $\rho_{1,2}$ is the Pearson correlation between data sets; and n is the sample size common to both data sets (Wilks 1995). Because of the serial correlation observed in the data stream, the sample size, n, was replaced by an effective sample size, n', which is estimated to be:

$$n' = n\left(\frac{1-\rho_0}{1+\rho_0}\right) \tag{7.2}$$

where ρ_0 is the estimated autocorrelation (at lag zero) of the time series.

First, a data set composed of "clear" days was generated from each of the ten sites. Clear and mostly clear days were manually selected at each site from the year-long data set. All cloud-contaminated days were excluded. Sample sizes ranged between 15 days at Stigler to 72 days at Idabel. Next, data were examined from all non-rain days. Sample sizes ranged between 57 days at Stigler to 173 days at Idabel.

Significance testing were conducted on data prior to instrument corrections being applied to the sonic data. The tests were repeated except with the corrections added. Results are listed in Table 7.1.

Table 7.1: Hypothesis test results for data collected from the super sites during clear and non-rain days; data in bold denote when the null hypothesis was rejected at the 5% level.

Site	No corrections	Corrections	No corrections	Corrections
	Clear days only		All non-rain days	
Alva	**1.725**	1.090	**5.485**	**2.857**
Bessie	**3.271**	**1.708**	**9.872**	**6.037**
Boise City	**1.806**	**1.620**	**5.586**	**4.062**
Burneyville	**1.741**	**4.050**	**3.984**	0.785
Foraker	**4.301**	**2.011**	**8.303**	**3.386**
Grandfield	**3.860**	0.524	**8.401**	0.576
Idabel	**2.555**	**2.288**	**10.517**	**7.534**
Marena	**2.906**	0.821	**9.444**	**3.797**
Norman	1.059	0.113	**6.170**	0.671
Stigler	**7.526**	**2.344**	**8.177**	**2.968**

The null hypothesis was rejected at all sites except Norman when only clear days were considered and without sonic corrections being applied. Thus, (Rn – GH) is greater than (SH + LH). The sample size at Norman was most likely too small to reject the hypothesis. Data from all ten sites proved significant at the 5% rejection criteria ($Z > 1.65$) when all days were considered. After sonic corrections were applied, (Rn-GH) > (SH+LH) still held true at most sites. The null hypothesis was rejected at all but a few sites. As discussed in Section 7.5.2, Alva, Grandfield, and Norman have the flattest terrain of the ten sites. The results suggest that topography may cause some underestimate in closure. Nevertheless, this study repeats the results of previous work by demonstrating that, at a majority of sites, (Rn-GH) > (SH+LH) even after appropriate instrument corrections are applied.

7.2 Tilt Correction

The correction for coordinate rotation accounts for sensor tilt (not properly leveled during installation) and for terrain slope. Coordinate rotation assumes planar rotation such that the u-v coordinates of wind are rotated to force w to equal zero. The details of this correction method are given in Appendix A.3.

Because the sensor tilt and terrain slope affect the EC measurements, each time the sonic anemometer is inspected for maintenance purposes could cause a new "tilt" to be observed in the observations. When considering a long-term data set of EC measurements, the tilt due to terrain slope should remain constant during the period. However, a tilt correction at the beginning of a project may not be applicable after several months of field exposed to atmospheric elements and after several site visits by maintenance personnel.

The stability of the tilt correction during the year long data set was examined by quantifying the slope error separately over three periods of two-week duration. The bi-weekly periods were chosen near the beginning, middle, and end of the data set; in this way, changes to the tilt of the sensor could be noted. Weather during the three periods was generally fair with little precipitation. Data collected during days with rainfall were excluded from the calculations. Data also were excluded when the azimuth angle of the wind was northerly (between 345° and 15°); the tower structure, located north of the sensor, obstructed proper ventilation to the anemometer. In addition, data were excluded when the estimated elevation angle of the sonic anemometer was > |4°|.

Sonic anemometer data were examined from the ten super sites during the periods of 1-14 October 1999; 1-14 January 2000; and 15-31 May 2000. Elevation and azimuth angles were computed from each set of measured u, v, and w components collected during each 5-minute period. These data are plotted for several selected sites for each 2-week period (Figs. 7.1 – 7.2). Next, the sonic lean angle (θ) and azimuth of the sonic lean angle (ϕ) were computed for each site (Table 7.2). As shown in Eq. (4.10), the sinusoidal fit of what was used to correct the raw data, is a function of the θ and ϕ angles.

Remarkably, the tilt correction remained relatively stable throughout the three 2-week periods. Figures 7.1 – 7.2 suggests that few changes are evident in the sinusoidal fit during the three periods for each site. A review of Table 7.2 reveals little variation among the three periods in either the maximum amplitude of the elevation angle or the azimuth angle associated with the maximum amplitude of the elevation angle. In general, the flatter the terrain, the less variant the data. In fact, the flatter the terrain, the less change observed in the rotation coordinates among time periods as listed in Table 7.2. Overall, the data remained relatively "well-behaved" with time. Thus, it can be concluded that a single sinusoidal fit can be applied to an entire year-long data set. Note that during this period of data collection, no sonic anemometers were removed or replaced.

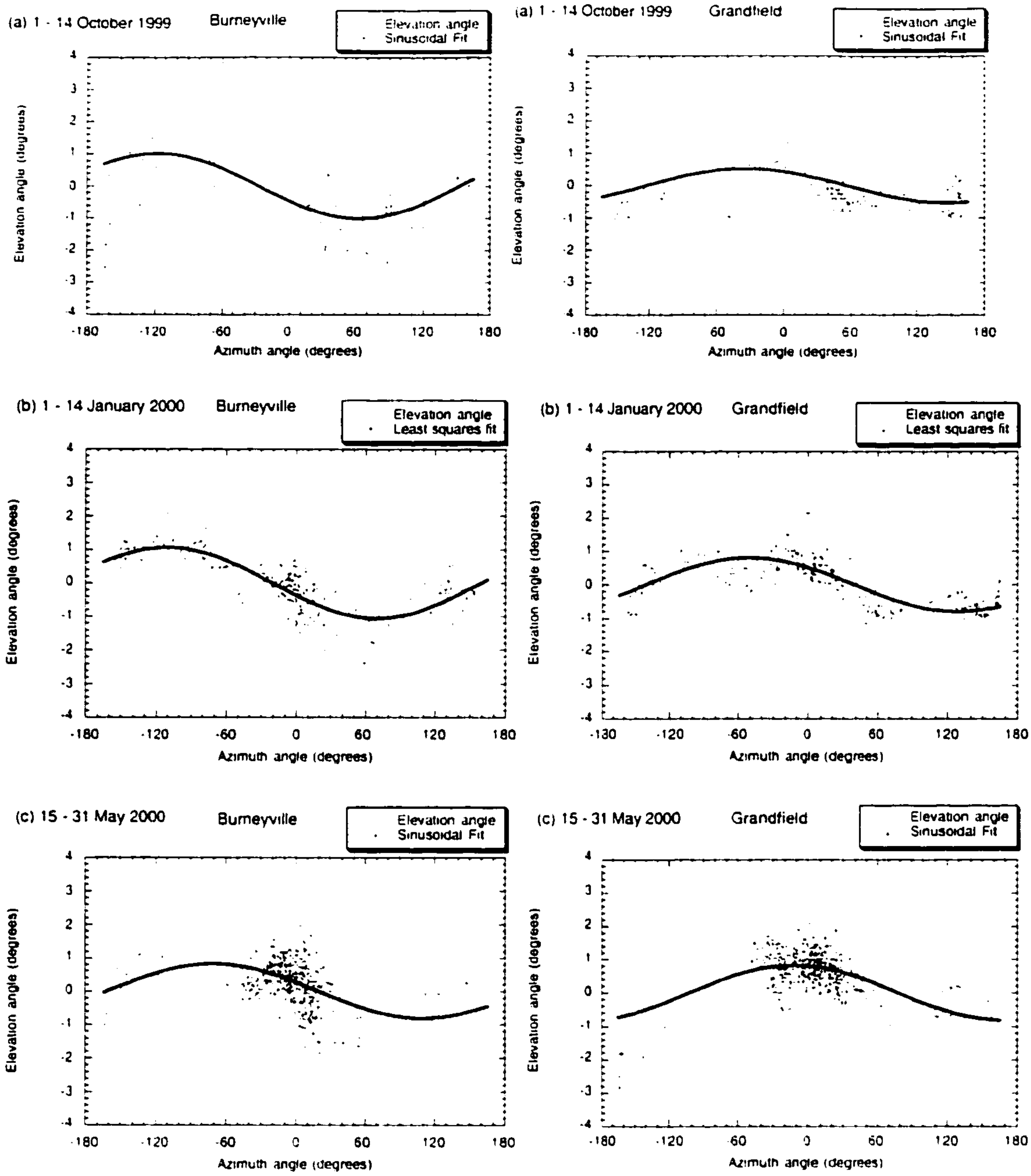

Figs. 7.1a-c: Elevation angle plotted as a function of the azimuth angle. Data is plotted for Burneyville and Grandfield.

Table 7.2: The calculated sonic lean angle and azimuth of the sonic lean angle for each super site for each selected time period.

	Sonic lean angle, θ (degrees)			Azimuth of the sonic lean angle, φ (degrees)		
	Oct 1-14 1999	Jan 1-14 2000	May 15-31 2000	Oct 1-14 1999	Jan 1-14 2000	May 15-31 2000
Alv2	0.88	0.63	0.62	85.13	62.4	77.98
Bess	1.78	1.93	1.46	-6.78	-2.16	15.85
Bois	0.29	0.45	0.65	47.29	41.77	23.44
Burn	1.01	1.05	0.81	-117.26	-110.82	-71.12
Fora	0.75	0.61	0.43	-171.37	-164.02	-123.58
Gra2	0.52	0.80	0.82	-33.69	-51.09	-12.39
Idab	1.02	1.08	0.70	-31.78	-50.00	-35.50
Mare	1.33	1.61	1.73	-22.60	-19.97	-15.34
Norm	0.42	0.58	0.55	1.95	5.52	7.25
Stig	1.07	0.83	1.07	73.47	68.56	70.97

The next question considered was how well the sinusoidal correction fit the sonic data. Although the estimated azimuth of the sonic lean angle was artificially restricted to lie between +/- 4° to accurately estimate the sinusoidal fit, large variance in the data were observed at several sites. Nevertheless, a qualitative inspection of plots from the three periods revealed that the sinusoidal fit represented the mean value at most sites. Data collected from Burneyville and Marena, however, indicated a significant departure from the sinusoidal fit. Terrain at these two sites is similar; the fine-scale, sloped terrain created micro-scale affects for which the sinusoidal fit was not designed.

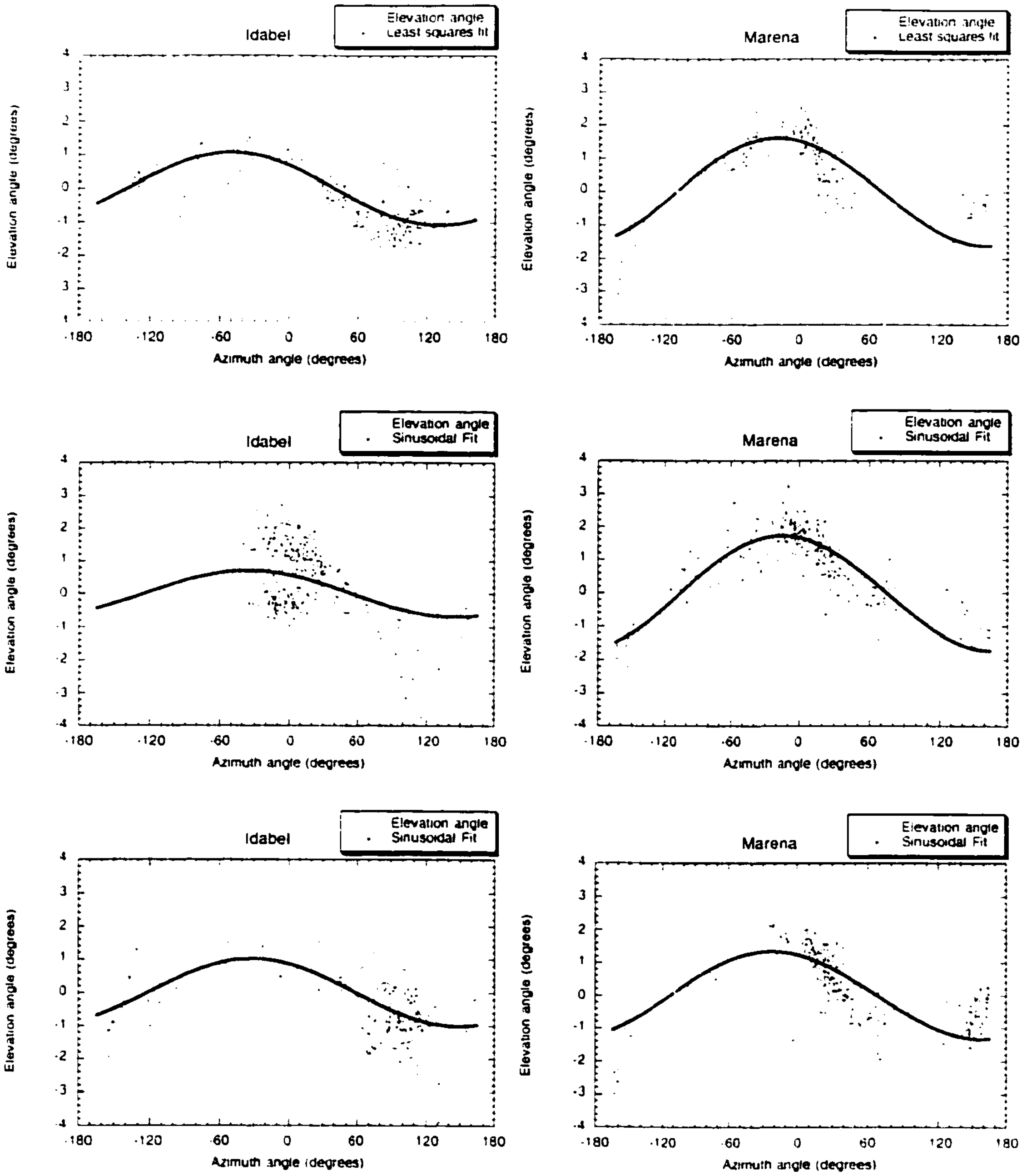

Fig. 7.2a-c: Elevation angle plotted as a function of the azimuth angle as estimated during three two-week periods. Data is plotted for Idabel and Marena.

7.3 Effect of Sonic Corrections

Results were examined as corrections were applied one-by-one to the sensible and latent heat fluxes. As described in Chapter 4, sensible heat fluxes were corrected for the effects of moisture (Schotanus et al. 1983), specific heat (Stull 1988), and tilt. Likewise, latent heat flux estimates were corrected for the effects of oxygen (Tanner et al. 1980), density variations (Webb et al. 1980) and tilt. The impact of each correction upon the aerodynamic flux is listed as the percentage of increase or decrease in the mean annual flux at each site (Tables 7.3 and 7.4).

Sensible heat fluxes decreased when corrected for variations in humidity (Schotanus et al. 1983). The temperature measurement by the sonic was determined to be a function of atmospheric moisture. To acquire correct measurements of atmospheric temperature requires removal of this effect. The result is a reduction of the sensible flux from that measured by the sonic anemometer. The flux was reduced only 1.1% at Grandfield but by a larger 4.7% at Stigler.

Conversely, sensible heat flux increased as the specific heat of air increased (Stull 1988), which in turn, increased as atmospheric moisture increased. The result is a greater sensible flux. Sensible heat fluxes increased from 1.3% at Bessie to as high as 7.3% at Stigler. Note that each correction is a tightly modulated function of atmospheric moisture. Because of the moister climate in eastern Oklahoma, sites such as Foraker, Stigler, and Idabel incurred the greatest flux change from following the corrections. The small data sample collected at Stigler during the summer months may not be representative of an annual mean.

The net effect of these two corrections (Schotanus et al. and Stull) upon sensible flux was significant. Increases in flux ranged from 0.8% to 3.4%. The small effect of the corrections on sensible heat flux at Bessie most likely results from a poor site exposure. The wind fetch at the Bessie site is poor because of small hills and rolling terrain in nearly every direction; the site itself sits atop a large hill. The relatively large effect observed at Stigler results from the small sample used and its eastern Oklahoma location.

The corrections for oxygen and those proposed by Webb et al. increased estimates of latent heat flux (Table 7.4). The oxygen density of air affects fluxes of latent heat when measured by a krypton hygrometer. The greater the flux, the greater the underestimate of latent heat by the krypton. A correction to account for this underestimate increased the estimated latent heat flux at all sites. Values increased from 2.9% at Foraker to as much as 10.7% at Boise City. The apparent large correction at Boise City was due to the smaller values of latent flux measured there compared to measurements at the more eastern sites.

Latent heat flux also is affected by density fluctuations caused by the fluxes themselves (Webb et al. 1980). The result is a significant underestimate in the measurement. The correction increased latent heat flux by 6.2% at Stigler to as much as 12.0% at Grandfield.

The total net increase in latent heat flux from the two corrections ranged from 10.3% at Stigler to a large 21.1% at Boise City. Overall, the impact of each correction on the measured flux remained consistent among the ten sites. Note the significant impact of the corrections on both the sensible and latent heat. Failure to include these corrections would lead to a significant underestimate in closure of the energy budget.

7.4 Mean Annual Closure Rates

Mean annual statistics of closure were examined for the ten super sites using data collected during clear days and on all non-rain days. Closure was examined at each site prior to and after sonic corrections were applied. Results for clear-sky conditions are summarized in Table 7.5. Table 7.5 lists the mean annual closure rate (X), the standard deviation of closure about the mean (σ), the range of closure during the year-long data set,

Table 7.3: Mean annual statistics of the impact of sonic corrections on sensible heat flux at each of the ten super sites collected on non-rain days.

Site	Schotanus et al. correction (%)	Stull correction (%)	Schotanus et al. and Stull corrections (%)
Alva	-2.8	4.5	2.2
Bessie	-2.4	1.3	0.8
Boise City	-1.4	2.2	2.1
Burneyville	-2.3	3.6	2.0
Foraker	-2.5	4.0	2.2
Grandfield	-1.1	1.8	1.2
Idabel	-3.4	5.6	2.4
Marena	-2.7	4.4	2.4
Norman	-2.5	3.2	2.1
Stigler	-4.7	7.3	3.4

Table 7.4: Mean annual statistics of the impact of sonic corrections on latent heat flux at each of the ten super sites collected on non-rain days.

Site	Oxygen correction (%)	Webb et al. correction (%)	Oxygen and Webb et al. corrections (%)
Alva	3.3	7.2	10.7
Bessie	5.4	10.1	15.4
Boise City	10.7	8.4	21.1
Burneyville	5.4	10.7	17.2
Foraker	2.9	8.4	11.3
Grandfield	5.8	12.0	18.0
Idabel	3.5	7.9	12.0
Marena	4.1	8.7	13.2
Norman	3.5	8.0	12.4
Stigler	3.5	6.2	10.3

the improvement in closure after the sonic corrections were applied (ΔX), the change in standard deviation after the sonic corrections were applied ($\Delta\sigma$), and the sample size.

The annual mean value of closure estimates on clear days ranged between 68.2% at Bessie to 87.4% at Grandfield. Mean closure at most sites ranged between 80 - 88%. By

Table 7.5: Mean annual statistics of closure at all ten super sites based upon data collected during clear days and non-rain days. Italicized data have all corrections applied.

Site	X (%)	σ (%)	Range (%)	ΔX (%)	Δσ (%)	Sample size (# of days)
Alva	87.0	22.4	49.0 - 180.7	7.8	-3.3	71
	94.8	*19.1*	*56.2 - 161.7*			*54*
Bessie	68.2	23.1	19.1 - 116.2	8.6	1.2	79
	76.8	*24.3*	*36.5 - 121.8*			*54*
Boise City	84.2	11.1	49.9 - 115.4	6.7	-0.3	67
	90.9	*10.8*	*68.0 - 115.1*			*46*
Burneyville	84.0	11.9	43.8 - 136.2	8.2	0.3	84
	92.2	*12.2*	*67.4 - 120.9*			*65*
Foraker	83.0	8.7	53.4 - 99.0	9.8	-1.4	58
	93.2	*6.1*	*76.4 - 106.2*			*42*
Grandfield	87.4	7.1	70.8 - 107.5	10.8	1.1	57
	98.2	*8.2*	*82.1 - 120.6*			*51*
Idabel	76.9	11.3	25.6 - 101.0	7.6	1.0	90
	84.5	*12.3*	*62.0 - 114.9*			*72*
Marena	85.0	10.1	63.3 - 137.0	6.9	-1.2	85
	91.9	*8.9*	*70.8 - 110.5*			*63*
Norman	86.7	12.4	45.5 - 107.2	14.0	1.7	41
	100.7	*14.1*	*73.0 - 125.6*			*33*
Stigler	78.1	10.5	48.8 - 105.5	10.6	-1.3	22
	88.7	*9.2*	*78.5 - 117.1*			*15*

including the appropriate sonic corrections, closure improved 6.7% at Boise City to as much as 14.0% at Norman. The corrected closure rates ranged between 76.8% at Bessie to 100.7% at Norman. Note that nearly all sites *underestimated* closure. The variance increased by 1.7% at Norman and decreased by 3.3% at Alva.

A comparison of information in Table 7.5 with that in Table 3.1 indicates a relationship exists between topography and closure (see Figs. 7.21 – 7.25). In general, it appears the flatter the site, the better the closure rate. This result is similar to findings by Stannard et al. (1991) observed during Monsoon-90. The effects of topography and instrument exposure - via stationarity and homogeneity - upon eddy correlation estimates still are not well understood. It is widely accepted that Monin-Obukhov theory fails in complex terrain; it may be that similar restraints should be adopted for use of eddy

Table 7.6: Mean annual statistics of closure at all ten super sites based upon data collected during non-rain days. Italicized data have all corrections applied.

Site	X (%)	σ (%)	Range (%)	ΔX (%)	Δσ (%)	Sample size (# of days)
Alva	84.5	22.5	21.7 - 184.0	7.9	-3.8	150
	92.4	*18.7*	*43.7 - 161.7*			*106*
Bessie	69.3	24.1	16.4 - 119.7	7.5	3.3	166
	76.8	*27.4*	*17.2 - 136.5*			*106*
Boise City	84.1	16.6	20.8 - 140.7	9.2	-0.2	138
	93.3	*16.4*	*68.0 - 187.4*			*90*
Burneyville	86.9	14.2	41.7 - 172.5	9.6	-0.7	206
	96.5	*13.5*	*67.4 - 124.6*			*149*
Foraker	83.2	13.2	13.8 - 133.0	12.7	-3.1	161
	95.9	*10.1*	*67.3 - 129.0*			*108*
Grandfield	88.5	7.2	70.8 - 107.5	11.0	2.1	126
	99.5	*9.3*	*78.7 - 124.1*			*111*
Idabel	77.9	14.5	25.6 - 164.3	7.6	2.0	216
	85.5	*16.5*	*36.9 - 120.8*			*166*
Marena	83.1	15.3	20.8 - 176.2	7.9	-5.7	192
	91.0	*9.6*	*70.8 - 123.5*			*135*
Norman	86.2	12.5	45.5 - 109.1	14.0	3.1	97
	100.2	*15.6*	*73.0 - 138.9*			*78*
Stigler	83.3	11.1	48.8 - 111.7	10.0	1.1	76
	93.3	*12.2*	*72.0 - 124.0*			*57*

covariance techniques. A discussion of the effect of topography upon closure is detailed in Section 7.5.2.

When the full-year data set was limited to non-rain days (Table 7.6), closure rates were similar to the results obtained using only days that were clear. Closure estimates ranged between 69.3% at Bessie prior to sonic corrections to 100.2% at Norman after corrections. In general, closure rates improved slightly at most sites when only non-rain days were used. Even so, the results were more variable than observed on clear days.

7.5 Trends in Closure at the 10 Super Sites

Closure is a complex summary of how well the overall surface energy budget is measured. Thus, many reasons exist for nonclosure at a particular site. Limitations with the instruments, site inhomogeneity, instrument exposure, and topographical effects contribute to increasing the observational error.

Closure rates were averaged over 24-hour periods at the ten super sites between 1 June 1999 and 31 May 2000 (Tables 7.5 and 7.6) for clear days only and for non-rain days only. The results duplicated that which was uncovered in previous studies. Aerodynamic fluxes were underestimated relative to the available energy, (Rn - G) > (SH + LH), and thus, closure was underestimated. However, results using OASIS data represent an improvement over published results based upon FIFE and SGP-97 (Table 2.1).

OASIS permits closure to be examined on a variety of time scales; such that long-term systematic errors can be identified as well as short-term variability due to instrument error. To detect systematic errors, closure should be determined at multiple sites. Monthly to seasonal changes in closure at multiple sites will provide insight into the underlying causes for non-closure.

First, trends in closure were examined as a percentage [Eq. (2.1)] and as a residual of the energy balance [Eq. (2.2)]. During the winter months, closure rates are poor simply as a consequence of the low magnitude of the flux values. This lack of closure results from a deficiency in the closure equation itself: the percentage error is sensitive to the magnitude of the fluxes. The greater the values of flux, the less sensitive to error is the percentage of closure. Thus, the residual of error is important to examine as well.

Days on which rainfall occurred were excluded, as were days when winds were between 330 and 30 degrees. The interference by the tall tower significantly affected sonic estimates. Thirty-minute averages were calculated using the 5-minute observations. Because daily totals of flux were needed, at least 44 of the 48 observations per day (> 92%) had to be available for that day of data to be included in the study. In addition, when a day of data was used, missing observations (up to 4) were interpolated from the time series. In this manner, a more accurate total of flux could be estimated for each day.

A percentage of closure was estimated daily for each super site (Fig. 7.3a-j). However, several sites, those at Boise City and Stigler, were not installed until mid-October while several other sites, Grandfield and Norman, had equipment failures during the year (Table 4.3). When estimating closure as a percentage, days also were excluded when (Rn – GH) < 1.5 MJ m^{-2} day^{-1} or when (SH + LH) < 1.5 MJ m^{-2} day^{-1}.

A review of the annual variation in the percentage of closure reveals similarity among the plots of data from the ten super sites. Bessie, Burneyville, Grandfield, Idabel, Marena, and Norman exhibited the same annual pattern of closure. Low closure rates (< 100%) during DOY 1 – 200 were followed by a 30 – 60 day period when closure was above 100%. Another period of low closure occurred during remaining days of the year. Data from sites at Boise City, Foraker, and Marena also showed a second period when the closure was near 100% (DOY 1 – 60). These three sites are the most northern of the ten sites studied.

A strong correlation among the ten sites in the annual trend of closure is evidence of an underlying systematic cause for non-closure. Because the pattern is so systematic and widespread, instrument exposure, terrain slope, and wind fetch unique to each site can be eliminated as the dominant factors in non-closure.

The daily closure rate was recalculated as the residual (MJ m^{-2} day^{-1}) and is shown in Figures 7.4a-j. As a residual, closure rates primarily reflect the annual cycle of incoming energy. However, a dramatic improvement in closure occurred between DOY 200 – 250 at the Bessie site; most other sites also recorded a similar improvement but in less dramatic fashion. Such a large shift in closure during mid-summer indicates that the closure problem was not caused by either net radiation or ground heat flux. Changes were not made to the net radiation sensors at this time. Furthermore, the total ground flux was not large enough to create the significant difference that was observed. An examination of the daily totals of net radiation and ground flux revealed little change beyond the annual cycle known to be in the year-long data set. Thus, the closure problem is contained within either the sensible and/or latent heat flux.

A review of the soil moisture and NDVI highlighted a drying, near-drought period between DOY 200 –250 during 1999. A lack of rainfall over most of the state during this period caused the upper levels of soil to dry significantly, which in turn, caused vegetation to wilt, increased stomatal resistance, and further dried the surface boundary layer. An examination of the daily totals of sensible and latent flux during the annual cycle revealed a dramatic increase in Bowen ratio during this same period of drying. In fact, closure rates became worse in the spring as the latent heat flux increased. During the period of drought, closure improved as the latent heat flux decreased sharply.

Annual trends of closure, and sensible and latent heat flux varied widely among the ten super sites. Because of that fact and to determine the impact of sensible and latent fluxes upon closure, daily estimates of Bowen ratio were plotted against daily estimates of closure (Figs. 7.5a-j). As is evident at almost every site, closure rates approached or even exceeded 100% as the Bowen ratio increased. The drier the site (i.e., the greater the sensible heat flux), the better the closure. Closure appeared particularly poor when the BR was less than 1.0. When the BR exceeded 1.0, closure was at or above 100%.

Figure 7.5a-j implies that latent heat flux is the primary cause for non-closure. Indeed, several previous experiments determined excellent closure in arid conditions (Stannard et al. 1994; Unland et al. 1996; Wright et al. 1992). However, Twine et al. (2000) disagreed; they claimed non-closure was created by both sensible and latent heat fluxes. To correct for non-closure, one should divide the residual of energy by the measured Bowen ratio.

If the majority of the closure error lies with measurement of the latent heat flux, the question remains: what is the cause of that error in the latent heat? Several hypotheses are proposed. First, routine cleaning of the hygrometer was not performed during 1999 at 9 of the 10 super sites. Failure to keep the krypton hygrometer clean increased the variance of all measurements. However, differences were not noted in the latent heat flux before and after the sensor was cleaned. The hygrometer at Idabel was cleaned on a regular basis during the entire period of study. Results from Idabel are the same as those from other sites. As a result, the real error lies within the latent heat flux.

A second reason latent heat flux was underestimated was caused by a physical separation of the krypton hygrometer and sonic anemometer. Koprov and Sokolov (1973) determined a 10% underestimate in flux when the lateral separation of sensors was 20 cm. The OASIS hygrometer and sonic anemometer are separated vertically by 15 cm. Kristensen et al. (1997) theorized that, when the scalar sensor was 20 cm above the anemometer, an underestimate of 18% would occur. However, when the scalar sensor was 20 cm below the anemometer, an error of only 2% occurred. To minimize errors due to sensor separation, OASIS placed the krypton hygrometer, the scalar component, 15 cm below the sonic anemometer.

A further look into the details of Figures 7.5a-j reveals variability of closure even among data with high Bowen ratio estimates. Large variability of these estimates within a site and among all sites is apparent. It appears as if topography may account for some degradation in closure. Stannard et al. (1991) demonstrated that, the flatter the site landscape, the better the closure. This situation appears to occur with OASIS data as well.

Results indicate that closure is strongly modulated by the Bowen ratio. During periods of high latent heat flux, closure was relatively low, and during very dry periods, closure was near or above 100%. To further explore this relationship, daily closure estimates were plotted versus the soil water potential (Figs. 7.6a-j). Soil water potential (kPa) is a measure of the amount of work needed to move a unit mass of water within the soil (Basara and Crawford 2000). In other words, it is a measure of the soil wetness. The drier the soil, the greater the soil water potential. In Figures 7.6a-j, the maximum value permitted (subjectively) was −10000 kPa; any observation greater in magnitude was assigned the value −10000 kPa. The more negative the observation, the drier the soil.

The results within Figure 7.6 reflect those in Figures 7.2 – 7.5. The wetter the soil, the lower the closure rate. For saturated soils, closure generally remained less than 100%; for drier soils, closure ranged from near 100% to 120%. Data from the sites at Alva, Boise City, Burneyville, Foraker, Marena, and Norman had a linear relationship between closure and soil water potential. The drier the soil, the greater the percentage of closure.

Closure was overestimated when the soils were dry. This problem with closure could indicate an overestimate in the ground heat flux. More specifically, it is likely that the soil water content was overestimated, as revealed in the Mesonet/ARM comparison in Chapter 6 (Fig. 6.14). The conversion of soil water potential to soil water content may create a positive bias (or higher values). If the soil water content was estimated to be too high, then the ground heat flux would be overestimated. The problem would be particularly apparent during dry conditions. An overestimate in ground heat flux leads to an underestimate in the available energy (Rn-GH), and subsequently, an overestimate in the closure rate.

Figure 6.14 demonstrated how, during saturated conditions, estimates of soil water content remained high even during wet periods, and that ground flux estimates were overestimated as well. Thus, closure estimates were lower than indicated by the measurements. Thus, errors in the estimate of soil water content could explain the overestimate in closure during dry periods. Unfortunately, correcting for errors in the soil water content further decreases the closure rates.

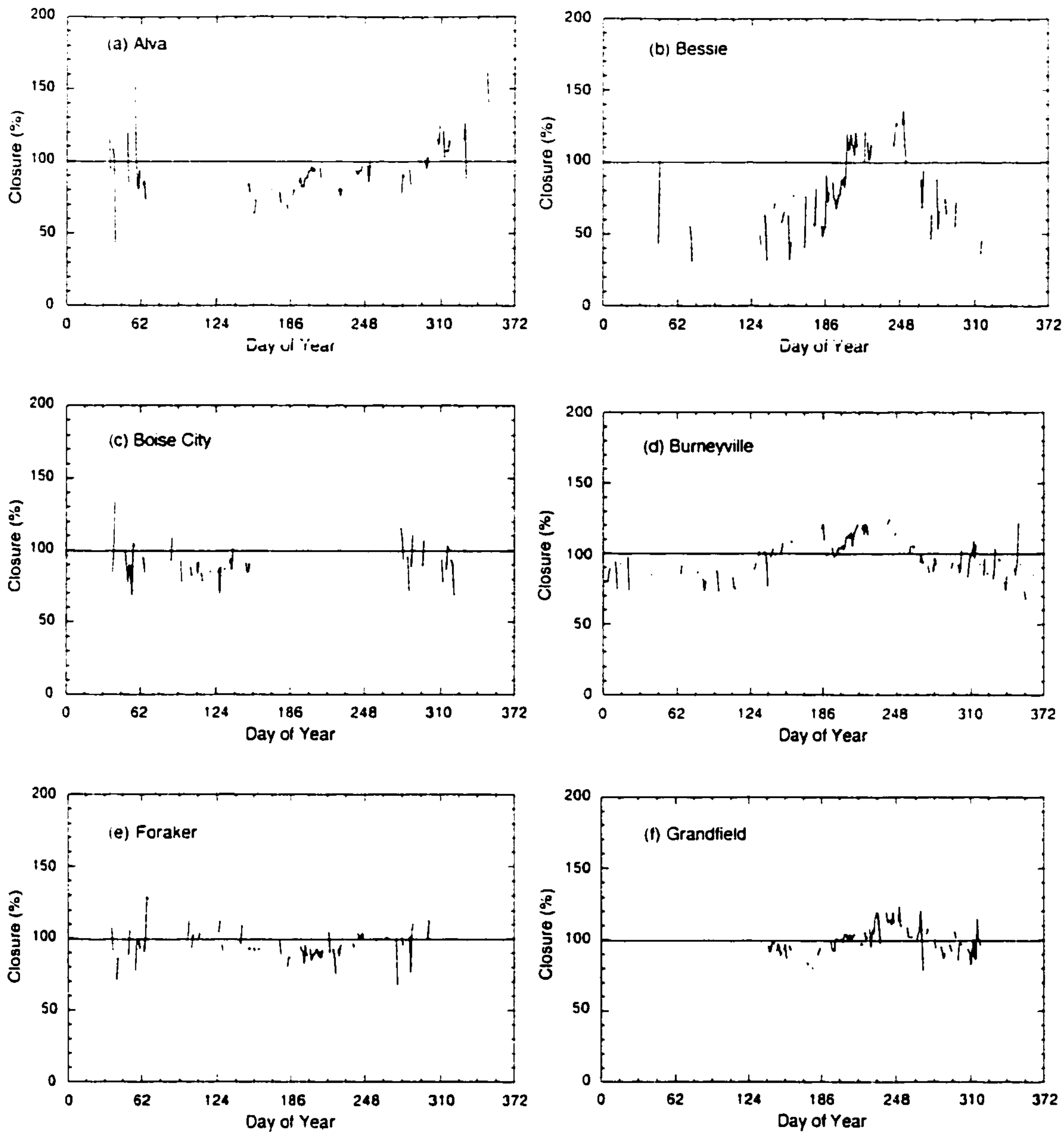

Fig. 7.3a-f: Daily estimates of closure (as a %) for each super site during 1 June 1999 to 31 May 2000.

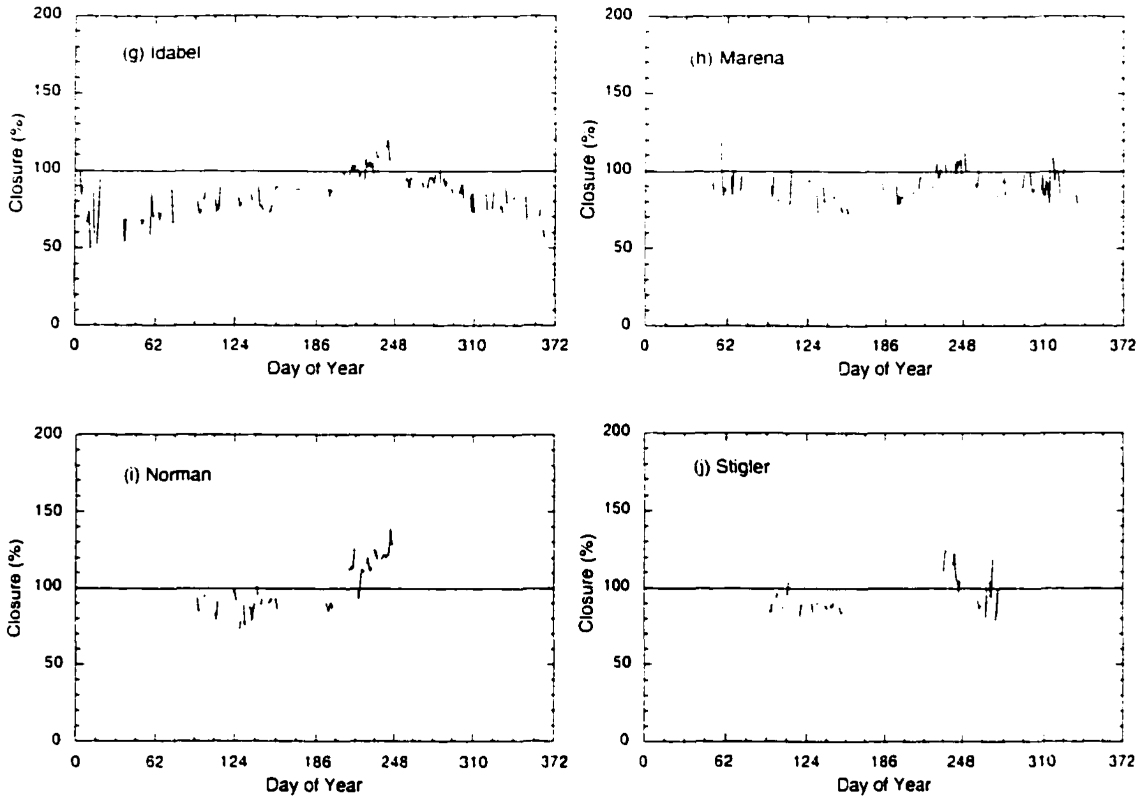

Fig. 7.3g-j: Daily estimates of closure (as a %) for each super site during 1 June 1999 to 31 May 2000.

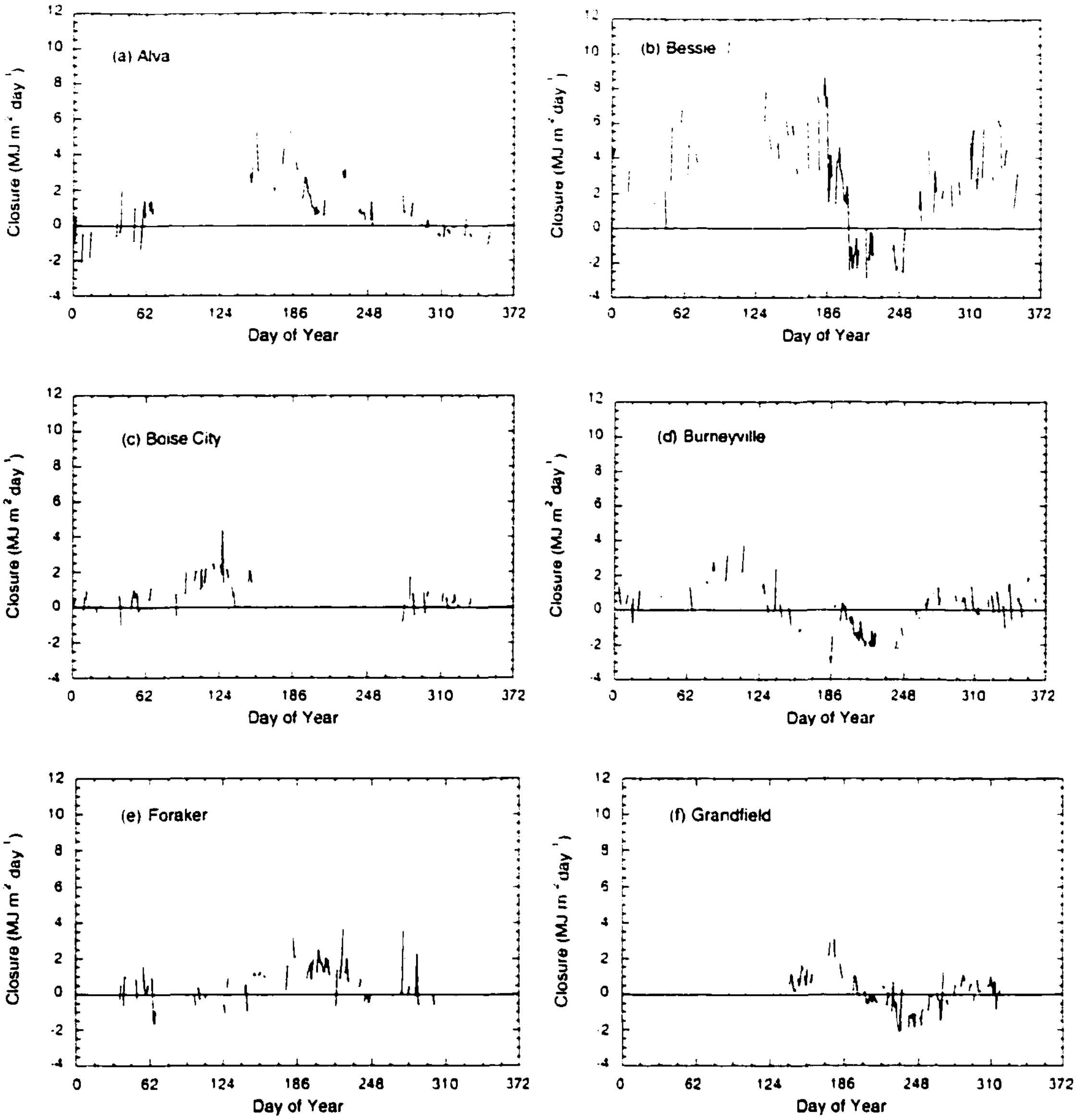

Figs. 7.4a-f: Daily estimates of closure (in MJ m^{-2} day^{-1}) for each super site during 1 June 1999 to 31 May 2000.

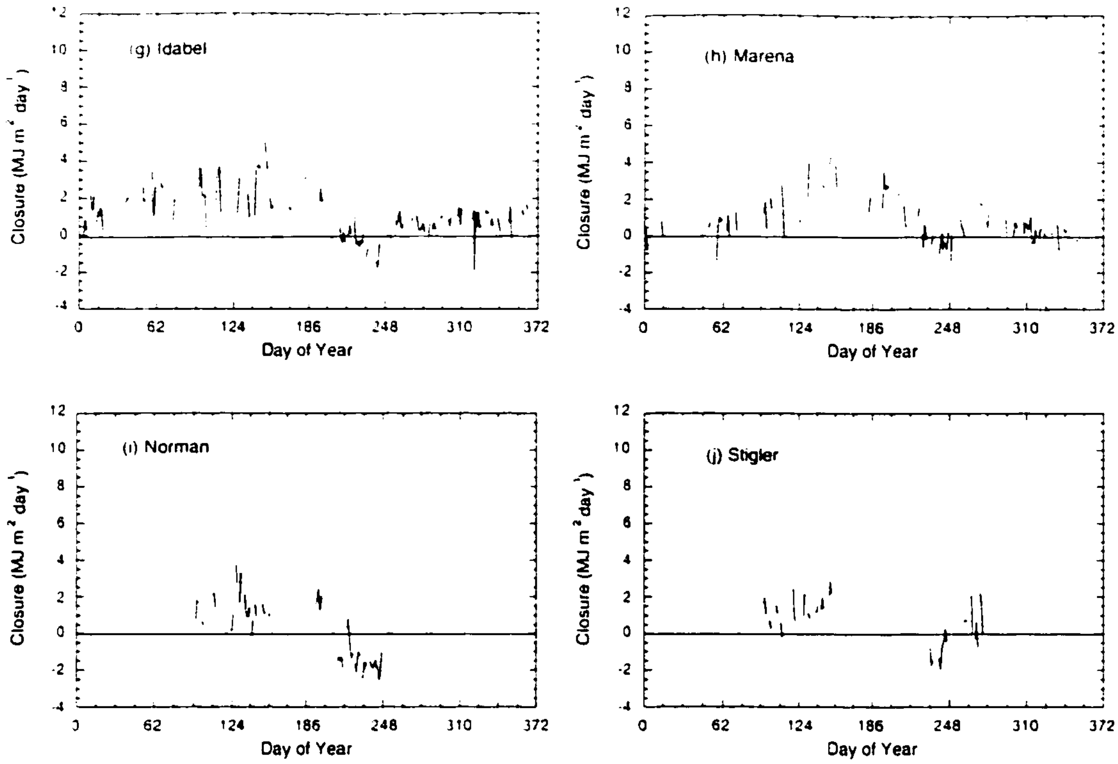

Figs. 7.4g-j: Daily estimates of closure (in MJ m^{-2} day^{-1}) for each super site during 1 June 1999 to 31 May 2000.

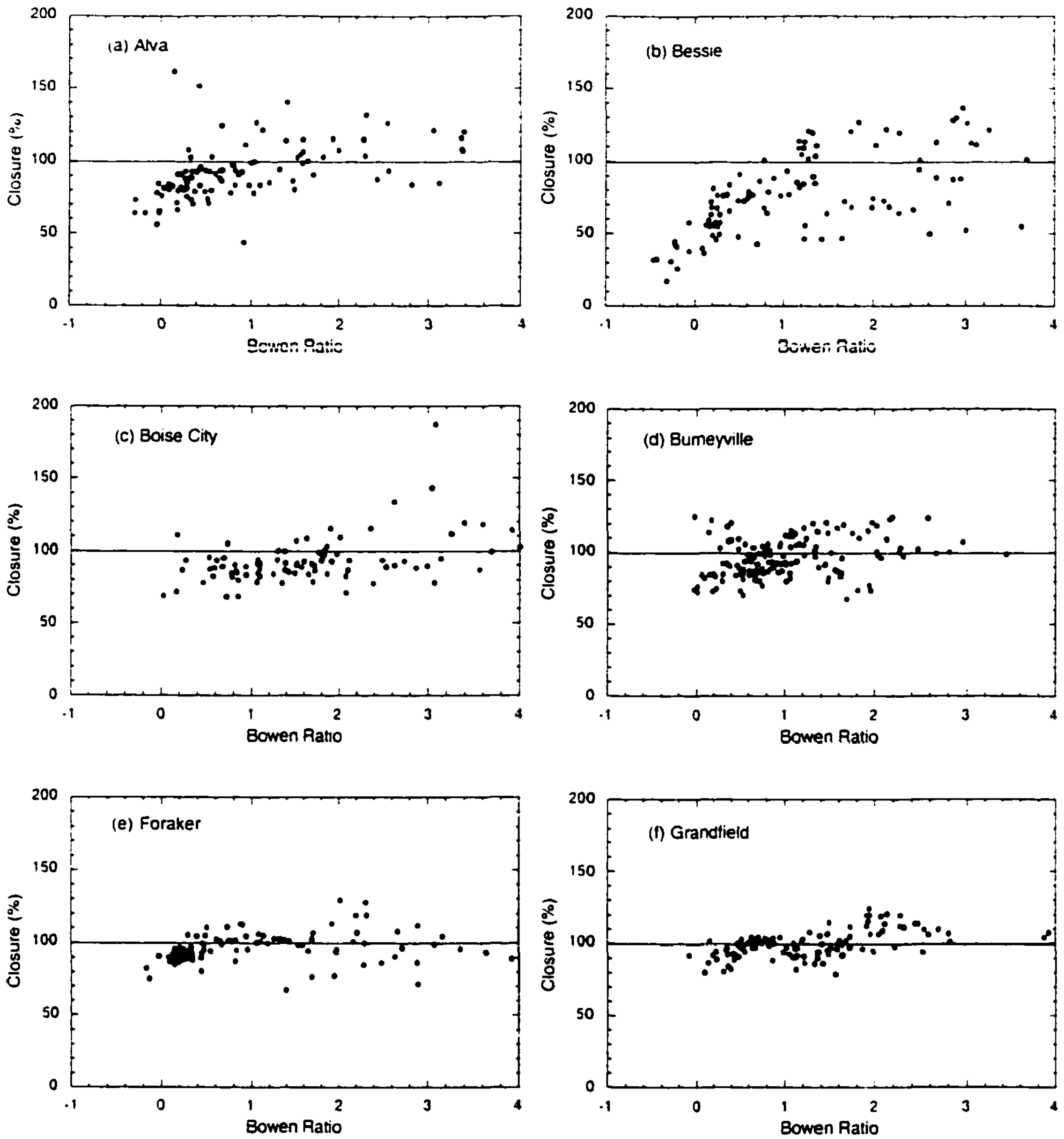

Figs. 7.5a-f: Daily estimates of closure (%) plotted as a function of the Bowen ratio. Data collected during 1 June 1999 to 31 May 2000.

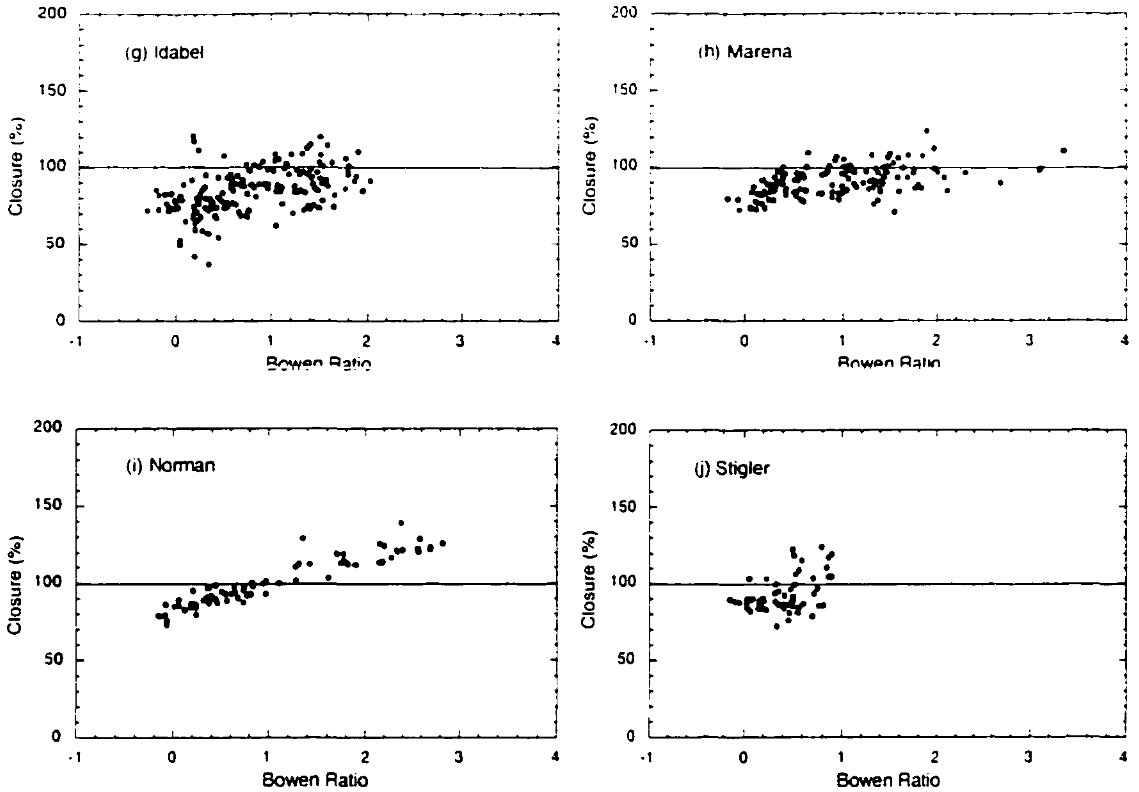

Figs. 7.5g-j: Daily estimates of closure (%) plotted as a function of the Bowen ratio. Data collected during 1 June 1999 to 31 May 2000.

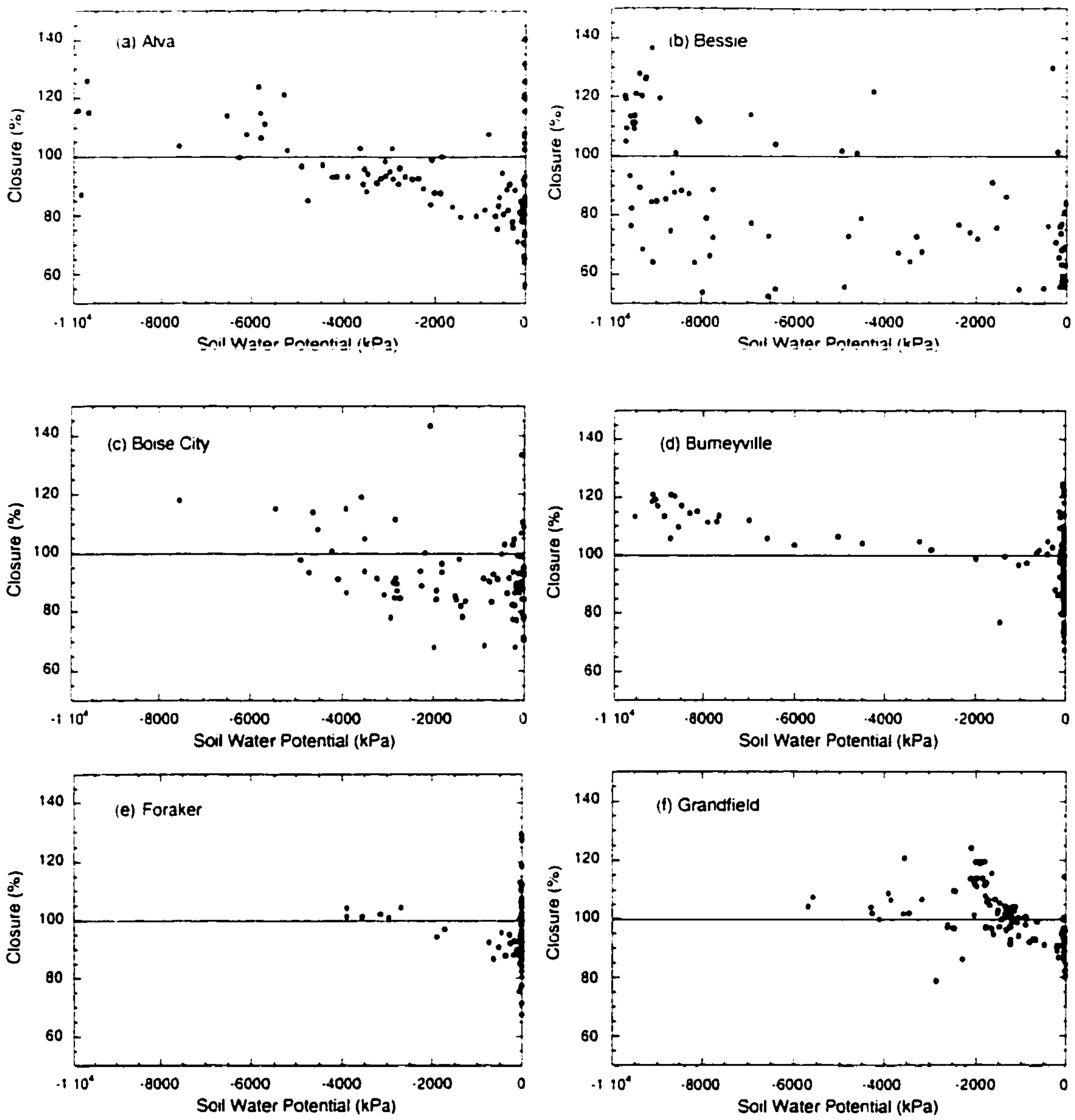

Fig. 7.6a-f: Daily estimates of closure (%) plotted as a function of soil water potential (kPa).

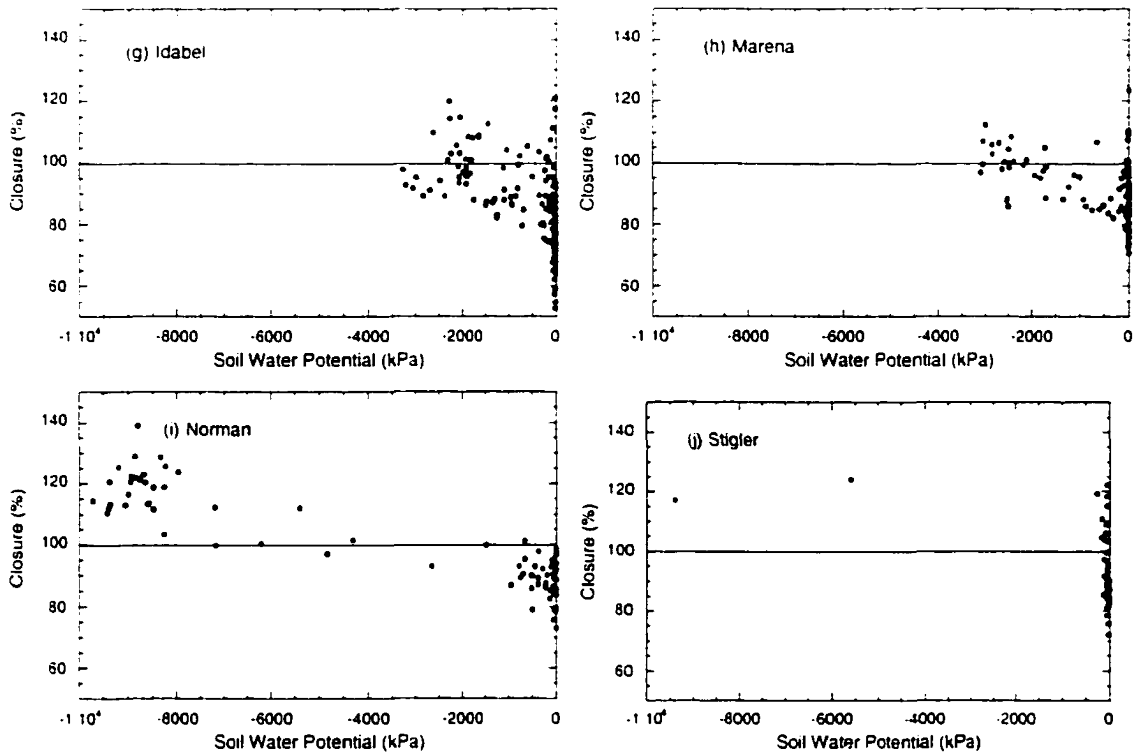

Fig. 7.6g-j: Daily estimates of closure (%) plotted as a function of soil water potential (kPa).

Diurnal averaging of the data was designed to reveal information regarding systematic error. Five-minute data were averaged diurnally for each month during the period between 1 June 1999 and 31 May 2000. Data from the 10 OASIS sites are shown in Figures 7.7 – 7.19.

Characteristics noted in the diurnally averaged plots of closure include a common diurnal pattern at ~ half of the sites. For example, sites at Boise City, Foraker, Grandfield, Norman, and Stigler measured a maximum closure rate at midday and a minimum closure rate during the early morning and late afternoon hours. Plots of the diurnally averaged estimates of Bowen ratio at Foraker (Fig. 7.12) showed a strikingly similar pattern to the pattern of closure. The relationship between closure and Bowen ratio, as demonstrated in Figure 7.5, appears to hold even across the diurnal cycle. As the Bowen ratio decreased to < 1, closure rates declined. As BR > 1.0, closure rates improved to ≥ 100%. This period during the mid-afternoon, a period with excellent closure (~ 100%), coincides with the daytime period when the greatest mixing and the lowest correlation between θ and q ($R^2_{\theta q}$) occurred (Barr et al. 1994). This increase in mixing of the PBL is due to the entrainment of warm, dry air above the boundary layer being mixed convectively to the surface.

All sites observed their lowest rate of closure during the early morning period prior to boundary layer mixing becoming established. This period of minimal Bowen ratio was followed by turbulent mixing that increased during the morning hours. As a result, dry air entrainment increased the Bowen ratio and increased closure rates.

A second characteristic was shared at Bessie, Burneyville, Idabel, and Marena. At these sites, a minimum in closure occurred during the early morning hours, but closure estimates increased during the day to reach a maximum during the late afternoon. In this scenario, the closure mean was asymmetric about solar noon. An examination of diurnal means of net radiation, ground, sensible, and latent heat fluxes uncovered an asymmetric diurnal pattern in latent heat flux. Latent heat flux was less than net radiation during the morning hours, but greater than net radiation during the late afternoon hours.

An earlier comparison between the EC and BR methods suggested that the EC method was unable to capture latent heat flux during the early morning hours (Figs. 6.34a-f). This problem led to an apparent underestimate in closure during the morning period. It appears this problem may be widespread and not necessarily a function of site properties (Figs. 7.7 – 7.19). The problem may also result from the relatively high height (4.5 m) at which the EC sensors were installed. Perhaps a lower height for these sensors would alleviate the problem described above (Chapter 8).

A third common pattern is the month-to-month variation in closure at several sites. A close relationship between closure and the Bowen ratio at Bessie was evident during June through August 1999 as both the Bowen ratio and closure rates increased. During September and November, both Bowen ratios and closure rates decreased. A similar pattern was observed at Burneyville, Grandfield, Idabel, Marena, and Norman.

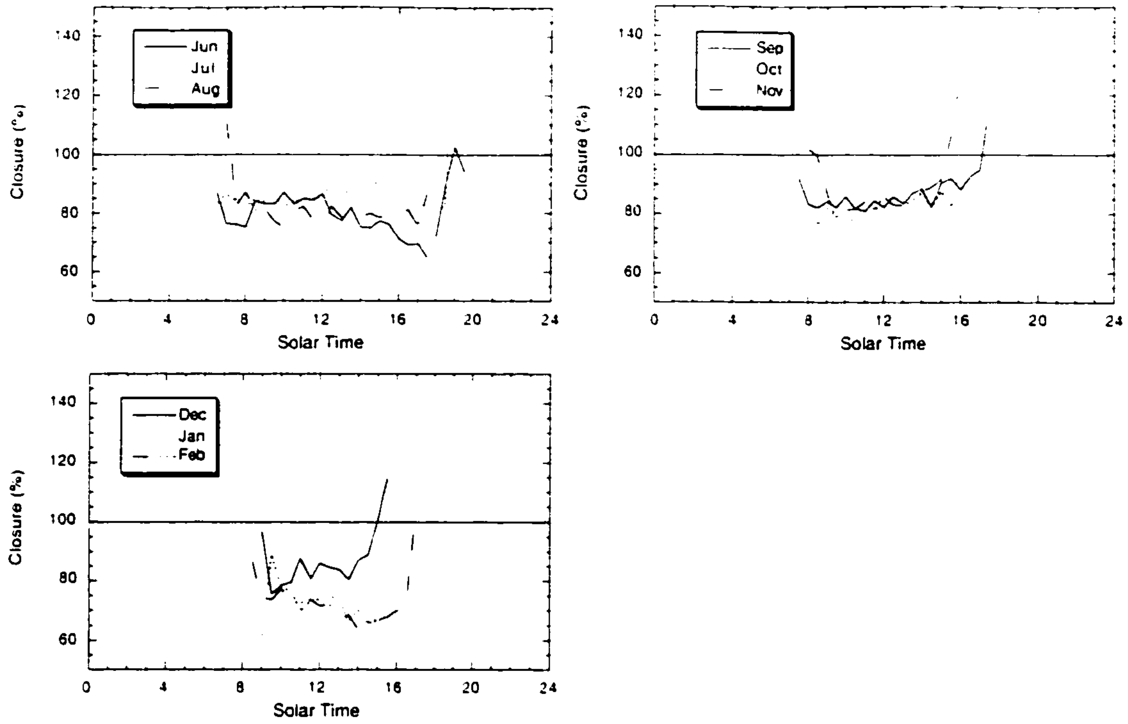

Fig. 7.7: Monthly-averaged estimates of closure plotted as a function of solar time. Data were collected at the Alva super site during 1 June 1999 – 31 May 2000.

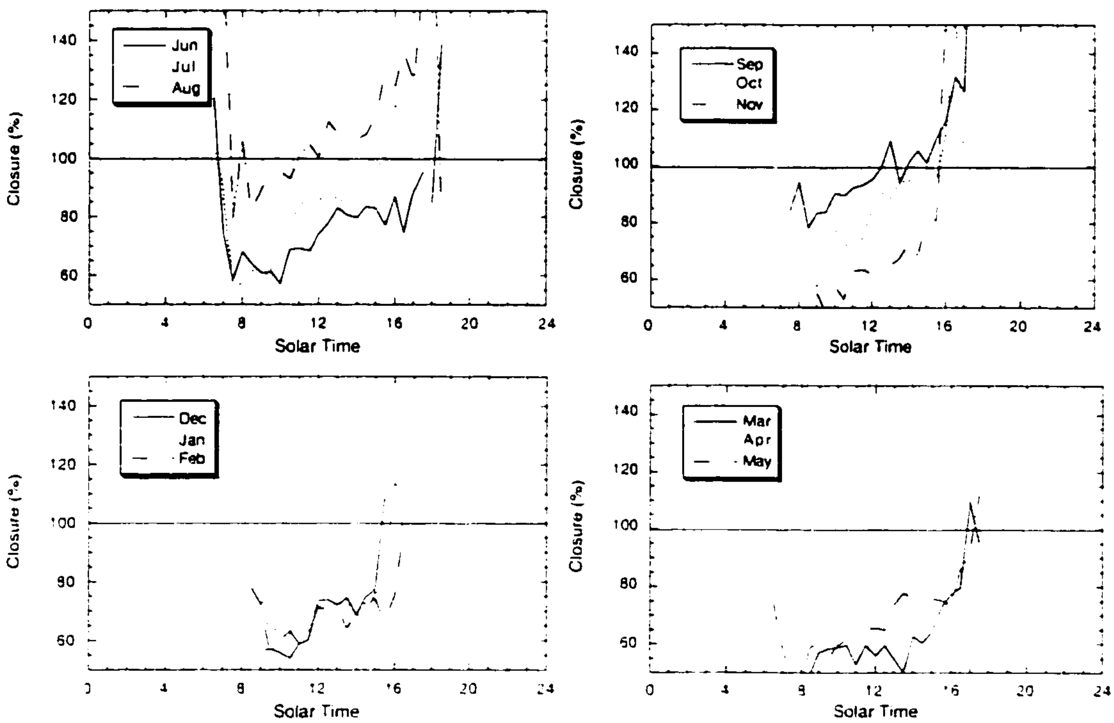

Fig. 7.8: Monthly-averaged estimates of closure plotted as a function of solar time. Data were collected at the Bessie super site during 1 June 1999 – 31 May 2000.

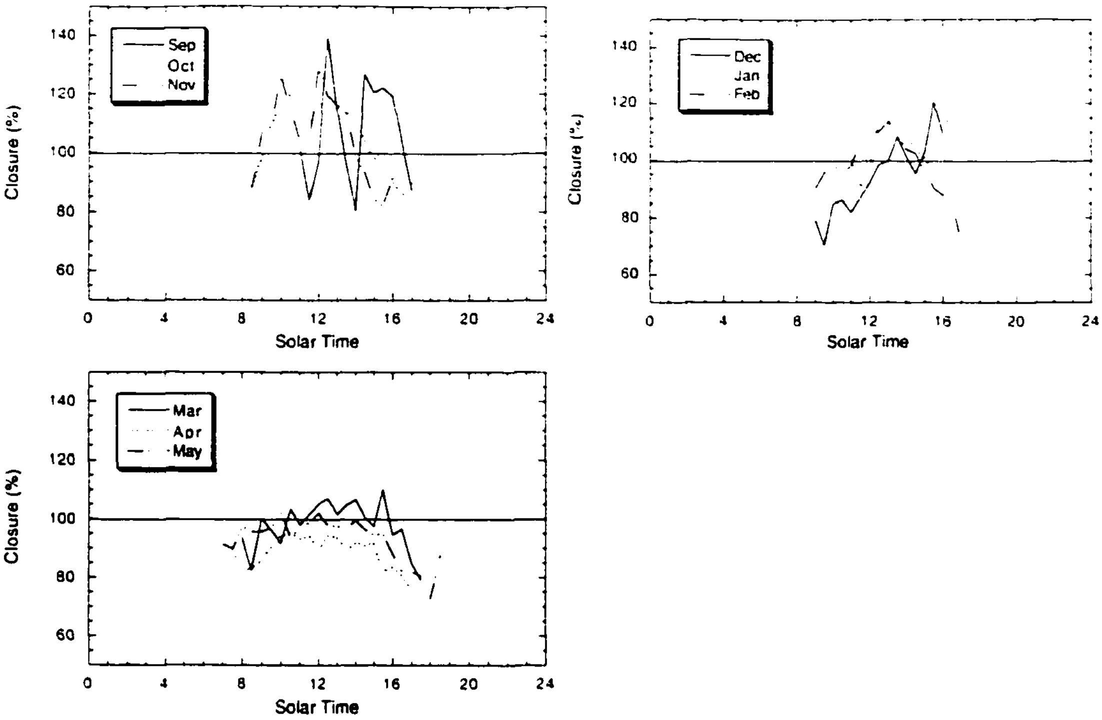

Fig. 7.9: Monthly-averaged estimates of closure plotted as a function of solar time. Data were collected at the Boise City super site during 1 June 1999 - 31 May 2000.

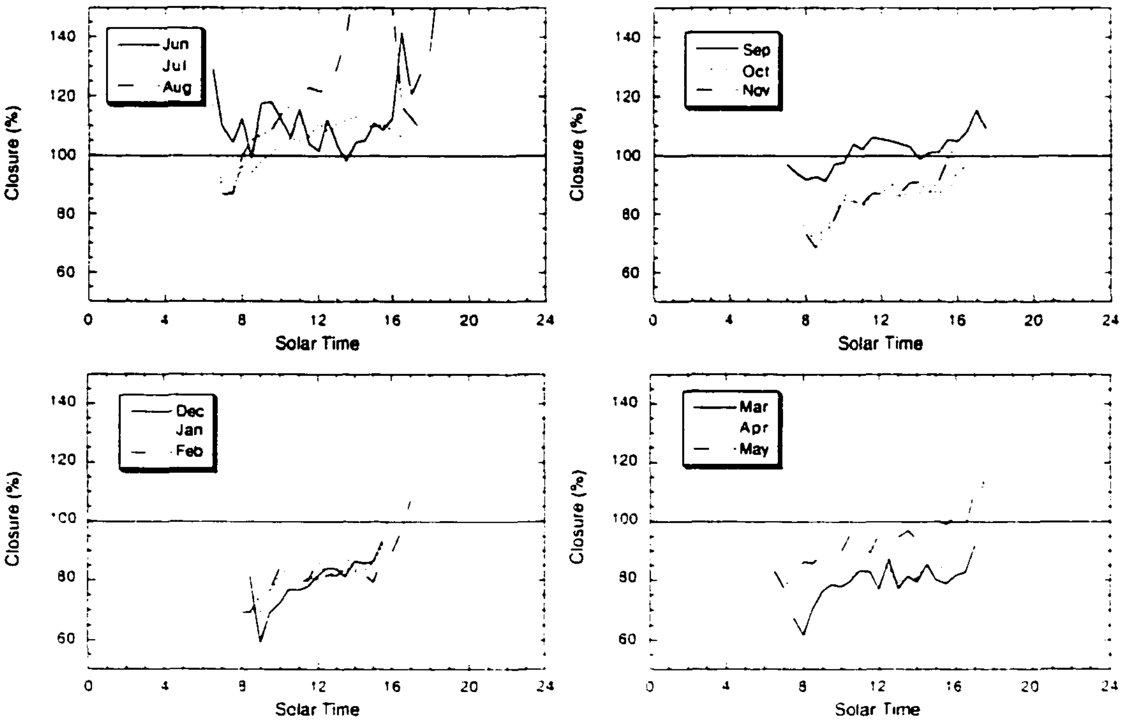

Fig. 7.10: Monthly-averaged estimates of closure plotted as a function of solar time. Data were collected at the Burneyville super site during 1 June 1999 – 31 May 2000.

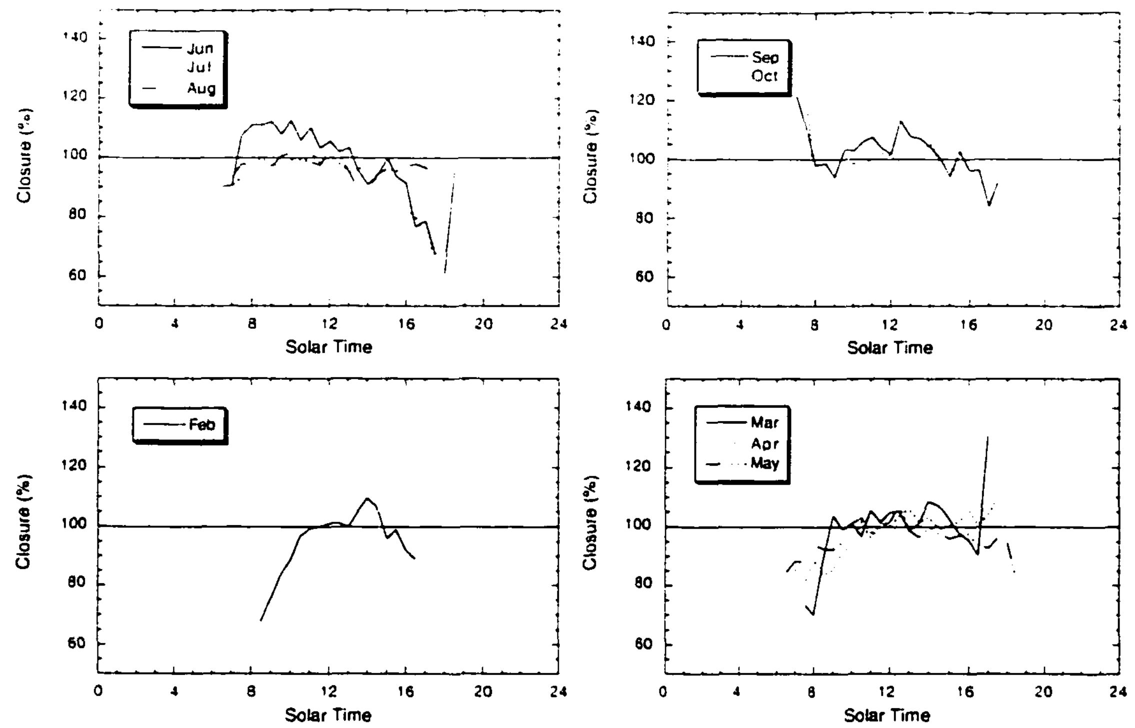

Fig. 7.11: Monthly-averaged estimates of closure plotted as a function of solar time. Data were collected at the Foraker super site during 1 June 1999 – 31 May 2000.

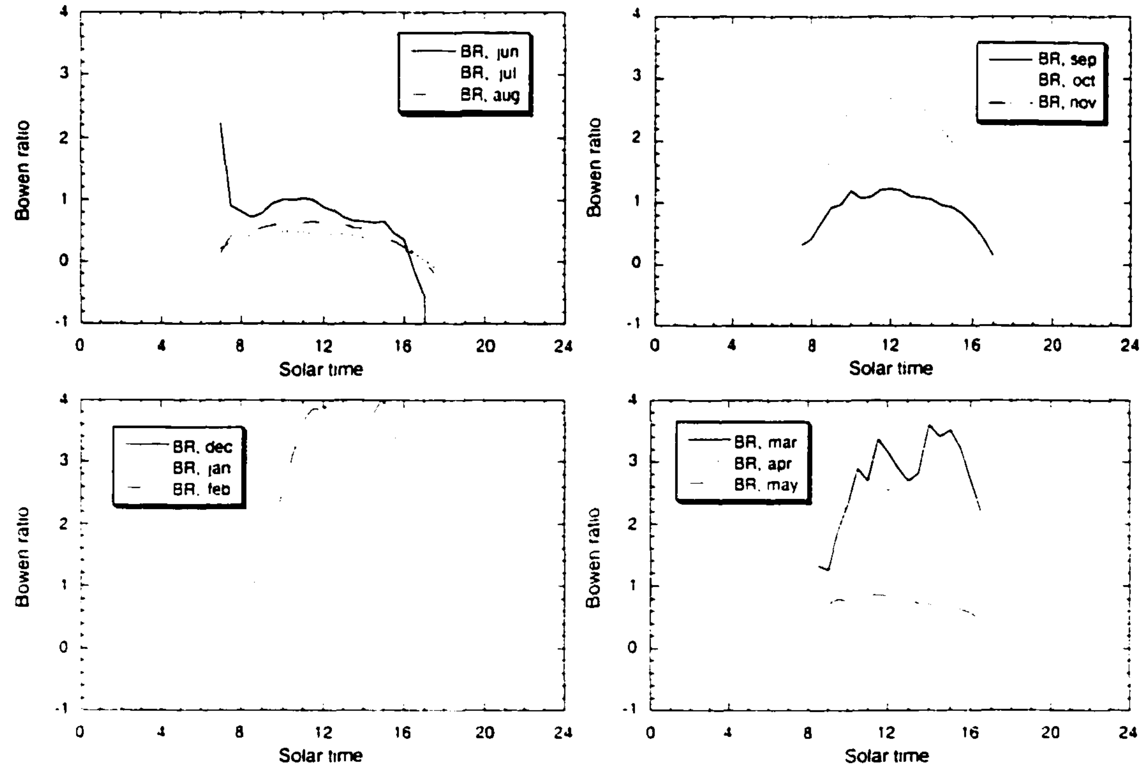

Fig. 7.12: Monthly-averaged estimates of the Bowen ratio plotted as a function of solar time. Data were collected at the Foraker super site during 1 June 1999 – 31 May 2000.

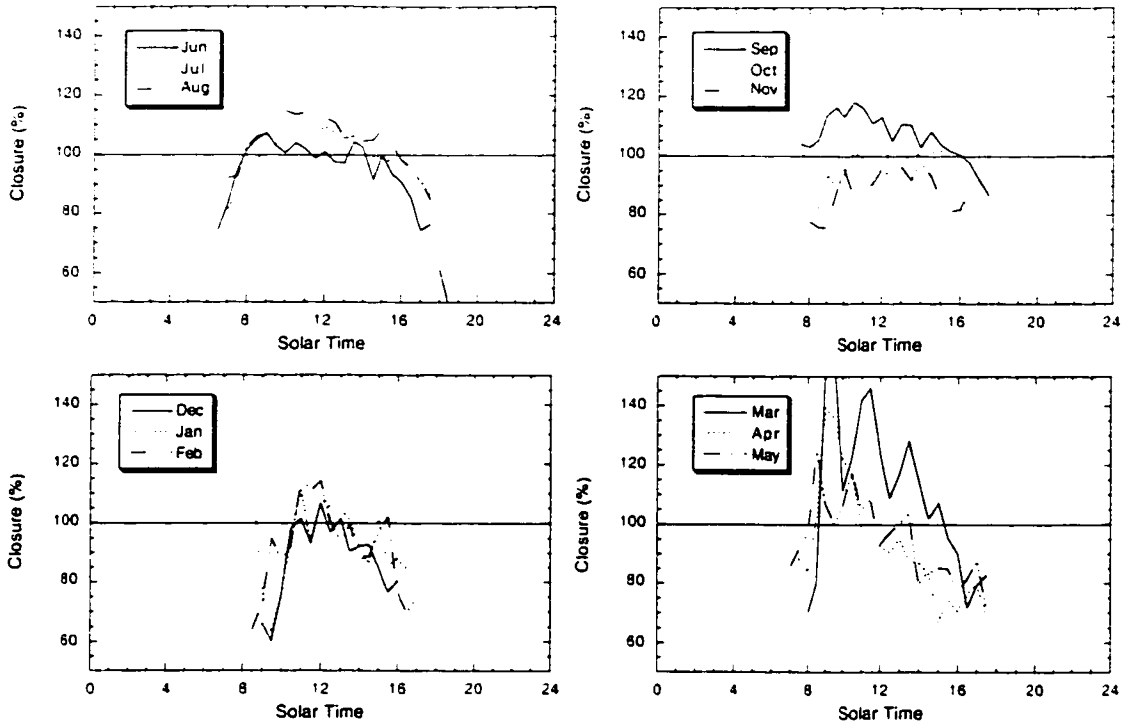

Fig. 7.13: Monthly-averaged estimates of closure plotted as a function of solar time. Data were collected at the Grandfield super site during 1 June 1999 – 31 May 2000.

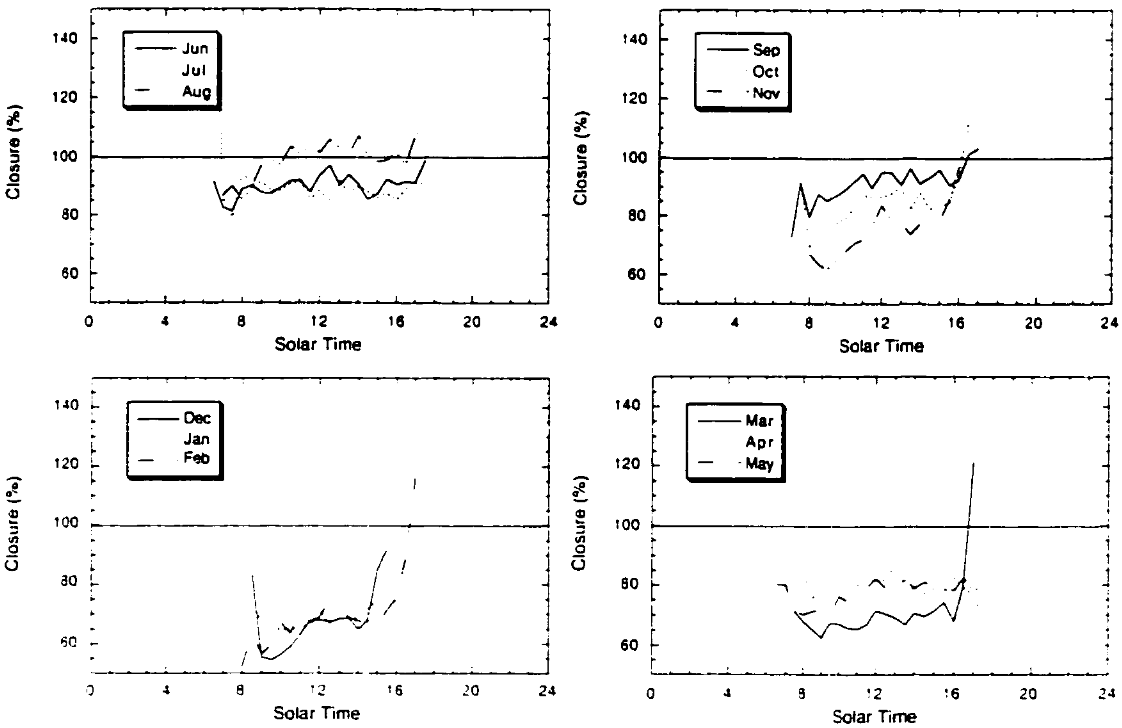

Fig. 7.14: Monthly-averaged estimates of closure plotted as a function of solar time. Data were collected at the Idabel super site during 1 June 1999 – 31 May 2000.

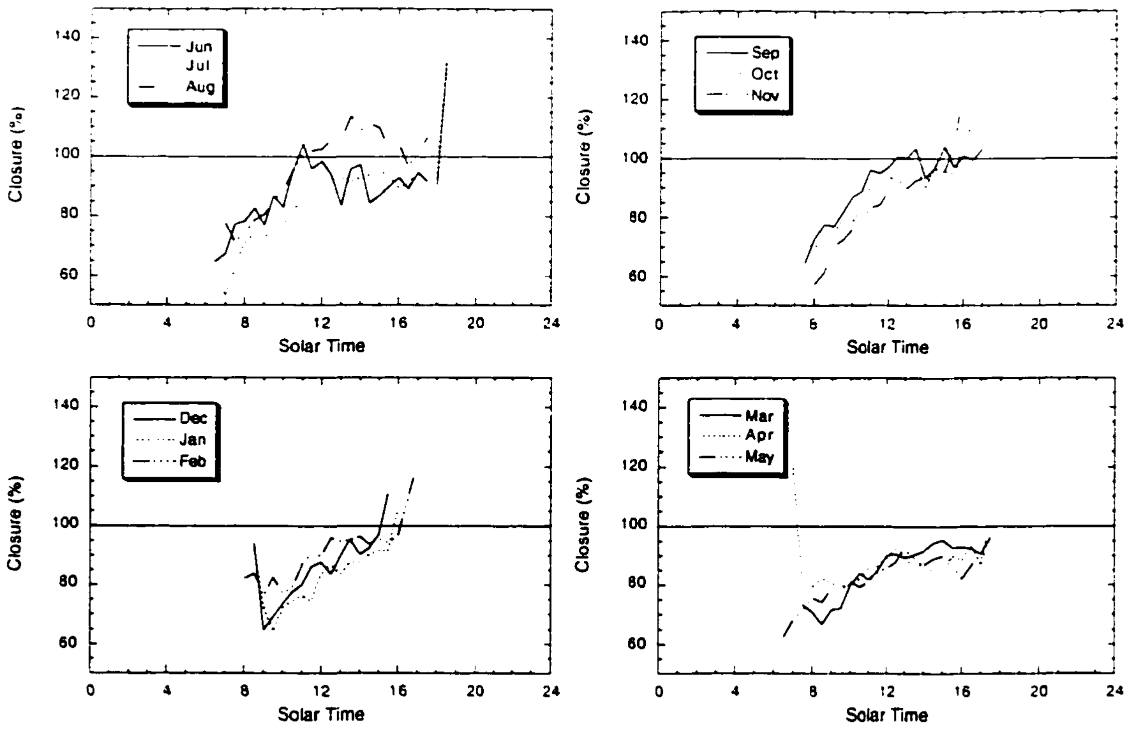

Fig. 7.15: Monthly-averaged estimates of closure plotted as a function of solar time. Data were collected at the Marena super site during 1 June 1999 – 31 May 2000.

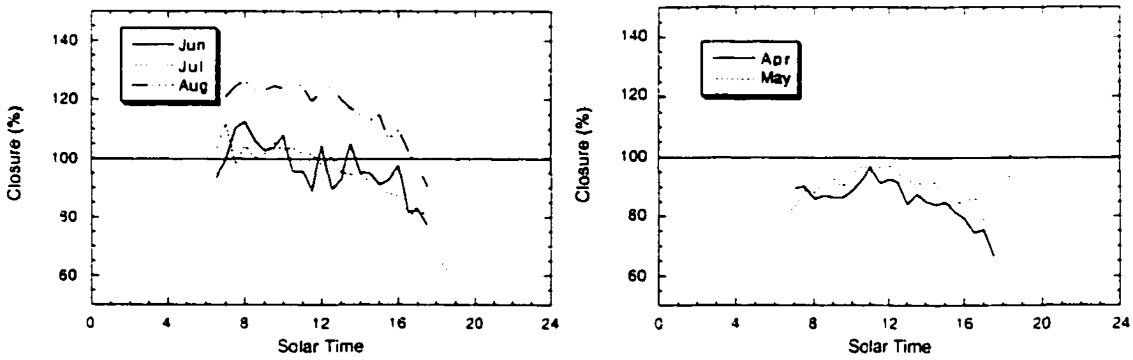

Fig. 7.16: Monthly-averaged estimates of closure plotted as a function of solar time. Data were collected at the Norman super site during 1 June 1999 – 31 May 2000.

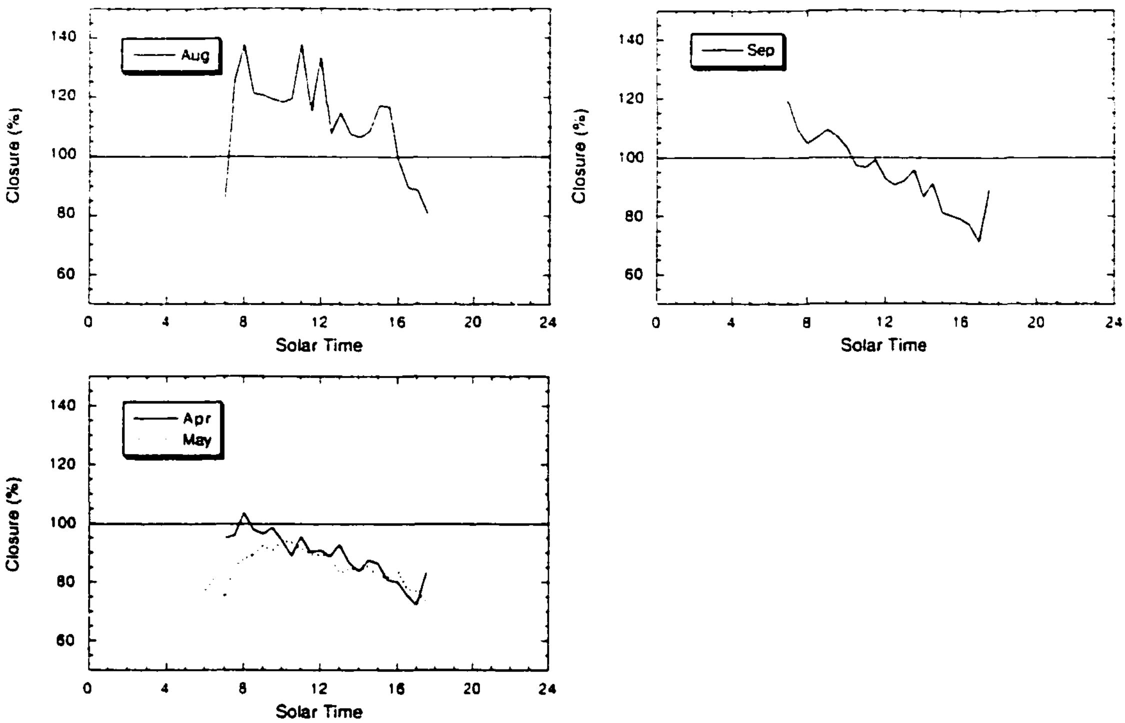

Fig. 7.17: Monthly-averaged estimates of closure plotted as a function of solar time. Data were collected at the Stigler super site during 1 June 1999 – 31 May 2000.

7.6 External Factors Influencing Closure

Several variables were examined to help explain the variance observed at the ten super sites. Closure assessed in light of the Bowen ratio, topography, and geographical location.

7.6.1 Bowen Ratio

The mean annual rate of closure at each site was plotted as a function of the mean annual of Bowen ratio (Fig. 7.20). Closure rates improved as the Bowen ratio increased. Some variance in closure resulted from differences in length of the data period. For instance, the data sample at Stigler and Norman was less than 80 days in length while the sample at Marena included 135 days of data. The site at Bessie was not included in Figure 7.20 because of a poor closure rate, mostly likely the result of rough and hilly terrain.

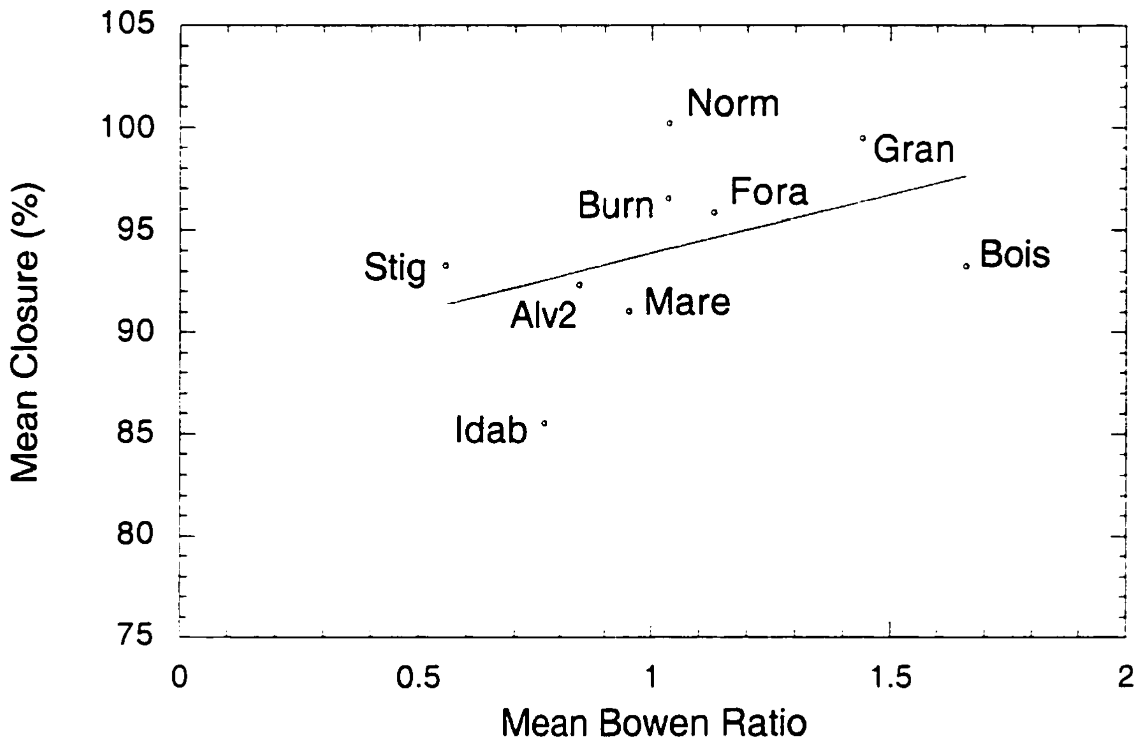

Fig. 7.20: Mean annual closure rate at each super site versus the mean annual Bowen ratio.

The Bowen ratio also had a strong influence on daily closure rates (Fig. 7.5). The comparison between the BR and EC methods in Chapter 6 indicated a failure to measure latent heat flux correctly during certain periods of the day, particularly during the early morning and late afternoon hours when the measured Bowen ratio was at a minimal value. Likewise, the annual cycle of closure at the ten sites showed remarkable improvement in closure rates during long-dry periods (Figs. 7.3 – 7.4). This result indicates that the energy budget is well measured during dry periods, but is poorly measured during periods when latent heating is at a maximum. Thus, the lack of an accurate measurement of latent heat flux is primarily responsible for the lack of closure.

7.5.2 Topography

Stannard et al. (1992) determined an inverse relationship between closure rate and topography with closure rates declining as surface roughness increased. A similar relationship was uncovered at the ten super sites. Topographical data at 30 m resolution was acquired from a digital elevation model of the United States Geological Survey. The average and standard deviation of elevation, slope, and aspect were calculated for each site. In addition, statistics of the topography were determined for the four cardinal directions (N, S, E, and W) from each Mesonet site so the effects of fetch could be investigated.

EC measurements are influenced by an upwind, land-surface area known as the "footprint" region. The size of the footprint area is a function of the height at which sensors were installed, atmospheric stability, and surface roughness. For a measurement height of 4.5 m and during stable conditions, the radius of influence extended beyond 0.5 km from the site. However, during neutral and unstable conditions, 0.5 km was the maximum radius of influence. For this study, land characteristics were assessed within a circular area about each site that was 500 m in radius.

The annual mean closure plotted as a function of mean slope (Fig. 7.21) illustrates a weak inverse relationship. Several of the flattest sites with near-zero terrain slope – like

Norman, Grandfield, and Burneyville - attained the greatest degree of closure. Likewise, three sites with the greatest terrain slope – Bessie, Marena, and Stigler – attained the worst closure rates. Note that Bessie and Idabel were not shown due to their poor closure rates. The worst closure rate was estimated at Bessie, a site with the greatest degree of terrain slope. Only the site at Idabel appeared as an outlier in Figure 7.21. Despite the relative flatness of the Idabel site, the closure rate at Idabel was much less than that observed at other flat sites. The low rate of closure at Idabel is likely caused by large values of latent heat flux (Fig. 7.20). Given its geographic location in southeast Oklahoma, nearby forests likely prevented a determination of the appropriate fetch to use in the Idabel computations. Roughness created by tall vegetation and trees create a similar effect to rough topography. Thus, the linear relationship between closure and terrain slope indicated that closure declined 2% per degree of terrain slope (Fig. 7.21). However, variance about the "best fit" relationship shows the relationship between mean slope and closure is weak.

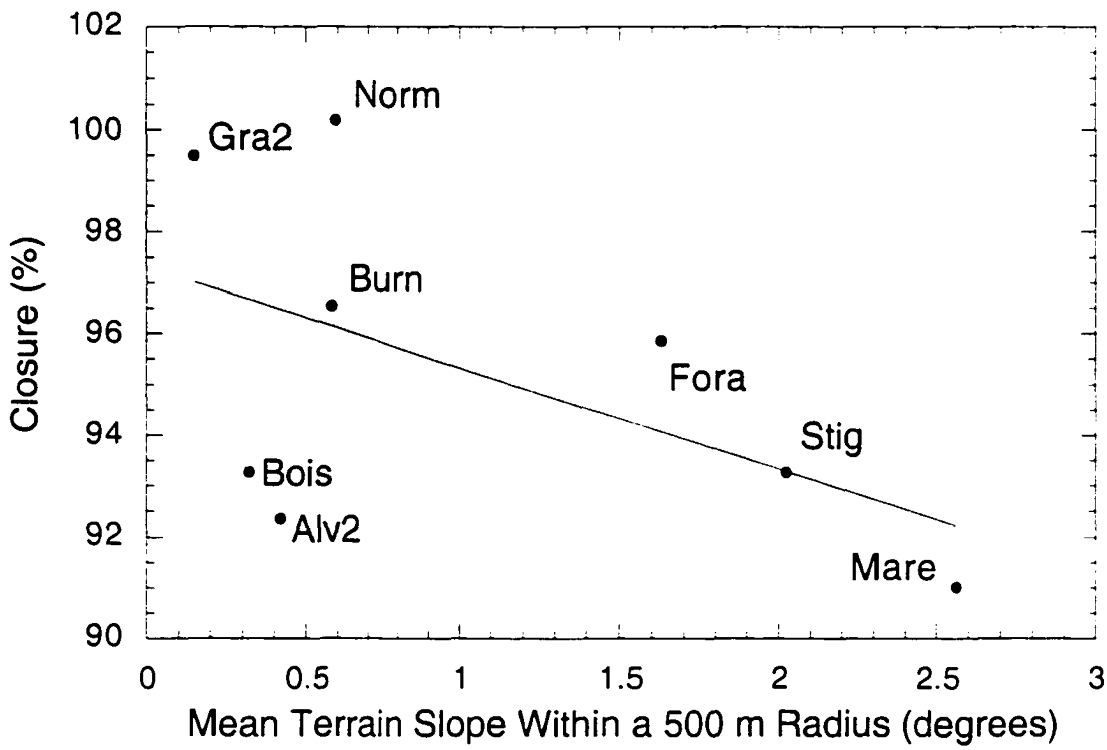

Fig. 7.21: Mean annual closure rates (%) as a function of the mean terrain slope (within a 0.5 km radius of each Mesonet site).

The correction for coordinate rotation removes much of the error due to the mean terrain slope. However, corrections are not possible in more complex topography. The annual mean of closure versus the standard deviation (σ) of terrain slope revealed results (Fig. 7.22) that were similar to those in Figure 7.21. Closure decreased at an average rate of 2% per degree of standard deviation of slope.

A t-test was performed to determine if the variance of slope had a significant impact on closure. The sites were stratified into two categories: those sites with a standard deviation of terrain slope < 0.5° and those sites with a standard deviation of terrain slope > 0.5°. The test for significance did not reveal a significant difference in closure between the

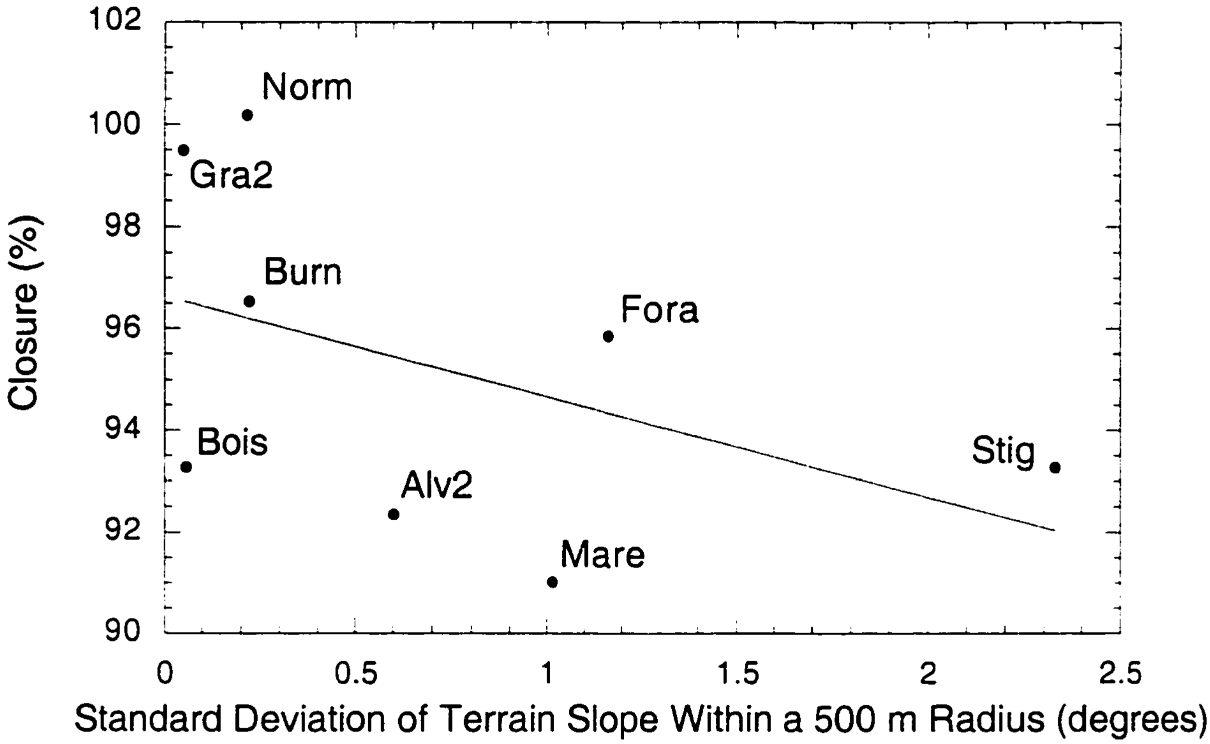

Fig. 7.22: Mean annual closure rates (%) plotted as a function of the standard deviation of terrain slope (within a 0.5 km radius at each Mesonet site).

two groups at the 10% confidence level. However, when data from the Idabel site were excluded, the t-test displayed a significant difference between the two groups. Likewise, a significant difference between the two groups occurred when data from Idabel and Bessie were excluded. Thus, a significant difference in closure is created by increased variance of topographical features.

The relationship between closure, elevation and terrain slope was investigated when wind direction was considered. The 5-minute observations of wind direction were stratified into one of 16 cardinal directions (e.g., N, NNE, NE, ENE...). Then, the prevailing wind direction in 30-minute time windows was determined (to match the time resolution of OASIS data). Unfortunately, topographical data had only been determined in four directions (N, S, E, and W). For Mesonet data to be compatible with this previous decision, the 30-minute means of closure were stratified into one of the four cardinal directions. These results, as a function of wind direction, are shown in Figures 7.23 – 7.25.

When stratified by cardinal directions for the prevailing flow, the mean elevation at a site had limited influence upon closure (Fig. 7.23a-j). Closure rates observed from the flattest sites at Alva, Grandfield, and Norman varied little with prevailing direction. Likewise, closure rates varied greatest at sites where topography varied the most. Closure rates from sites at Bessie, Foraker, and Marena showed large variance in closure with changes in the prevailing wind direction. On the other hand, Idabel is nearly flat and yet the data revealed a large variance in closure with prevailing direction. The site at Stigler, a hilly site, showed little variation in closure versus changes in the prevailing wind direction.

The variance in elevation at a site seemed to have a stronger impact upon closure estimates (Fig. 7.24a-j). The most topographically variable sites - Bessie, Foraker, and Marena - had a strong negative correlation with the standard deviation in elevation. With increased variance in elevation, closure rates declined sharply. As the topography became more gently varying, closure rates improved. Data from several of the flatter sites (Alva, Norman, and Stigler) decreased their closure with increased variability of the land-surface in one of the cardinal directions. Sites at Boise City, Burneyville, and Idabel showed no relationship between the variance of the topography and closure.

In summary, the effects of topography upon closure are difficult to discern without more detailed study. Results should be repeated using geographical data with 16 directions. In addition, the impact of nearby forests and tall grasses affect fetch, which may dampen or inhibit a clear topographical signal.

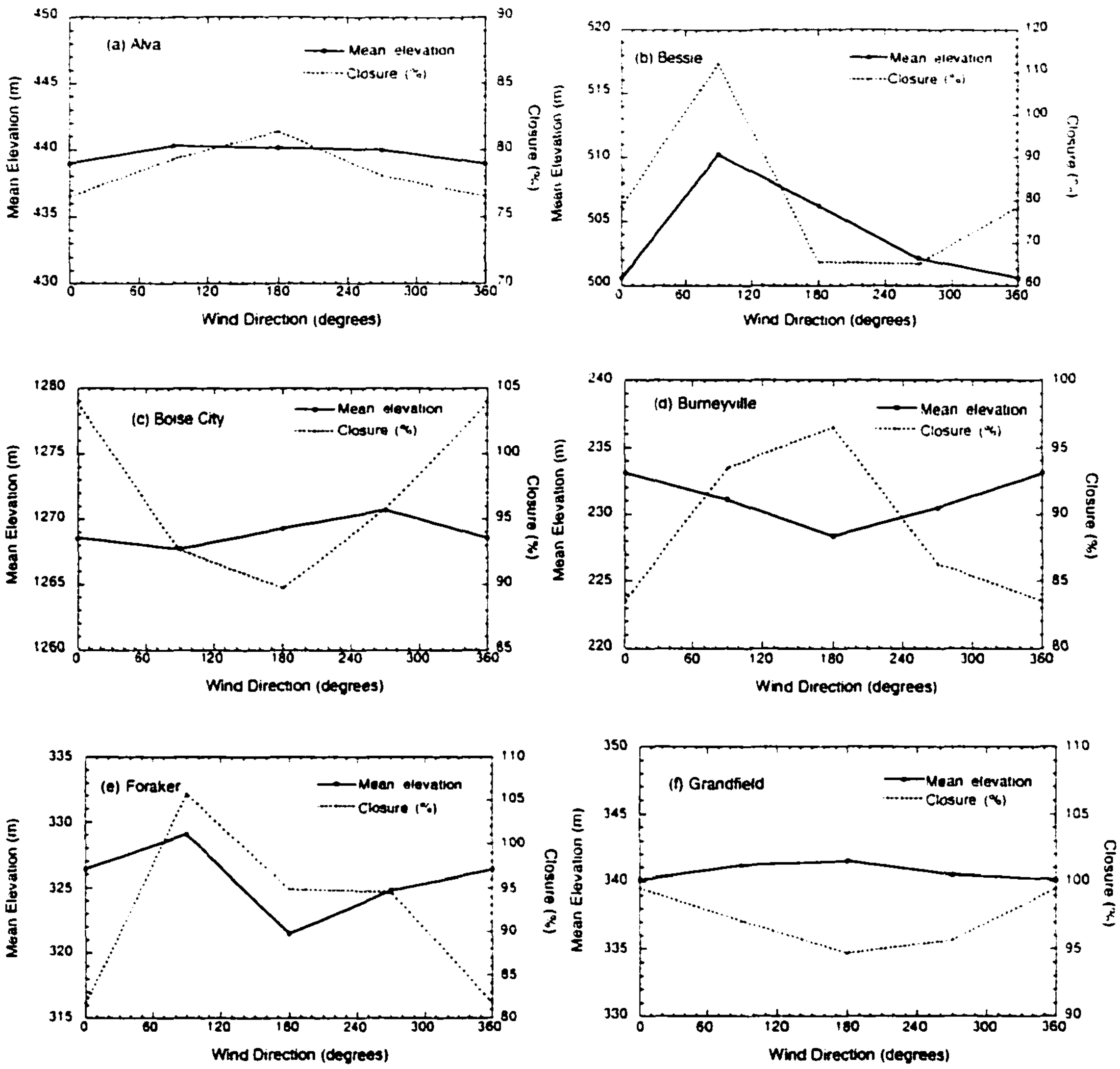

Figs. 7.23a-f: Mean elevation (m) and closure (%) plotted as a function of prevailing wind direction (degrees).

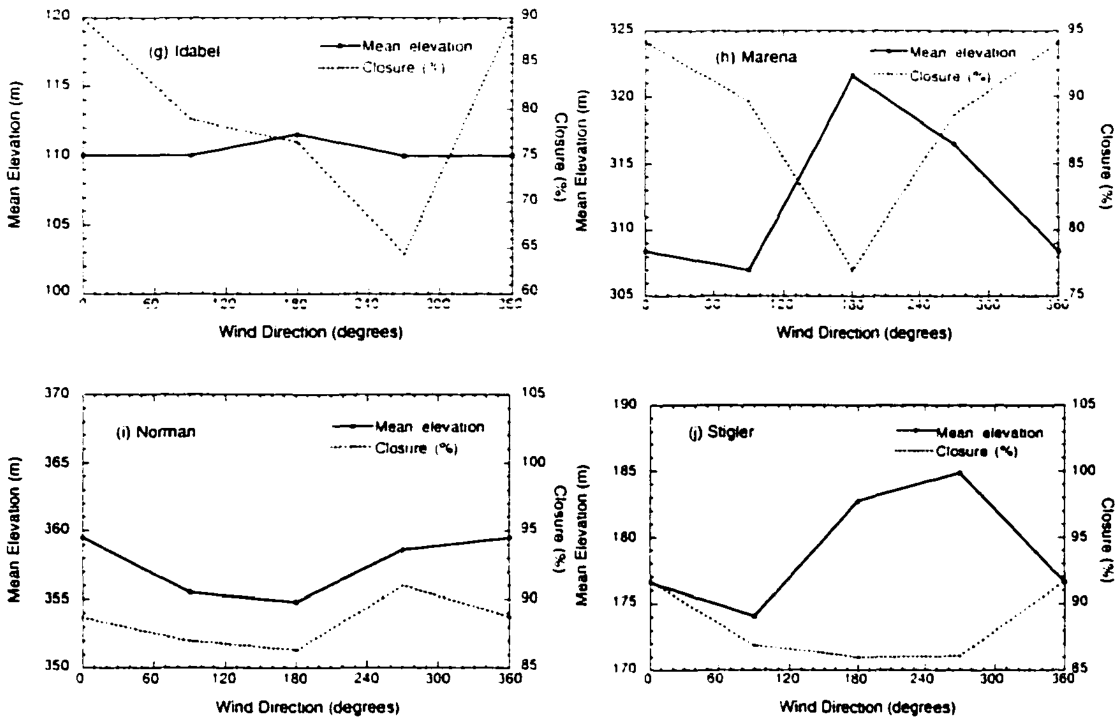

Figs. 7.23g-j: Mean elevation (m) and closure (%) plotted as a function of prevailing wind direction (degrees).

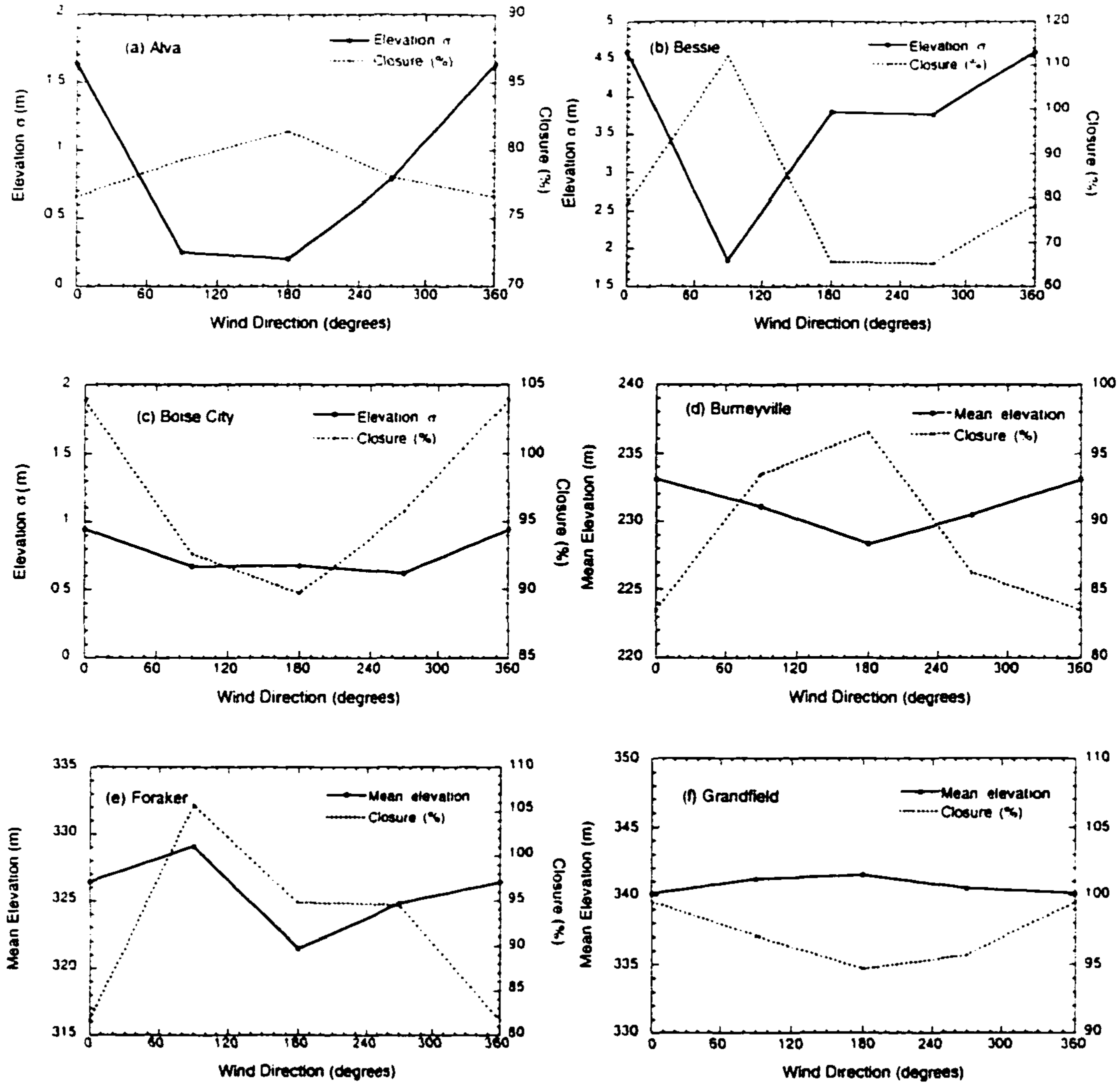

Figs. 7.24a-f: Standard deviation of elevation (m) and closure (%) plotted as a function of prevailing wind direction (degrees).

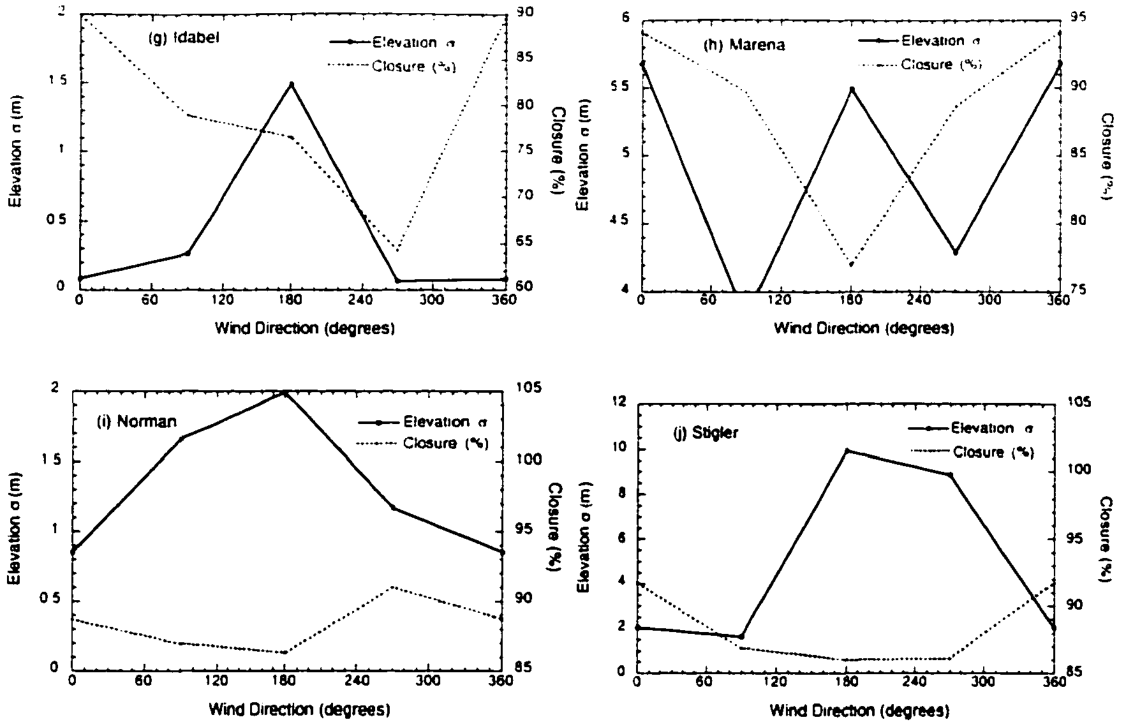

Figs. 7.24g-j: Standard deviation of elevation (m) and closure (%) plotted as a function of prevailing wind direction (degrees).

7.5.3 Geographic Location

The climate and vegetation of Oklahoma are influenced by the geography of Oklahoma. Terrain slopes upwards from southeast toward northwest Oklahoma. Forests dominate eastern Oklahoma while agriculture and prairie grasses are more common in the western half. Native vegetation reflects the climate across the state with southeast portions receiving more than 1300 mm of rain per year and northwest portions receiving less than 500 mm per year. The combined effects of a wetter climate and more variable terrain and forests in eastern Oklahoma produce poor closure rates (<90%) while a relatively dry climate, flat terrain and short grasses in western Oklahoma produce good to excellent closure rates (>90%). Closure rates as a function of longitude reflects a weak relationship. Closure rates only improve hardly at all from east to west across Oklahoma. The site at Bessie is an outlier in Figure 7.25. The poor closure rate at Bessie is reflective of steep terrain in that limited portion of western Oklahoma.

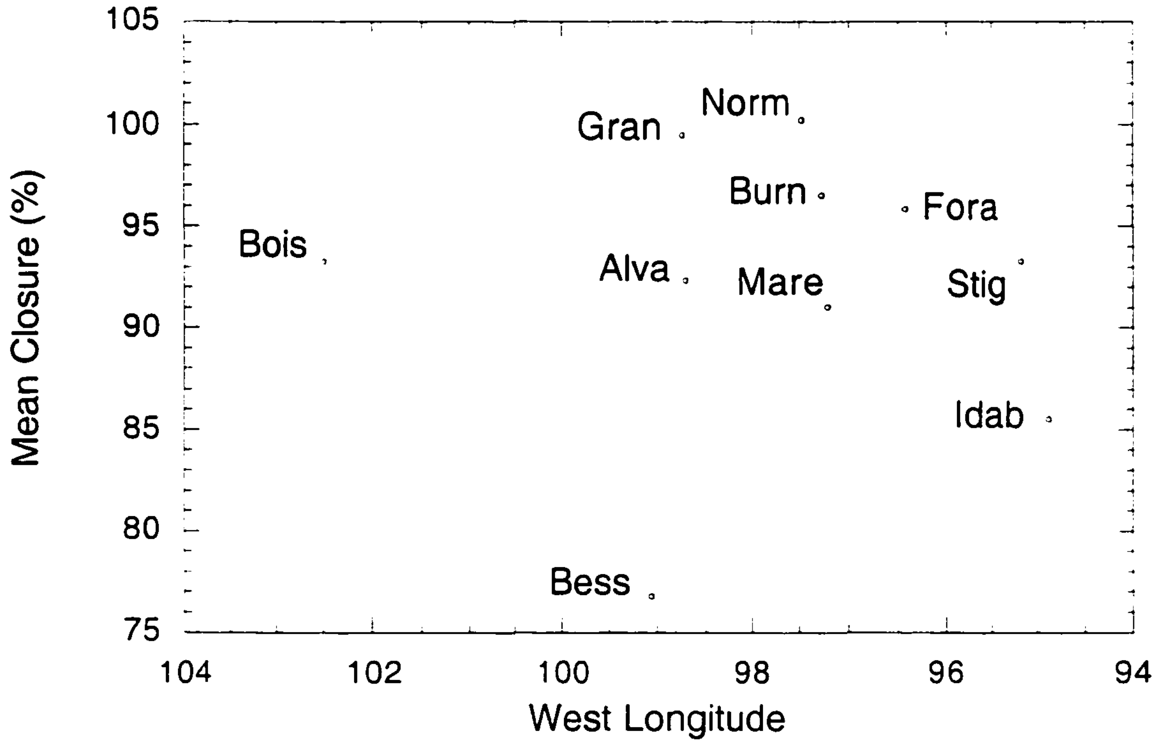

Fig. 7.25: Mean annual closure rate (%) plotted as a function of site longitude.

Chapter 8: System Error

Introduction

Error by the observing system are created when, despite properly working instruments, the observation still does not represent the "real" atmosphere. A persistent systematic error in energy budget studies has been the fact that SH and LH fluxes are underestimated EC systems. Thus, this continued failure to close the energy budget has been an inextricable problem since EC systems were introduced. The origin of this systematic error is part of an ongoing debate and likely has more than one source. Reasons for non-closure are most likely unique to each study. Unfortunately, the sensitivity of surface measurements to subtle variations in the design of instruments, fetch, topography, and surface heterogeneity have limited most short-term studies from solving this fundamental system error.

The OASIS data set was designed to provide long-term measurements from multiple sites so that system errors could be isolated. With that issue settled, other causes of closure error are considered. Reasons for non-closure have been suggested by many other investigators and each are considered in this chapter. These reasons include an overestimate of the available energy, a mismatch in source areas, horizontal flux divergence, surface heterogeneity, fetch issues, and instrument error.

8.1 The Overestimate of Available Energy

Sensible and latent heat fluxes are difficult parameters to measure accurately. Failure to close the energy budget has been synonymous with the underestimate of sensible and latent heat fluxes. Nevertheless, an overestimate of net radiation and/or an underestimate in ground heat flux can lead to a similar failure to close the energy budget (because less than 100% of the energy budget can be accounted for).

The primary concern that impacts closure is systematic errors (bias) with either measurement of net radiation or ground heat flux. A comparison of data from similar instruments revealed only a minimal systematic bias with either measurement. As demonstrated by Halldin and Lindroth (1992) and by Field et al. (1992) and as illustrated in Figures 5.3 and 6.6 – 6.7, significant differences in calibration were observed between different models of radiometers. Observations from the CNR1 when compared to observations from a 4-component PSP/PIR radiometer system manufactured by Eppley (Section 5.1) revealed how the CNR1 *underestimated* net radiation by ~ 40 Wm^{-2} at midday. A second test compared the CNR1 estimates with the SIRS estimates from the ARM site at Foraker. This study revealed how the CNR1 *overestimated* relative to SIRS by as much as 5% (Fig. 6.6). Unfortunately, the absolute "true" value of net radiation is unknown.

Systematic errors in ground heat flux are more difficult to identify. Only at the co-located ARM site could the ground flux be independently evaluated against another system. Annual variations in ground heat flux between the two systems was ~ +/- 1 MJ m^{-2} day^{-1}. During the growing season, the Mesonet estimates of ground flux were greater than estimates from ARM while during the cool season the Mesonet estimates were less than those from ARM. This overestimate in closure is likely caused by an overestimate in soil moisture during the dry period due, in part, to error in the conversion of matric soil water potential to soil water content (Fig. 6.14).

The available energy measured at the Mesonet site at Foraker was nearly equal to the available energy measured at the ARM site (Figs. 6.16 – 6.18). The overestimate in radiation by the CNR1, when compared to SIRS was compensated by an equal overestimate in the ground heat flux at the Mesonet site. Thus, differences in available energy between the two observing systems were within +/- 1 MJ m^{-2} day^{-1} (Fig. 6.32). The residual error from closure during the year ranged as high as +4 MJ m^{-2} day^{-1}. Thus, only 25% of the closure error could be explained by an overestimate in available energy. Based upon a comparison of data from the Mesonet and ARM sites and based upon prior results in the scientific literature, error in the measurement of net radiation and ground heat flux likely had only a small contribution to the closure error.

8.2 Mismatch in Source Areas and Horizontal Flux Divergence

One difficulty that occurs when estimating closure is to ensure that each of the four components of the energy budget represent measurements from similar source regions. This problem arises from the fact that observations of net radiation and ground heat flux are point measurements while the eddy covariance measurements are areal estimates. The technique of EC measures fluxes, which are sometimes influenced by land properties as far as one kilometer upwind.

A *mismatch in source areas* occurs when the available energy measured by the net radiometer and ground flux sensors is not equal to the available energy incident upon the larger area measured by the EC system (Stannard et al. 1994). The problem is created because the Rn and GH terms are point measurements acquired near the tower whereas the EC measurement represents an areal estimate from a much larger footprint.

To limit these effects, previous scientific experiments used flat agricultural fields with a known roughness length (e.g., FIFE, Nie et al. 1992; SGP-97, Twine et al. 2000).

To minimize the problem of measuring fluxes from multiple source areas, each component of the energy budget should be representative of the landscape near the observation site. However, given the nature of the point measurements in the soil, this requirement is not possible to meet unless hundreds of ground flux plates and PRTDs are placed across an area that is 0.5 - 1 km in diameter. Because the measurement of net radiation represents a small footprint, the higher above ground the net radiometer is placed, the greater the footprint area. In turn, the greater the surface area that is sampled, the more surface heterogeneity can impact the radiation measurement. Unfortunately, longwave radiation is emitted by molecules of air. Thus, the higher the radiometer is mounted, the greater the radiation that is emitted by air molecules between the radiometer and ground surface emit longwave radiation.

Fortunately, the problem of multiple source areas is limited to relatively flat terrain. This concern does not greatly impact data from the ten OASIS super sites. Yet, a mismatch in source areas becomes significant when measuring energy components across sloped terrain. The varying aspects of sloped terrain create large differences in available energy (Stannard et al. 1994).

A problem related to estimating closure is *horizontal flux divergence*. Horizontal flux divergence is created when energy from the flux of sensible or latent heat is advected into the source area under study. For example, an irrigated system upwind of a grazed site would create a greater influx of latent heat into the source area and exceed the latent flux exiting the source area. Several studies demonstrated that local advection creates areas of vertical divergence of the aerodynamic fluxes (Brakke et al. 1978; Lang et al. 1983). These areas of advection are prominent at leading edge of a discontinuity in surface properties. Typically, this type of discontinuity results from variations in vegetation type or height, roughness, or even surface wetness (Lloyd et al. 1997).

Stannard et al. (1994) listed several reasons why horizontal flux divergence does not have a significant impact upon closure. They suggested those areas producing large values of sensible and latent heat flux tended to offset one another. Thus, areas with large values of sensible flux can only produce small values of latent heat flux, and vice versa. Wet areas with large values of latent heat flux tend to be cooler and produce small values of sensible flux; dry areas produce large values of sensible flux and only small values of latent heat flux. Thus, the sum of SH and LH remains nearly the same as the available energy. Thus, flux divergence has a minimal impact upon closure estimates.

8.3 Surface Heterogeneity

Surface heterogeneity is the primary reason why measurements from multiple source areas and estimates of horizontal flux divergence are often in error. Variations in the type, moisture, and temperature of soils, and vegetation height and type create significant differences in the thermal characteristics of soil and the fluxes of energy that result. For example, two heat flux plates separated by only a meter could measure the soil heat flow from two different surface regimes. Thus, the use of at least three heat flux plates and three PRTDs has been recommended by previous studies to account for surface heterogeneity (Fritschen and Gay 1979; Massman 1993). The Mesonet uses two heat flux plates and two PRTDs to measure soil heat flux.

As the surrounding landscape become more uniform, closure estimates improve. Assuming that systematic errors do not occur in the instruments, differences in measurements obtained from several heat flux plates and several PRTDs provide a measure of heterogeneity of the surface vegetation and soil characteristics. For example, in a patchy landscape composed of 50% bare soil and 50% vegetation, two flux plates and two PRTDs likely would measure different fluxes if one plate (and PRTD) sampled the bare soil while the other pair sampled the vegetated surface.

This hypothesis was tested by examining differences in the measurements from two PRTDs and two flux plates (Tables 8.1 and 8.2). The mean annual difference in soil heat flow as estimated by two flux plates is plotted in Figure 8.1. For heavily vegetated sites, both sets of sensors were expected to measure a similar thermal regime. For example, little difference was noted between the two flux plates at Foraker and Idabel (Fig. 8.1). On the other hand, sparsely vegetated land-cover should increase the variability between sensor observations. Data from Grandfield revealed large differences in the measurements from the two flux plates (Fig. 8.1). Furthermore, data from the western-most sites appeared to be more variable than did data from sites in eastern Oklahoma. This contrast was most likely a result of sparse vegetation at the western sites. Unfortunately, using only two sets of sensors does not capture the spatial variability needed to quantify characteristics of the landscape.

Because the mean annual closure varied systematically across Oklahoma, surface heterogeneity likely impacted closure estimates.

The scientific literature does not agree on which climate conditions create the greatest surface homogeneity. Lloyd et al. (1997) found that rainy periods with wet surface conditions and neutral surface layers produced better closure rates than were observed during drier periods. They concluded that drier periods led to greater surface heterogeneity and a more unstable surface layer. Thus, the areal extent of the footprint region was limited. On the other hand, Unland et al. (1996) determined that convective precipitation greatly impacted surface homogeneity at a desert site. Using a small network of rain gages deployed across a 40 m x 50 m area during the monsoon season. Unland et al. discovered that rainfall varied by about 20% during convective storms and 5% during the passage of frontal systems. They concluded that point samples of rainfall were not representative during convective periods.

Basara et al. (2001) examined the spatial variability of soil moisture at a 5 cm depth from 12 sample locations within a 20 m x 20 m plot. They found that variability in soil water content among the 12 sample locations was greatest during saturated conditions and least during wilting conditions. The small observing plot actually became more homogeneous during dry periods. Thus, the spatial variability of soil moisture observed at the Mesonet site near Norman supported the results from Unland et al.

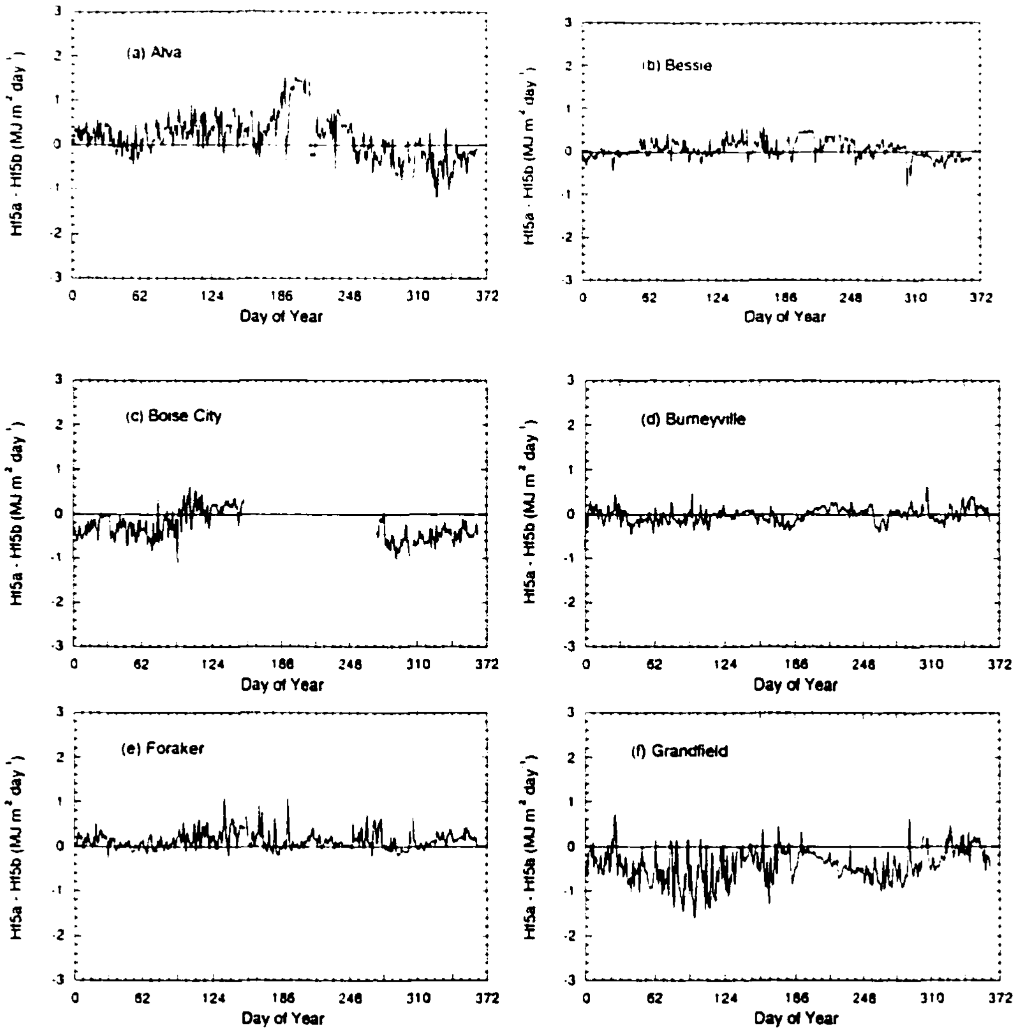

Fig. 8.1a-f: Daily totals of the difference between heat flux plates plotted at each of the ten super sites. Data were collected from 1 June 1999 to 31 May 2000.

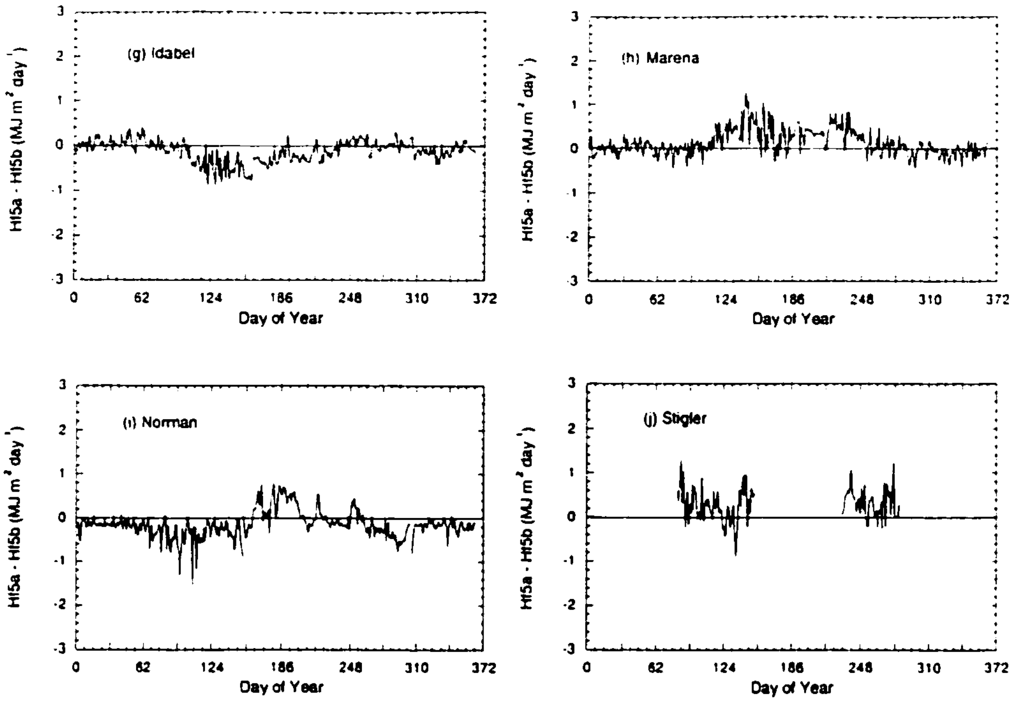

Fig. 8.1g-j: Daily totals of the difference between heat flux plates plotted at each of the ten super sites. Data were collected from 1 June 1999 to 31 May 2000.

Table 8.1: The annual mean (X) and standard deviation (σ) of integrated temperature (°C) as measured by the two PRTDs at each super site during 1 June 1999 and 31 May 2000.

	X (°C)		σ (°C)		ΔX (°C)	Δσ (°C)
	Prta	Prtb	Prta	Prtb		
Alv2	16.99	16.46	9.55	8.91	0.53	1.12
Bess	19.19	18.78	9.83	10.04	0.41	0.84
Bois	10.41	10.24	7.75	6.72	0.16	1.44
Burn	20.0	20.0	9.12	8.59	0.01	1.25
For a	15.58	15.57	8.37	8.45	0.01	0.50
Gra2	19.87	20.32	10.01	11.06	-0.46	1.89
Idab	20.20	20.25	8.40	8.47	-0.05	0.61
Mare	18.43	17.71	9.12	8.57	0.71	0.90
Norm	19.25	19.48	9.83	10.30	-0.23	1.18
Stig	21.9	21.7	6.49	6.54	0.16	0.92

Table 8.2: The annual mean (X) and standard deviation (σ) of heat flux (Wm^{-2}) as measured by the two heat flux plates at each super site during 1 June 1999 and 31 May 2000.

	X (Wm^{-2})		σ (Wm^{-2})		ΔX (Wm^{-2})	Δσ (Wm^{-2})
	Hf5a	Hf5b	Hf5a	Hf5b		
Alv2	2.43	0.52	31.4	19.6	1.91	14.1
Bess	0.65	0.20	28.4	25.7	0.45	6.75
Bois	-2.85	0.62	26.9	23.5	-3.47	8.27
Burn	0.74	0.97	19.9	23.3	-0.22	7.01
Fora	0.68	-0.82	29.5	29.2	1.50	5.48
Gra2	0.05	4.90	30.7	43.4	-4.86	15.81
Idab	1.27	2.82	20.0	24.6	-1.55	8.78
Mare	1.72	0.15	38.1	26.8	1.56	0.90
Norm	-0.71	1.06	38.1	35.7	-1.77	7.75
Stig	5.87	2.53	48.0	34.4	3.34	17.3

The presence of plant material also complicates this scenario. During dry conditions, vegetation can draw moisture from lower soil depths to create areas of high ET at the surface. The surface landscape can be considered homogeneous only during severe drought conditions when the volume of soil moisture diminishes below wilting levels or during periods of senescence. Prior scientific results determined the best closure rates were measured in arid or semi-arid environments (Barr et al. 1994; Unland et al. 1996). However, the more arid sites also were among the flattest sites tested. As a result, the degree of closure could have been dependent upon either the aridity or the topography of the site.

The temporal variability of closure at the 10 super sites may have been impacted by changes in the landscape. The variability of closure was less when the Bowen ratio was small (<1.0), and greatest when the Bowen ratios was large (> 1.0). For example, the standard deviation of closure was 15.3 Wm^{-2} when the BR < 1.0 and was 16.1 Wm^{-2} when BR > 1.0. Thus, Lloyd et al. (1997) appear correct in their conclusions. During wet conditions, closure rates were less variable (despite a systematic underestimate in closure). During dry conditions, closure rates were more variable across Oklahoma as localized areas of surface heterogeneity impacted the estimates of flux estimates. While this hypothesis does not explain the systematic underestimate in closure when Bowen ratios were small, variability in the surface landscape could explain the large variability in closure when sensible heat flux is very strong. However, an F-test for significance (Wilks 1994) failed to support the existence of a significant difference in the variance among closure rates. An extended data set is essential to determine the impact of surface heterogeneity upon closure.

8.4 Fetch

A fourth problem affecting closure is fetch which refers to the region upwind from the sensors that could impact measurements. For EC systems, an adequate fetch is critical to base study results on the assumptions of stationarity and homogeneity. Surface heterogeneity can invalidate the statistical assumptions and the accuracy of EC estimates. For instance, a mixture of short grasses and forests near a site can create large spatial variations in roughness and, thereby, limit the homogeneity of the statistical sample.

Another problem in using an EC system is the distortion of air movement through the tower. Flow distortion of the wind field by the tower does impact flux estimates (e.g., Fig. 6.23). Distortion of the wind field minimizes the covariance between the vertical wind and other scalar components. As a result, the wind field is not representative of the mean flow. Thus, EC fluxes are underestimated when surface winds are from the north. Terrain and trees have a similar effect. The size, shape and height of the obstacle, its distance from the tower, wind speed and direction, and atmospheric stability determine their impact upon estimates of flux. Fritschen et al. (1992) found that complex terrain and fetch issues create significant errors in sensible and latent fluxes.

The ten super sites were examined to assess when fetch might be a problem. Fetch was the main factor in determining which Mesonet sites would become a super sites. Only sites with the flattest, least obstructed fetch were chosen.

Closure was expected to vary significantly with wind direction. It also was expected to be significantly less than 100% when fetch problems arose. Thus, closure was assessed in light of topography (Chapter 7). Lloyd et al. (1997) observed that the effects of fetch and heterogeneity decreased as measurements were averaged over long periods of time. For example, closure rates at Bessie were poor because of the nearby sloped terrain. At Idabel, fetch problems arose from nearby trees and forests. However, on an annual and seasonal basis, variations in closure at different sites were similar.

8.5 Instrument Error

Instrument error is the most common cause for not being able to account for 100% of energy (i.e., closing the energy budget). When EC systems were first introduced in the 1960s and 1970s, rapid-sampling temperature sensors were used with an array of vertically-mounted propeller anemometers to estimate sensible heat flux. Often, latent flux was estimated as the residual. The minimal stall speeds of the anemometer introduced problems as did the frequency response and the separation between the propeller and temperature sensor. The results were frequent underestimates of flux. As instruments and software improved, these problems had less and less impact on the estimates of flux. However, a number of instrument problems persist, and they were discussed in Chapters 3, 4, and 5.

The OASIS data set has been used to address the instrument problems described earlier. The key advantage of ten OASIS sites having the same set of instruments is that site-to-site variability can be investigated without having the problem of measurement bias between differing sensors. The disadvantage of using similar instruments is that a bias inherent in one measurement is repeated at all ten sites. Instrument problems, which could lead to a systematic underestimate in EC fluxes, are discussed below. They include: frequency response, aliasing of the data, height of the measurements, and separation of the sonic anemometer and krypton hygrometer.

8.5.1 Frequency Response

Before high-speed digital technologies became readily available, adequate sampling of eddy covariance flux was difficult. Corrections often were included to account for high frequency flux that could not be measured by low frequency sampling. Thus, an EC system must sample the range of measurements needed to create an accurate closure.

Within the surface boundary layer, energy transfer by eddies typically occurs at frequencies defined by:

$$f = nz/U \qquad (8.1)$$

where f is the normalized frequency, n is cyclical frequency (Hz), z is the measurement height (m), and U is the mean wind speed (ms^{-1}; Verma, 1990). A range of frequencies typically measured by sonic anemometers is between 0.001 and 2.

To evaluate the OASIS configuration of sensors, a maximum frequency of ~ 2 was assumed. Because the sonic anemometers were installed at a height of 4.5 m, n = (2)(U) / (4.5). The range of frequencies ranged between 0.44 Hz and 4.44 Hz when the mean wind speed was between 1 and 10 m s^{-1}, respectively. The CSAT3 sampled at a rate of 8 Hz, nearly twice the maximum required frequency required to prevent aliasing of the data. Thus, the sampling rate used by OASIS was adequate to capture the necessary range of the turbulent spectrum. More stable conditions require use of a higher frequency for sampling, while less frequent sampling is required during more unstable conditions.

8.5.2 Sensor Height

The height at which the EC sensors were installed affects the percentage of flux that can be observed. Installation of the sonic anemometer too high above ground or too low creates an underestimate of flux. Furthermore, the preferred height of installation is dependent upon the frequency response of the instrument, the mean wind speed, and an adequate fetch available to the sensor. The minimum height of installation (z_{min}) is recommended to be:

$$z_{min} = \frac{2\bar{U}}{n} \tag{8.2}$$

where U is the mean wind speed and n is the sampling frequency (Verma 1990). Thus, the measurement height of 4.5 m seems adequate based upon Eq. (8.2) when wind speeds are less than 18 ms^{-1}. The maximum height of measurement is determined by the areal extent of a homogeneous fetch which is available to the site. The greater the footprint area, the greater the maximum height can be. In general, a fetch-to-height ratio of 100:1 is used (Leclerc and Thurtell 1990). Thus, a measurement height of 4.5 m yields a fetch of ~ 450 m in all directions around each site. While this ratio assumption is not valid in some situations, it is valid at most of the ten sites. The footprint of the aerodynamic flux defines the fetch-to-height ratio, which is a function of stability, roughness, and height at which measurements are acquired (Schuepp et al. 1990). During daytime convection created by radiational heating of the earth's surface, the fetch-to-height ratio can be relaxed to much less than 100:1; during stable conditions, the required fetch ratio is several times greater (Horst and Weil 1994). Thus, the validity of OASIS measurements (and closure) are dependent upon the stability at sites where a proper fetch can not be guaranteed.

8.5.3 Sensor Separation

Until recently, sensible heat flux had to be estimated using two separate systems. A set of propeller anemometers were installed at various heights on an observation tower to measure the fluctuations in vertical wind speed. A fast-response temperature sensor was needed to measure the fluctuations in temperature. Using a new generation of sonic anemometers, eddy fluctuations in wind and temperature are made from the same volume of space, eliminating sensor separation error when estimating sensible heat flux. However, two separate sensors still are required to estimate latent heat flux. The covariance between variables decreases as the distance between systems increases. As the measured covariance decreases, the estimated flux rates also decrease, which causes closure rates to become worse. The minimum separation distance between sensors is limited by flow distortion which causes one sensor to impact the measurements from another sensor.

Kaimal (1975) recommended that the maximum separation distance (d_l) between sensors be limited to

$$d_l = \frac{(z-d)}{6\pi} \tag{8.3}$$

where z is the measurement height and d is the displacement height as defined by surface vegetation. For OASIS, assuming a maximum displacement height of 1.0 m, the maximum separation distance should be less than 0.186 m. The sonic anemometer and krypton hygrometer used by OASIS are vertically separated by 0.15 m.

Kristensen et al. (1997) observed that the measurement errors due to the separation of sensors is a function of the ratio of the distance between sensors to the scale of turbulence. The scale of turbulence increases with height. Thus, the ratio of separation of the sensors to turbulence scale decreases relative to the turbulent eddies observed. Thus, the measurement error diminishes as a function of height. In addition, Kristensen et al. found asymmetry in the error when sensors are displaced vertically. Because measurement error is minimized when the scalar sensor (krypton hygrometer) is deployed below the anemometer, the krypton hygrometer was placed below the sonic anemometer. For the sensor deployment used by OASIS, flux error due to sensor separation is estimated at less than 2%.

Measurement errors (in LH) created by the vertical separation of OASIS sensors decreases the degree to which closure can be attained. Because closure rates are strongly modulated by the Bowen ratio, sensor separation is a reason why closure is underestimated. However, care was taken to minimize problems measurement which resulted from sensor separation.

Chapter 9: Summary and Concluding Remarks

The hypothesis of this dissertation was that *the surface energy budget can be closed even in complex terrain when instrumentation error, topography, surface heterogeneity, and sampling differences are addressed with care.* To investigate the validity of this hypothesis, a year of data from the OASIS Project was collected and quality assured. Then, an exhaustive analysis of the closure problem was completed using data from ten OASIS sites. A comparison between a Bowen ratio system of ARM and an eddy correlation system of OASIS permitted a unique examination of the closure problem.

This dissertation is among the first attempts at explaining the causes for non-closure of the surface energy budget. Many previous works have examined the closure obtained from specific projects (e.g., Stannard et al. 1991; Nie et al. 1992; Lloyd et al. 1997; Twine et al. 2000), and many theories have been offered to explain consistent underestimates of flux. Yet, there has been little effort made to investigate why a systematic error in closure is observed. In addition, no "climatology" of closure has ever been attempted. Few long-term studies had been conducted. The scientific community needs to know when data is most reliable from field experimentation, and so a general knowledge of closure becomes important. Because of high costs and technological limitations, most field studies were limited in time and space. With projects such as OASIS and ARM, long-term changes in closure have been examined for seasonally and spatially dependent bias.

Results from model and satellite validation become suspect when long-term and spatial biases are detected.

A complete examination of closure required development of the OASIS data set. Data collected over a period of 12 months from ten OASIS sites across Oklahoma were processed and quality assured. Quality assurance of the data included many sensor intercomparisons and field studies, such as OASIS-98 and OASIS-2000. The principal results from analyzing this data set are as follows.

1. A multi-year study from 1998 to 2000 quantified differences in the measurement of net radiation among 5 independent radiation systems: the CNR1, PSP/PIR, and SIRS 4-component radiometers and the Q*6.1 and NR-Lite net radiometers.
2. The field performance of the new domeless NR-Lite was investigated and quantified for the first time (Brotzge and Duchon 2000). It was concluded that the performance of the NR-Lite was comparable to other net radiometers and could be used during long-term field studies.
3. Several algorithms used to correct for solar heating of pyrgeometers were compared (Brotzge and Duchon 2000).
4. Measurement uncertainty was quantified for each of the four components of the energy budget as estimated by the OASIS super sites (see Chapter 5).
5. Investigation of the correction algorithms applied to sonic anemometer data revealed how the performance of eddy correlation methods varied with geography and climate (see Section 7.4).

Once the data set was completed and measurement uncertainty quantified, closure was explicitly examined. First, the eddy correlation system used by OASIS was compared with the Bowen ratio system used by ARM. Differences between systems were related to variations in closure as measured at the OASIS site. Second, closure was observed at the ten super sites of OASIS. Systematic variations in closure among the ten sites were related to differences in climate, soil characteristics, and topography.

An examination of the ARM and OASIS systems, located approximately 100 m apart, revealed significant differences. Variations in ground fluxes, soil moisture, and Bowen ratio between sites highlighted problems associated with surface heterogeneity. Diurnal variations between the BR and EC systems revealed several reasons for the underestimate in closure by the EC system. Principal results from the BR/EC comparison are listed below.

1. Significant differences were observed in soil wetness and soil heat flow between the ARM and Mesonet systems (see Section 6.2.2). Seasonal variations in soil wetness were observed between the two systems, particularly during dry periods. Such differences could be caused by problems in calibration or surface heterogeneity. Differences between systems measuring diurnal variations in ground heat flux were consistent with a more vegetated surface at the ARM site and a more bare soil cover at the Mesonet site.

2. Little annual variation was noted in the differences between systems in either net radiation or ground heat flux (Section 6.4). On the other hand, significant seasonal variations were noted between the ARM and Mesonet systems in measurements of sensible and latent fluxes.
3. Closure at the Mesonet site was estimated at less than 100% using the EC system. Closure approached 100% after boundary layer mixing during the late morning and afternoon. Closure was observed to be lowest during stable and transitional periods during the early morning and late afternoon.
4. The minimum closure rates observed daily by the EC system coincided with a lower estimate of latent heat when compared to the ARM BR system. The daily underestimate in closure appears to result from a failure by the EC system to correctly measure early-morning and late-afternoon latent heat flux.
5. The BR and EC systems partitioned available energy differently into sensible and latent heat fluxes (Section 6.4). The BR system favored a partitioning into sensible heat flux while the EC system favored latent heat flux. Either instrument error or erroneous theoretical assumptions behind the BR method could have created differences in the estimates of the Bowen ratio.
6. Flux comparisons highlighted a complex relationship between soil wetness, vegetation, and Bowen ratio (Section 6.2.3). A small BR was observed during August despite limited soil moisture while during February, a large BR was measured over saturated soils. In both cases, the measured BR

more accurately reflected evapotranspiration from vegetation quantified by NDVI estimates. Such a relationship diminishes the need for direct measurements of soil moisture.

Similarity in closure among the ten super sites of OASIS highlighted several results. Seasonal and diurnal variations were combined with climate and topographical information to identify causes for the systematic errors in closure (Section 7.5). Results are listed as follows.

1. Estimates of closure were found to be a strong function of Bowen ratio. Closure was at or greater than 100% during periods with high sensible heat flux; closure was much less than 100% during periods of high latent heat flux. The mean closure rate was estimated at 98.7% when BR > 1.0; the mean closure rate was 86.6% when BR < 1.0.
2. Closure rates varied proportionally to the wetness of the soil. During dry periods, closure rates were near or above 100%; during wet periods, closure rates were lowest. Closure rates varied with BR and soil wetness because latent heat flux was underestimated.
3. Closure rates varied with topography at several sites. The more variable the topography, the lower the closure rate. Topographical *variability* cannot be corrected by coordinate rotation.

The results of this dissertation provide a framework for conducting future field studies of the surface energy budget. Even when measurement uncertainty is minimized, system errors can introduce significant and systematic bias. Recommendations for future field programs include the following.

1. At least three different net radiation sensors should be used to minimize measurement uncertainty. As demonstrated in Chapter 4, differences in treatment of sensor heating can lead to significant differences between measurements.

2. Multiple ground flux sensors should be used to measure soil heat flow, the integrated soil temperature, and soil moisture. As shown in Fig. 6.10, large differences in soil moisture are observed among the five sensors used by ARM. The exact number of sensors required has yet to be determined, and is most likely a function of soil characteristics. It can be assumed that the greater the number of soil sensors used, the better the soil heterogeneity is measured.

3. The correction for the vertical separation of sensors described by Villalobos (1997) should be applied when possible. The study by Villalobos quantifies the effect of sensor separation and provides a ready correction. While this dissertation used the results from Kristensen et al. (1997) to reduce sensor separation errors, the magnitude of the errors is unknown.

4. Eddy correlation systems should be used at several measurement heights. Multiple EC systems allow for vertical divergence to be quantified. In addition, differences in the measured Bowen ratio between heights permit different source regions to be identified (see Tanner 1988).

Results of this dissertation have provided an explanation for the systematic underestimate in closure. It is assumed that closure is measured correctly very near the ground. However, the higher the measurements, the larger the source region and the greater the surface heterogeneity included in the measurement. The fetch area also is much greater during stable and transitional periods than during unstable conditions. Errors in closure are greatest during stable and transitional periods possibly due to the much larger footprint regions. Heterogeneity in surface properties combined with the limitations in sampling frequency and averaging interval lead to an underestimate in closure. The underestimate in closure appears manifest in differences in measurement of latent heat flux primarily because of its importance during the stable and transitional periods. In addition, problems with sensor separation and sensor maintenance may reduce measurements of latent heat flux during stable and transitional periods. The exact cause for the underestimate in closure remains unknown. However, closure improved with increased PBL mixing, with decreased latent heat flux, and with flat terrain.

The hypothesis of this dissertation is that *the surface energy budget can be closed even in complex terrain when instrumentation error, topography, surface heterogeneity, and sampling differences are addressed with care.* This hypothesis cannot be rejected based upon the results described herein. Closure was found to be near 100% during those periods when systematic errors caused by measurement uncertainty, surface heterogeneity, and topography were minimized. Mean annual closure rates at 8 of the 10 super sites ranged between 90 and 100%, much higher than closure rates estimated by field programs such as FIFE and SGP-97.

The OASIS data set compiled for this study provides a unique data set available to the scientific community. Measurement uncertainty has been quantified through a series of field experiments. An analysis of closure increases confidence in the data that, during certain periods of time, nearly all components of the energy budget are measured correctly. Such a data set can provide scientists with the most accurate data from which to conduct model and satellite verification.

The work from this dissertation also provides the scientific community with a model for conducting future energy balance studies. Recommendations are provided to limit instrument and system error. In addition, many competing theories concerning closure have been discussed, and ways to limit each of these errors are described.

Finally, results from this work should prompt greater awareness of using closure as a tool for quality control of energy balance data. This work has shown preferred diurnal and seasonal periods when the energy balance is measured nearest 100%. Hopefully, this result will prompt further research in identifying and limiting problems associated with measurement of all energy budget components. Only when errors during stable and transitional periods and during high latent flux periods are reduced further can closure be systematically improved.

References

Alados-Arbolas, L., J. Vida, and J. I. Jimenez, 1988: Effects of solar radiation on the performance of pyrgeometers with silicon domes. *J. Atmos. Oceanic Technol.*, **5**, 666-670.

Albrecht, B., and S. K. Cox, 1977: Procedures for improving pyrgeometer performance. *J. Appl. Meteor.*, **16**, 188-197.

Anderson, S.P., and M. F. Baumgartner, 1998: Radiative heating errors in naturally ventilated air temperature measurements made from buoys. *J. Atmos. Oceanic Technol.*, **15**, 157-173.

Barr, A.G., K.M. King, T.J. Gillespie, G. Den Hartog, and H.H. Neumann, 1994: A comparison of Bowen Ratio and eddy correlation sensible and latent heat flux measurements above deciduous forest. *Bound.-Layer Meteor.*, **71**, 21-41.

Basara, J.B., and T.M. Crawford, 2000: Improved installation procedures for deep-layer soil moisture measurements. *J. Atmos. Oceanic Technol.*, **17**, 879 – 884.

Betts, A. K., and J. H. Ball, 1997: Albedo over the boreal forest. *J. Geophys. Res.*, **102**, 28901-28909.

Blad, B. L., and N. J. Rosenberg, 1974: Lysimetric calibration of the Bowen ratio-energy balance method for evapotranspiration. *J. Appl. Meteor.*, **13**, 227-236.

Bowen, I.S., 1926: The ratio of heat losses by conduction and by evaporation from any water surface. *Phys. Rev.*, **27**, 779-787.

Brakke, T.W., S.B. Verma, and N.J. Rosenberg, 1978: Local and regional components of sensible heat advection. *J. Appl. Meteor.*, **17**, 955-963.

Brock, F.V. and S.J. Richardson, 2001: Meteorological measurement systems. Oxford Press, 200 pp.

Brock, F.V., K.C. Crawford, R.L. Elliott, G.W. Cuperus, S.J. Stadler, H.L. Johnson, and M.D. Eilts, 1995: The Oklahoma Mesonet: a technical overview. *J. Atmos. Oceanic Technol.*, **12**, 5-19.

Brotzge, J. A., 1997: A preliminary evaluation to measuring sensible heat fluxes using the Oklahoma Mesonet. M.S. Thesis, School of Meteorology, University of Oklahoma, Norman, 125 pp. [Available from 100 E. Boyd, Suite 1210, Norman, OK 73019].

Brotzge, J.A., and K.C. Crawford, 2000: Estimating sensible heat flux from the Oklahoma Mesonet. *J. Appl. Meteor.*, **39**, 102-116.

Brotzge, J.A., and C.E. Duchon, 2000: A field comparison among a domeless net radiometer, two 4-component net radiometers, and a domed net radiometer. *J. Atmos. Oceanic Technol.*, in press.

Brotzge, J.A., S.J. Richardson, C.M. McAloon, 2001: The OASIS Project network for monitoring the surface energy budget. *Eleventh Symp. on Meteor. Observations and Instrumentation*, AMS, 14 – 19 January.

Brotzge, J.A., S.J. Richardson, C.E. Duchon, S.E. Fredrickson, and D.L. Grimsley, 1999a: Evaluation of a domeless net radiometer. *Thirteenth Conf. on Bound.-Lay. Turb.*, Amer. Met. Soc., Dallas, TX, Jan 10-15.

Brotzge, J.A., S.J. Richardson, K.C. Crawford, T.W. Horst, F.V. Brock, K.S. Humes, Z. Sorbjan, and R.L. Elliott, 1999b: The Oklahoma Atmospheric Surface-layer Instrumentation System (OASIS) Project. *Thirteenth Conf. on Bound.-Lay. Turb.*, Amer. Met. Soc., Dallas, TX, Jan.10-15.

Brotzge, J.A., K.C. Crawford, and C.H. Marshall, Jr., 1998: Estimating sensible heat flux from the Oklahoma Mesonet: A comparison to ARM. *Tenth Symp. on Meteor. Obs. and Instr.*, Amer. Met. Soc., Phoenix, AZ, Jan 11-16.

Brutsaert, W., 1982: *Evaporation into the Atmosphere*. D. Reidel, Boston, MA, 299 pp.

Duchon, C.E., and G.E. Wilk, 1994: Field comparisons of direct and component measurements of net radiation under clear skies. *J. Appl. Meteor.*, **33**, 245-251.

Dugas, W. A., L.J. Fritschen, L. W. Gay, A. A. Held, A. D. Matthias, D. C. Reicosky, P. Steduto, and J. L. Steiner, 1991: Bowen ratio, eddy correlation, and portable chamber measurements of sensible and latent heat flux over irrigated spring wheat. *Agric. and For. Meteor.*, **56**, 1-20.

Dyer, A. J., 1961: Measurements of evaporation and heat transfer in the lower atmosphere by an automatic eddy-correlation technique. *Quart. J. R. Meteor. Soc.*, **87**, 401-412.

Dyer, A. J., 1981: Flow distortion by supporting structures. *Bound.-Layer Meteor.*, **20**, 243-251.

Dyer, A. J., J. R. Garratt, R.J. Francey, I.C. McIlroy, N.E. Bacon, P. Hyson, E.F. Bradley, O.T. Denmead, L.R. Tsvang, Y.A. Volkov, B. M. Koprov, L.G. Elagina, K. Sahashi, N. Monji, T. Hanafusa, O. Tsukamoto, P. Frenzen, B.B. Hicks, M. Wesely, M. Miyake, andW. Shaw, 1982: An international turbulence comparison experiment (ITCE 1976). *Bound.-Layer Meteor.*, **21**, 181-209.

Enz, J.W., J.C. Klink, and D.G. Baker, 1975: Solar radiation effects on pyrgeometer performance. *J. Appl. Meteor.*, **14**, 1297-1302.

Field, R. T., L. J. Fritschen, E. T. Kanemasu, E. A. Smith, J. B. Stewart, S. B. Verma, and W.P. Kustas, 1992: Calibration, comparison, and correction of net radiation instruments used during FIFE. *J. Geophys. Res.*, **97**, 18681-18695.

Foken, T., and B. Wichura, 1996: Tools for quality assessment of surface-based flux measurements. *Ag. and For. Meteor.*, **78**, 83-105.

Fritschen, L.J., and L. W. Gay, 1979: Environmental Instrumentation. Springer-Verlag, 216 pp.

Fritschen, L.J., and J.R. Simpson, 1989: Surface energy and radiation balance systems: general description and improvements. *J. Appl. Meteor.*, **28**, 680 – 689.

Fritschen, L.J, P. Qian, E. T. Kanemasu, D. Nie, E. A. Smith, J. B. Stewart, S. B. Verma, and M. L. Wesely, 1992: Comparisons of surface flux measurement systems used in FIFE 1989. *J. Geophy. Res.*, **97**, 18697-18713.

Fuchs, M. and C. B. Tanner, 1968: Calibration and field test of soil heat flux plates. *Soil Sci. Soc. Amer. Proc.*, **32**, 326-328.

Geissbuhler, P., R Siegwolf, W Eugster, 2000: Eddy covariance measurements on mountainslopes: The advantage of surface-normal sensor orientation over a vertical set-up. *Bound.-Layer Meteor.*, **96**, 371-392.

Halldin, S., and A. Lindroth, 1992: Errors in net radiometery: Comparison and evaluation of six radiometer designs. *J. Atmos. Oceanic Technol.*, **9**, 762-783.

Halliwell, D.H., and W. R. Rouse, 1989: A comparison of sensible and latent heat flux calculations using the Bowen Ratio and aerodynamic methods. *J. Atmos. Oceanic Technol.*, **6**, 563-574.

Heiser, M.D., and P.J. Sellers, 1995: Production of a filtered and standardized surface flux data set for FIFE 1987. *J. Geophys. Res.*, **100**, 25631-25643.

Hicks, B. B., 1970: The measurement of atmospheric fluxes near the surface: A generalized approach. *J. Appl. Meteor.*, **9**, 386-388.

Holtslag, A. A. M., and P. Van Ulden, 1983: A simple scheme for daytime estimates of the surface fluxes from routine weather data. *J. Clim. Appl. Meteor.*, **22**, 517-529.

Horst, T.W., and J.C. Weil, 1994: Footprint estimation for scalar flux measurements in the atmospheric surface layer. *Bound.-Layer Meteor.*, **59**, 279-296.

Hukseflux, cited 1999: Heat flux and heat transfer science. [Available on-line from http://www.hukseflux.com/heat%20flux/heatflux.htm.]

Kaimal, J. C., and J. A. Businger, 1963: A continous wave sonic anemometer-thermometer. *J. Appl. Meteor.*, **2**, 156-164.

Kaimal, J.C., and J.E. Gaynor, 1991: Another look at sonic thermometry. *Bound.-Layer Meteor.*, **56**, 401-410.

Kaimal, J.C., J.C. Wyngaard, Y. Izuma, and O.R. Cote, 1972: Spectral characteristics of surface layer turbulence. *Quart. J. R. Meteor.*, **98**, 563-589.

Kanemasu, E. T., S. B. Verma, E. A. Smith, L. J. Fritschen, M. Wesely, R. T. Field, W. P. Kustas, H. Weaver, J. B. Stewart, R. Gurney, G. Panin, and J. B. Moncrieff, 1992: Surface flux measurements in FIFE: An overview. *J. Geophys. Res*, **97**, 18547-18555.

Kizer, M.A., and R.L. Elliott, 1991: Eddy correlation systems for measuring evapotranspiration. Trans. of the ASAE, 34, 387 – 392.

Koprov, B. M., and D. Y. Sokolov, 1973: Spatial correlation functions of velocity and temperature components in the surface layer of the atmosphere. *Izv. Atmos. and Oceanic Phys.*, **9**, 178-182.

Kristensen, L., J. Mann, S.P. Oncley, and J.C. Wyngaard, 1997: How close is close enough when measuring scalar fluxes with displaced sensors? *J. Atmos. Oceanic Technol.*, **14**, 814-821.

Kustas, W.P., D.C. Goodrich, M.S. Moran, S.A. Amer, L.B. Bach, J.H. Blanford, A. Chehbouni, H. Claassen, W. E. Clements, P.C. Doraiswamy, P. Dubois, T.R. Clarke, C.S. T. Daughtry, D.I. Gellman, T.A. Grant, L.E. Hipps, A.R. Huete, K.S. Humes, T.J. Jackson, T.O. Keefer, W.D. Nichols, R. Parry, E.M. Perry, R.T. Pinker, P.J. Pinter, Jr., J. Qi, A. C. Riggs, T.J. Schmugge, A. M. Shutko, D. I. Stannard, E. Swiatek, J.D. van Leeuwen, J. van Zyl, A. Vidal, J. Washburne, and M. A. Weltz, 1991: An interdisciplinary field study of the energy and water fluxes in the atmosphere-biosphere system over semiarid rangelands: description and some preliminary results. *Bull. Amer. Meteor. Soc.*, **72**, 1683-1705.

Lang, A.R.G., K.G. McNaughton, C. Fazu, E.F. Bradley, and E. Ohtaki, 1983: Inequality of eddy transfer coefficients for vertical transport of sensible and latent heats during advective inversions. *Bound.-Layer Meteor.*, **25**, 25-41.

Leclerc, M. Y. and G.W. Thurtell. 1990: Markovian anaylsis: Footprint prediction of scalar fluxes. *Bound.-Layer Meteor.*, **52**, 247-258.

Lee, X., and T.A. Black, 1993: Atmospheric turbulence within and above a Douglas fir stand. Part II. Eddy fluxes of sensible heat and water vapour. *Bound.-Layer Meteor.*, **64**, 369-389.

Lloyd, C.R., P. Bessemoulin, F.D. Cropley, A.D. Culf, A.J. Dolman, J. Elbers, B. Heusinkveld, J.B. Moncrieff, B. Monteny, and A. Verhoef, 1997: A comparison of surface fluxes at the HAPEX-Sahel fallow bush sites. *J. Hydrology*, **188-89**, 400-425.

Massman, W.J., 1993: Errors associated with the combination method for estimating soil heat flux. *Soil Sci. Soc. Am. J.*, **57**, 1198-1202.

McAloon, C., S.J. Richardson, J.A. Brotzge, T.W. Horst, and S. Semmer, 1999: Preliminary Results from the OASIS98 Field Project. *Thirteenth Conf. on Bound.-Lay. Turbul.*, Amer. Met. Soc., Dallas, TX, Jan 10-15.

McAloon, C., S.J. Richardson, J.A. Brotzge, and T.W. Horst, 2000: Preliminary Results from the OASIS2000 Field Project. *Fourteenth Conf. on Bound.-Lay. Turbul.*, Amer. Met. Soc., Aspen, CO.

McBean, G.A., 1972: Instrument requirements for eddy correlation measurements. *J. Appl. Meteor.*, **11**, 1078-1084.

McNeil, and Shuttleworth, 1975: Comparative measurements of the energy fluxes over a pine forest. *Bound.-Layer Meteor.*, **9**, 297-313.

McMillen, R.T., 1988: An eddy correlation technique with extended applicability to non-simple terrain. *Bound.-Layer Meteor.*, **43**, 231-245.

Moore, C.J., 1986: Frequency response corrections for eddy correlation systems. *Bound.-Layer Meteor.*, **37**, 17-35.

Motha, R.P., S.B. Verma, and N.J. Rosenberg, 1979: Exchange coefficients under sensible heat advection determined by eddy correlation. *Agric. Meteor.*, **20**, 273-280.

Nie, D., E. T. Kanemasu, L. J. Fritschen, H. L. Weaver, E. A. Smith, S. B. Verma, R. T. Field, W. P. Kustas, and J. B. Stewart, 1992: An intercomparison of surface energy flux measurement systems used during FIFE 1987. *J. Geophys. Res.*, **97**, 18715-18724.

Ohmura, Al., 1982: Objective criteria for rejecting data for Bowen Ratio flux calculations. *J. Appl. Meteor.*, **21**, 595-598.

Ohmura, A., E.G. Dutton, B. Forgan, C. Frohlich, H. Gilgen, H. Hegner, A. Heimo, G. Konig-Langlo, B. McArthur, G. Muller, R. Philipona, R. Pinker, C.H. Whitlock, K. Dehne, and M. Wild, 1998: Baseline Surface Radiation Network (BSRN/WCRP): New precision radiometry for climate research. *Bull. of Amer. Meteor. Soc.*, **79**, 2115-2136.

Panofsky, H.A., and J.A. Dutton, 1984: Atmospheric Turbulence. John Wiley and Sons, Inc., New York, 397 pp.

Paulson, C.A., 1970: The mathematical representation of wind speed and temperature profiles in the unstable atmospheric surface layer. *J. Appl. Meteor.*, **9**, 857-861.

Perez, M., L. Alados-Arboledas, 1999: Effects of natural ventilation and solar radiation on the performance of pyrgeometers. *J. Atmos. Oceanic Technol.*, **16**, 174-180.

Peixoto, J.P., and A.H. Oort, 1992: Physics of Climate. American Institute of Physics, New York, 520 pp.

Richardson, S.J., 1995: Multiplate radiation shields: Investigating radiational heating errors. *PhD Dissertation*, U. of Oklahoma, 134 pp. [Available from 100 E. Boyd, Suite 1210, Norman, OK 73019.]

Schotanus, P., F.T.M. Nieuwstadt, and H.A.R. De Bruin, 1983: Temperature measurements with a sonic anemometer and its application to heat and moisture fluxes. *Bound.-Layer Meteor.*, **26**, 81-93.

Schuepp, P.H., M.Y. Leclerc, J.I. Macpherson, and R.L. Desjardins, 1990: Footprint prediction of scalar fluxes from analytical solutions of the diffusion equation. *Bound.-Layer Meteor.*, **50**, 355-373.

Sellers, P.J., and F.G. Hall, 1992: FIFE in 1992: results, scientific gains, and future research directions. *J. Geophys. Res.*, **97**, 19091-19109.

Shaw, R., 1985: On diffusive and dispersive fluxes in forest canopies. *The Forest-Atmosphere Interaction.* B.A. Hutchinson and B.B. Hicks, Eds. D. Reidel, 407-419.

Shafer, M.A., and T.W. Hughes, 1996: Automated quality assurance of data from the Oklahoma Mesonetwork. Twelfth International Conf. on Interactive Info. and Proc. Systems for Meteor., Ocean., and Hydrology, Atlanta, GA.

Shafer, M. A., C. A. Fiebrich, D. S. Arndt, S. E. Fredrickson, and T. W. Hughes, 2000: Quality assurance procedures in the Oklahoma Mesonetwork. *J. Atmos. Oceanic Techn.*ol., **17**, 474 – 494.

Shuttleworth, W.J., 1991: Insight from large-scale observational studies of land/atmosphere interactions. *Surveys in Geophysics*, **12**, 3-20.

Shuttleworth, W.J., J.H.C. Gash, C.R. Lloyd, C.J. Moore, J. Roberts, A. De O. M. Filho, G. Fisch, V. De P. S. Filho, M. De N. G. Ribeiro, L. C. B. Molion, L. D. De Abreu Sa', J. C. A. Nobre, O. M. R. Cabral, S. R. Patel, and J. C. De Moraes, 1984: Eddy correlation measurements of energy partition for Amazonian forest. *Quart. J. R. Met. Soc.*, **110**, 1143-1162.

Smith, E.A., G.B. Hodges, M. Bacrania, H.J. Cooper, M.A. Owens, R. Chappell, W. Kincannon, 1997: BOREAS Net Radiometer Engineering Study. Report to the National

Aeronautical Space Administration, Grant NAG5-2447, Florida State University, Tallahassee, FL, 51 pp.

Stannard, D.I., J.H. Blanford, W.P. Kustas, W.D. Nichols, S.A. Amer, T.J. Schmugge, and M.A. Weltz, 1994: Interpretation of surface flux measurements in heterogeneous terrain during the Monsoon '90 experiment. *Water Res. Res.*, **30**, 1227-1239.

Stokes, G.M. and S. E. Schwartz, 1994: The Atmospheric Radiation Measurement (ARM) Program: Programmatic background and design of the Cloud and Radiation Test Bed. *Bull. Amer. Meteor. Soc.*, **75**, 1201 – 1221.

Stull, R.B., 1988: An introduction to boundary layer meteorology. Kluwer Academic Publishers, Boston, MA, 666 pp.

Suomi, V. E., 1957: Energy budget studies and development of the sonic anemometer for spectrum analysis. AFCRC Tech. Report 56-274, University of Wisconsin, Dept. of Meteorology, 91 pp.

Swinbank, W. C., 1951: The measurement of vertical transfer of heat and water vapor by eddies in the lower atmosphere. *J. Meteor.*, **8**, 135-145.

Tanner, C. B., 1960: Energy balance approach to evapotranspiration from crops. *S. Sci. Soc. of Amer. Proc.*, **24**, 1-9.

Tanner, B.D., 1984: Measurements with a portable eddy correlation system. Presented at International Symposium in memory of Dr. F. Sauberer. Vienna, Austria, 23 – 25 October.

Tanner, B.D., 1988: Use requirements for Bowen ratio and eddy correlation determination of evapotranspiration. Planning now for irrigation and drainage in the 21st century. Ed. DeLynn R. Hay, ASCE, Lincoln, NE, 782 pp.

Tanner, B.D., M.S. Tanner, W.A. Dugas, E.C. Campbell, and B.L. Bland, 1985: Evaluation of an operational eddy correlation system for evapotranspiration measurement. In Advances in evapotranspiration, Proc. Of the National Conference on Advances in Evapotranspiration, 87 – 99, St. Joseph, MI. ASAE.

Tanner, C.B., E. Swiatek, and J.P. Greene, 1993: Density fluctuations and use of the Krypton hygrometer in surface flux measurements. *Irrigation and drainage systems*, 945-950.

Thom, A.S., J.B. Stewart, H.R. Oliver, and J.H.C. Gash, 1975: Comparison of aerodynamic and energy budget estimates of fluxes over a pine forest. *Quart. J. R. Met. Soc.*, **101**, 93-105.

Twine, T.E., W.P. Kustas, J.M. Norman, D.R. Cook, P.R. Houser, T.P. Meyers, J.H. Prueger, and P.J. Starks, 2000: Correcting eddy covariance flux underestimates over a grassland. *Agric. and Forest Meteor.* **103**, 279-300.

Unland, H. E., P. R. Houser, W.J. Shuttleworth, and Z.-L. Yang, 1996: Surface flux measurement and modeling at a semi-arid Sonoran Desert site. *Agri. And For. Meteor.*, **82**, 119-153.

van Loon, W.K.P., H.M.H. Bastings, and E. J. Moors, 1998: Calibration of soil heat flux sensors, *Ag. and For. Meteor.*, **92**, 1-8.

Verma, S.B., 1990: Micrometeorological methods for measuring surface fluxes of mass and energy. *1 Instrumentation for Studying Vegetation Canopies for Remote Sensing in Optical and Thermal Infrared Regions*, N. S. Goel and J. M. Norman, Eds., Harwood Academic Publishers, 99 – 115.

Verma, S.B., D. D. Baldocchi, D. E. Anderson, D. R. Matt, and R. J. Clement, 1986: Eddy fluxes of CO_2, water vapor, and sensible heat over a deciduous forest. *Bound-Layer Meteor.*, **36**, 71-91.

Vickers, D., and L. Mahrt, 1997: Quality control and flux sampling problems for tower and aircraft data. *J. Atmos. Oceanic Technol.*, **14**, 512-526.

Webb, E. K., G. I. Pearman, and R. Leuning, 1980: Correction of flux measurements for density effects due to heat and water vapour transfer. *Quart. J. R. Met. Soc.*, **106**, 85-100.

Wilks, D.S., 1995: Statistical methods in the atmospheric sciences. Academic Press, New York, NY, 464 pp.

Wyngaard, J.C., 1982: Comments on flow distortion by supporting structures. *Bound.-Layer Meteor.*, **22**, 263-265.

Appendix

Appendix A: Profile gradient estimate of sensible heat flux

Sensible heat flux is estimated using Mesonet observations of air temperature at 1.5 m and 9 m (z_{t1} and z_{t2}, respectively) and wind speed at 2.0 m and 10 m (z_{u1} and z_{u2}, respectively). For the OASIS Project, a gradient profile method was chosen. This method is based upon Paulson (1970) and modified by T. Horst (1998, private communication). See Brotzge and Crawford (2000) for additional details.

The sensible heat flux, H [W m^{-2}], can be derived for stable and unstable stratification as:

$$H = -\rho C_p [u_* \theta_*]. \tag{A.1}$$

where u_* [m s^{-1}] is the friction velocity, θ_* is a scaling temperature [°C], C_p [J deg^{-1} kg^{-1}] is the specific heat at constant pressure, and ρ is air density [kg m^{-3}]. Next we solve for u_* and θ_*. We begin with the integrated form of the nondimensional gradients of momentum and temperature as described by Paulson:

$$u = \frac{u_*}{k}\left[\ln\left(z/z_o\right) - \psi\left(z_u/L\right)\right] \tag{A.2}$$

$$\theta = \frac{\theta_*}{k}\left[\ln\left(z/z_o\right) - \psi\left(z_t/L\right)\right] \tag{A.3}$$

where z_0 [m] is the roughness coefficient, ψ_u and ψ_t are the stability functions for momentum and heat, respectively, and L [m] is the Obukhov length. The von Karman constant (k) has been set to 0.40. Equations (2) and (3) are each applied at the two levels of measurement, z_1 and z_2 [m]. The finite difference between levels is then:

$$u_2 - u_1 = \Delta\overline{U} = \frac{u_*}{k}\left[\ln\left(z_{u2}/z_{u1}\right) - \psi\left(z_{u2}/L\right) + \psi\left(z_{u1}/L\right)\right] \tag{A.4}$$

$$\theta_2 - \theta_1 = \Delta\bar{\theta} = \frac{\theta_*}{k}\left[\ln\left(\frac{z_{t2}}{z_{t1}}\right) - \psi\left(\frac{z_{t2}}{L}\right) + \psi\left(\frac{z_{t1}}{L}\right)\right] \tag{A.5}$$

The values for u. and θ. may then be rewritten as:

$$u_* = \frac{k\Delta\bar{U}}{\ln\left(\frac{z_{u2}}{z_{u1}}\right) - \psi_{u2} + \psi_{u1}} \tag{A.6}$$

and

$$\theta_* = \frac{k\Delta\bar{\theta}}{\ln\left(\frac{z_{t2}}{z_{t1}}\right) - \psi_{t2} + \psi_{t1}} \tag{A.7}$$

Finally, by substitution of (6) and (7) into (1):

$$H = -\rho C_p\left[\frac{k^2\Delta\bar{U}\Delta\bar{\theta}}{\chi}\right]. \tag{A.8}$$

The denominator χ is defined as a function of stability. For unstable conditions,

$$\chi = \left[\ln\left(\frac{z_{u2}}{z_{u1}}\right) - \psi_{u2} + \psi_{u1}\right]\left[\ln\left(\frac{z_{t2}}{z_{t1}}\right) - \psi_{t2} + \psi_{t1}\right] \tag{A.9}$$

and for stable conditions,

$$\chi = \left[\ln\left(\frac{z_{u2}}{z_{u1}}\right) + \beta\left(\frac{(z_{u2} - z_{u1})}{L}\right)\right]\left[\ln\left(\frac{z_{t2}}{z_{t1}}\right) + \beta\frac{(z_{t2} - z_{t1})}{L}\right] \tag{A.10}$$

where β is set equal to 5. The stability functions for momentum (ψ_u) and heat (ψ_t) are defined by Paulson (1970) as:

$$\psi_{u(1,2)} = 2\ln\left[\frac{1 + x_{u(1,2)}}{2}\right] + \ln\left[\frac{1 + x_{u(1,2)}^2}{2}\right] + 2Tan^{-1}\left[\frac{1 - x_{u(1,2)}}{1 + x_{u(1,2)}}\right] \tag{A.11}$$

$$\psi_{t(1,2)} = 2\ln\left[\frac{1 + x_{t(1,2)}^2}{2}\right] \tag{A.12}$$

with

$$x_{u(1,2)} = \left[1 - \gamma \frac{z_{u(1,2)}}{L}\right]^{\frac{1}{4}} \quad (A.13)$$

$$x_{t(1,2)} = \left[1 - \gamma \frac{z_{t(1,2)}}{L}\right]^{\frac{1}{4}} \quad (A.14)$$

where $\gamma = 16$. and the Obukhov length is defined as:

$$L = \frac{-u_*^3 c_p \rho T_m}{kgH} \quad (A.15)$$

where g [ms^{-2}] is gravity, and T_m [K] is the arithmetic mean temperature within the depth of the tower. Equation (13) (equation (14)) is applied at each level where wind speeds (temperatures) are measured, in this case at z_{u1} and z_{u2} to yield x_{u1} and x_{u2} (z_{t1} and z_{t2} to yield x_{t1} and x_{t2}).

For unstable conditions, z/L is equivalent to the Richardson number (z/L = Ri) when $\phi_h = \phi^2_m$ as explained by Businger (1988):

$$\xi = z/L = Ri \frac{\left[\ln(z_{u2}/z_{u1})\right]^2}{\ln(z_{t2}/z_{t1})} \quad (A.16)$$

The Richardson number is calculated in finite difference form as:

$$Ri = \frac{g}{T_m} z_m \frac{\Delta\bar{\theta}}{(\Delta\bar{U})^2} \quad (A.17)$$

where z_m [m] is the geometric mean of the temperature measurement height, and $\Delta\bar{\theta}$ [K] and $\Delta\bar{U}$ [ms^{-1}] are the vertical temperature and wind speed gradients, respectively. The geometric mean of the measurement height, z_m, is defined as:

$$z_m = {(z_{u1} z_{u2})} \Big/ {(z_{t1} z_{t2})^{1/2}} . \quad (A.18)$$

For stable conditions, ξ is generally not equal to Ri. Because the temperature and wind speed are not measured at the same heights ($z_{u1} \neq z_{t1}$), a quadratic form has been applied:

$$\xi = \frac{-b + \sqrt{b^2 - 4ac}}{2a}. \tag{A.19}$$

Derived from equations (A.2) and (A.3), it can be shown that:

$$a = \frac{\beta(z_{t2} - z_{t1})}{z_m} - Ri\left[\frac{\beta(z_{u2} - z_{u1})}{z_m}\right]^2 \tag{A.20}$$

$$b = \ln\left({z_{t2}}/{z_{t1}}\right) - 2Ri\ln\left({z_{u2}}/{z_{u1}}\right)\beta\left[\frac{(z_{u2} - z_{u1})}{z_m}\right] \tag{A.21}$$

$$c = -Ri\left[\ln\left({z_{u2}}/{z_{u1}}\right)\right]^2. \tag{A.22}$$

If, however,

$$1/\beta > Ri\left[\frac{(z_{u2} - z_{u1})^2}{z_m(z_{t2} - z_{t1})}\right]. \tag{A.23}$$

then there is no solution, and the flux is undefined.

Derived from Equations (A.2) and (A.3), Equation (A.4) is derived as follows:

Given:

$$u_* = \frac{k\Delta u}{\ln\left({z_{u2}}/{z_{u1}}\right) - \psi_m\left({z_{u2}}/{L}\right) + \psi_m\left({z_{u1}}/{L}\right)}$$

$$T_* = \frac{k\Delta T}{\ln\left({z_{T2}}/{z_{T1}}\right) - \psi_h\left({z_{T2}}/{L}\right) + \psi_h\left({z_{T1}}/{L}\right)}$$

$$\frac{z_m}{L} = \frac{g}{T}\frac{kz_m}{u_*^3}u_*T_* = \frac{g}{T}\frac{kz_m}{u_*^2}T_*$$

$$\frac{z_m}{L} = \frac{g}{T} z_m \frac{\Delta T}{(\Delta u)^2} \frac{\left[\ln\left(\frac{z_{u2}}{z_{u1}}\right) - \psi_m\left(\frac{z_{u2}}{L}\right) + \psi_m\left(\frac{z_{u1}}{L}\right)\right]^2}{\left[\ln\left(\frac{z_{T2}}{z_{T1}}\right) - \psi_h\left(\frac{z_{T2}}{L}\right) + \psi_h\left(\frac{z_{T1}}{L}\right)\right]}$$

If z/L > 0, then

$$\psi_m = \psi_h = -\beta\left(\frac{z}{L}\right)$$

$$\frac{z_m}{L} = \frac{g}{T} z_m \frac{\Delta T}{(\Delta u)^2} \frac{\left[\ln\left(\frac{z_{u2}}{z_{u1}}\right) - \psi_m\left(\frac{z_{u2}}{L}\right) + \psi_m\left(\frac{z_{u1}}{L}\right)\right]^2}{\left[\ln\left(\frac{z_{T2}}{z_{T1}}\right) - \psi_h\left(\frac{z_{T2}}{L}\right) + \psi_h\left(\frac{z_{T1}}{L}\right)\right]}$$

$$Ri_m = \frac{g}{T} \frac{z_m \Delta T}{(\Delta u)^2}$$

$$\frac{z_m}{L}\left[\ln\left(\frac{z_{T2}}{z_{T1}}\right) + \frac{\beta(z_{T2} - z_{T1})}{L}\right] = Ri_m\left[\ln\left(\frac{z_{u2}}{z_{u1}}\right) + \frac{\beta(z_{u2} - z_{u1})}{L}\right]^2$$

$$\zeta\left[\ln\left(\frac{z_{T2}}{z_{T1}}\right) + \left(\frac{\beta(z_{T2} - z_{T1})}{z_m}\right)\zeta\right] = Ri_m\left[\ln^2\left(\frac{z_{u2}}{z_{u1}}\right) + 2\ln\left(\frac{z_{u2}}{z_{u1}}\right)\beta\frac{z_{u2} - z_{u1}}{z_m}\zeta + \beta^2\left(\frac{z_{u2} - z_{u1}}{z_m}\right)^2\zeta^2\right]$$

$$\left[\beta\left(\frac{\Delta z_T}{z_m}\right) - Ri_m\left(\frac{\beta\Delta z_u}{z_m}\right)^2\right]\zeta^2 + \left[\ln\left(\frac{z_{T2}}{z_{T1}}\right) - 2Ri_m\ln\left(\frac{z_{u2}}{z_{u1}}\right)\beta\left(\frac{\Delta z_u}{z_m}\right)\right]\zeta - Ri_m\ln^2\left(\frac{z_{u2}}{z_{u1}}\right) = 0$$

$$\zeta = \frac{-b \pm \sqrt{b^2 - 4ac}}{2a}$$

$$b^2 - 4ac = \ln^2\left(\frac{z_{T2}}{z_{T1}}\right) - 4Ri_m\ln\left(\frac{z_{u2}}{z_{u1}}\right)\ln\left(\frac{z_{T2}}{z_{T1}}\right)\beta\left(\frac{\Delta z_u}{z_m}\right) + 4Ri_m^2\ln^2\left(\frac{z_{u2}}{z_{u1}}\right)\beta^2\left(\frac{\Delta z_u}{z_m}\right)^2 +$$

$$4Ri_m\ln^2\left(\frac{z_{u2}}{z_{u1}}\right)\left[\beta\left(\frac{\Delta z_T}{z_m}\right) - Ri_m\left(\beta\frac{\Delta z_u}{z_m}\right)^2\right]$$

Assuming $z_{T2} = z_{u2}$ and $z_{T1} = z_{u1}$, then

$$b^2 - 4ac = \ln^2\left(\frac{z_2}{z_1}\right)\left[1 - 4Ri_m\beta\frac{\Delta z}{z_m} + 4Ri_m^2\beta^2\left(\frac{\Delta z}{z_m}\right)^2 + 4Ri_m\beta\frac{\Delta z}{z_m} - 4Ri_m^2\beta^2\left(\frac{\Delta z}{z_m}\right)^2\right] = \ln^2\left(\frac{z_2}{z_1}\right)$$

where

$$b = \ln\left(\frac{z_2}{z_1}\right)\left[1 - 2Ri_m\beta\frac{\Delta z}{z_m}\right]$$

$$2a = 2\beta\frac{\Delta z}{z_m}\left[1 - Ri_m\beta\frac{\Delta z}{z_m}\right]$$

$$\zeta = \frac{\ln\left(\frac{z_2}{z_1}\right)\left[2Ri_m\beta\frac{\Delta z}{z_m} - 1 \pm 1\right]}{2\beta\frac{\Delta z}{z_m}\left[1 - Ri_m\beta\frac{\Delta z}{z_m}\right]}$$

If positive, then $\zeta = \dfrac{\ln\left(\frac{z_2}{z_1}\right)Ri_m}{\left[1 - Ri_m\beta\frac{\Delta z}{z_m}\right]}$.

Appendix B: Estimation of soil water potential and soil water content

A. Soil water potential

First, each sensor is applied an individual calibration slope (m) and intercept (b):

$$dT_{ref} = m * dT_{sensor} + b$$

where dT_{ref} is the reference sensor and dT_{sensor} is the individual sensor. Second, the temperature differential is converted to a soil water potential:

$$\psi = \frac{1}{a}\left[\frac{dT_w - dT_d}{dT_{ref} - dT_d} - 0.9\right]^{1/n}$$

where ψ is the soil water potential (kPa), dT_d = 4.0 C, dT_w = 1.45 C, a = -0.01 kPa, and n = 0.77.

B. Soil Water Content

The soil water content is then empirically derived as a function of potential:

$$\theta = \theta_r + \frac{\theta_s - \theta_r}{\left[1 + \left(a(-\psi/100)\right)^n\right]^{(1-1/n)}}$$

where θ is the soil water content (m^3m^{-3}), θ_r is the residual water content, θ_s is the saturated soil water content, and α and n are empirical constants.

Appendix C: Coordinate axis rotation

Coordinate axis rotation is used to correct for the tilt error imposed by either the tilt of the sonic anemometer or the slope of the underlying topography. Observations of the orthogonal u, v, and w components of wind are rotated about an axis until the mean vertical wind speed is zero.

As shown in Section 4.a, a least-squares fit is applied to the data to determine three unknowns: a, b, and c. The equation

$$w = a + bu + cv \qquad \text{(C.1)}$$

is used to determine a, b, and c. The observations of u, v, and w, are the 5-minute means of wind. From Eq. (C.1), the values for a, b, and c are then used to determine the lean angle (θ) and the azimuth of the lean angle (ϕ) as follows:

$$\theta = Tan^{-1}\left(\sqrt{b^2 + c^2}\right) \qquad \text{(C.2)}$$

$$\varphi = Tan^{-1}\left(\frac{c}{b}\right) \qquad \text{(C.3)}$$

Once θ and ϕ are determined, the actual observations then can be rotated. First, a coordinate rotation matrix is developed from the values for θ and ϕ. The matrix components are developed as follows:

$\gamma=\mathrm{sqrt}(\cos(\theta)^2 + \sin(\theta)^2\cos(\phi)^2)$

$A[1,1] = \cos(\theta)/\gamma$
$A[1,2] = 0$
$A[1,3] = -\sin(\theta)\cos(\phi)/\gamma$

$A[2,1] = (\sin(\theta)\sin(\phi))(-\sin(\theta))(\cos(\phi)/\gamma)$
$A[2,2] = (\cos(\theta)(\cos(\theta)/\gamma)$
$A[2,3] = -(\sin(\theta)\sin(\phi))(\cos(\theta)/\gamma)$

$A[3,1] = \sin(\theta)\cos(\phi)$
$A[3,2] = \sin(\theta)\sin(\phi)$
$A[3,3] = \cos(\theta)$

Once the rotation matrix has been formed, the wind component means, scalar covariances, and wind covariances can be easily rotated into the actual mean wind. The wind component means and scalar covariances are rotated as follows:

Let $B[a_1\ \ a_2\ \ a_3]$ be the vector of wind component means u, v, w. The rotated vector of winds are found simply by vector-matrix multiplication:

$D[b_1\ \ b_2\ \ b_3] = [A] * B$

The scalar covariances are rotated in a similar fashion, e.g. with the vector B $[a_1\ \ a_2\ \ a_3]$ where $a_1 = u'T'$, $a_2 = v'T'$, $a_3 = w'T'$.

The wind covariances are rotated in a slightly more complicated manner since all three dimensions of wind speed must be rotated. A 3x3 matrix of wind speed covariances are formed as:

$$[B] = \begin{bmatrix} u'u' & u'v' & u'w' \\ v'u' & v'v' & v'w' \\ w'u' & w'v' & w'w' \end{bmatrix}$$

The rotated matrix [D] is found by matrix multiplication as:

$[D] = [A]^t\,[B]\,[A]$.